Non-Newtonian Effects and Taylor–Aris Dispersion in Rivulet Flow

This thesis is submitted to the University of Strathclyde for the degree of Doctor of Philosophy in the Faculty of Science by

Fatemah Hussain Habib Al Mukahal

Department of Mathematics and Statistics

University of Strathclyde

Glasgow, UK

August 2017

Declaration of Authenticity and Author's Rights

This thesis is the result of the author's original research. It has been composed by the author and has not been previously submitted for examination which has led to the award of a degree.

Signed:

Date:

I dedicate this work to my husband Ali AlAtawi, my daughters Zainab and Khaula, without whom this thesis could have been finished one year earlier, and to my parents for their endless love, continual prayers and encouragement.

Acknowledgements

First and foremost I will thank Almighty Allah, the compassionate, the almighty Merciful, who kindly helped me and granted me the courage and strength to accomplish my thesis. It would not have been possible to write this thesis without the aid and support of the most kind people around me, to only some of whom it is possible to give particular indication here.

Above all, I would like to thank my dearest husband Ali and my beloved parents Hussain and Shukariah for their unconditional love, endless patience and continuous support at all times. They have given me their unequivocal support throughout my studies for which my mere expression of thanks likewise does not suffice.

The success of this thesis is indebted to the extensive support and assistance from both of my supervisors, Prof. Stephen K. Wilson. and Dr. Brian R. Duffy. I would like to express my heartfelt gratitude and sincere appreciation to them for their guidance, invaluable advice, supervision, encouragement, invaluable knowledge and kindness to me throughout this work. Words could not be enough to express my gratitude for the wonderful job they did. Also, thank you for all the opportunities you provided me to contribute in conferences and to gain greater intellectual insights into academic life.

I also take the opportunity to thank the Ministry of Education, Kingdom of Saudi Arabia and King Faisal University for financial support via an Academic Staff Training Fellowship and for making my PhD research program possible at

the University of Strathclyde. I would also like to acknowledge the academic and technical support at Department of Mathematics and Statistics in the University of Strathclyde and its staff, particularly Dr. Ronnie Wallace and Mrs. Irene Spencer, for all their help during my studies.

Finally, I extend my deepest thanks to my daughters Zainab (six years) and Khaula (one year) to whom I cannot adequately express in just a few words how much I love them. While I am absorbed in this project, they provided a loving home and motivated me at every step. Thank you for making me delighted and cheery when I needed it, especially your birth moments in Glasgow.

Abstract

In this thesis we use a combination of analytical and numerical methods to analyse two aspects of the steady flow of rivulets of fluid, namely the effects of non-Newtonian rheology, and the transport of a passive solute in a rivulet of Newtonian fluid.

In Chapters 2–4 we consider rivulet flow of non-Newtonian fluids. Firstly, we obtain the solution for unidirectional gravity-driven flow of a uniform thin rivulet of a power-law fluid down a planar substrate, and then we use this solution to describe the flow of a rivulet with prescribed constant contact angle but slowly varying semi-width down a slowly varying substrate, specifically the flow in the azimuthal direction around the outside of a large horizontal circular cylinder. Secondly, we use the solution for unidirectional flow to describe the flow of a rivulet with prescribed constant semi-width but slowly varying contact angle down a slowly varying substrate. Thirdly, we consider rivulet flow of generalised Newtonian fluids down a vertical planar substrate. In particular, we obtain the solutions for rivulet flow of a Carreau fluid and of an Ellis fluid, highlighting their similarities and differences.

In Chapters 5 and 6 we investigate both the short-time advection and the long-time Taylor–Aris dispersion of a passive solute in uniform non-thin and thin rivulets, respectively, of a Newtonian fluid undergoing steady unidirectional flow driven by gravity and/or a prescribed uniform surface shear stress on a vertical planar substrate. In particular, we obtain an explicit expression for the effective

diffusivity of the solute in a thin rivulet as a function of the surface shear stress, the volume flux along the rivulet, and either the semi-width or the contact angle of the rivulet.

Contents

Chapter 1

Introduction

This thesis concerns two aspects of the steady flow of rivulets of fluid, namely the effects of non-Newtonian rheology, and the transport of a passive solute in a rivulet of Newtonian fluid.

1.1 Rivulet Flow

When a continuous fluid film flows over a substrate, it may break up into one or more rivulets, as shown in Figure 1.1. A rivulet (sometimes also called a trickle) can be defined as a narrow stream of fluid that shares a curved free surface with the surrounding atmosphere, with contact angles at the three-phase contact lines where the substrate, fluid and the surrounding atmosphere are all in contact. A key feature of rivulet flow is that it is long and slender, with the flow predominantly along the rivulet (*i.e.* in the direction of the longer length scale). Rivulets can occur in small-scale flows as well as in large-scale flows.

The flow of rivulets of both Newtonian and non-Newtonian fluids is a fundamental fluid mechanics problem of enduring theoretical and experimental interest both in its own right and as a prototype problem for a variety of more complex flows. Here we give three specific reasons motivating the study of this problem.

Firstly, rivulets of non-Newtonian fluids occur in a wide range of devices in

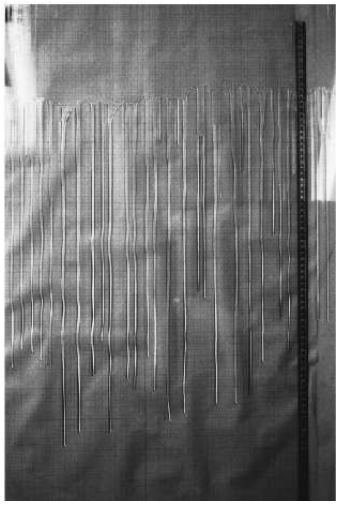

Figure 1.1: Image showing a gravity-driven film breaking into a series of rivulets down a substrate inclined at angle $\pi/4$ to the horizontal, from an experiment by Hocking *et al.* [56]. Reprinted from Hocking *et al.* [56] with permission, copyright 1999, from American Institute of Physics.

engineering processes and industrial technology, including condensers and heat exchangers (see, for example, Vlasogiannis *et al.* [127]), as well as in the use of catalysts in trickle-bed reactors (see, for example, Maiti *et al.* [75]) and in desalination plants (see, for example, Semiat *et al.* [112]). Other important situations in which rivulets often appear are any industrial processes in which painting or coating is involved, such as in the manufacture of vehicles. In such situations it is very important to prevent the formation of rivulets (which might be affected by any non-uniformities in the temperature of the substrate or the thickness of the coating) as they could seriously degrade the quality of the coating (see, for example, Myers [90]). A more commonly encountered everyday occurrence of rivulets includes the pouring of sauce over a dessert (as shown in Figure 1.2(a)).

Secondly, on large scales, rivulet flow can occur in geophysical contexts such as the spreading flow of mud, the flow of lava from a volcanic eruption, and the cascade of an avalanche of snow down a mountain. These types of flow have motivated several authors to use theoretical and experimental approaches to address various aspects of the problem of rivulet flow, such as Coussot [23] for flows of mud, and Griffiths [52] for flows of lava (as shown in Figure 1.2(b)). An

(a)  (b) 

Figure 1.2: (a) Image showing rivulets encountered when pouring sauce over a dessert. Photograph courtesy of fotor [45]. (b) Image showing a rivulet flow of lava [62].

(a)  (b) 

Figure 1.3: (a) Image showing rainwater on the window of a moving vehicle. Photograph by Prof. S. K. Wilson. (b) Image showing ice accretion on an aircraft wing. Photograph courtesy of Aviation Education Multimedia Library [72].

important factor in rivulet flow in these contexts is the temperature of the ice or lava, because slight temperature differences lead to relatively large variations in their rheological properties.

Thirdly, there are many situations in which rivulet flow occurs in the presence of external forces, such as those due to an external airflow, for example, rivulets of rainwater on the windows of a rapidly moving vehicle on a rainy day (as shown in Figure 1.3(a)), and the rivulets of de-icing fluid that form on aircraft wings during flight (as shown in Figure 1.3(b)) (see, for example, Myers and Charpin [88], Myers *et al.* [89], Sullivan *et al.* [118], and Paterson *et al.* [99] and the references therein). Another interesting phenomenon involving rivulets subject to an external airflow is the Rain–Wind-Induced Vibrations (RWIVs) of the cables of cable-stayed bridges, in which rivulets of rainwater that form on the cables interact with the wind and play a crucial role on the occurrence of substantial vibrations of the cables (see, for example, Robertson *et al.* [106]).

However, despite the widespread occurrence of non-Newtonian rheology in many of the practical occurrences of rivulet flow described above, there has been surprisingly little theoretical work on rivulet flow of non-Newtonian fluids. The work presented in Chapters 2–4 of the present thesis goes some way to rectifying this shortfall.

In Chapters 2–4 of this thesis we shall be concerned with understanding rivulet flows of non-Newtonian fluids, and so in Section 1.2 we present a general introduction to Newtonian and non-Newtonian fluids, and we will then describe them in more mathematical detail in Section 1.3. As we shall be concerned primarily with thin rivulets, in Section 1.4 we give an overview of thin-film flows, and in Sections 1.5–1.10 we describe various aspects of rivulet flow. Also, in Chapters 5 and 6 we will consider the transport of a passive solute in rivulet flows of a Newtonian fluid, and so in Section 1.11 we give a brief overview of the concept of dispersion of a solute in a flowing fluid.

1.2 Newtonian and Non-Newtonian fluids

We can classify any fluid as either Newtonian or non-Newtonian depending on its behaviour when it flows. A Newtonian fluid is one for which the relationship between the stress tensor and the rate-of-strain tensor is linear with the coefficient of the proportionality in this relationship, namely the viscosity, being a constant. The viscosity of a fluid can be thought of as a measure of the frictional resistance to the flow of the fluid. A non-Newtonian fluid is one whose behaviour deviates from that of a Newtonian fluid.

In order to help our understanding of the different types of non-Newtonian fluids, we need to have an understanding of rheology. The term rheology, which was coined by E. C. Bingham in 1929 (see, for example, Barnes *et al.* [13] and Morrison [83]), is defined as the study of the deformation and flow of matter.

There has been a considerable appreciation of the importance of the study of rheology in many fields such as chemical engineering, in which an understanding of how non-Newtonian fluids behave under stress is of considerable practical interest (see, for example, Morrison [83], Tanner [120], and Tanner and Walters [121]).

Some common fluids that exhibit non-Newtonian rheology are pharmaceutical products (for example, creams and foams), polymer solutions, suspensions, quicksand and foodstuffs such as ketchup, cornflour and dairy products (for example, cream and yoghurt), whose physical properties change when a shear stress is applied. For example, toothpaste becomes runnier and flows more easily when it is squeezed from a toothpaste tube (*i.e.* its viscosity decreases with increasing shear rate), but returns to an almost solid state when the shear stress is removed (*i.e.* its viscosity increases). This most common non-Newtonian behaviour is known as shear-thinning or pseudoplastic behaviour. Specifically, shear-thinning materials exhibit a decrease in their viscosity under an increase in shear rate. However, other fluids show the converse behaviour; for example, cornflour mixed with water becomes "thicker" when subjected to a high shear (*i.e.* its viscosity increases and it behaves like a solid), but it becomes "thinner" when subjected to a low shear. Quicksand has similar properties to cornflour solutions, with the consequence that the best way to escape from quicksand is to try move slowly and thereby to reduce its viscosity. This converse behaviour occurs for shear-thickening or dilatant fluids; such materials exhibit an increase in their viscosity under an increase in shear rate.

Shear-thinning and shear-thickening behaviour are not the only non-Newtonian effects. In particular, some non-Newtonian fluids exhibit surprising behaviour associated with viscoplasticity and/or viscoelasticity. Viscoplastic materials behave essentially like a solid unless the shear stress exceeds a critical value, known as the yield stress, above which they deform and begin to flow. Viscoelastic materials exhibit characteristics of both viscous and elastic behaviour. Examples

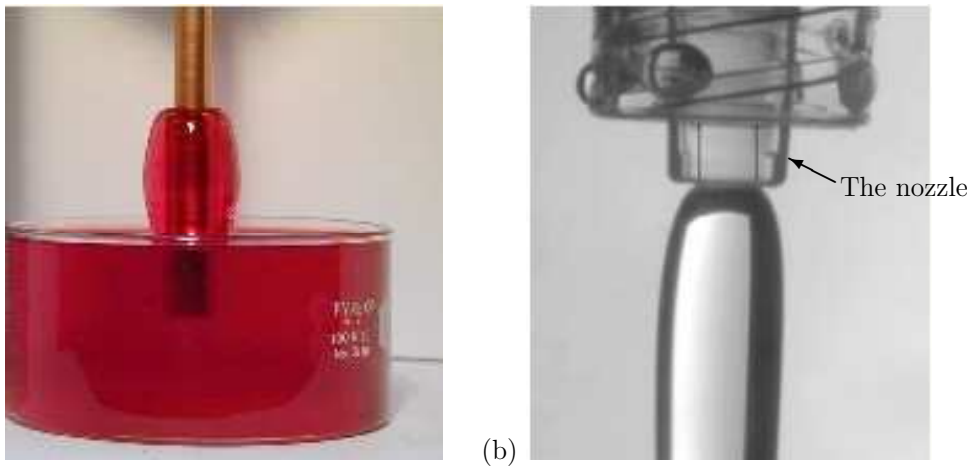

Figure 1.4: Viscoelastic behaviour. (a) Rod-climbing exhibited by a solution of a polystyrene polymer in polybutene oil generated by clockwise or anticlockwise rotation of the rod. (b) Die-swell exhibited by a solution of 1% polyacylamide in a mixture of 50% glycerol and 50% water when extruded through a nozzle. Photographs courtesy of Gareth McKinley's Non-Newtonian Fluid Dynamics Research Group at MIT [77].

of the surprising behaviour associated with the latter are rod climbing (the so-called Weissenberg effect), in which a fluid climbs up a rod spun in a container of the fluid, as shown in Figure 1.4(a)), and also die swell, in which a fluid flowing through a capillary swells when it emerges into the atmosphere, as shown in Figure 1.4(b) (see, for example, Boger and Walters [19] and Morrison [83]).

1.3 Mathematical Modelling in Rheology

In this section we give a brief overview of the mathematical modelling of non-Newtonian fluids, and describe in detail the three main models used in this thesis.

The flow of an incompressible fluid of constant density ρ is described by Cauchy's balance of momentum (*i.e.* the equation of motion),

$$\rho \frac{D\mathbf{u}}{Dt} = \rho \mathbf{f} + \nabla \cdot \underline{\underline{\boldsymbol{\sigma}}}, \tag{1.1}$$

and the mass-conservation equation (*i.e.* the continuity equation),

$$\nabla \cdot \mathbf{u} = 0, \tag{1.2}$$

where $\mathbf{f}$ denotes any body force per unit mass acting on the fluid (e.g. gravity or electromagnetic forces), $\underline{\underline{\boldsymbol{\sigma}}}$ is the symmetrical Cauchy stress tensor, $D/Dt = \partial/\partial t + \mathbf{u} \cdot \nabla$ is the material time derivative, $\mathbf{u}$ is the fluid velocity, ∇ is the usual vector differential gradient operator, and t denotes time. Note that the Cauchy equation (1.1) is valid for all fluids, including both Newtonian and non-Newtonian fluids. We decompose $\underline{\underline{\boldsymbol{\sigma}}}$ as

$$\underline{\underline{\boldsymbol{\sigma}}} = -p\underline{\underline{\mathbf{I}}} + \underline{\underline{\boldsymbol{\sigma}}}', \tag{1.3}$$

where p is the fluid pressure, $\underline{\underline{\mathbf{I}}}$ is the identity tensor, and $\underline{\underline{\boldsymbol{\sigma}}}'$ is the extra-stress tensor, that is, the part of the stress other than the pressure. What distinguishes different fluids in (1.1) is the way in which $\underline{\underline{\boldsymbol{\sigma}}}'$ is related to deformation, that is, to kinematic variables; this is given by a relation known as the constitutive equation of the fluid (see, for example, Barnes *et al.* [13]).

1.3.1 A Newtonian Fluid

The constitutive equation of a Newtonian fluid is given by

$$\underline{\underline{\boldsymbol{\sigma}}}' = 2\mu\underline{\underline{\mathbf{e}}}, \tag{1.4}$$

where μ is the fluid viscosity, and $\underline{\underline{\mathbf{e}}}$ is the rate-of-strain tensor, given by

$$\underline{\underline{\mathbf{e}}} = \frac{1}{2}\left(\nabla\mathbf{u} + (\nabla\mathbf{u})^{\mathrm{T}}\right). \tag{1.5}$$

Substituting equations (1.3)–(1.5) into the equation of motion (1.1) yields the familiar equation of motion for an incompressible Newtonian fluid, namely the Navier–Stokes equation:

$$\rho\frac{D\mathbf{u}}{Dt} = -\nabla p + \rho\mathbf{f} + \mu\nabla^2\mathbf{u}. \tag{1.6}$$

In order to determine solutions to the mass-conservation equation (1.2) and Navier–Stokes equation (1.6), it is necessary to impose appropriate initial and boundary conditions on the velocity and pressure.

At any boundary S between a fluid and a solid, the tangential component of velocity is continuous and satisfies the no-slip condition

$$[\mathbf{u} \cdot \mathbf{t}]_1^2 = 0 \quad \text{on} \quad S, \tag{1.7}$$

where $\mathbf{t}$ denotes a unit vector tangent to S, while the normal component of velocity is also continuous and satisfies the no-penetration condition

$$[\mathbf{u} \cdot \mathbf{n}]_1^2 = 0 \quad \text{on} \quad S, \tag{1.8}$$

where $\mathbf{n}$ denotes the unit vector normal to S, and $[\cdot]_1^2$ denotes the change in a quantity across S. In particular, at any boundary S moving with velocity $\mathbf{U}$ the no-slip condition (1.7) and the no-penetration condition (1.8) become

$$\mathbf{u} \cdot \mathbf{t} - \mathbf{U} \cdot \mathbf{t} = 0, \tag{1.9}$$

$$\mathbf{u} \cdot \mathbf{n} - \mathbf{U} \cdot \mathbf{n} = 0, \tag{1.10}$$

respectively. Together, equations (1.9) and (1.10) mean that the velocity of the fluid is continuous everywhere and is equal to the velocity of the boundary, that is,

$$\mathbf{u} = \mathbf{U} \quad \text{on} \quad S. \tag{1.11}$$

Also, at any boundary S between two fluids the stress-balance equation

$$[\underline{\boldsymbol{\sigma}} \cdot \mathbf{n}]_1^2 = \gamma(\nabla \cdot \mathbf{n})\mathbf{n} - \nabla\gamma \quad \text{on} \quad S \tag{1.12}$$

is satisfied, where γ is the coefficient of surface tension on S and $\nabla \cdot \mathbf{n}$ is the mean

curvature of S. The surface tension arises from the imbalance of molecular forces on the surface. In the special case of constant γ, the balances of the normal and tangential stress are therefore given by

$$[\mathbf{n} \cdot \underline{\underline{\boldsymbol{\sigma}}} \cdot \mathbf{n}]_1^2 = \gamma \nabla \cdot \mathbf{n}, \tag{1.13}$$

$$[\mathbf{t} \cdot \underline{\underline{\boldsymbol{\sigma}}} \cdot \mathbf{n}]_1^2 = 0, \tag{1.14}$$

respectively, on S. In addition, at any boundary S between two fluids, on the assumption that the fluid particles on the boundary remain on the boundary, we also have the kinematic condition, given by

$$\frac{DF}{Dt} = 0 \quad \text{on} \quad S, \tag{1.15}$$

where $F(\mathbf{x}, t) = 0$ is the equation for the boundary. The volume flux of fluid across any surface S is given by

$$Q = \iint_S \mathbf{u} \cdot \mathbf{n} \, \mathrm{d}S, \tag{1.16}$$

where $\mathbf{n}$ is again the unit vector normal to S.

To solve unsteady problems we must impose initial conditions for $\mathbf{u}$ and p of the form

$$\mathbf{u}(\mathbf{x}, t = 0) = \mathbf{u}_0(\mathbf{x}), \quad p(\mathbf{x}, t = 0) = p_0(\mathbf{x}), \tag{1.17}$$

where $t = 0$ is the initial time and $\mathbf{x}$ denotes the position vector.

1.3.2 Generalised Newtonian Fluids

A generalised Newtonian fluid is one for which the equation of motion (1.1) again holds, but for which the viscosity varies with either the shear rate q or the shear stress τ, so that the relation between stress and shear rate is non-linear.

Specifically, for such fluids the viscosity is prescribed either as a function $\mu = \mu(q)$ of the shear rate q given by

$$q = \left(2\,\mathrm{tr}\left(\underline{\underline{\mathbf{e}}}^2\right)\right)^{1/2}, \tag{1.18}$$

or as a function $\mu = \mu(\tau)$ of the measure of stress τ given by

$$\tau = \left(\frac{1}{2}\mathrm{tr}\left(\underline{\underline{\boldsymbol{\sigma}}}'^2\right)\right)^{1/2}. \tag{1.19}$$

Use of (1.4)–(1.19) shows that μ, q and τ are related by

$$\tau = \mu q. \tag{1.20}$$

In practice, one or the other of the forms $\mu = \mu(q)$ or $\mu = \mu(\tau)$ may be considerably more convenient to use than the other (such as, for example, when one of them is prescribed explicitly whereas the other is known only implicitly).

In this thesis we shall firstly focus on the simplest generalised Newtonian fluid whose viscosity is usually expressed in the form $\mu = \mu(q)$, namely a power-law fluid (sometimes also called the Ostwald–de Waele fluid; see Barnes *et al.* [13]), for which the viscosity is directly proportional to a power of the shear rate, so that the constitutive equation takes the form

$$\underline{\underline{\boldsymbol{\sigma}}}' = 2\mu(q)\underline{\underline{\mathbf{e}}}, \qquad \mu(q) = \mu_N q^{N-1}, \tag{1.21}$$

where the power-law index N and the consistency parameter of the fluid μ_N are constants. Note that the dimensions of μ_N depend on N. In this case, the measure of the stress, τ, takes the form $\tau = \mu(q)q = \mu_N q^N$. In practice, N is usually found to lie between 0.1 and 1, although values outside this range do occur, see Barnes *et al.* [13]. So, in order to investigate the full range of possible

Table 1.1: Values of the physical parameters in the power-law model (1.21) for various well-known materials for particular ranges of shear rates, where μ_N is the consistency parameter of the fluid and N is the power-law index. Data taken from Barnes *et al.* [13].

Material	μ_N [$\mathbf{Pa\,s^N}$]	N	**Shear rate range** [$\mathbf{s^{-1}}$]
Ball-point pen ink	10	0.85	10^0–10^3
Fabric conditioner	10	0.6	10^0–10^2
Molten chocolate	50	0.5	10^{-1}–10^2
Skin cream	250	0.1	10^0–10^2

behaviour in this thesis, we shall allow N to take any positive value.

Table 1.1 shows parameter values for some examples of shear-thinning fluids modelled by the power-law model given by (1.21).

Because of its inherent simplicity, the power-law fluid has been used widely to study the rheological behaviour of both shear-thinning fluids (μ decreases with q) when $0 < N < 1$ and shear-thickening fluids (μ increases with q) when $N > 1$ over a wide range of flow conditions. When $N = 1$ the special case of a Newtonian fluid with constant viscosity is recovered.

Although the power-law fluid offers the simplest example of non-Newtonian behaviour, it suffers from a major shortcoming, namely that it is valid over only a limited range of shear rates; in particular, a power-law fluid predicts an unphysically large viscosity at low shear rates for shear-thinning fluids and small viscosity at low shear rates for shear-thickening fluids. For example, in steady unidirectional pressure-driven flow in a channel, since the shear rate is zero on the mid-line of the channel, the viscosity of a shear-thinning power-law fluid would be infinite there (Myers [91]). Moreover, it is found experimentally that real non-Newtonian fluids exhibit Newtonian behaviour with finite nonzero viscosities at both zero and infinite shear rates, but this behaviour is not captured by the power-law model. Despite the shortcomings of the power-law model, it has proved useful in many situations and is the most popular and widely used non-Newtonian model. Its shortcoming can be rectified by using more complicated models such as the Carreau fluid and the Ellis fluid, which we now describe.

Table 1.2: Values of the physical parameters in the Carreau fluid (1.22) for various well-known materials, where μ_0 and μ_∞ ($\leq \mu_0$) are the viscosities at zero and infinite shear rate, respectively, λ is a (finite) relaxation time, and N (≤ 1) is a measure of the shear-thinning behaviour. Data taken from Tanner [120].

Material	μ_0 **[Pa s]**	μ_∞ **[Pa s]**	λ **[s]**	N
0.75% Separan-30 in a mixture of 95% water and 5% glycerol	10.6	0.01	8.04	0.364
2% polyisobutylene in Primol 355	923	0.15	191	0.358
7% Aluminum soap in decalin and m-cresol	89.6	0.01	1.41	0.2
Phenoxy-A at 485 K	1.24×10^4	0	7.44	0.728

Another example of a generalised Newtonian fluid whose viscosity is usually expressed in the form $\mu = \mu(q)$ is a Carreau fluid (see, for example, Tanner [120] and Myers [91]), given by

$$\mu = \mu_\infty + \frac{\mu_0 - \mu_\infty}{\left(1 + \lambda^2 q^2\right)^{(1-N)/2}}, \tag{1.22}$$

where μ_0 and μ_∞ ($\leq \mu_0$) are the viscosities at zero and infinite shear rate, respectively, λ is a (finite) relaxation time, and N (≤ 1) is a measure of the shear-thinning behaviour (specifically, the smaller the value of N, the greater the rate of shear thinning). A Newtonian fluid may be recovered from a Carreau fluid in the limits $\lambda \to 0$, $\lambda \to \infty$, $N \to 1$ and $\mu_\infty \to \mu_0$. Table 1.2 shows parameter values for some examples of shear-thinning fluids modelled by the Carreau model given by (1.22).

An example of a generalised Newtonian fluid whose viscosity is usually expressed in the form $\mu = \mu(\tau)$ is an Ellis fluid (see, for example, Barnes, Hutton and Walters [13]), sometimes known as the Meter model [80], given by

$$\mu = \mu_\infty + \frac{\mu_0 - \mu_\infty}{1 + \left(\dfrac{\tau}{\tau_{\mathrm{av}}}\right)^{\alpha-1}}, \tag{1.23}$$

Table 1.3: Values of the physical parameters in the Ellis fluid (1.23) for four aqueous solutions of Natrosol 250, Type H (hydroxyethyl cellulose, high viscosity grade), where μ_0 and μ_∞ ($\leq \mu_0$) are the viscosities at zero and infinite shear rate, respectively, $\tau_{\rm av}$ is the (non-zero) value of the stress τ when μ takes the average value $\mu = \mu_{\rm av} = (\mu_0 + \mu_\infty)/2$, and α (≥ 1) is a measure of the shear-thinning behaviour. Data taken from Meter and Bird [80].

Concentration	μ_0 **[Pa s]**	μ_∞ **[Pa s]**	$\tau_{\rm av}$ **[dyn cm^{-2}]**	α
0.3%	0.023	0.00122	78	2.02
0.5%	0.109	0.0015	76	2.19
0.7%	0.386	0.00185	106	2.54
1%	2.03	0.0025	173	3.1

where $\tau_{\rm av}$ is the (non-zero) value of the stress τ when μ takes the average value $\mu = \mu_{\rm av} = (\mu_0 + \mu_\infty)/2$, and α (≥ 1) is a measure of the shear-thinning behaviour (specifically, the larger the value of α, the greater the rate of shear thinning). A Newtonian fluid may be recovered from an Ellis fluid in the limits $\tau_{\rm av} \to \infty$, $\mu_\infty \to \mu_0$ and $\alpha \to 1$. A conventional Ellis fluid (see, for example, Myers [91] and Kieweg [67]), which has zero viscosity in the limit of infinite stress $\tau \to \infty$, corresponds to the special case $\mu_\infty = 0$. Table 1.3 shows parameter values for some examples of shear-thinning fluids modelled by the Ellis model given by (1.23).

1.3.3 Viscoplastic Fluids

An important class of non-Newtonian fluids are viscoplastic fluids, whose behaviour obeys the generalised Newtonian model with a yield stress. Many constitutive equations have been used to model viscoplastic fluids (see, for example, the early review article by Bird *et al.* [17]). Perhaps the simplest model of such a fluid is a biviscosity fluid (see, for example, Lipscomb and Denn [73] and Gartling and Phan-Thien [47]), given by

$$\mu = \begin{cases} \mu_0 & \text{for} \quad q \leq q_{\rm c}, \\ \mu_\infty + (\mu_0 - \mu_\infty)\,\dfrac{q_{\rm c}}{q} & \text{for} \quad q > q_{\rm c}, \end{cases} \tag{1.24}$$

or, equivalently,

$$\mu = \begin{cases} \mu_0 & \text{for } \tau \leq \tau_c, \\ \dfrac{\mu_\infty}{1 - \left(\dfrac{\mu_0 - \mu_\infty}{\mu_0}\right)\dfrac{\tau_c}{\tau}} & \text{for } \tau > \tau_c, \end{cases} \tag{1.25}$$

where q_c and τ_c denote a critical shear rate and a yield stress, respectively, related by $\tau_c = \mu_0 q_c$. For a biviscosity fluid there will be a transition from a constant viscosity to a non-constant viscosity across any surface within the fluid on which $q = q_c$ or, equivalently, $\tau = \tau_c$. A Bingham fluid behaves like a perfectly rigid solid plug when the stress is less than the yield stress but otherwise it behaves like a viscous fluid; in particular, a Bingham fluid may be obtained from a biviscosity fluid (1.24) in the distinguished limit $\mu_0 \to \infty$ and $q_c \to 0$ with $\mu_0 q_c$ held fixed.

Other popular models that have been used to describe the behaviour of a viscoplastic fluid are the Herschel–Bulkley model and the Casson model (see, for example, Barnes [12]), defined by

$$\begin{aligned} \tau &= \tau_c + \mu_\infty q^N \quad \text{for} \quad \tau \geq \tau_c, \\ \sqrt{\tau} &= \sqrt{\tau_c} + \sqrt{\mu_\infty q} \quad \text{for} \quad \tau \geq \tau_c, \end{aligned} \tag{1.26}$$

respectively, where $\tau = 0$ for $\tau \leq \tau_c$. Figure 1.5 shows a summary of the relationships between the stress, τ, and the shear rate, q, for Newtonian and generalised Newtonian fluids, including the Bingham and Herschel–Bulkley models.

1.4 Mathematical Modelling of Thin-Film Flows

In this section we give a brief overview of classical lubrication theory for a thin layer of fluid between a substrate and an unknown free surface using the approach pioneered by Reynolds [105]. The same approach may also be applied to many other situations, including journal bearings, pressure-driven flow in a

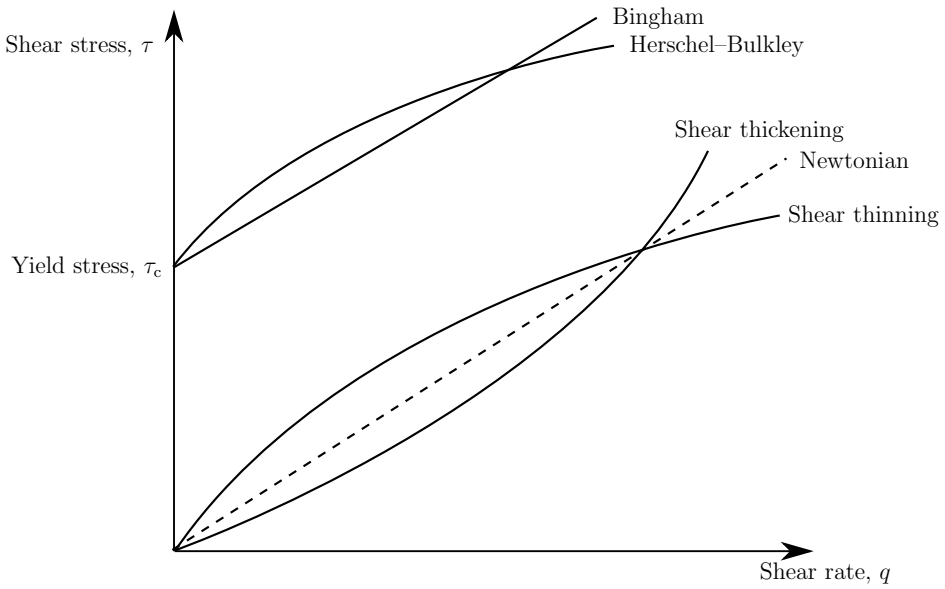

Figure 1.5: Sketch of the relationship between the shear stress, τ, and shear rate, q, for Newtonian and generalised Newtonian fluids, including the Bingham and Herschel–Bulkley models. The constant slope of the Newtonian flow curve is its viscosity.

slowly varying channel and squeeze films (in which a thin-film of fluid is squeezed between two prescribed boundaries moving toward each other). In most of this thesis (specifically Chapters 2–4 and 6 but not Chapter 5) we will use this theory to analyse the flow of uniform rivulets on an inclined substrate in cases when the cross-sectional profile of the rivulet transverse to the direction of flow is thin.

In general, the governing equations (1.2) and (1.6) must be solved numerically; however, we can often apply some practically relevant approximations to the equations and boundary conditions to permit the possibility of at least some analytical progress; this is because in practice some physical effects can dominate others, and it is a good approximation to retain only the dominant effects. For example, the introduction of an appropriate small aspect ratio allows simplification of the governing equations by neglecting terms that are small compared to others, and often results in equations where analytical progress can be made. In particular, if a film of fluid is sufficiently thin, the governing equations can be greatly simplified via a thin-film or lubrication approximation based on the

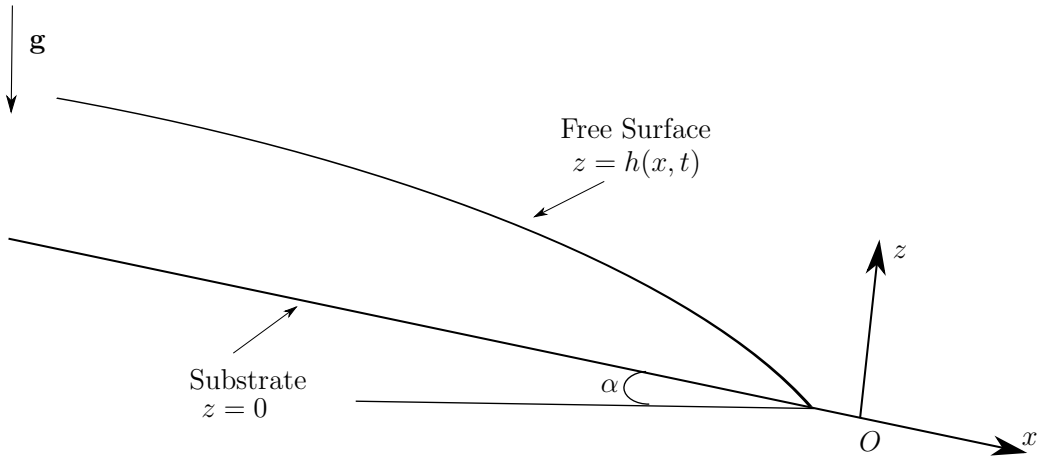

Figure 1.6: Sketch of unsteady two-dimensional gravity-driven flow of fluid draining down a planar substrate inclined at an angle α to the horizontal.

smallness of the aspect ratio of the film, given by

$$\delta = \frac{H}{L} \ll 1, \tag{1.27}$$

where $H = \delta L$ and L are typical lengthscales in the transverse and longitudinal directions, respectively, in which the fluid predominantly flows in the longitudinal direction.

We will present the idea of this approximation by considering a simple problem, namely, the unsteady two-dimensional gravity-driven flow of fluid on an inclined planar substrate. Consider two-dimensional flow of a thin-film of Newtonian fluid with constant density ρ and viscosity μ down a planar substrate inclined at an angle α ($0 \leq \alpha \leq \pi$) to the horizontal, as shown in Figure 1.6. We choose Cartesian coordinates Oxz with the x-axis and z-axis taken to be in the longitudinal (*i.e.* along the substrate) and transverse (*i.e.* normal to the substrate) directions, respectively. The substrate is at $z = 0$, and we denote the free surface of the fluid by $z = h$, where $h = h(x,t)$ is the film thickness, and again t denotes time. The velocity and pressure of the fluid are denoted by $\mathbf{u} = (u(x,z,t), 0, w(x,z,t))$ and $p = p(x,z,t)$, respectively. We non-dimensionalise and scale the system

appropriately by writing

$$\begin{gathered} x = Lx^*, \quad z = \delta L z^*, \quad h = \delta L h^*, \quad t = \frac{L}{U} t^*, \\ u = Uu^*, \quad w = \delta U w^*, \quad p = p_0 + \rho g \delta L p^*, \quad Q = \delta U L Q^*, \end{gathered} \tag{1.28}$$

where p_0 denotes the constant atmospheric pressure, and g denotes acceleration due to gravity. With the star superscripts immediately dropped for clarity, equations (1.2) and (1.6) become

$$u_x + w_z = 0, \tag{1.29}$$

$$\delta^2 Re(u_t + uu_x + wu_z) = -\delta p_x + \sin\alpha + \delta^2 u_{xx} + u_{zz}, \tag{1.30}$$

$$\delta^4 Re(w_t + uw_x + ww_z) = -p_z - \cos\alpha + \delta^2(\delta^2 w_{xx} + w_{zz}), \tag{1.31}$$

where $Re = \rho UL/\mu$ denotes the non-dimensional Reynolds number of the flow, which is the ratio of inertial forces to viscous forces, and $U = \rho g \delta^2 L^2/\mu$ is taken to be the relevant velocity scale, which leads to $Re = \rho^2 g \delta^2 L^3/\mu^2$

We take the reduced Reynolds number, defined by $Re^* = \delta^2 Re \ll 1$, to be small; in particular, this condition may be satisfied even if the Reynolds number itself is not small. Therefore, at leading order in the thin-film limit $\delta \to 0$, the governing equations (1.29)–(1.31) reduce to

$$u_x + w_z = 0, \tag{1.32}$$

$$\sin\alpha + u_{zz} = 0, \tag{1.33}$$

$$-p_z - \cos\alpha = 0, \tag{1.34}$$

respectively. Equations of this types are often called the lubrication equations. Also, at leading order in δ the boundary conditions of no-slip (1.9) and no-

penetration (1.10) on the substrate are given by

$$u = w = 0 \quad \text{on} \quad z = 0. \tag{1.35}$$

At the free surface $z = h$ the unit normal and relevant unit tangent vector are given by

$$\mathbf{n} = \frac{(-\delta h_x, 1)}{(1 + \delta^2 h_x^2)^{1/2}}, \quad \mathbf{t} = \frac{(1, \delta h_x)}{(1 + \delta^2 h_x^2)^{1/2}}, \tag{1.36}$$

respectively, and so the normal stress component $\mathbf{n} \cdot \underline{\underline{\boldsymbol{\sigma}}} \cdot \mathbf{n}$, the tangential stress component $\mathbf{t} \cdot \underline{\underline{\boldsymbol{\sigma}}} \cdot \mathbf{n}$, and the mean curvature $\nabla \cdot \mathbf{n}$ are given by

$$\mathbf{n} \cdot \underline{\underline{\boldsymbol{\sigma}}} \cdot \mathbf{n} = \frac{1}{1 + \delta^2 h_x^2} \left(-\frac{p}{\delta^2} - p h_x^2 - 2 u_z h_x + 2 w_z + \delta^2 \left(2 u_x h_x^2 - 2 w_x h_x \right) \right), \tag{1.37}$$

$$\mathbf{t} \cdot \underline{\underline{\boldsymbol{\sigma}}} \cdot \mathbf{n} = \frac{1}{1 + \delta^2 h_x^2} \left(\frac{u_z}{\delta} + \delta \left(w_x - 2 u_x h_x + 2 w_z h_x - u_z h_x^2 \right) - \delta^3 w_x h_x^2 \right), \tag{1.38}$$

$$\nabla \cdot \mathbf{n} = -\frac{\delta h_{xx}}{(1 + \delta^2 h_x^2)^{3/2}}. \tag{1.39}$$

Therefore, at leading order in the limit $\delta \to 0$ the normal stress-balance and tangential stress-balance equations (1.13) and (1.14) reduce to

$$p = -C_{\mathrm{a}}^{-1} h_{xx}, \tag{1.40}$$

$$u_z = 0, \tag{1.41}$$

respectively, at $z = h$, where

$$C_{\mathrm{a}} = \frac{\rho g L^2}{\delta \gamma} \tag{1.42}$$

is the appropriate capillary number, which is the ratio of viscous forces and surface-tension forces, and which we have taken to be $O(1)$. Note that the latter choice is appropriate for this particular problem, but it may not be appropriate

in other situations. Also, the kinematic condition (1.15) is given by

$$\frac{D(h-z)}{Dt} = 0 \quad \text{on} \quad z = h(x,t), \tag{1.43}$$

which yields

$$h_t + uh_x - w = 0, \tag{1.44}$$

which may also be rewritten as

$$h_t + Q_x = 0, \tag{1.45}$$

where $Q = Q(x,t)$ (from (1.16)), defined by

$$Q = \int_0^h u \, \mathrm{d}z, \tag{1.46}$$

is the volume flux of fluid per unit width draining in the longitudinal direction.

In the case when the effects of surface tension are negligible (*i.e.* $C_{\mathrm{a}}^{-1} \to 0$ or $C_{\mathrm{a}} \to \infty$) the solution to (1.32)–(1.34) for the pressure p and the velocity $\mathbf{u}$ subject to the no-slip and no-penetration conditions (1.35) on $z = 0$ and the balances of normal stress (1.40) and tangential stress (1.41) on $z = h$, is given by

$$p = \cos\alpha(h - z), \quad u = \frac{\sin\alpha}{2}(2hz - z^2), \quad w = -\frac{\sin\alpha}{2}h_x z^2. \tag{1.47}$$

Therefore the volume flux per unit width across a station $x =$ constant, down the substrate, is given by

$$Q = \int_0^h u \, \mathrm{d}z = \frac{\sin\alpha}{3}h^3, \tag{1.48}$$

and so the kinematic condition (1.45) leads to the partial differential equation for

the free surface profile h, namely

$$h_t + \sin\alpha\, h^2 h_x = 0. \tag{1.49}$$

Hence, the net effect of the lubrication approximation is to replace the mass-conservation equation (1.2) and Navier–Stokes equation (1.6) with a single partial differential equation for h, namely (1.49), so that the solutions for the pressure p and velocity $\mathbf{u}$ for the two-dimensional unsteady flow of a thin-film of a Newtonian fluid given by (1.47) are known completely once (1.49) is solved.

Huppert [61] solved (1.49) by using the method of characteristics to obtain the implicit solution

$$h = f\left(x - h^2 t \sin\alpha\right), \tag{1.50}$$

where $f = f(x)$ is the initial free surface shape of the film at $t = 0$. As time progresses the flow of the bulk of the fluid approaches the unique similarity solution

$$h = \left(\frac{x}{t\sin\alpha}\right)^{1/2}, \tag{1.51}$$

which is independent of the initial shape $f = f(x)$. This similarity solution predicts that the height of the free surface varies with x and t according to $x^{1/2}$ and $t^{-1/2}$. Huppert [61] truncated this solution appropriately to find the expression for the "nose" (*i.e.* the front) of the flow at time t, denoted by $x = x_N(t)$, namely

$$x_N(t) = \left(\frac{9A^2 t\sin\alpha}{4}\right)^{1/3}, \tag{1.52}$$

where A is the initial volume (*i.e.* area) of the film per unit width in the y direction, given by

$$A = \int_0^{x_N} h(x,t)\,\mathrm{d}x; \tag{1.53}$$

the solution for h is then given by (1.51) for $0 \leq x \leq x_N$. The effects of surface

tension, which are neglected in this analysis, become important near the nose of the flow $x = x_N(t)$. The similarity solution (1.51)–(1.53) of Huppert [61] is in excellent agreement with his own experimental measurements.

More generally, as a result of the simplicity of the equations arising in lubrication theory, which has been widely used to make analytical and numerical progress in thin-film flow problems, there has been a vast amount of scientific research using this approach, and there are several comprehensive review articles covering various aspects of this theory (see, for example, Oron *et al.* [94], Colinet *et al.* [22] and Craster and Matar [24]).

1.5 Flow of a Thin Rivulet Down a Planar Substrate

In Chapters 2–4 we will consider steady gravity-driven flow of a rivulet of non-Newtonian fluid, and in Chapters 5 and 6 we will consider steady flow of a rivulet of a Newtonian fluid driven by gravity and/or a uniform surface shear stress on the free surface of the rivulet. In this Section we introduce some key concepts and ideas that will be used in all of these Chapters; in particular, in Subsections 1.7.1 and 1.7.2 we summarise the main results of Wilson and Duffy [131] and Duffy and Moffatt [31], respectively, both of whom considered steady unidirectional gravity-driven flow of a rivulet of a Newtonian fluid with constant contact angle draining down a slowly varying substrate, in Subsection 1.7.3 we summarise the main results of Paterson *et al.* [97] who considered a "converse" situation of flow of a rivulet of a Newtonian fluid with constant semi-width but varying contact angle draining down a slowly varying substrate, in Section 1.9 we summarise the main results of Smith [114] and Duffy and Moffatt [32], both of whom considered gravity-driven flow of a non-uniform rivulet on an inclined planar substrate, and in Section 1.10 we review other relevant previous work on rivulet flow.

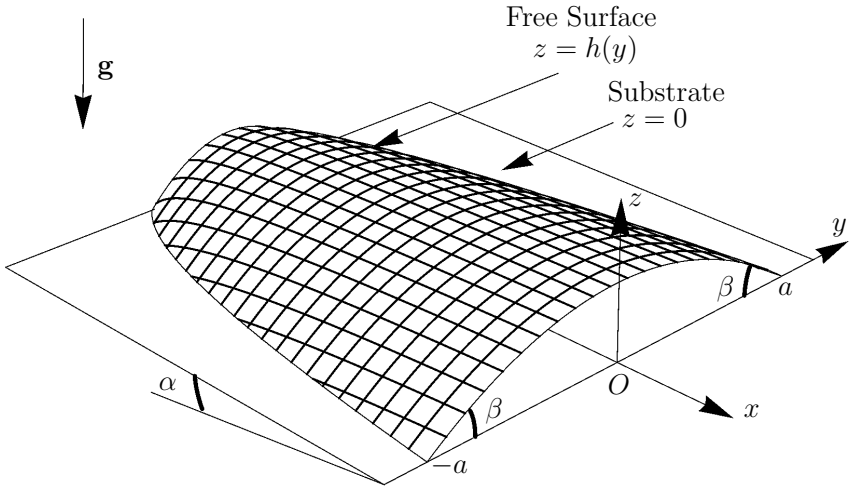

Figure 1.7: Sketch of steady gravity-driven flow of a symmetric rivulet draining down a planar substrate inclined at an angle α to the horizontal.

Consider steady gravity-driven draining of a symmetric rivulet of Newtonian fluid with constant density ρ, viscosity μ and coefficient of surface tension γ, and of constant volume flux Q down a planar substrate inclined at an angle α ($0 \leq \alpha \leq \pi$) to the horizontal, as shown in Figure 1.7.

The case $0 \leq \alpha < \pi/2$ corresponds to flow down the upper side of the substrate (a sessile rivulet), the case $\pi/2 < \alpha \leq \pi$ corresponds to flow down the lower side of the substrate (a pendent rivulet), and the case $\alpha = \pi/2$ corresponds to flow down a vertical substrate. We adopt the Cartesian coordinates $Oxyz$ shown in Figure 1.7, with the x-axis parallel to the substrate, the y-axis horizontal and the z-axis normal to the substrate at $z = 0$. We denote the free surface profile of the rivulet by $z = h$, where $h = h(x, y)$ is the thickness of the rivulet, the contact angle by $\beta = \beta(x, y)$, the semi-width of the rivulet by $a = a(x)$ (so that $h = 0$ at the contact lines $y = \pm a$) and the thickness of the rivulet at $y = 0$ (not necessarily the maximum thickness) by $h_{\rm m} = h(x, 0)$. The velocity

$\mathbf{u} = (u(x,y,z), v(x,y,z), w(x,y,z))$ and pressure $p = p(x,y,z)$ are governed by the mass-conservation and Navier–Stokes equations (1.2) and (1.6), respectively.

We consider flow of a thin rivulet (with, in particular, $\beta \ll 1$) for which the length scale in the z direction is much smaller than the length scale in the y direction, which, in turn, is much smaller than the length scale in the x direction, and hence we re-scale and non-dimensionalise the variables appropriately by writing

$$\begin{gathered} x = Lx^*, \quad y = \epsilon L y^*, \quad z = \epsilon\delta L z^*, \quad a = \epsilon L a^*, \quad \beta = \delta\beta^*, \\ h = \epsilon\delta L h^*, \quad u = \frac{\rho g \epsilon^2 \delta^2 L^2}{\mu} u^*, \quad v = \frac{\rho g \epsilon^3 \delta^2 L^2}{\mu} v^*, \quad w = \frac{\rho g \epsilon^3 \delta^3 L^2}{\mu} w^*, \\ p = p_0 + \rho g \epsilon \delta L p^*, \quad Q = \frac{\rho g \epsilon^4 \delta^3 L^4}{\mu} Q^*, \end{gathered} \tag{1.54}$$

where L is an appropriate longitudinal length scale, p_0 denotes the constant atmospheric pressure, g denotes acceleration due to gravity, ϵ ($\ll 1$) is the transverse aspect ratio of the rivulet, and δ ($\ll 1$) is the longitudinal aspect ratio of the rivulet. With the star superscripts omitted for clarity, the mass-conservation and Navier–Stokes equations (1.2) and (1.6) become

$$u_x + v_y + w_z = 0, \tag{1.55}$$

$$Re^*(uu_x + vu_y + wu_z) = -\epsilon\delta p_x + \sin\alpha + (\epsilon^2\delta^2 u_{xx} + \delta^2 u_{yy} + u_{zz}), \tag{1.56}$$

$$\epsilon Re^*(uv_x + vv_y + wv_z) = -\delta p_y + \epsilon(\epsilon^2\delta^2 v_{xx} + \delta^2 v_{yy} + v_{zz}), \tag{1.57}$$

$$\epsilon\delta Re^*(uw_x + vw_y + ww_z) = -p_z + \cos\alpha + \epsilon\delta(\epsilon^2\delta^2 w_{xx} + \delta^2 w_{yy} + w_{zz}), \tag{1.58}$$

where

$$Re^* = \frac{\rho^2 g \epsilon^4 \delta^4 L^3}{\mu^2} \tag{1.59}$$

is an appropriately defined reduced Reynolds number which differs from the reduced Reynolds number defined in Section 1.4 by the factor of ϵ^4; this is because in Section 1.4 the appropriate length scale in the transverse direction is δL but

here it is $\epsilon\delta L$. Provided that $Re^* \ll 1$ is sufficiently small then at leading order in ϵ equations (1.55)–(1.58) reduce to the lubrication equations

$$u_x + v_y + w_z = 0, \tag{1.60}$$

$$\sin\alpha + u_{zz} = 0, \tag{1.61}$$

$$-\delta p_y + \epsilon v_{zz} = 0, \tag{1.62}$$

$$-p_z - \cos\alpha = 0. \tag{1.63}$$

These governing equations are to be integrated subject to the no-slip and no-penetration conditions (from (1.9) and (1.10)) at the substrate $z = 0$:

$$u = v = w = 0, \tag{1.64}$$

the usual normal and tangential stress balances (from (1.13) and (1.14)) at the free surface $z = h(y)$:

$$p = -C_{\mathrm{a}}^{-1} h_{yy}, \tag{1.65}$$

$$u_z = v_z = 0, \tag{1.66}$$

and the condition of zero thickness at the contact-lines:

$$h = 0 \quad \text{and} \quad h_y = \mp\beta \quad \text{at} \quad y = \pm a, \tag{1.67}$$

where

$$C_{\mathrm{a}} = \frac{\rho g \epsilon^2 L^2}{\gamma} \tag{1.68}$$

denotes the appropriate capillary number, which differs from the capillary number given by (1.42) by the factor of ϵ^2/δ; this is because in Section 1.4 the dominant contribution of the surface-tension force is γh_{xx}, whereas here it is γh_{yy}. We define the capillary length ℓ by $\ell = (\gamma/\rho g)^{1/2}$, and then choose $\epsilon = \ell/L$, corresponding

to taking $C_{\rm a} = 1$ without loss of generality. The kinematic condition (1.15) at the free surface $z = h$ may be written in the form

$$\bar{u}_x + \bar{v}_y = 0, \tag{1.69}$$

where the local fluxes $\bar{u} = \bar{u}(x, y)$ and $\bar{v} = \bar{v}(x, y)$ are given by

$$\bar{u} = \int_0^h u \, \mathrm{d}z, \quad \bar{v} = \int_0^h v \, \mathrm{d}z. \tag{1.70}$$

Integrating (1.62) subject to (1.65) at $z = h$ gives the solution for the pressure p, namely

$$p = \cos\alpha(h - z) - h_{yy}, \tag{1.71}$$

while integrating (1.60) and (1.61) twice subject to (1.64) at $z = 0$ and (1.66) at $z = h$ gives the solution for the velocity $\mathbf{u}$, namely

$$\begin{aligned} u &= \frac{\sin\alpha}{2}(2hz - z^2), \\ \epsilon v &= -\frac{\delta p_y}{2}(2hz - z^2), \\ \epsilon\delta w &= -\frac{\epsilon\delta \sin\alpha h_x z^2}{2} + \frac{\delta^2 z^2}{2}\left(p_{yy}h + p_y h_y - \frac{z}{3}p_{yy}\right). \end{aligned} \tag{1.72}$$

Therefore from (1.70) the local fluxes $\bar{u}$ and $\bar{v}$ are given by

$$\bar{u} = \frac{\sin\alpha}{3}h^3, \quad \epsilon\bar{v} = -\frac{\delta p_y}{3}h^3, \tag{1.73}$$

and hence the volume flux of fluid along the rivulet, $Q = Q(x)$, is given by

$$Q = \int_{-a}^{a} \bar{u} \, \mathrm{d}y = \frac{2\sin\alpha}{3}\int_0^a h^3 \, \mathrm{d}y. \tag{1.74}$$

In the present work we shall be concerned with situations in which Q takes a prescribed constant value $Q = \bar{Q}$. We will consider only a thin rivulet that varies

much more slowly in the x-direction than in the y-direction; in particular, we will take x-derivatives to be much smaller than y-derivatives, *i.e.* the case $\epsilon \ll \delta \ll 1$. Physically this corresponds to the rivulet being thin and slowly varying. Note that both of the alternative cases $\epsilon = O(\delta) \ll 1$ and $\delta \ll \epsilon \ll 1$ are also possible; however, the former case $\epsilon = O(\delta)$ would require rather specific parameter values, and in the latter case $\delta \ll \epsilon \ll 1$ the rivulet varies much more slowly in the y-direction than in the x-direction; in particular, y-derivatives are much smaller than x-derivatives. Physically this corresponds to the rivulet being very thin. Neither of these two alternative case is considered here.

1.6 Unidirectional Flow of a Thin Uniform Rivulet Down a Planar Substrate

The pioneering analysis of the steady unidirectional flow of a uniform rivulet (*i.e.* a rivulet with constant width and cross-sectional profile) of a Newtonian fluid down an inclined substrate was performed by Towell and Rothfeld [124]. In particular, they obtained the free surface profile of the rivulet and the numerical solution for the velocity, and found that their solutions were in good agreement with their own experimental results. Allen and Biggin [8] used the lubrication approximation to obtain an expression for the velocity profile and found good agreement between their first-order-accurate asymptotic solution and their numerical solution. Bentwich *et al.* [16] extended the analysis employed by Allen and Biggin [8] to develop numerical results for the flow on an inclined substrate and a vertical substrate for a greater range of contact angles of the rivulet by producing a four-term expansion for the velocity. Duffy and Moffatt [31] followed the approach of Allen and Biggin [8] to obtain the leading order asymptotic solution in the limit of a thin rivulet with constant non-zero contact angle and prescribed volume flux on an inclined substrate and interpreted their results as describing

the locally unidirectional flow of a slowly varying rivulet down a slowly varying substrate, and, in particular, as describing the flow in the azimuthal direction round a large horizontal cylinder. In this Section we will explain these concepts in more detail.

A feature of rivulet flow down an inclined planar substrate is that when $\epsilon \ll \delta$, so that $\epsilon/\delta \to 0$ in the limit $\epsilon \to 0$, the flow is unidirectional, as sketched in Figure 1.8; at leading order in ϵ and δ the velocity will be of the form $\mathbf{u} = u(y,z)\mathbf{i}$ and therefore the governing equations (1.61)–(1.63) become

$$\sin\alpha + u_{zz} = 0, \tag{1.75}$$

$$-p_y = 0, \tag{1.76}$$

$$-p_z - \cos\alpha = 0, \tag{1.77}$$

together with the boundary conditions (1.64)–(1.67), namely

$$u = 0 \quad \text{on} \quad z = 0, \tag{1.78}$$

$$p = -h_{yy} \quad \text{and} \quad u_z = 0 \quad \text{on} \quad z = h, \tag{1.79}$$

and

$$h = 0 \quad \text{and} \quad h_y = \mp\beta \quad \text{on} \quad y = \pm a. \tag{1.80}$$

In cases when β is prescribed, δ can be defined by $\delta = \beta$, corresponding to taking $\beta^* = 1$ without loss of generality (this choice was made by Duffy and Moffatt [31]). On the other hand, in cases when a is prescribed, δ can be defined by $\delta = (\mu\bar{Q}/\rho g\ell^4)^{1/3}$, corresponding to taking $\bar{Q}^* = 1$ without loss of generality (this choice was made by Paterson *et al.* [97]). However, in this Section we leave δ unspecified and retain both β and $\bar{Q}$ in order to keep the subsequent presentation as general as possible.

In the general case of non-zero contact angle $\beta > 0$ (*i.e.* the case when the

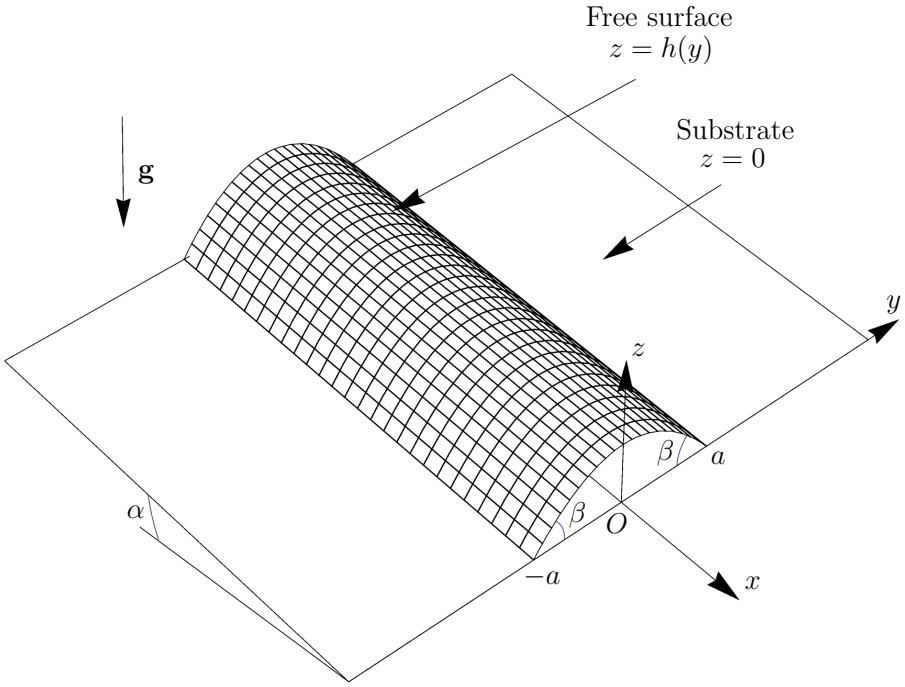

Figure 1.8: Sketch of steady gravity-driven flow of a thin uniform rivulet draining down a planar substrate inclined at an angle α to the horizontal.

fluid wets the substrate non-perfectly) Duffy and Moffatt [31] showed, by integrating (1.75)–(1.77) subject to the boundary conditions (1.78) and (1.79), that the solutions for the pressure p and velocity u, are given by

$$p = \cos\alpha(h - z) - h_{yy}, \quad u = \frac{\sin\alpha}{2}(2hz - z^2). \tag{1.81}$$

The local longitudinal flux $\bar{u} = \bar{u}(y)$ is given by

$$\bar{u} = \int_0^h u \, \mathrm{d}z = \frac{\sin\alpha}{3} h^3, \tag{1.82}$$

and hence the volume flux of fluid along the rivulet, Q, is given by

$$Q = \int_{-a}^{a} \bar{u} \, \mathrm{d}y = \frac{2\sin\alpha}{3} \int_0^a h^3 \, \mathrm{d}y. \tag{1.83}$$

Also the solution for p given by (1.81) with (1.76) leads to a third-order ordinary

differential equation for the free surface profile, namely

$$(h_{yy} - \cos\alpha\, h)_y = 0, \tag{1.84}$$

which when integrated subject to the contact-line conditions (1.80) yields the free surface profile

$$h = \beta \times \begin{cases} \dfrac{\cosh ma - \cosh my}{m \sinh ma} & \text{if } \ 0 \le \alpha < \dfrac{\pi}{2}, \\ \dfrac{a^2 - y^2}{2a} & \text{if } \ \alpha = \dfrac{\pi}{2}, \\ \dfrac{\cos my - \cos ma}{m \sin ma} & \text{if } \ \dfrac{\pi}{2} < \alpha \le \pi, \end{cases} \tag{1.85}$$

the maximum thickness of the rivulet h_{m}

$$h_{\mathrm{m}} = \beta \times \begin{cases} \dfrac{1}{m} \tanh \dfrac{ma}{2} & \text{if } \ 0 \le \alpha < \dfrac{\pi}{2}, \\ \dfrac{a}{2} & \text{if } \ \alpha = \dfrac{\pi}{2}, \\ \dfrac{1}{m} \tan \dfrac{ma}{2} & \text{if } \ \dfrac{\pi}{2} < \alpha \le \pi, \end{cases} \tag{1.86}$$

and the volume flux

$$Q = \frac{\beta^3 \sin\alpha}{9m^4} f\,(ma)\,, \tag{1.87}$$

where the function $f(ma)$ is defined by

$$f(ma) = \begin{cases} 15ma \coth^3 ma - 15 \coth^2 ma - 9ma \coth ma + 4 & \text{if } \ 0 \le \alpha < \dfrac{\pi}{2}, \\ \dfrac{12}{35}\,(ma)^4 & \text{if } \ \alpha = \dfrac{\pi}{2}, \\ -15ma \cot^3 ma + 15 \cot^2 ma - 9ma \cot ma + 4 & \text{if } \ \dfrac{\pi}{2} < \alpha \le \pi, \end{cases} \tag{1.88}$$

where we have introduced the notation $m = \sqrt{|\cos\alpha|}$.

In the special case of zero contact angle $\beta = 0$ (*i.e.* the case when the fluid wets the substrate perfectly) Wilson and Duffy [131] showed that equations (1.83)

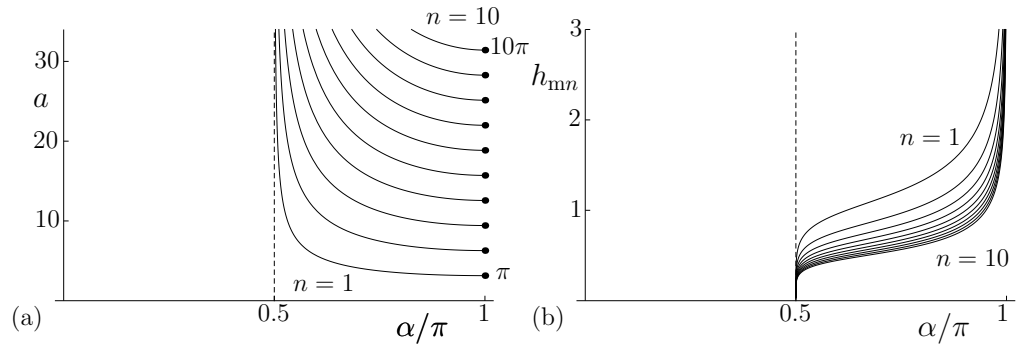

Figure 1.9: Plots of (a) the semi-width a, and (b) the maximum thickness $h_{\mathrm{m}n}$ as functions of α/π given by (1.90), for $n = 1$, all when $\bar{Q} = 1$, for a rivulet of perfectly wetting fluid.

and (1.84) have no solutions for h corresponding to sessile rivulets or rivulets on a vertical substrate (*i.e.* on the upper side of the substrate, $0 \leq \alpha \leq \pi/2$), but for pendent rivulets (*i.e.* on the lower side of the substrate, $\pi/2 < \alpha \leq \pi$) they have infinitely many solutions, namely

$$a = \frac{n\pi}{m}, \quad h = \frac{h_{\mathrm{m}n}}{2}(1 - (-1)^n \cos my), \tag{1.89}$$

where $h_{\mathrm{m}n}$ is the maximum thickness of the rivulet, given by

$$h_{\mathrm{m}n} = 2\left(\frac{3\bar{Q}m}{5n\pi \sin\alpha}\right)^{1/3}, \tag{1.90}$$

for $n = 1, 2, 3, \ldots$, where we have again used the notation $m = \sqrt{|\cos\alpha|}$. In particular, the solutions (1.89) and (1.90) show that the semi-width a varies with α and does not depend on the prescribed flux $\bar{Q}$, but that the thickness of the rivulet varies with $\bar{Q}$ according to $h \propto \bar{Q}^{1/3}$. All of these solutions are physically realisable in the sense that they satisfy $h \geq 0$ for $0 \leq y \leq a$, and the higher-branch solutions (*i.e.* $n = 2, 3, \ldots$) are arrays of n identical contiguous rivulets each of which is a suitably re-scaled copy of the lowest-branch solution (*i.e.* $n = 1$).

Figures 1.9(a) and 1.9(b) show plots of the semi-width a and the maximum thickness $h_{\mathrm{m}n}$ as functions of the scaled inclination angle α/π for various values

of n for $\bar{Q} = 1$, respectively.

1.7 Flow of a Thin Slowly Varying Rivulet Down a Slowly Varying Substrate

The solution described in Section 1.6 for unidirectional flow of a thin uniform rivulet down a planar substrate, as sketched in Figure 1.8, also provides the leading-order solution for the *locally* unidirectional flow of a slowly varying rivulet down a *slowly varying* substrate, for example, the flow in the azimuthal direction from the top ($\alpha = 0$) to the bottom ($\alpha = \pi$) of a large horizontal cylinder of a rivulet with prescribed contact contact angle $\beta = \bar{\beta}$ (≥ 0) but *slowly varying* semi-width $a = a$. Note that α is now the *local slope* of the substrate, and rather than being constant it varies slowly in the downstream direction. Note also that "slowly varying" in this situation means that both the azimuthal aspect ratio, $\epsilon = \ell/R \ll \beta$, and the reduced Reynolds number, $Re^* \ll 1$, are sufficiently small, where R is the radius of the cylinder. In particular, both of these conditions are satisfied if the cylinder is sufficiently large.

We will consider two types of rivulet flow, one in which the contact angle has a prescribed value $\beta = \bar{\beta}$ (but the semi-width a is unknown and is to be determined as part of the solution), and one in which the semi-width has a prescribed (nonzero) value $a = \bar{a}$ (but the contact angle β is unknown and is to be determined as part of the solution). Specifically, in Subsections 1.7.1 and 1.7.2 we describe a rivulet with prescribed constant contact angle $\beta = \bar{\beta} = 0$ and $\beta = \bar{\beta} > 0$, respectively, but (unknown) slowly varying semi-width $a = a(\alpha)$. In Subsection 1.7.3 we describe a rivulet with prescribed constant semi-width $a = \bar{a}$ but (unknown) slowly varying contact angle $\beta = \beta(\alpha)$.

The key results of Duffy and Moffatt [31], Wilson and Duffy [131] and Paterson *et al.* [97] are relevant to the work in Chapters 2–4 on rivulet flow of

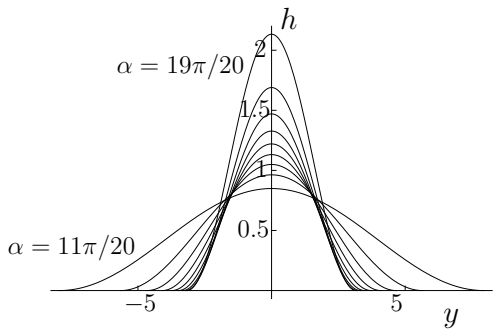

Figure 1.10: Plot of the cross-sectional free surface profile $z = h(y)$ given by (1.89) and (1.91) at $\alpha = 11\pi/20, 12\pi/20, \ldots, 19\pi/20$ on the lower half of cylinder for $n = 1$, all when $\bar{Q} = 1$, for a rivulet of perfectly wetting fluid.

non-Newtonian fluid.

1.7.1 A Rivulet of a Perfectly Wetting Fluid with Constant Contact Angle ($\bar{\beta} = 0$)

Unlike in flow down an inclined substrate, in flow down a slowly varying substrate only the case $n = 1$ in (1.89) and (1.90) is realisable, because it is impossible for $n \geq 2$ identical (but slowly varying) rivulets to be contiguous for all α.

Wilson and Duffy [131] used the solution (1.89) and (1.90) with $n = 1$ to describe flow of a slowly varying rivulet with zero contact angle $\beta = \bar{\beta} = 0$ (*i.e.* a perfectly wetting fluid), the solution for h, a and h_m then varying slowly with α.

Applying the condition of prescribed volume flux, $Q = \bar{Q}$, with Q given by $Q = (5\pi \sin\alpha h_\mathrm{m}^3)/24m$, yields an explicit solution for the maximum thickness $h_\mathrm{m} = h_\mathrm{m1}$ given by

$$h_\mathrm{m1} = 2\left(\frac{3\bar{Q}m}{5\pi \sin\alpha}\right)^{1/3}. \tag{1.91}$$

Figure 1.10 shows a plot of the cross-sectional free surface profile h as a function of y given by (1.89) and (1.91) at various values of α on the lower half of the cylinder, for $\bar{Q} = 1$ and $n = 1$.

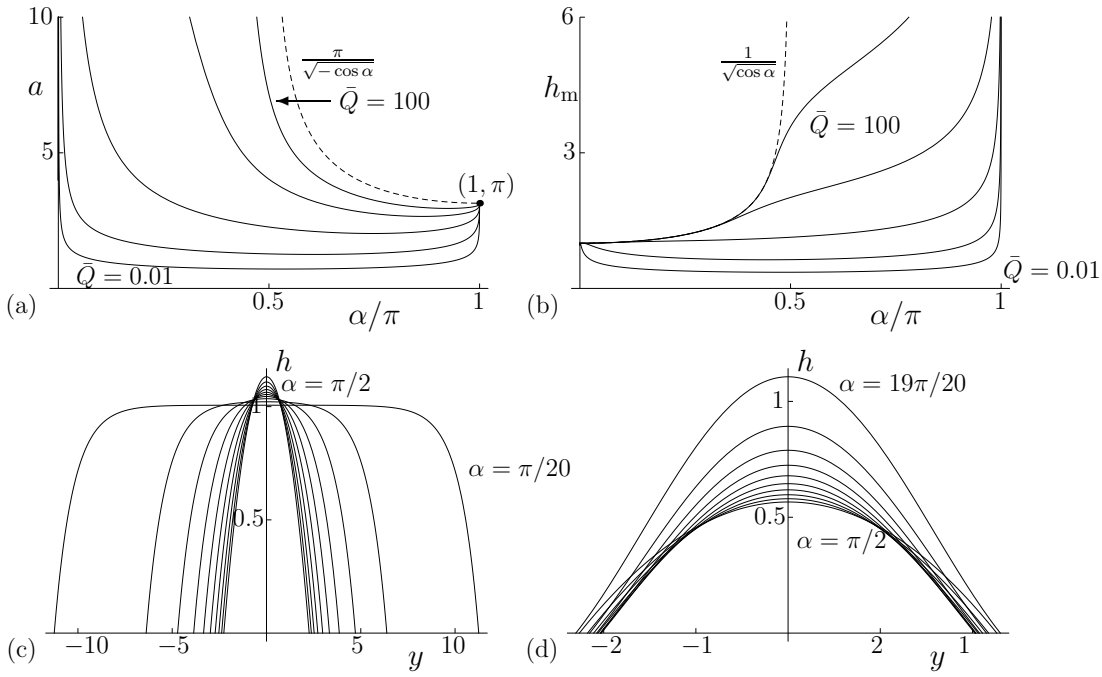

Figure 1.11: Plots of (a) the semi-width a, (b) the maximum thickness $h_{\rm m}$ as functions of α/π for $\bar{Q} = 0.01$, 0.1, 1, 10, 100, the cross-sectional free surface profile $z = h(y)$ at (c) $\alpha = \pi/20$, $\pi/10, \ldots, \pi/2$ on the upper half of cylinder, and (d) $\alpha = \pi/2$, $11\pi/20, \ldots, 19\pi/20$ on the lower half of the cylinder when $\bar{Q} = 1$, for a rivulet of non-perfectly wetting fluid.

1.7.2 A Rivulet of Non-Perfectly Wetting Fluid with Constant Contact Angle ($\bar{\beta} > 0$)

Duffy and Moffatt [31] used the solution (1.85)–(1.88) to describe flow of a slowly varying rivulet with non-zero contact angle $\beta = \bar{\beta} > 0$ (*i.e.* non-perfectly wetting fluid) down a slowly varying substrate. The solution (1.85) reveals that, unlike in the case $\bar{\beta} = 0$ described above, solutions exist for both sessile and pendent rivulets. However, applying the condition of prescribed volume flux, $Q = \bar{Q}$ with Q given by (1.87), yields a transcendental algebraic equation for the semi-width a which can, in general, be solved only numerically or asymptotically.

Figures 1.11(a) and 1.11(b) show plots of the semi-width a and the maximum thickness $h_{\rm m}$ as functions of the scaled inclination angle α/π for various values of $\bar{Q}$, respectively. Figures 1.11(c) and 1.11(d) show plots of the cross-sectional free surface profile h as a function of y at various values of α on the top half of the cylinder and the bottom half of the cylinder, respectively, for $\bar{Q} = 1$, illustrating

that near the top $\alpha = 0$ of the cylinder the rivulet becomes wide with finite thickness, while it becomes infinitely deep and of finite width near the bottom $\alpha = \pi$ of the cylinder.

1.7.3 A Rivulet with Constant Semi-width $a = \bar{a} > 0$

Paterson *et al.* [97] used the solution (1.85)–(1.88) together with the corresponding solution for a rivulet of a perfectly wetting fluid to describe flow of a slowly varying rivulet with prescribed constant semi-width $a = \bar{a}$ (≥ 0) (*i.e.* pinned contact lines) but slowly varying contact angle down a slowly varying substrate. In particular, setting $Q = \bar{Q}$ and $a = \bar{a}$ in (1.87) yields an *explicit* solution for β, namely

$$\beta = \left(\frac{9\bar{Q}m^4}{f(m\bar{a})\sin\alpha} \right)^{1/3}, \tag{1.92}$$

and h is then given explicitly by (1.85). Note that β (and hence the rivulet) does not have top-to-bottom symmetry. The global behaviour of the rivulet in this case is qualitatively different from that of a rivulet with prescribed constant contact angle described in Subsections 1.7.1 and 1.7.2. A rivulet can have constant semi-width all the way around the cylinder only if the rivulet is sufficiently narrow (specifically only if $\bar{a} \leq \pi$), but for a wider rivulet (specifically for $\bar{a} > \pi$) there is a critical value of α on the lower half of the cylinder, denoted by α_{depin} ($\pi/2 < \alpha_{\text{depin}} < \pi$) and given by solving $m\bar{a} = \pi$ to obtain

$$\alpha_{\text{depin}} = \cos^{-1}\left(-\frac{\pi^2}{\bar{a}^2}\right) \quad \text{for} \quad \bar{a} > \pi, \tag{1.93}$$

at which the contact angle is equal to zero, $\beta = 0$, and beyond which there is no physically realisable solution with constant width $a = \bar{a}$. Note that α_{depin} is a monotonically decreasing function of $\bar{a}$ satisfying $\alpha_{\text{depin}} = \pi + O((\bar{a}-\pi)^{1/2}) \to \pi^-$ as $\bar{a} \to \pi^+$ and $\alpha_{\text{depin}} = \pi/2 + O(\bar{a}^{-2}) \to \pi/2^+$ as $\bar{a} \to \infty$. Paterson *et al.* [97] assumed that the contact lines de-pin at $\alpha = \alpha_{\text{depin}}$ and that thereafter the rivulet

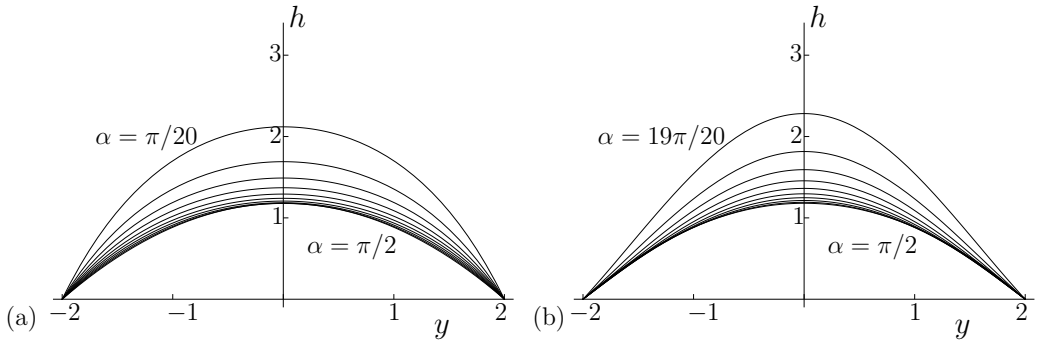

Figure 1.12: Plots of the cross-sectional free surface profile $z = h(y)$ at (a) $\alpha = \pi/20, \pi/10, \ldots, \pi/2$ on the upper half of cylinder, and (b) $\alpha = \pi/2, 11\pi/20, \ldots, 19\pi/20$ on the lower half of the cylinder when $\bar{Q} = 1$, for a narrow rivulet of non-perfectly wetting fluid with prescribed constant semi-width $\bar{a} = 2$ $(< \pi)$

drains from $\alpha = \alpha_{\text{depin}}$ to the bottom of the cylinder with zero contact angle $\beta = 0$ and slowly varying semi-width a. This behaviour is a special case of the more general scenario in which a rivulet with prescribed constant width de-pins and possibly re-pins at a prescribed non-zero value of the contact angle.

1.7.3.1 A Narrow Rivulet with $\bar{a} \leq \pi$

A narrow rivulet with $\bar{a} \leq \pi$ can flow all the way from the top to the bottom of the cylinder. Figure 1.12 shows plots of h given by (1.85) for a narrow rivulet with prescribed constant semi-width $\bar{a} = 2$ $(< \pi)$ as a function of y at various values of α on the top of the cylinder and the bottom of the cylinder, respectively.

1.7.3.2 A Wide Rivulet with $\bar{a} > \pi$

A wide rivulet with $\bar{a} > \pi$ can flow all the way from the top to the bottom of the cylinder only by flowing from $\alpha = \alpha_{\text{depin}}$ $(\pi/2 < \alpha_{\text{depin}} < \pi)$, where α_{depin} is given by (1.93), to the bottom of the cylinder with de-pinned contact lines and zero contact angle according to the solution for a rivulet of a perfectly wetting fluid given by (1.89) with $n = 1$. Figures 1.13 (a) and (b) show plots of the contact angle β and the maximum thickness h_{m} as functions of α/π for a range of values of $\bar{a}/\pi$. Figures 1.13(c) and 1.13(d) show plots of h given by (1.89)

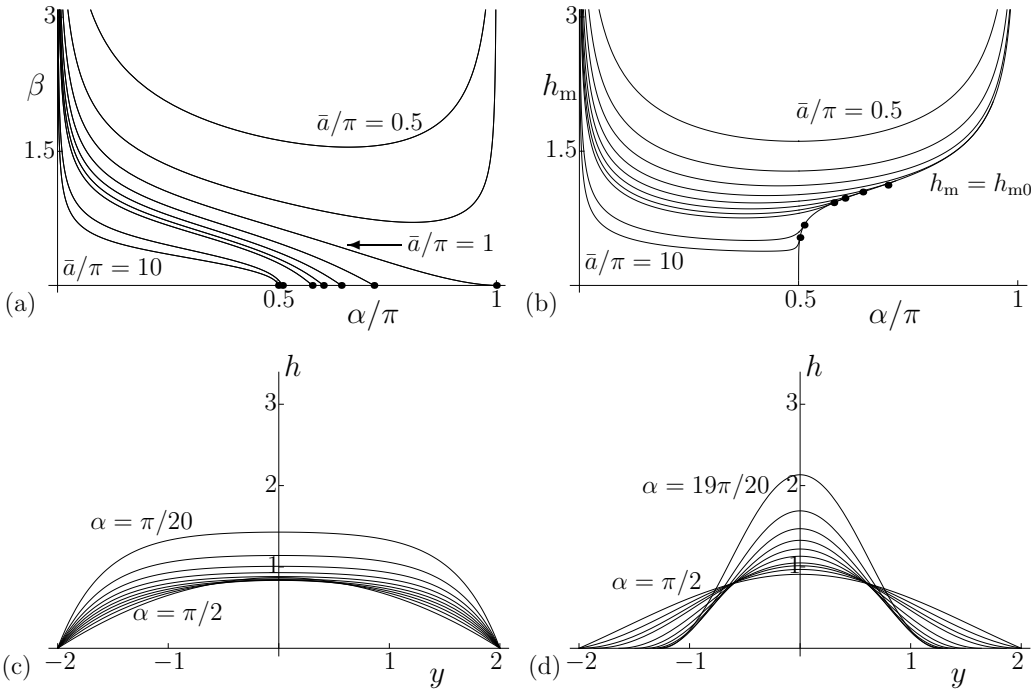

Figure 1.13: Plots of (a) the contact angle β given by (1.92), (b) the maximum thickness $h_{\rm m}$ as functions of α/π for $\bar{a}/\pi = 0.5$, 0.75, 1, 1.25, 1.5, 2, 5, 10 when $\bar{Q} = 1$, the cross-sectional free surface profile $z = h(y)$ at (c) $\alpha = \pi/20, \pi/10, \ldots, \pi/2$ on the upper half of cylinder, and (d) $\alpha = \pi/2, 11\pi/20, \ldots, 19\pi/20$ on the lower half of the cylinder for a wide rivulet $\bar{a} = 5$ whose contact lines de-pin at zero contact angle $\beta = \bar{\beta} = 0$. In part (c), the corresponding solutions for a rivulet with zero contact angle $\beta = 0$ given by (1.89) with $n = 1$ and (1.91) are also included. De-pinning occurs at $\alpha = \alpha_{\rm depin}$ for $\bar{a} > \pi$, and the points at which this happens are denoted by dots.

with $n = 1$ and (1.85) for a wide rivulet with prescribed constant semi-width $\bar{a} = 5$ ($> \pi$) as a function of y at various stations around the cylinder, including $\alpha = \alpha_{\rm depin} \simeq 1.9766$, illustrating that the rivulet becomes thick with zero contact angle and finite semi-width π near the bottom of the cylinder.

1.8 Unidirectional Flow of a Thin Rivulet of Non-Perfectly Wetting Fluid on a Vertical Substrate Subject to a Uniform Longitudinal Surface Shear Stress

In this Section we summarise some of the key results of Wilson and Duffy [132] who considered the flow of a thin rivulet of non-perfectly wetting fluid with constant non-zero contact angle on a vertical substrate subject to a uniform longitudinal surface shear stress τ, relevant to the work in Chapter 6 on advection and Taylor–Aris dispersion of a passive solute in such a rivulet.

The flow is governed by (1.75)–(1.77) with $\alpha = \pi/2$ and $\epsilon \ll \delta$, subject to the no-slip condition at the substrate (1.78) and the normal stress balance $(1.79)_1$. We consider the situation when $\beta > 0$ is prescribed, and we set $\delta = \beta$. We nondimensionalise and scale τ with $\beta\rho g\ell$, so that the tangential stress balance is now given by

$$u_z = \tau \quad \text{on} \quad z = h. \tag{1.94}$$

Also the contact-line conditions are again given by (1.80) with $\beta = 1$. As in Section 1.6, at leading order in ϵ and δ we obtain

$$p = \frac{1}{a}, \quad u = \frac{2hz - z^2}{2} + \tau z, \quad h = h_{\rm m}\left(1 - \frac{y^2}{a^2}\right), \tag{1.95}$$

$$Q = \frac{32ah_{\rm m}^3}{105} + \frac{8\tau a h_{\rm m}^2}{15}, \quad h_{\rm m} = \frac{a}{2}. \tag{1.96}$$

Figure 1.14 shows a sketch of Q given in (1.95) as a function of a for various values of τ. The flux Q (which may be positive or negative depending on the relative strengths of the effects of gravity and shear-stress) is, for $\tau \geq 0$, a monotonically increasing function of a, but for $\tau < 0$, Q decreases to a minimum value $Q = Q_{\rm min}$ at $a = a_{\rm min}$, where

$$Q_{\rm min} = -\frac{3087\tau^4}{5120} < 0 \quad \text{and } a_{\rm min} = -\frac{21\tau}{8} < 0, \tag{1.97}$$

and then increases monotonically, taking the value $Q = 0$ at $a = a_0 = -7\tau/2$. Wilson and Duffy [132] analysed and categorised all of the possible cross-sectional flow patterns into five types which we denote as type I to type V. We denote the minimum and maximum fluid velocities over the rivulet by $u_{\rm min}$ and $u_{\rm max}$, respectively, which satisfy $u_{\rm min} \leq 0$ and $u_{\rm max} \geq 0$. Wilson and Duffy [132] showed that when $\tau \geq 0$ (*i.e.* when the prescribed shear stress acts in the same direction as gravity) the velocity is downwards throughout the rivulet (*i.e.* $u \geq 0$), and the maximum velocity $u_{\rm max} = a(a + 4\tau)/8$ occurs at the apex of the rivulet at $y = 0$ and $z = h_{\rm m}$ (type I), but when $\tau < 0$ (*i.e.* when the prescribed shear stress opposes gravity) the velocity is upwards near the edges of the rivulet (*i.e.* $u < 0$), but it can be downwards elsewhere. In the latter case, when $a \leq -2\tau$ the velocity is upwards throughout the rivulet, and the minimum velocity $u_{\rm min} = a(a+4\tau)/8$ occurs at the apex (type V), but when $a > -2\tau$ there is a region of downwards flow in the centre of the rivulet, and the maximum velocity $u_{\rm max} = (a+2\tau)^2/8$ occurs within the rivulet at $y = 0$, $z = h_{\rm m} + \tau$ and the minimum velocity $u_{\rm min} = \tau^2/2$ occurs on the free surface at $y = \pm a(1+2\tau/a)^{1/2}$, $z = -\tau$ (type II when $a > -4\tau$, type III when $a = -4\tau$, and type IV when $-2\tau < a < -4\tau$).

When $\bar{Q} > 0$ there is a single rivulet solution in which a is a monotonically decreasing function of τ, but when $\bar{Q} < 0$ there are two rivulet solutions (in the

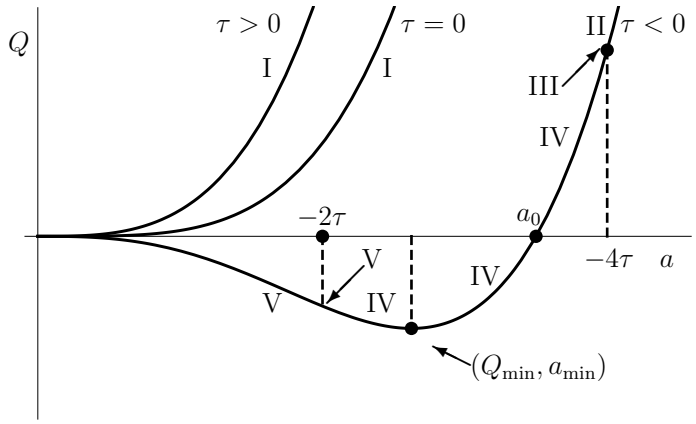

Figure 1.14: Sketch of the flux Q as a function of the semi-width a in gravity- and shear-stress-driven flow in a thin rivulet on a vertical substrate showing when the five different types of flow pattern occur in each of the cases $\tau > 0$, $= 0$, and < 0.

narrower one of which is a monotonically increasing function of τ satisfying $0 < a < a_{\min}$ and in the wider one of which a is a monotonically decreasing function of τ satisfying $a_{\min} < a < a_0$) when $\tau < \tau_{\max}$, where $\tau_{\max} = -(-5120\bar{Q}/3087)^{1/4}$, one solution in which $a = a_{\min}$ when $\tau = \tau_{\max}$, and no rivulet solution when $\tau_{\max} < \tau < 0$.

1.9 Non-uniform Rivulet Flow Down an Inclined Planar Substrate

Situations involving non-uniform rivulets have also been considered. In this Section we summarise the main results of Smith [114] and Duffy and Moffatt [32], both of whom considered gravity-driven flow of a non-uniform rivulet on an inclined planar substrate.

The steady gravity-driven flow of a slender non-uniform rivulet flowing either from a point source or to a point sink of a prescribed flux, $Q = \bar{Q}$, down an inclined planar substrate was studied by Smith [114] and Duffy and Moffatt [32] in the cases of weak and strong surface-tension effects, respectively. Smith [114] neglected the surface-tension contribution in comparison with the lateral spreading due to gravity (*i.e.* $\rho g \cos\alpha$). Thus he had $|\rho g h \cos\alpha| \gg |\gamma h_{yy}|$, that

is, $\rho g H|\cos\alpha| \gg \gamma H/(\epsilon L)^2$, leading to $C_{\rm a}^{-1} \ll |\cos\alpha|$ (*i.e.* the effect of surface tension in this case weak). Therefore, at leading order the kinematic condition (1.69) with (1.73) yields the governing partial differential equation for the free surface profile h, namely

$$\cos\alpha \left(h^3 h_y\right)_y - \sin\alpha \left(h^3\right)_x = 0, \tag{1.98}$$

which is to be integrated subject to $Q = \bar{Q}$ and the contact-line conditions (1.79). Hence Smith [114] obtained the similarity solution

$$h = h_{\rm m}\left(1 - \frac{y^2}{a^2}\right), \quad a = (cx)^{3/7}, \tag{1.99}$$

where $h_{\rm m}$ and the constant c are given by

$$h_{\rm m} = \frac{3c\tan\alpha}{14(cx)^{1/7}}, \quad c = \frac{7\cot\alpha}{3}\left(\frac{105\bar{Q}}{4\sin\alpha}\right)^{1/3}. \tag{1.100}$$

This (unique) similarity solution predicts that the rivulet has a transverse profile (1.99) with a single global maximum $h = h_{\rm m}$ at $y = 0$, and that its width increases or decreases according to $x^{3/7}$ and its height correspondingly decreases or increases according to $x^{-1/7}$. The solutions (1.99) may be interpreted for both sessile rivulets and pendent rivulets; specifically, solutions for $\cos\alpha > 0$ (so that $c > 0$) represent widening and shallowing sessile rivulets in $x > 0$ and solutions for $\cos\alpha < 0$ (so that $c < 0$) represent narrowing and deepening pendent rivulets in $x < 0$.

Duffy and Moffatt [32] used Smith's [114] work to include the effect of surface tension, in situations in which $\rho g\cos\alpha$ is much less than surface tension. Hence, they had $|\rho g h\cos\alpha| \ll |\gamma h_{yy}|$, that is, $\rho g H|\cos\alpha| \ll \gamma H/(\epsilon L)^2$, leading to $C_{\rm a}^{-1} \gg |\cos\alpha|$ (*i.e.* the effect of surface tension in this case is strong). Therefore, at leading order the kinematic condition (1.69) with (1.73) yields the partial

differential equation for the free surface profile h, namely

$$(h^3 h_{yyy})_y + \sin\alpha (h^3)_x = 0, \tag{1.101}$$

which is to be integrated subject to $Q = \bar{Q}$ and the contact-line condition (1.79). Duffy and Moffatt [32] obtained a one-parameter family of similarity solutions parametrised by a constant parameter $G_0 \geq 0$ in which the free surface profile is given by

$$h = h_{\rm m}\left(1 - \frac{y^2}{a^2}\right)\left(G_0 - \frac{Sy^2}{24a^2}\right), \quad a = (cx)^{3/13}, \tag{1.102}$$

where $h_{\rm m}$ and the constant c are given by

$$h_{\rm m} = \frac{3c\sin\alpha}{13(cx)^{1/13}}, \quad c = \frac{13}{3\sin\alpha}\left(\frac{3\bar{Q}}{I\sin\alpha}\right)^{1/3}, \tag{1.103}$$

where $S = \mathrm{sgn}(c)$ and the function $I = I(G_0)$ is defined by

$$I = \int_{-1}^{1}\left[(1-\eta^2)\left(G_0 - \frac{S\eta^2}{24}\right)\right]^3 \mathrm{d}\eta = \frac{32}{35}G_0^3 - \frac{4S}{315}G_0^2 + \frac{1}{6930}G_0 - \frac{S}{1297296}. \tag{1.104}$$

Physically realisable similarity solutions are obtained only for $G_0 \geq 1/24$ when $S = 1$, in which case the rivulet has a transverse profile (1.102) with a single global maximum $h = h_{\rm m}$ at $y = 0$. In contrast, such solutions are obtained for all values $G_0 \geq 0$ when $S = -1$, in which case the rivulet has a transverse profile (1.102) with a single global maximum $h = h_{\rm m}$ at $y = 0$ for $G_0 \geq 1/24$ but two equal global maxima $h/h_{\rm m} = (1 + 24G_0)^2/96$ at $y/a = \pm((1 - 24G_0)/2)^{1/2}$ and a local minimum $h = h_{\rm m}$ at $y = 0$ for $0 \leq G_0 < 1/24$.

Therefore, the similarity solutions (1.102) predict that the width of the rivulet increases or decreases according to $x^{3/13}$ and the height of the rivulet correspondingly decreases or increases according to $x^{-1/13}$. Solutions for $S = 1$ (so that $c > 0$) represent widening and shallowing rivulets in $x > 0$, and solutions for $S = -1$ (so that $c < 0$) represent narrowing and deepening rivulets in $x < 0$.

1.10 Review of Previous Literature on Rivulet Flow

In addition to the studies discussed in detail in Sections 1.5–1.9 there has been considerable work on the flow of rivulets. In this Section we discuss other relevant previous work on rivulet flow of Newtonian and non-Newtonian fluids, and, more generally, thin-film flows of non-Newtonian fluids.

1.10.1 Gravity-Driven Rivulet Flow

At the beginning of Section 1.5 we discussed some of the early work on steady unidirectional flow of a rivulet of a Newtonian fluid down an inclined substrate by Towell and Rothfeld [124], Allen and Biggin [8], Bentwich *et al.* [16] and Duffy and Moffatt [31].

The work by Duffy and Moffatt [31] has been extended by Wilson and Duffy [129] to consider the rivulet draining down a locally non-planar substrate and a slowly varying substrate for a variety of convex and concave transverse substrate profiles. In particular, they found that a rivulet can run continuously from the top to the bottom of a large horizontal cylinder only if the transverse profile of the substrate is a sufficiently shallow trough; if the profile is a deeper trough then a rivulet is not possible near the bottom of the cylinder while if the profile is a ridge then a rivulet is not possible near the top of the cylinder. Eres *et al.* [38] carried out numerical simulations of a thin film driven by gravity and/or surface shear-stress that is perturbed at its leading edge such that rivulets form, in the cases of a perfectly wetting and a non-perfectly wetting fluid. In the former case and the case of small non-zero contact angles, the rivulets are wedge-shaped, for larger contact angles the rivulets have constant width, and for contact angles that are larger still the rivulets split into distinct droplets, as shown in Figure 1.15. Holland *et al.* [57] considered a rivulet that is uniformly hotter or

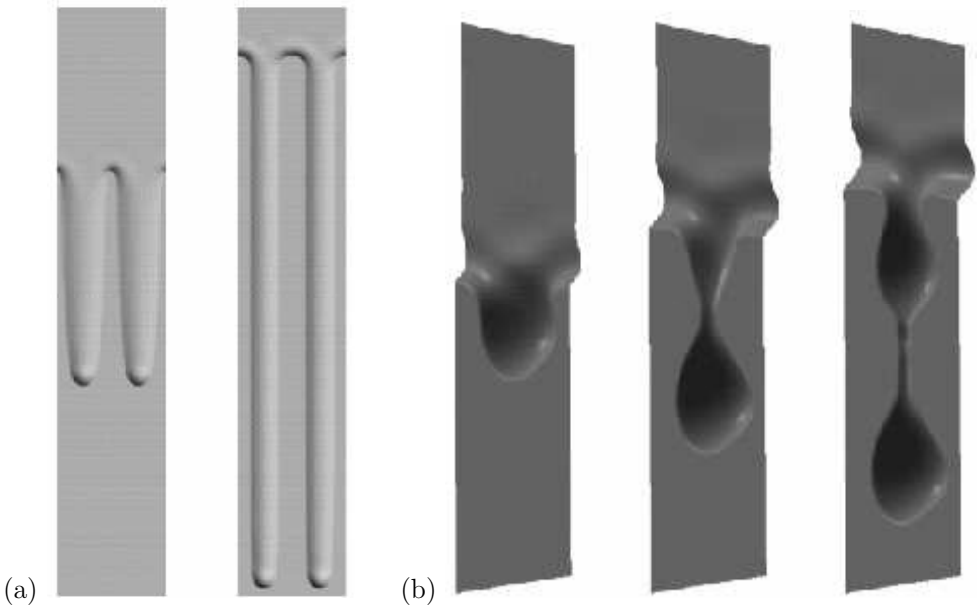

Figure 1.15: Numerical simulations of (a) a gravity-driven thin film draining down a vertical substrate that breaks into steadily translating pattern of wedge-shaped rivulets (on the left) and continuously growing constant-width rivulets (on the right), and (b) a shear-stress-driven thin film draining down a vertical substrate that breaks into distinct droplets, computed by Eres *et al.* [38]. In part (a), the contact angle increases from left to right. In part (b), time increases from left to right. Reprinted with permission from Eres *et al.* [38], copyright 2000, American Institute of Physics.

uniformly colder than the surrounding atmosphere, and for which the surface tension of the fluid varies linearly with temperature (*i.e.* thermocapillary force); they found that the variation in surface tension drives a transverse flow that leads to the fluid particles spiralling down the rivulet in helical vortices. Wilson and Duffy [130] studied the effects of thermoviscosity on a rivulet draining down a heated or cooled slowly varying substrate for three different viscosity models, namely a linear, an exponential and an Eyring model, and found that when the atmosphere is strongly cooled the rivulet becomes wide and deep, whereas when the atmosphere is strongly heated it becomes narrow and shallow. Duffy and Wilson [33] extended the work by Wilson and Duffy [130] to the case of a rivulet of perfectly wetting fluid. Other studies of a rivulet of perfectly wetting fluid include those by Kuibin [68] and by Alekseenko *et al.* [6], who considered the draining of a pendent rivulet down the underside of an inclined cylinder. In particular, Kuibin [68] obtained the leading-order asymptotic solution for a thin

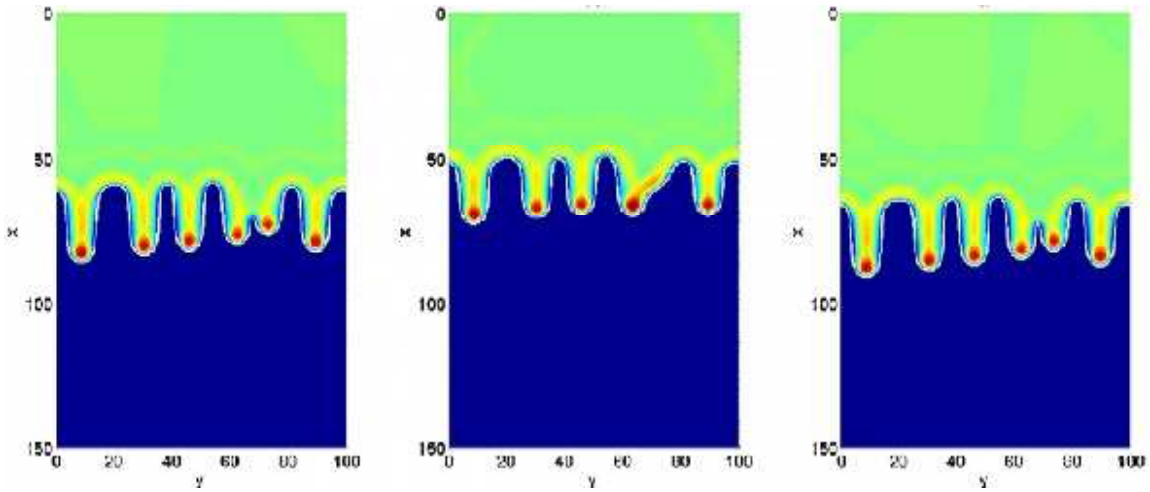

Figure 1.16: Numerical simulations of a gravity-driven thin film over a planar substrate that breaks into rivulets, computed by Slade *et al.* [113] for various value of the surface-tension gradient, namely zero on the left, -0.25 in the centre and 0.25 on the right. Reprinted with permission from Slade *et al.* [113], copyright, 2013, Elsevier.

and narrow rivulet in the limit of small contact angle on the underside of an inclined locally parabolic substrate. Schwartz [111] studied the fingering (*i.e.* rivulets) phenomenon in gravitational flow within the lubrication approximation and obtained time-dependent numerical solutions. Slade *et al.* [113] also captured fingering at the contact line of a thin film on an inclined planar substrate driven by gravity, as shown in Figure 1.16, and examined the effect of Marangoni stresses and surface topography on the formation of the rivulets. Evans *et al.* [41] obtained numerical solutions to the three-dimensional model for fluid flow on the outside of a rotating horizontal cylinder (*i.e.* coating flow) derived by Evans *et al.* [40], which included the effects of rotation, gravity, surface tension and axial variation, and reproduced features observed in their own experiments, namely the rivulets and rings of fluid as the speed of rotation increases. Leslie *et al.* [71] considered the steady flow of a thin ring of fluid with constant non-zero contact angle draining on the inside or outside of a rotating horizontal cylinder, and found that there is a maximum mass of fluid that can be supported against gravity for a given rotation speed or, equivalently, there is a minimum rotation speed required to support a given mass of fluid. In particular, at the critical mass (or rotation speed) the free

surface of the rivulet exhibits a corner on the lower half of the cylinder on the side that is rising with the rotation.

Studies of the steady unidirectional flow of a uniform non-thin rivulet of Newtonian fluid have been performed by Perazzo and Gratton [100], who derived the exact solutions of the Navier–Stokes equation for a sessile rivulet draining down an inclined planar substrate. In particular, Perazzo and Gratton [100] derived the exact solution for the velocity within a semi-circular rivulet by solving the appropriate Poisson equation in the domain defined by the cross-section of the rivulet. Their work was extended by Tanasijczuk *et al.* [119] to consider both sessile and pendent rivulets draining down an inclined planar substrate.

1.10.2 Experiments on Rivulets

Experimental work on the development of rivulets from a film of fluid has been carried out by many authors. For example, Johnson *et al.* [63] conducted an experiment that showed a film of fluid of constant volume flux breaking into a series of rivulets at the leading edge, the exact shape of these rivulets being found to depend on the inclination of the substrate to the horizontal. Zhang *et al.* [142] observed three flow patterns, namely complete film flow, the formation of dry patches, and the formation of rivulets, while studying fluid draining in a falling film microreactor. Howell *et al.* [58] theoretically and experimentally considered steady gravity-driven flow of a thin rivulet draining down a flexible beam, as shown in Figure 1.17, and found that the weight of the fluid causes the deflection of the beam to increase, which in turn, enhances the spreading of the rivulet.

1.10.3 Stability of Rivulet Flow

There is a considerable body of work, for example, by Schmuki and Laso [110], Young and Davis [140], Nakagwa [92], Nakagwa and Scott [93], Benilov [15], Diez *et al.* [29, 30], Wilson and Duffy [132], Wilson *et al.* [136], Herrada *et al.* [55],

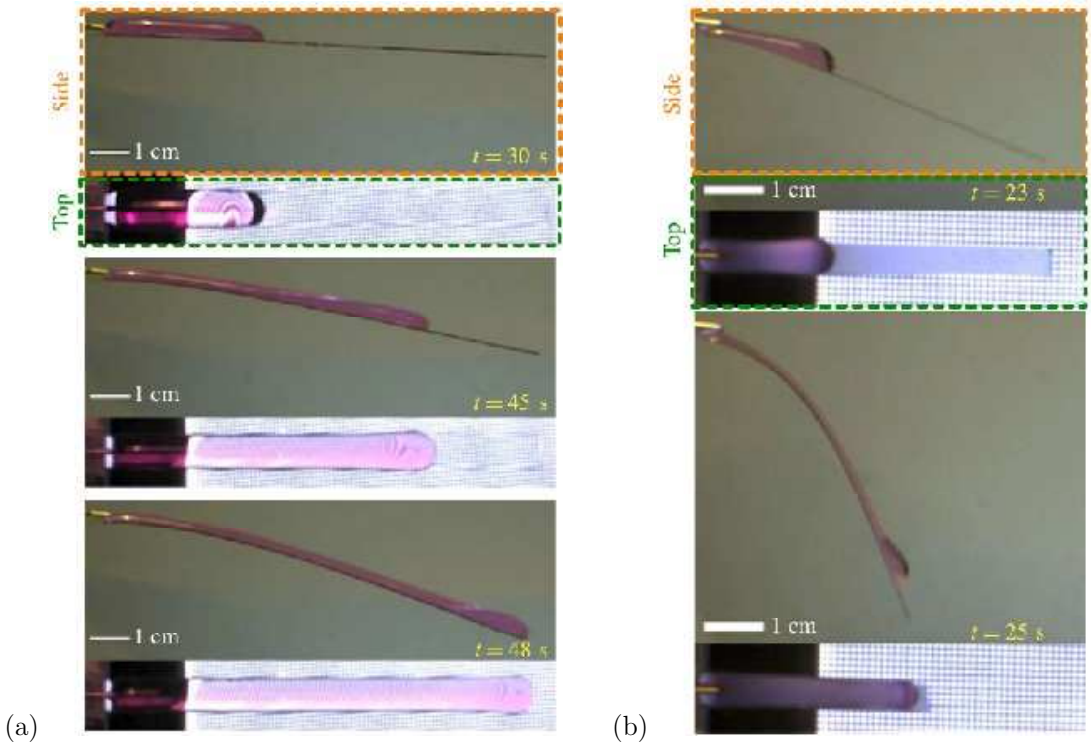

Figure 1.17: Images of the flow of a thin rivulet draining down a flexible beam, obtained by Howell *et al.* [58]. The deflection of the beam increases from the lowest value in (a) to the largest value in (b). Reprinted with permission from Howell *et al.* [58], copyright 2016, Cambridge University Press.

Mikielewicz and Moszynski [81], and El-Genk and Saber [37], using a variety of methods to obtain considerable insight into the study of stability of rivulet flow. In particular, there are a variety of situations in which continuous films are unstable and break up, and could split up into a series of rivulets. In particular, there are several types of flow regime involving rivulets draining down an inclined substrate. In their experiments, Schmuki and Laso [110] studied the effects of the inclination angle of the substrate, the flow rate, surface tension, the substrate material and the fluid viscosity on flow of fluid draining down an inclined substrate. In particular, they observed five distinct flow regimes depending on the flow rate: first, a regime of continuous film flow; second, a regime of droplet flow; third, a regime of steady flow of a thin uniform rivulet; fourth, a regime of a continuous flow of a steady meandering rivulet; and fifth, a regime of unsteady flow of an oscillating rivulet, as shown in Figure 1.18. In particular, Schmuki

Figure 1.18: Images of the five regimes of gravity-driven rivulet flow obtained by Schmuki and Laso [110], namely (from left to right) droplet flow, a uniform rivulet, film flow, a meandering rivulet and an oscillating rivulet. Reprinted from Schmuki and Laso [110] with permission from Cambridge University Press.

and Laso [110] compared the energies of the different configurations and obtained predictions as to when the transitions from a uniform rivulet to a meandering rivulet and from a meandering rivulet to multiple rivulets occur. Young and Davis [140] studied the stability of a rivulet draining down a vertical substrate in three different cases, namely fixed contact lines, fixed contact angles and contact angles that are smooth functions of the speed of the moving contact line. In their experiments, restricted to a single type of fluid on a single substrate, Nakagawa and Scott [93] and Nakagawa [92] investigated the gravity-driven flow of a rivulet, and found four regimes of flow depending on the flow rate, namely droplet flow, a stable meandering rivulet, an oscillating rivulet and also a braided rivulet, the latter regime being associated with a periodic increase and decrease of the width of the rivulet. In their experiments, Mertens *et al.* [79] observed a braided regime of rivulet flow with a constant flow rate draining down an inclined substrate, and suggested that braiding could be a result of the interaction between surface tension tending to decrease the width of the rivulet and inertia tending to increase it. Birnir *et al.* [18] derived a model for a regime of meandering rivulet flow and found that this meandering is triggered by a small disturbance in the flow rate. Le Grand-Piteira *et al.* [50] found experimentally that the meandering regime of rivulet flow is possible only if the flow rate is below a critical value and that this

value increases with the fluid viscosity. Daerr *et al.* [25] subsequently suggested that the most important factor in meandering behaviour is fluid inertia.

The break-up of a film on a substrate has been investigated by several authors. Mikielewicz and Moszynski [81] analysed the critical condition for the break-up of a film of uniform thickness draining under gravity down a vertical substrate into a periodic array of identical rivulets. Specifically, by equating the energies of the two states and minimising the energy of the rivulet state per unit width of the film, they specified the critical thickness above which it is energetically favourable for the film to remain as a film but below which it is energetically favourable for it to break up into rivulets. El-Genk and Saber [37] used numerically calculated solutions for the velocity of a rivulet to investigate the break-up of a film on a vertical substrate by using a minimum total energy argument, and the validity of their calculations was demonstrated by comparison with experimental results, while Kabov [65] provided an overview of studies on the heat transfer to a thin film falling down a heated substrate, and its breakup into rivulets.

Benilov [15] considered the stability of the gravity-driven flow of a thin sessile or pendent rivulet with constant width on an inclined substrate, and found that the former is always stable whereas the stability of the latter depends on the width of the rivulet and the angle of the inclination of the substrate. Diez *et al.* [29, 30] considered the stability of a "static rivulet" (*i.e.* a ridge of fluid) on an inclined substrate, both on a macroscopic scale where gravitational effects are dominant and on a microscopic scale where van der Waals forces are dominant, and discussed the evolution of static rivulets of finite length. Myers *et al.* [89] investigated the flow of a rivulet on an inclined substrate subject to gravity and a uniform longitudinal surface shear stress, and solved the problem analytically and numerically for a thin rivulet. In particular, they used an energy-minimisation argument to calculate when it is energetically favourable for the rivulet to split into two subrivulets, and hypothesised that a purely gravity-driven rivulet may

split into two subrivulets whereas a purely shear-driven rivulet will never split. Wilson and Duffy [133, 132] reconsidered the splitting of both a perfectly wetting rivulet on an inclined substrate and a non-perfectly wetting rivulet on a vertical substrate subject to a longitudinal shear stress. In particular, Wilson and Duffy [132] showed that a purely shear-driven rivulet may split into two subrivulets (*i.e.* that the conjecture of Myers *et al.* [89] is false), while Wilson *et al.* [136] showed that in the purely gravity-driven case, there is a minimum thickness below which it is energetically favourable for a film to break up into rivulets, and there is a maximum thickness above which it is energetically favourable for a single rivulet to break up.

1.10.4 Rivulets in the Presence of an External Airflow

Rivulets of fluid subject to significant surface-shear-stress forces are of importance in many industrial contexts such as distillation, coating processes and heat exchangers. Accordingly, such flows have received considerable attention from a variety of authors. Saber and El-Genk [108] studied the effect of an external airflow on a film on an inclined or a vertical substrate subject to gravity and a non-uniform shear stress on its free surface, and predicted the minimum thickness of the film before break-up occurs. They found that if the shear stress is directed down the substrate then increasing its strength decreases the minimum thickness, whereas if the shear stress is directed up the substrate (while the flow remains downwards everywhere) then increasing its strength increases the minimum thickness. Mikielewicz and Moszynski [82] used a conformal mapping technique to obtain the exact solution for the velocity of a rivulet when the flow is driven purely by gravity and purely by a prescribed uniform longitudinal surface shear stress on its free surface. Wilson *et al.* [134] obtained similarity solutions for a rivulet of power-law fluid draining down an inclined substrate subject to a uniform longitudinal shear stress on its free surface in the cases of both weak and

strong surface tension. As summarised in Section 1.8, Wilson and Duffy [132] found that there are five possible flow patterns that the rivulet may take; the same five flow patterns were found to be the only possibilities by Sullivan *et al.* [118] in the case of a pendent rivulet of perfectly wetting fluid on a slowly varying substrate subject to a uniform longitudinal shear stress. Sullivan *et al.* [117] considered both a gravity-driven rivulet on a vertical substrate and a rivulet on a horizontal substrate driven by a longitudinal shear stress, subject to a prescribed uniform transverse shear stress, and discussed the cases when both contact lines are pinned and when one or both contact lines de-pin. Paterson *et al.* [98] considered the possible scenario of pinning and subsequent de-pinning of a rivulet with constant contact angle and the possible de-pinning and subsequent re-pinning of a rivulet with constant width as they flow in the azimuthal direction from the top to the bottom of a large horizontal cylinder subject to a uniform transverse shear stress. In particular, they showed that in the presence of a surface shear stress there exists an infinitely wide two-dimensional film of uniform thickness that covers part of the upper half of the cylinder and breaks up to a single rivulet with constant contact angle.

1.10.5 Waves on Rivulets

There has also been considerable work on waves on rivulets by many authors. Young and Davis [140] found the appearance of kinematic-wave instabilities on a wide rivulet draining unidirectionally down a vertical substrate. The wave motion of rivulets was measured experimentally for the first time by Alekseenko *et al.* [7] for fluid draining down the bottom part of an inclined cylinder; they found that the natural wave (which appears because of a hydrodynamical instability of rivulet flow) and an excited wave (which appears because of an external forcing) have some similarities when their frequencies coincide. This study was extended by Alekseenko *et al.* [5] for a range of the physical parameters, including various

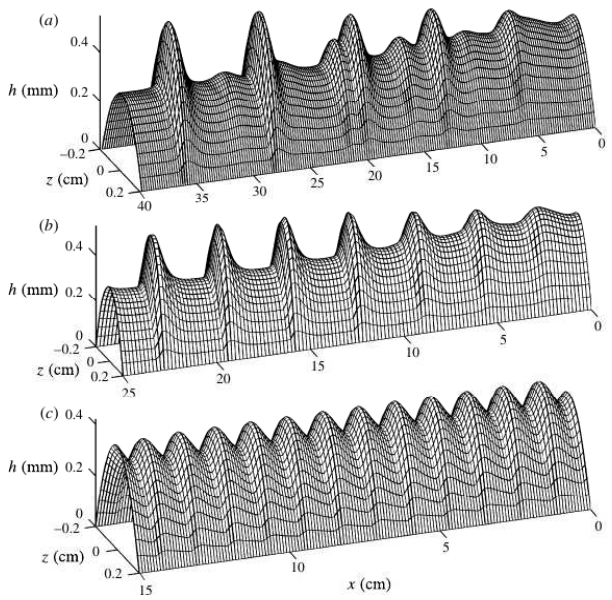

Figure 1.19: Numerical simulations of three-dimensional waves on the surface of the rivulet draining down a vertical substrate, computed by Alekseenko *et al.* [3]. The forcing frequency increases from lowest value in (a) to the largest value in (c). Reprinted from Alekseenko *et al.* [3] with permission from Cambridge University Press.

physical properties of the fluids. In particular, they found that the amplitude of the wave (which is defined by the difference between the maximum and minimum values of the rivulet thickness) decreases with increase of the excitation frequency for all the fluids. Alekseenko *et al.* [4] also studied the appearance of the three-dimensional surface wave on a rivulet draining down a vertical substrate, and showed that the structure of the wave depends strongly on the contact angle. Alekseenko *et al.* [3] carried out numerical simulations of surface waves on a rivulet draining down a vertical substrate, and obtained various characteristics of linear and nonlinear excited waves on the rivulet as functions of the forcing frequency for a variety of Reynolds numbers and contact angles, as shown in Figure 1.19. Alekseenko *et al.* [3] compared their calculations with the experimental results of Alekseenko *et al.* [4] for two different fluids, namely a 45% solution of ethanol in water (WES) and a 25% water–glycerine solution (WGS), and showed that their model predicts step-wise waves with low forcing frequencies on a rivulet of WGS and waves with no capillary ripple in front of the main peak on a rivulet of WES, both of which are consistent with the experimental results of Alekseenko *et al.*

[4].

1.10.6 Studies of Rivulet Flow of Non-Newtonian Fluids

As already pointed out, despite the widespread occurrence of non-Newtonian rheology in many of the practical occurrences of rivulet flow, there has been surprisingly little theoretical work on rivulet flow of non-Newtonian fluids. Rare exceptions include the work by Rosenblat [107] on rivulet flow of a viscoelastic fluid. Specifically Rosenblat [107] extended the work of Towell and Rothfeld [124] to investigate the flow of a uniform rivulet of a viscoelastic fluid draining down an inclined substrate, and found that one effect of the elasticity is to drive a transverse flow (absent in the Newtonian case) which causes the fluid particles to spiral down the rivulet in two counter-rotating helical vortices. Balmforth *et al.* [11] and Wilson *et al.* [135] investigated rivulet flow of a viscoplastic material. In particular, Wilson *et al.* [135] studied the flow both of a thin slowly varying rivulet of a biviscosity fluid and of a Bingham fluid down a cylindrical substrate, and found that near the top of the cylinder the flow of a rivulet of Bingham fluid comprises two regions with different viscosities; the flow consists of an infinitely wide rigid and stationary plug, while elsewhere it consists of two "levées" at the sides of the rivulet and a central region in which the flow near the free surface is a pseudoplug whose velocity does not vary normally to the substrate, separated from the fully plastic flow near the substrate by a pseudoyield surface which is the surface that separates the yielded and unyielded regions. Wilson *et al.* [134] considered steady flow of a non-uniform rivulet for a power-law fluid on an inclined substrate driven by either gravity or a prescribed shear stress at the free surface of the fluid for both weak and strong surface-tension effects. In general, they found that the solutions for a shear-stress-driven rivulet are qualitatively similar to those for a gravity-driven rivulet. In particular, for purely gravity-driven flow, they recovered the solutions of Wilson and Burgess [128], whereas for purely

shear-stress-driven flow, they found that the rivulet widens according to $x^{1/3}$ and thins according to $x^{1/6}$, where x is the longitudinal coordinate. Yatim *et al.* [138, 139] used a variety of analytical and numerical methods to derive unsteady similarity solutions for gravity-driven flow of a thin rivulet of a Newtonian and a power-law fluid down an inclined substrate. In particular, the solutions of Yatim *et al.* [138] correspond to a rivulet with a fixed nose with either a single-humped or double-humped cross-sectional profile that widens (for a pendent rivulet) or thins (for a sessile rivulet) with distance along the rivulet, while the solutions of Yatim *et al.* [139] predict that at any time the rivulet widens or narrows according to $|x|^{(2N+1)/2(N+1)}$ and thickens or thins according to $|x|^{N/(N+1)}$ as it flows down the substrate, where N is the power-law index. Yatim *et al.* [137] showed that a rivulet of a shear-thinning fluid subject to a weak shear stress is wider and thicker than a corresponding rivulet of a Newtonian fluid; whereas such a rivulet subject to a strong shear stress is narrower and thinner than a corresponding rivulet of a Newtonian fluid.

1.10.7 Thin-Film Flows of Non-Newtonian Fluids

While there has been very little work on rivulet flow of non-Newtonian fluids, there has been intensive work on other closely related free surface flows of non-Newtonian fluids. Matsuhisa and Bird [76] provided analytical and numerical solutions for isothermal and non-isothermal flow of an Ellis fluid. Myers [91] provided comparisons between predictions of the thin-film flow of three generalised Newtonian fluids, namely power-law, Carreau and Ellis fluids down an inclined substrate and in a channel, and showed that the velocities of the Ellis and Newtonian fluids are relatively similar whereas the power-law fluid indicates significant flattening in the central region where it approaches plug flow. The two-dimensional flow of a thin film of a power-law fluid on an inclined substrate, subject to a uniform longitudinal surface shear stress, was studied by Pascal and

D'Alessio [96]. They examined analytically and numerically the linear and nonlinear stability of the film and found that an upward shear stress has a stabilising effect. Jossic *et al.* [64] gave comparisons between the behaviour of shear-thinning and Newtonian models of tear films in the eye and man-made substitutes, during blinking. Hu and Kieweg [59] incorporated the effects of surface tension for gravity-driven flow of power-law shear-thinning fluids on an incline in order to simulate a capillary ridge and the fingering instability in a two-dimensional model. They indicated that optimizing the shear-thinning index can prevent the occurrence of fingering instabilities. Hu and Kieweg [60] extended the above work to study the three-dimensional flow of power-law fluids based on their linear stability analysis and numerical simulations to show, in particular, how the effects of shear-thinning would influence the finger growth. They showed that the wavelengths for Newtonian and shear-thinning fluids are exactly the same on a vertical substrate whereas for a less-inclined substrate the wavelengths for Newtonian fluids are shorter than those for shear-thinning fluids. Kheyfets and Kieweg [67] developed a three-dimensional model for gravity-driven flow of an Ellis fluid to study the spreading speed of polymeric solutions and to validate the numerical methods with experiments; however, they did not incorporate surface-tension effects and therefore could not simulate fingering instabilities. Sayag and Worster [109] reported experimental studies to validate theoretical predictions concerning axisymmetric gravity currents of a power-law fluid. In particular, they analysed constant-volume and constant-flux release of axisymmetric spreading of an aqueous suspension of Xanthan gum of 1% concentration by weight. Pritchard *et al.* [102] studied the flow of a shallow layer of a generalised Newtonian fluid on an inclined substrate; in particular, they presented the kinematic-wave solution for a Carreau fluid and showed that the effect of shear thinning on these solutions is to increase the wave speed.

Rimming flow of non-Newtonian fluids has been investigated by, amongst

others, Fomin *et al.* [43], who studied the flow of a power-law fluid and obtained analytical solutions in the particular case when the power-law index is equal to 1/2, and Fomin *et al.* [44], who studied the flow of a thin polymeric film on the inner wall of a uniformly rotating horizontal cylinder.

1.11 Dispersion of a Solute in a Flowing Fluid

In Chapters 5 and 6 of this thesis we consider advection and Taylor–Aris dispersion of a passive solute in steady unidirectional flow of uniform non-thin and thin rivulets, respectively, of a Newtonian fluid down a vertical planar substrate when the flow is driven by gravity and/or a uniform shear stress on its free surface. Accordingly, this section gives a brief overview of the concept of dispersion of a solute in a flowing fluid.

The study of solute dispersion in a flowing fluid has long been an active area of research, partly because it is a fascinating topic scientifically, and partly because of its wide range of applications in the fields of, for example, chemical engineering, ecological dynamics, petroleum production, and physiological fluid dynamics. Examples of dispersion include the spread of pollutants in the environment (see, for example, [126]), chromatographic separation in chemical engineering (see, for example, [54]), and the transport of dissolved drugs in the blood (see, for example, [125]).

If a solute is injected into a flowing fluid then it disperses (that is, it is advected by the flow and diffuses), and its concentration $c(x, y, z, t)$ satisfies the advection–diffusion equation

$$\frac{\partial c}{\partial t} + \mathbf{u} \cdot \nabla c = D \nabla^2 c, \tag{1.105}$$

where D is the molecular diffusivity, t denotes time, $\mathbf{u}$ is the fluid velocity, and ∇^2 denotes the three-dimensional Laplacian operator.

The dispersion of a solute in a steadily flowing fluid after a sufficiently long

time is due to a remarkable phenomenon called *Taylor–Aris dispersion* (or often simply just Taylor dispersion), named after Taylor [122, 123] and Aris [9]. In particular, Taylor [122, 123] performed the pioneering theoretical and experimental analysis of dispersion (first observed experimentally by Griffiths [51]) of a slug of solute injected into a fluid solvent undergoing steady unidirectional flow along a straight pipe of circular cross-section. The explanation of this phenomenon was a remarkable achievement, but perhaps not even Taylor could have anticipated that his work would have such widespread application in so many different areas.

In his experiment Griffiths [51] used a drop of fluorescent solution as a marker in a stream of water flowing through a pipe to measure the viscosity of water. In particular, he observed that the marker spread out symmetrically from a point which moved with the mean speed of the flow in the pipe. Later, Taylor [122] performed his own experiments, in which he used potassium permanganate as the solute and water as the solvent. Taylor [122] explained Griffiths's [51] observation by means of a series of intuitive arguments. In particular, Taylor [122, 123] showed analytically using these arguments that any initially finite distribution of the solute will, as a consequence of the combined effect of advection by the flow and radial diffusion, eventually become uniform over the cross-section of the pipe and take up a symmetric Gaussian profile axially; this Gaussian profile moves with the mean speed of the flow $\bar{u}$, and spreads axially over a distance of $O((D_{\text{eff}}t)^{1/2})$ with an effective diffusivity, D_{eff}, which is larger than the molecular diffusivity D, and which is defined by

$$D_{\text{eff}} = D\left(1 + \frac{\text{Pe}^2}{48}\right), \tag{1.106}$$

where a is the radius of the pipe and $\text{Pe} = \bar{u}a/D$ is the appropriate Péclet number, which is defined to be the ratio of advective effects on the concentration of solute to diffusive effects. In particular, Taylor [122] showed that the mean concentration

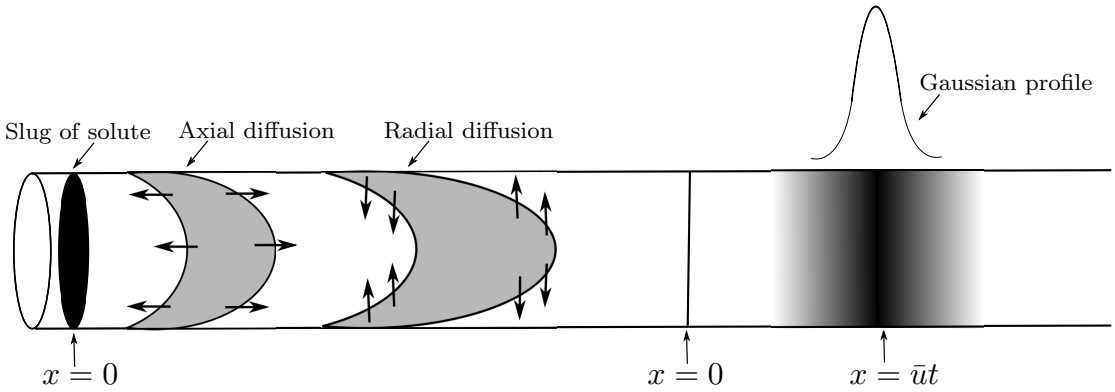

Figure 1.20: Sketch of the Taylor–Aris dispersion problem, representing the dispersion of a slug of solute injected into steady unidirectional flow along a straight pipe of circular cross-section, showing the slug of the solute injected at the initial time $t = 0$, the axial diffusion, and the radial diffusion. The sketch also shows a section of the pipe at a much later time when the slug has moved downstream with the mean velocity of the flow $\bar{u}$ and spread symmetrically over a distance $O((D_{\text{eff}}t)^{1/2})$ forming a Gaussian profile.

satisfies a simple advection–diffusion equation with effective diffusivity D_{eff} given by (1.106).

1.11.1 Physical Mechanism of Taylor–Aris Dispersion in a Pipe

As discussed by Probstein [103] and Leal [69], the physical mechanism of Taylor–Aris dispersion for flow in a pipe may be explained as follows. If an asymmetric slug of solute is injected into the pipe, then at small times a radial inhomogeneity is established, in which the slug is distorted into a parabolic profile due to the parabolic velocity profile of the flow, as illustrated in Figure 1.20. Thus advection of the solute by the flow enlarges the axial extent over which the solute is present and contributes to enhancing the axial dispersion, so that a radial concentration gradient is established. As a consequence, at longer time, radial diffusion plays a role on the dispersion mechanism: the radial diffusion acting at the rear of the slug causes the particles from the lower-velocity wall region to move to the higher-velocity central region, thereby causing the rear of the slug to speed up, while doing the opposite to the front of the slug. Thus the net effect of radial diffusion is

to compress the mixing zone between the slug of solute and the solvent (whereas the net effect of axial diffusion is to elongate it). Thus the radial diffusion inhibits the axial dispersion. As time progresses, as a result of the combined effect of axial advection and radial diffusion, the initially asymmetric slug is symmetrically distributed axially, and has a Gaussian profile.

1.11.2 Transport of a Passive Solute in a Pipe

Consider the evolution of an axisymmetric concentration of solute, c, as a function of the axial distance x, radial distance r and time t in a steady unidirectional Poiseuille flow in a pipe of circular cross-section with axial velocity of the form $\mathbf{u} = 2\bar{u}\,(1 - r^2/a^2)\,\mathbf{k}$, for which the advection–diffusion equation (1.105) becomes

$$\frac{\partial c}{\partial t} + 2\bar{u}\left(1 - \frac{r^2}{a^2}\right)\frac{\partial c}{\partial x} = D\left(\frac{\partial^2 c}{\partial r^2} + \frac{1}{r}\frac{\partial c}{\partial r} + \frac{\partial^2 c}{\partial x^2}\right). \tag{1.107}$$

If we assume that the distribution of the solute at the middle of the pipe is smooth and symmetric, and that there is no flux of the solute through the walls of the pipe, then the appropriate boundary conditions are

$$\frac{\partial c}{\partial r} = 0 \quad \text{on} \quad r = 0, a. \tag{1.108}$$

In addition, we assume that the slug of solute is injected at some initial time $t = 0$ with a prescribed initial distribution $c(x, r, 0) = c_0(x, r)$, occupying a (possibly infinite) portion $x_1 \le x \le x_2$ of the pipe, with x_1 and x_2 prescribed. The mean concentration over the cross-section of the pipe, $\bar{c} = \bar{c}(x, t)$, is simply defined by

$$\bar{c} = \frac{1}{A}\int_0^{2\pi}\int_0^a c\, r\, \mathrm{d}r\, \mathrm{d}\theta, \tag{1.109}$$

where $A = \pi a^2$ denotes the cross-sectional area of the pipe.

1.11.3 Advection of a Passive Solute in a Pipe

In his famous paper, Taylor [122] explained the physical idea of his dispersion argument by first describing the transport of the solute by advection alone. At sufficiently small times after the slug of solute is injected, specifically for $t \ll a^2/D$ (so that the radial diffusion time a^2/D is short compared with the advection time $L/\bar{u}$, where L is an appropriate longitudinal lengthscale), as we discussed in Subsection 1.11.1, axial advection is dominant over radial diffusion, and as a consequence the effects of radial diffusion may be ignored. Thus, in this case the governing equation (1.107) for c reduces simply to the advection equation

$$\frac{\partial c}{\partial t} + 2\bar{u}\left(1 - \frac{r^2}{a^2}\right)\frac{\partial c}{\partial x} = 0, \tag{1.110}$$

which has general solution

$$c(x, r, t) = c_0\left(x - 2\bar{u}\left(1 - \frac{r^2}{a^2}\right)t, r\right), \tag{1.111}$$

reflecting the fact that the position of the particle of solute that is at $x = x_0$ at $t = 0$ is at $x = x_0 + 2\bar{u}\,(1 - r^2/a^2)\,t$ at time t, where $c_0(x, r) = c(x, r, 0)$. It is appropriate to non-dimensionalise and scale x and t with L and $L/\bar{u}$, respectively. Taylor [122] considered first a simple situation in which the solute initially takes the form of a semi-infinite slug of uniform concentration c_0 in $x \leq 0$ with $c = 0$ in $x > 0$ at $t = 0$, where c_0 is a constant. He found that the solution for the mean concentration $\bar{c}$ is piecewise linear in x down the pipe, specifically

$$\frac{\bar{c}}{c_0} = \begin{cases} 1 & \text{if } x < 0, \\ 1 - \dfrac{x}{u_{\max}t} & \text{if } 0 \leq x \leq u_{\max}t, \\ 0 & \text{if } x > u_{\max}t, \end{cases} \tag{1.112}$$

where $u_{\max} = 2\bar{u}$ is the maximum velocity of the fluid. He then considered the situation in which the solute takes the form of a finite slug of uniform concentration c_0 in $0 \leq x \leq \Delta$ with $c = 0$ in $x < 0$ and $x > \Delta$ at $t = 0$, where both c_0 and the length of the slug Δ (> 0) are constants. He found that $\bar{c}$ is again piecewise linear in x down the pipe; specifically in this case the solution for $\bar{c}$ at time t is given by

$$\frac{\bar{c}}{c_0} = \begin{cases} 0 & \text{if } x < 0, \\ \dfrac{x}{u_{\max} t} & \text{if } 0 < x \leq u_{\max} t, \\ 1 & \text{if } u_{\max} t < x \leq \Delta, \\ \dfrac{u_{\max} t - x + \Delta}{u_{\max} t} & \text{if } \Delta < x \leq \Delta + u_{\max} t, \\ 0 & \text{if } x > \Delta + u_{\max} t, \end{cases} \tag{1.113}$$

for $t \leq \Delta / u_{\max}$ and by

$$\frac{\bar{c}}{c_0} = \begin{cases} 0 & \text{if } x < 0, \\ \dfrac{x}{u_{\max} t} & \text{if } 0 < x \leq \Delta, \\ \dfrac{\Delta}{u_{\max} t} & \text{if } \Delta < x \leq u_{\max} t, \\ \dfrac{u_{\max} t - x + \Delta}{u_{\max} t} & \text{if } u_{\max} t < x \leq \Delta + u_{\max} t, \\ 0 & \text{if } x > \Delta + u_{\max} t, \end{cases} \tag{1.114}$$

for $t > \Delta / u_{\max}$, where again $u_{\max} = 2\bar{u}$.

1.11.4 Taylor–Aris Dispersion of a Passive Solute in a Pipe

Taylor [122] went on to consider the change in the concentration of the solute at sufficiently long times after the slug of solute is injected, specifically for $t \gg$

a^2/D, for which times the radial concentration gradients are large enough that the effect of diffusion in the radial direction is not negligible. In this case the concentration c satisfies the full advection–diffusion equation (1.107). Taylor [122] again considered the situation in which the solute initially takes the form of a finite slug of non-uniform concentration $c(x, r, 0)$ in $0 \leq x \leq \Delta$, where Δ is again constant, with $c = 0$ in $x < 0$ and $x > \Delta$. He showed that the mean concentration $\bar{c}(x, t)$ defined by (1.109) is governed by a simple advection–diffusion equation given by

$$\frac{\partial \bar{c}}{\partial t} + \bar{u}\frac{\partial \bar{c}}{\partial x} = D_{\text{eff}}\frac{\partial^2 \bar{c}}{\partial x^2}, \tag{1.115}$$

where the effective diffusivity D_{eff} is given by (1.106). We do not attempt to reproduce his intuitive arguments here, because in Chapter 5 we will present an alternative derivation via the method of multiple scales. Taylor [122, 123] showed that the conditions under which this analysis is valid (and which are satisfied in his experiment) are

$$\frac{4L}{a} \gg \text{Pe} \gg \sqrt{48} \simeq 6.9282. \tag{1.116}$$

The relevant solution of (1.115) at large times is the evolving Gaussian profile given by

$$\bar{c}(x, t) = \frac{\bar{c}_0 \Delta}{\sqrt{4\pi D_{\text{eff}} t}} \exp\left(-\frac{(x - \bar{u}t)^2}{4D_{\text{eff}} t}\right), \tag{1.117}$$

where $\bar{c}_0 = M/(\pi a^2 \Delta)$ and M is the initial mass of solute. Figure 1.21 shows results from Taylor's experiments giving the distribution of the mean concentration $\bar{c}/\bar{c}_0$ as a function of x at three different times, and illustrating that Taylor's theoretical result given by (1.117) is in very good agreement with his experimental results. Taylor [122] fitted his data at measured positions at the three times 1740 s, 2160 s and 2490 s, respectively, to the Gaussian-function solution given by (1.117), and using this procedure determined D_{eff} and hence D, which he found ranged from 0.5×10^{-5} to $1.5 \times 10^{-5}\,\text{cm}^2\,\text{s}^{-1}$.

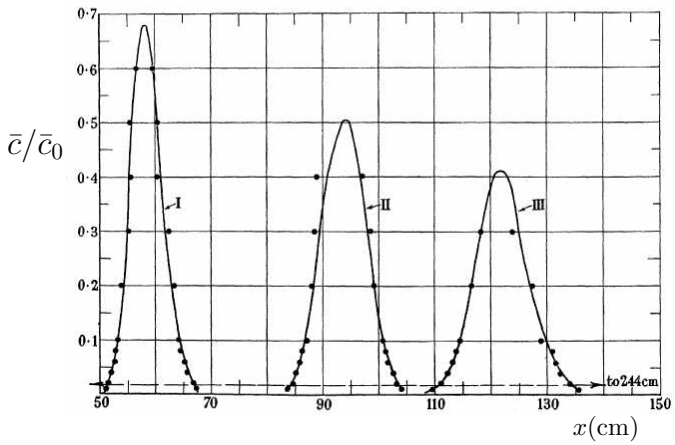

Figure 1.21: Image showing the mean concentration distribution $\bar{c}/\bar{c}_0$ centred at three positions along the pipe at three different times, measured by Taylor [122]. The solid curves I, II and III are the Gaussian-function solutions given by (1.117) at three times 1740 s, 2160 s and 2490 s, respectively. The dashed line is the distribution that would be due to pure advection, for comparison with curve III, and the dots indicate the experimental results. Reprinted from Taylor [122], Copyright, 1953, with permission from Proc. Roy. Soc. London A.

1.11.5 Derivations of Taylor Dispersion

Since the pioneering work of Taylor [122] (which had over 4900 citations on Google Scholar on 8$^{\text{th}}$ June 2017) a variety of derivations of Taylor's intuitive result have been presented by many different authors using a variety of analytical methods, such as the method of moments (Aris [9]) and the method of multiple scales (Pagitsas *et al.* [95], Fowler [46]), as well as methods based on the Centre-Manifold Theorem (Mercer and Roberts [78]), Liapunov–Schmidt reduction (Ratnakar and Balakotaiah [104]), and Fourier series (Lungu and Moffatt [74]). Aris [9] used the so-called method of moments in which he calculated the three total moments of the concentration $c(x, r, t)$ and the mean concentration $\bar{c}(x, t)$ in the forms

$$M_n(t) = \frac{2}{a^2} \int_{-\infty}^{\infty} \int_0^a x^n c(x, r, t) r \, \mathrm{d}r \, \mathrm{d}x \tag{1.118}$$

and

$$\overline{M}_n(t) = \int_{-\infty}^{\infty} x^n \bar{c}(x, t) \, \mathrm{d}x, \tag{1.119}$$

respectively, for $n = 0, 1, 2$, from which he derived the effective diffusivity, D_{eff}, given by (1.106), without any restriction on the value of Pe, and he presented a

more detailed treatment of unidirectional flow in a pipe of arbitrary cross-section and flow profile. Gill and Sankarasubramanian [48] used a generalised dispersion model for steady flow in a pipe to derive an advection–diffusion equation with a time-dependent effective diffusivity. They showed that for $t < 1/2$ their effective diffusivity decreases with decrease of the radius of the non-uniform initial slug of solute, and for $t \geq 1/2$ it is in agreement with Taylor–Aris dispersion for all values of the radius. Pagitsas *et al.* [95] showed, using the method of multiple scales, that the limiting value of D_{eff} in a rectangular channel in the limit of small aspect ratio is about eight times larger than D_{eff} in the corresponding two-dimensional case. In particular, they emphasized that for sufficiently short times this result is obtained by ignoring the side walls of the channel whereas for sufficiently long times the solute is affected by the perturbing presence of the side walls, so that D_{eff} increases. Using Aris's method Fan and Hwang [42] and Prenosil and Jarvis [101] considered Taylor–Aris dispersion of a solute in a non-Newtonian power-law fluid flowing through a circular pipe, and draining down an inclined substrate, respectively, and provided an expression for D_{eff} for the fluid in terms of the power-law index N. Zhang and Frigaard [143] used the method of multiple scales, as developed by Pagitsas *et al.* [95], to examine the displacement between two generalised Newtonian miscible fluids in channels and to derive an asymptotic approximation for the leading order concentration. They emphasized that increasing either the yield stress or the shear-thinning behaviour leads to the decrease of D_{eff}. Chatwin [20] developed an asymptotic series solution of (1.105) in powers of $t^{-1/2}$. In particular, he obtained the first three terms of this series, which provide an adequate approximation to $\bar{c}$ for $Dt/a^2 \geq 0.2$, and explained the weak effect of the initial mean concentration on the approach of the series to the Gaussian profile. Mercer and Roberts [78] described Taylor–Aris dispersion of a contaminant for flows in slowly varying channels of various cross-sections, for which they showed the convergence of their asymptotic approximation of

solutions of (1.105). In particular, they derived a higher-order approximation of (1.105), as used by Gill and Sankarasubramanian [48], to show the effect of variable diffusivity D in the velocity of the mean concentration and the dispersion of the contaminant, the latter of which is reduced if D decreases. A systematic method based on the Liapunov–Schmidt technique of bifurcation theory to obtain reduced-order models with modified inlet and initial conditions directly from the governing equation for the cross-sectionally mean concentration was developed by Ratnakar and Balakotaiah [104]. Recently, Adrover and Cerbelli [1] carried out numerical simulations of the dispersion of solutes in finite-length microtubes for a variety of Péclet numbers. A more complete history of different methods of analysing dispersion can be found in the article by Young and Jones [141].

The analysis of Taylor–Aris dispersion of a solute may also apply to the transport of heat, possibly with different boundary conditions. For example, Lungu and Moffatt [74] considered the effect of wall conductance on heat dispersion in Poiseuille flow through a circular pipe and a two-dimensional channel, and used Fourier transformations to obtain a series solution. They showed that for large times the effective diffusivity, D_{eff}, is a decreasing function of the wall conductance.

The effect of the geometry of the channel on the dispersion of a solute has been investigated by a considerable number of studies. Chatwin and Sullivan [21], Pagitsas *et al.* [95], Dutta [35], Dutta *et al.* [36], Guell *et al.* [53], and Ajdari *et al.* [2] studied the effect of width-to-depth aspect ratio on the effective diffusivity in pressure-driven flow in a channel of arbitrary cross-section. In particular, using the thin-film approximation, Guell *et al.* [53] and Ajdari *et al.* [2] showed that the effective diffusivity is governed by the width of the cross-section instead of, as might have been expected, by the much smaller depth of the channel, and they provided formulae for dispersion in channels of triangular, parabolic and elliptical cross-sectional profiles.

1.11.6 Transport in Rivulet Flows in Microfluidic Devices

One of the most important issues in microfluidic devices is the optimisation of transport (*i.e.* the mixing and dispersion) of a solute at small Reynolds numbers and small aspect ratios (see, for example, the reviews by Stone *et al.* [116] and Darhuber and Troian [28], and Lee *et al.* [70]). Rivulet flows can arise in such devices. Herrada *et al.* [55] proposed a technique for producing micro-bubbles with a controlled size from the breakup of a rivulet of gas in a microfluidic channel. Darhuber and Troian [28] explained how a rivulet on a microstripe may split into droplets due to thermocapillary forces. Kabov *et al.* [66] investigated experimentally the heat transfer to a rivulet flowing in minichannels and microchannels driven by gravity and a co-current gas flow; they found that in the former the rivulet widens with an increase in the effective gravity whereas in the latter gravity does not effect the shape of the rivulet. Darhuber *et al.* [27] and Darhuber *et al.* [26] investigated advective and diffusive mixing in narrow rivulets on chemically micropatterned surfaces. In particular, the latter identified micromixing analogous to Taylor–Aris dispersion for appropriate parameter ranges, in which an increase in D leads to an increase in the mixing time, and hence to a decrease in the mixing efficiency. However, with the notable exception of the work of Darhuber *et al.* [26], there has been surprisingly little theoretical work on transport of solutes in microfluidic flows with free surfaces and, in particular, on the study of the dispersion of a passive solute in a rivulet flow.

1.12 Outline of Thesis

In this thesis we analyse two aspects of the steady flow of rivulets of fluid, namely the effects of non-Newtonian rheology and the advection and dispersion of a passive solute in a rivulet of Newtonian fluid.

In Chapter 2 we use lubrication theory to obtain the solution for unidirec-

tional gravity-driven flow of a uniform thin rivulet of a power-law fluid down a planar substrate, and then we use this solution to describe the flow of a rivulet with prescribed constant contact angle but slowly varying semi-width down a slowly varying substrate, specifically flow in the azimuthal direction around the outside of a large horizontal circular cylinder. It is shown how the solution depends strongly on the value of the power-law index of the fluid. Another notable qualitative departure from Newtonian behaviour is that, whereas the mass of a rivulet of a Newtonian or a shear-thinning fluid is theoretically infinite, the mass of a rivulet of a shear-thickening fluid is finite.

In Chapter 3 we use the solution for unidirectional flow that was obtained in Chapter 2 to describe the flow of a rivulet with prescribed constant width but slowly varying contact angle down a slowly varying substrate. In particular, we describe how the shape of the rivulet of prescribed semi-width and the velocity within it depend on the power-law index N, and it is shown that whereas neither the shape of the rivulet nor the velocity within it vary monotonically with N, its mass always decreases monotonically with N.

In Chapter 4 we consider rivulet flow of generalised Newtonian fluids down a vertical planar substrate. In particular, we obtain the solutions for rivulet flow of a Carreau fluid and of an Ellis fluid, highlighting their similarities and differences. The behaviour of rivulets of nearly Newtonian fluids, rivulets with small or large prescribed flux, and rivulets of strongly shear-thinning Carreau and Ellis fluids is described.

In Chapters 5 and 6 we investigate both the short-time advection and the long-time Taylor–Aris dispersion of a passive solute in uniform non-thin and thin rivulets, respectively, of a Newtonian fluid undergoing steady unidirectional flow driven by gravity and/or a prescribed uniform surface shear stress on a vertical planar substrate. An explicit expression for the effective diffusivity of the solute in a thin rivulet as a function of the surface shear stress, the volume flux along the

rivulet, and either the semi-width or the contact angle of the rivulet is obtained.

Finally, in Chapter 7 we summarise the results and main findings of the thesis, and suggest some directions for possible future work.

1.13 Presentations and Publications

Aspects of the work described in Chapters 2 and 3 have been presented at the 4th joint British Mathematical Colloquium (BMC) and British Applied Mathematics Colloquium (BAMC) held in Cambridge from 30th March to 2nd April 2015, at the Rheologists in Scotland Meeting II held in Glasgow in the University of Strathclyde on 26th May 2015, at the 28th Scottish Fluid Mechanics Meeting held in Glasgow on 28th May 2015, and at the 11th European Coating Symposium held in Eindhoven, The Netherlands from 9th to 11th September 2015. Aspects of the work described in Chapter 4 have been presented at the British Society of Rheology Winter Meeting 2015: Microrheology and Microfluidics held in Glasgow in the University of Glasgow from 14th to 15th December 2015, and at the SIAM UKIE Annual Meeting held in Glasgow in the University of Strathclyde on 12th January 2017. Aspects of the work described in Chapter 6 have been presented at the British Applied Mathematics Colloquium held in Guilford in the University of Surrey from 10th to 12th April 2017, at the 30th Scottish Fluid Mechanics Meeting held in Glasgow in the University of Strathclyde on 19th May 2017, and at Flow17 held in Paris, France from 3rd to 5th July 2017.

Furthermore, aspects of the work in Chapters 2–4 have been presented by my primary supervisor Prof. Stephen K. Wilson at Viscoplastic Fluids: From Theory to Application held in Banff in Canada from 25th to 30th October 2015, and at the British Society of Rheology Midwinter Meeting 2016 held in Reading in the University of Reading from 12th to 14th December 2016. Aspects of the work in Chapter 6 has been recently presented by Prof. Stephen K. Wilson at UK Fluids

Conference held in Leeds in the University of Leeds from 7th to 9th September 2017.

A full account of the work in Chapter 2 has been published in Physics of Fluids (Al Mukahal *et al.* [84]), a full account of the work in Chapter 3 has been published in the Journal of Non-Newtonian Fluid Mechanics (Al Mukahal *et al.* [87]), and a full account of the work in Chapter 6 has been recently accepted for publication in Proceedings of the Royal Society A (Al Mukahal *et al.* [86]). A full account of the work contained in Chapter 4 (Al Mukahal *et al.* [85]) has been submitted for publication.

Chapter 2

A Rivulet of a Power-Law Fluid with Constant Contact Angle Draining Down a Slowly Varying Substrate

The work in this Chapter generalises that of Duffy and Moffatt [31] for the case of Newtonian fluid, as described in Sections 1.6 and 1.7, to a corresponding analysis for a power-law fluid.

There has been relatively little theoretical work on rivulet flow of non-Newtonian fluids; this Chapter begins to rectify this by analysing the locally unidirectional steady gravity-driven flow of a thin rivulet of a power-law fluid with prescribed volume flux down a locally planar substrate. First we obtain the solution for unidirectional flow of a uniform rivulet down a planar substrate, and then we use it to obtain the solution for a slowly varying rivulet with prescribed constant (nonzero) contact angle draining down a slowly varying substrate, specifically flow in the azimuthal direction around the outside of a large horizontal circular cylinder.

2.1 Rivulet Flow Down a Planar Substrate

2.1.1 Problem Formulation

In this Chapter we shall be concerned with flow of an incompressible power-law fluid with velocity $\mathbf{u}$ and pressure p for which, as described previously in Subsection 1.3.2, the extra stress $\underline{\underline{\boldsymbol{\sigma}}}'$ is related to the rate of strain $\underline{\underline{\mathbf{e}}} = \left(\nabla\mathbf{u} + (\nabla\mathbf{u})^{\mathrm{T}}\right)/2$ by $\underline{\underline{\boldsymbol{\sigma}}}' = 2\mu(q)\underline{\underline{\mathbf{e}}}$, where $\mu(q) = \mu_N q^{N-1}$ is the shear-rate-dependent viscosity, $q = \left(2\,\mathrm{tr}(\underline{\underline{\mathbf{e}}}^2)\right)^{1/2}$ is the shear rate, and the power-law index N and the consistency parameter μ_N are constants. The fluid is shear thinning when $0 < N < 1$ and shear thickening when $N > 1$; the special case $N = 1$ corresponds to a Newtonian fluid with constant viscosity μ_1. The measure of the stress, τ, defined by $\tau = \left(\mathrm{tr}\left(\underline{\underline{\boldsymbol{\sigma}}}'^2\right)/2\right)^{1/2}$, takes the form $\tau = \mu(q)q = \mu_N q^N$. The velocity $\mathbf{u}$ and the pressure p satisfy the mass-conservation and momentum-balance equations for such a fluid, which take the forms

$$\nabla\cdot\mathbf{u} = 0, \qquad \rho\frac{D\mathbf{u}}{Dt} = -\nabla p + \rho\mathbf{g} + \mu_N\nabla\cdot\left(q^{N-1}\left(\nabla\mathbf{u} + (\nabla\mathbf{u})^{\mathrm{T}}\right)\right), \tag{2.1}$$

where ρ, $\mathbf{g}$ and t denote the fluid density, acceleration due to gravity, and time, respectively.

Consider unidirectional steady gravity-driven flow of a thin uniform rivulet of a power-law fluid with prescribed volume flux down a planar substrate inclined at an angle α to the horizontal, as shown in Figure 2.1. The case $0 \leq \alpha < \pi/2$ corresponds to flow down the upper side of the substrate (a sessile rivulet), and the case $\pi/2 < \alpha \leq \pi$ corresponds to flow down the lower side of the substrate (a pendent rivulet); the special case $\alpha = \pi/2$ corresponds to flow down a vertical substrate, and will be considered in detail in Subsection 2.1.3. With reference to the Cartesian coordinates $Oxyz$ shown in Figure 2.1, the substrate is at $z = 0$; the cross-sectional free surface profile of the rivulet is denoted by $z = h(y)$ and

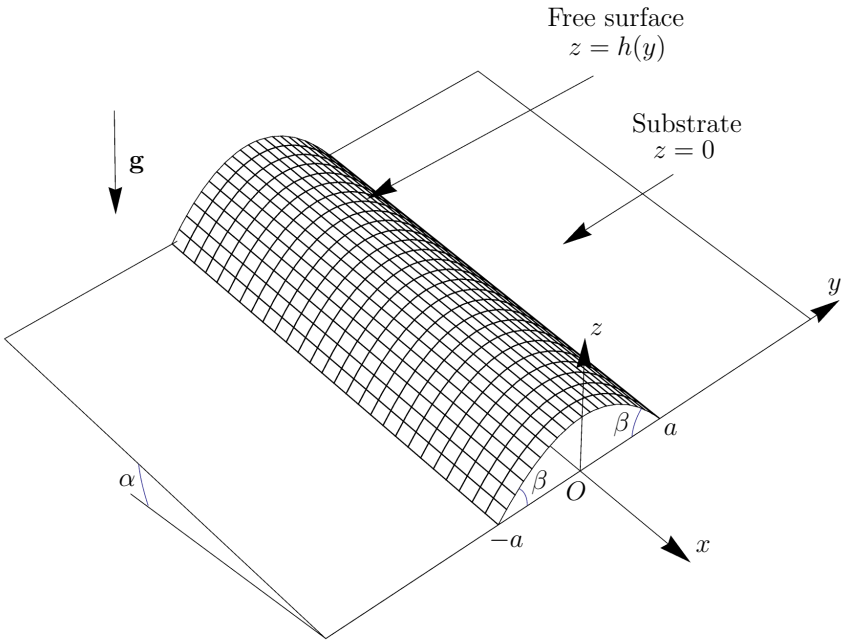

Figure 2.1: Sketch of the unidirectional steady gravity-driven flow of a thin uniform rivulet of a power-law fluid of prescribed volume flux down a planar substrate inclined at an angle α to the horizontal.

the semi-width of the rivulet by a, the fluid occupying $-a \leq y \leq a$. We consider the situation in which the contact angle of the fluid, β (> 0), has a prescribed (nonzero) value, but the semi-width a is unknown and is to be determined as part of the solution. Not only is this flow of interest in its own right, but also it forms the basis for studying the flow of a slowly varying rivulet with constant contact angle down a slowly varying substrate described in Section 2.2.

With a velocity of the form $\mathbf{u} = u(y, z)\mathbf{i}$, the shear rate is $q = \left(u_y^2 + u_z^2\right)^{1/2}$, but since the rivulet is thin we have $q = |u_z|$ to the usual accuracy of thin-film theory; moreover, since $u_z \geq 0$ for the type of flow under consideration, we have $q = u_z$. Therefore (2.1) reduces to

$$0 = -p_x + \rho g \sin\alpha + \mu_N (u_z^N)_z, \qquad 0 = -p_y, \qquad 0 = -p_z - \rho g \cos\alpha, \tag{2.2}$$

to be integrated subject to the boundary conditions of no slip on the substrate

$z = 0$, and balances of normal and tangential stress on the free surface:

$$u = 0 \ \text{ on } \ z = 0, \qquad u_z = 0 \ \text{ and } \ p = p_{\mathrm{a}} - \gamma h'' \ \text{ on } \ z = h, \tag{2.3}$$

where p_{a} denotes atmospheric pressure, γ denotes the coefficient of surface tension of the fluid, and a prime denotes differentiation with respect to y. In addition, h satisfies the contact-line conditions

$$h = 0 \ \text{ and } \ h' = \mp\beta \ \text{ at } \ y = \pm a. \tag{2.4}$$

The volume flux of fluid along the rivulet, Q, is given by

$$Q = \int_{-a}^{a} \int_{0}^{h} u \, \mathrm{d}z \, \mathrm{d}y, \tag{2.5}$$

which will be taken to have a prescribed value $Q = \bar{Q}$.

We non-dimensionalise and scale the variables appropriately by writing

$$\begin{gathered} y = \ell y^*, \quad a = \ell a^*, \quad z = \beta \ell z^*, \quad h = \beta \ell h^*, \quad u = U u^*, \\ p = p_a + \rho g \beta \ell p^*, \quad Q = \beta \ell^2 U Q^*, \quad q = \frac{U}{\beta \ell} q^*, \quad \mu = \bar{\mu} \mu^*, \quad \tau = \rho g \beta \ell \tau^*, \end{gathered} \tag{2.6}$$

where $\ell = (\gamma/\rho g)^{1/2}$ is the capillary length, $U = (\rho g \beta^{N+1} \ell^{N+1}/\mu_N)^{1/N}$ is an appropriate velocity scale, and $\bar{\mu} = \mu_N (U/\beta\ell)^{N-1}$ is an appropriate viscosity scale. Note that the scales U and $\bar{\mu}$ depend on μ_N and N, and that the scaled contact angle is $\beta^* \equiv 1$ and the scaled viscosity is $\mu^* = q^{*N-1}$. From now on we use non-dimensional quantities (omitting the stars, for clarity).

2.1.2 Solution

From $(2.2)_3$ and (2.3) the solution for p is

$$p = \cos\alpha(h - z) - h'', \tag{2.7}$$

and then $(2.2)_2$ gives

$$(h'' - \cos\alpha\, h)' = 0, \tag{2.8}$$

representing a transverse balance between gravity and surface-tension effects. Since (2.8) does not depend on viscous effects, the general form of solution for h will be independent of N; in particular, it will be the same as that for a Newtonian fluid (and indeed for any generalised Newtonian fluid).

The solution of (2.4) and (2.8) for h is

$$h = \begin{cases} \dfrac{\cosh ma - \cosh my}{m \sinh ma} & \text{if } \ 0 \le \alpha < \dfrac{\pi}{2}, \\ \dfrac{a^2 - y^2}{2a} & \text{if } \ \alpha = \dfrac{\pi}{2}, \\ \dfrac{\cos my - \cos ma}{m \sin ma} & \text{if } \ \dfrac{\pi}{2} < \alpha \le \pi, \end{cases} \tag{2.9}$$

where we have introduced the notation $m = \sqrt{|\cos\alpha|}$. We note that the rivulet is symmetric about its centreline $y = 0$, and so its maximum thickness $h_{\rm m} = h(0)$ occurs at $y = 0$, and is given by

$$h_{\rm m} = \begin{cases} \dfrac{1}{m} \tanh \dfrac{ma}{2} & \text{if } \ 0 \le \alpha < \dfrac{\pi}{2}, \\ \dfrac{a}{2} & \text{if } \ \alpha = \dfrac{\pi}{2}, \\ \dfrac{1}{m} \tan \dfrac{ma}{2} & \text{if } \ \dfrac{\pi}{2} < \alpha \le \pi. \end{cases} \tag{2.10}$$

It may be shown that, whereas for $0 < \alpha \le \pi/2$ the solution (2.9) is valid for any $ma \ge 0$, for $\pi/2 < \alpha \le \pi$ it is physically realisable (specifically, $h \ge 0$ for $-a \le y \le a$) only if $ma < \pi$. As yet the semi-width a in (2.9) is unknown.

From $(2.2)_1$ and (2.3) the solution for u is

$$u = \frac{N}{N+1} (\sin\alpha)^{\frac{1}{N}} \left(h^{\frac{N+1}{N}} - (h-z)^{\frac{N+1}{N}} \right), \tag{2.11}$$

representing a longitudinal balance between gravitational and viscous effects. The maximum velocity $u_{\max}$, given by

$$u_{\max} = \frac{N}{N+1} \left(\sin\alpha \, h_{\mathrm{m}}^{N+1} \right)^{\frac{1}{N}}, \tag{2.12}$$

occurs at the apex of the rivulet, *i.e.* at $y = 0$, $z = h_{\mathrm{m}}$. The shear rate q, viscosity $\mu = q^{N-1}$, and shear stress $\tau = \mu q = q^N$ vary across the rivulet, and are given by

$$q = [\sin\alpha \, (h-z)]^{\frac{1}{N}}, \qquad \mu = [\sin\alpha \, (h-z)]^{\frac{N-1}{N}}, \qquad \tau = \sin\alpha \, (h-z). \tag{2.13}$$

In particular, in the shear-thickening case ($N > 1$) the viscosity μ decreases monotonically from its value $(\sin\alpha \, h)^{(N-1)/N}$ at the substrate $z = 0$ to zero at the free surface $z = h$, whereas in the shear-thinning case ($N < 1$) it increases monotonically from $(\sin\alpha \, h)^{(N-1)/N}$ at $z = 0$ and becomes infinite at $z = h$. Despite the shortcomings associated with the power-law model (namely, a zero or infinite viscosity at the free surface), the other features of the flow are well behaved; in particular, the velocity u, shear rate q, and shear stress τ are finite everywhere (the latter being linear in z, as required by the balance of momentum in the x direction).

From (2.5) and (2.11) the flux of fluid along the rivulet, Q, is

$$Q = \frac{N}{2N+1} (\sin\alpha)^{\frac{1}{N}} \int_{-a}^{a} h^{\frac{2N+1}{N}} \, \mathrm{d}y. \tag{2.14}$$

Performing the quadrature here, with h given by (2.9), we find that Q is given

by

$$Q = \frac{1}{9}\left(\frac{\sin\alpha}{m^{3N+1}}\right)^{\frac{1}{N}} f_N(ma)\,, \tag{2.15}$$

where the function $f_N(ma)$ is defined by

$$f_N(ma) = \lambda_N \times \begin{cases} {}_2F_1\left(\frac{1}{2}, \frac{3N+1}{N}; \frac{7N+2}{2N}; \tanh^2\frac{ma}{2}\right)\tanh^{\frac{3N+1}{N}}\frac{ma}{2} & \text{if } 0 \le \alpha < \frac{\pi}{2}, \\ \left(\frac{ma}{2}\right)^{\frac{3N+1}{N}} & \text{if } \alpha = \frac{\pi}{2}, \\ {}_2F_1\left(\frac{1}{2}, \frac{3N+1}{N}; \frac{7N+2}{2N}; -\tan^2\frac{ma}{2}\right)\tan^{\frac{3N+1}{N}}\frac{ma}{2} & \text{if } \frac{\pi}{2} < \alpha \le \pi, \end{cases} \tag{2.16}$$

in which ${}_2F_1$ denotes the hypergeometric function, and where we have introduced λ_N defined by

$$\lambda_N = \frac{18\sqrt{\pi}\,\Gamma\left(\frac{2N+1}{N}\right)}{\Gamma\left(\frac{7N+2}{2N}\right)} = 36\,\mathrm{B}\left(\frac{3}{2}, \frac{2N+1}{N}\right), \tag{2.17}$$

where Γ and B denote Gamma and Beta functions, respectively. To complete the solution we must solve (2.15) with $Q = \bar{Q}$ to obtain the semi-width a; this depends on the form of $f_N(ma)$ in (2.16), and therefore also on the form of λ_N in (2.17).

Figure 2.2 shows a plot of λ_N as a function of N, illustrating that λ_N increases monotonically with N, satisfying

$$\lambda_N = 18\sqrt{\pi}N^{3/2} + O(N^{5/2}) \to 0^+ \quad \text{as} \quad N \to 0^+, \tag{2.18}$$

$$\lambda_N = \frac{48}{5} - \frac{16}{25}(31 - 15\log 4)\,N^{-1} + O(N^{-2}) \to \frac{48}{5}^- \quad \text{as} \quad N \to \infty, \tag{2.19}$$

and taking the value $192/35 \simeq 5.48571$ at $N = 1$.

Figure 2.3 shows plots of $f_N(ma)$ as a function of ma in the cases (a) $0 \le \alpha < \pi/2$ and (b) $\alpha = \pi/2$, and as a function of ma/π ($0 \le ma/\pi \le 1$) in the case (c)

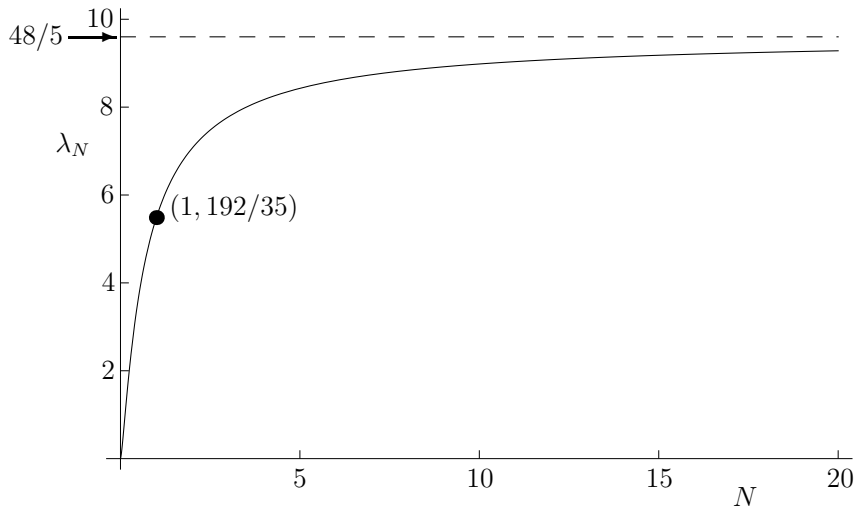

Figure 2.2: Plot of λ_N defined in (2.17) as a function of N, together with its asymptotic value 48/5 in the limit $N \to \infty$. The dot denotes the Newtonian value 192/35 at $N = 1$.

$\pi/2 < \alpha \leq \pi$, for a range of values of N. Figure 2.3 illustrates that in all cases $f_N(ma)$ increases monotonically with ma, and, in particular,

$$f_N(ma) \sim \lambda_N \left(\frac{ma}{2}\right)^{\frac{3N+1}{N}} = O\left((ma)^{\frac{3N+1}{N}}\right) \to 0^+ \tag{2.20}$$

in the limit $ma \to 0^+$,

$$f_N(ma) \sim \frac{18N}{2N+1} ma = O(ma) \to \infty \tag{2.21}$$

in the limit $ma \to \infty$ for $0 \leq \alpha < \pi/2$, $f_N(ma) = \lambda_N \, (ma/2)^{(3N+1)/N} = O\left(ma^{(3N+1)/N}\right) \to \infty$ in the limit $ma \to \infty$ for $\alpha = \pi/2$, and

$$f_N(ma) \sim 9 \left(\frac{2}{\kappa_N(\pi - ma)}\right)^{\frac{2N+1}{N}} = O\left((\pi - ma)^{-\frac{2N+1}{N}}\right) \to \infty \tag{2.22}$$

in the limit $ma \to \pi^-$ for $\pi/2 < \alpha \leq \pi$, where we have introduced κ_N defined by

$$\kappa_N = \left(\frac{(2N+1)\Gamma\left(\frac{3N+1}{N}\right)}{2\sqrt{\pi} N \, \Gamma\left(\frac{5N+2}{2N}\right)}\right)^{\frac{N}{2N+1}} = \left[\frac{2N}{2N+1} \mathrm{B}\left(\frac{1}{2}, \frac{5N+2}{2N}\right)\right]^{-\frac{N}{2N+1}}. \tag{2.23}$$

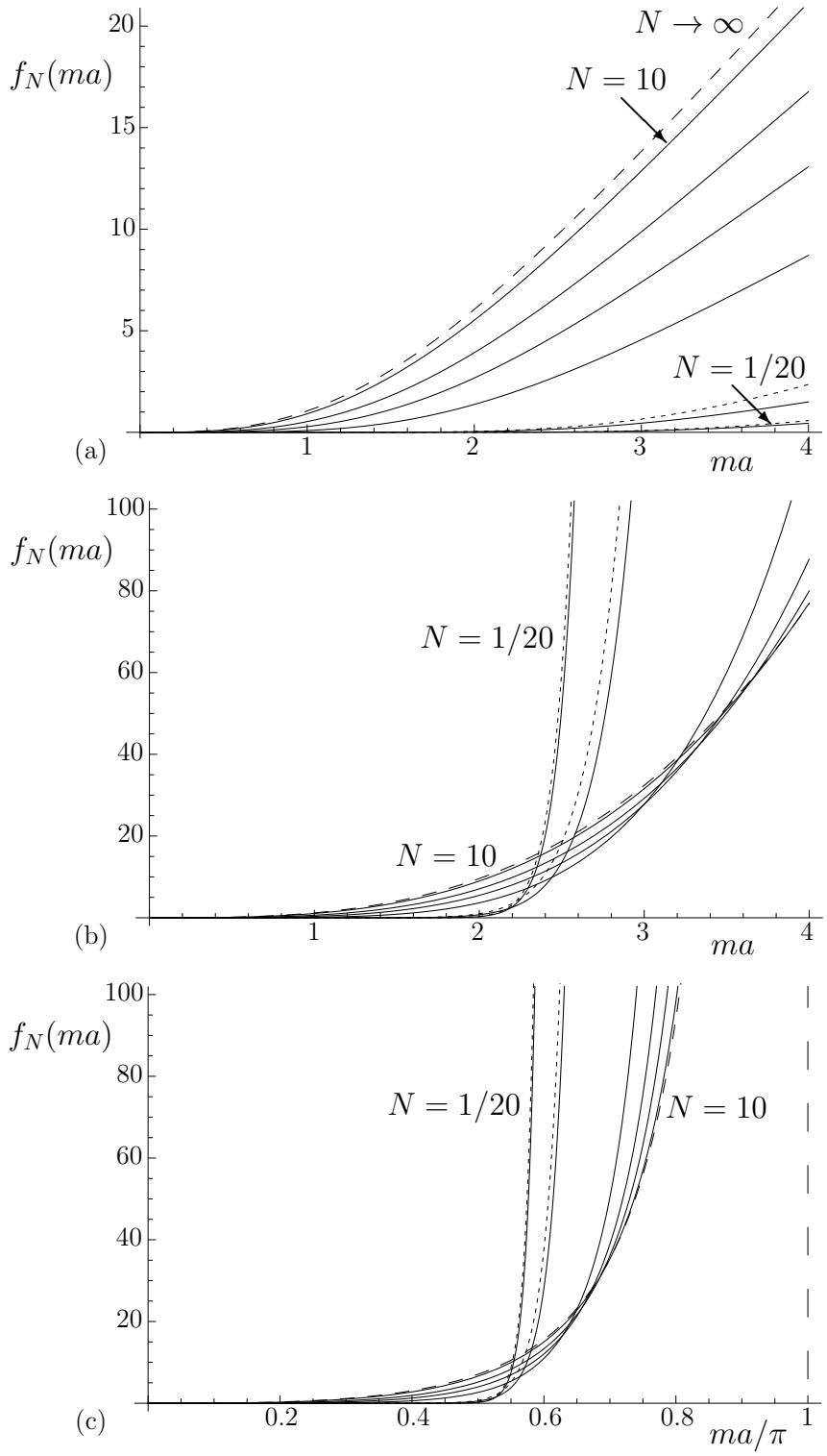

Figure 2.3: Plots of $f_N(ma)$ defined in (2.16) as a function of ma in the cases (a) $0 \leq \alpha < \pi/2$ and (b) $\alpha = \pi/2$, and as a function of ma/π ($0 \leq ma/\pi \leq 1$) in the case (c) $\pi/2 < \alpha \leq \pi$, for $N = 1/20$, $1/10$, $1/2$, 1, 2 and 10. The dotted lines show the leading-order asymptotic solution in the limit $N \to 0^+$, $\hat{f}_N$, defined in (2.24) and plotted for $N = 1/20$ and $N = 1/10$, and the dashed lines show the leading-order asymptotic solution in the limit $N \to \infty$, f_∞, defined in (2.26). The vertical long-dashed line in (c) marks the maximum value of $ma = \pi$ beyond which there are no physically realisable solutions for h.

We conclude that (2.15) has a solution a for any prescribed N, α and $\bar{Q}$, and that this solution is unique. [In fact, the function $f_N(ma)$ given in $(2.16)_3$ for $\pi/2 < \alpha \leq \pi$ has infinitely many branches in $ma \geq 0$; however, since only the branch in $0 \leq ma \leq \pi$ leads to physically realisable solutions for h, we shall ignore the branches beyond $ma = \pi$.] The transcendental nature of (2.15) means that, in general, it must be solved numerically for a.

Figure 2.3 also shows that when $0 \leq \alpha < \pi/2$, $f_N(ma)$ is an increasing function of N for all ma, but when $\pi/2 \leq \alpha \leq \pi$ it is an increasing function of N for sufficiently small values of ma but a decreasing function of N for sufficiently large values of ma; therefore the curves for different values of N in Figures 2.3(b) and (c) (but not those in Figure 2.3(a)) cross each other.

For future reference, we note that in the limit $N \to 0^+$ we have $f_N(ma) \sim \hat{f}_N(ma)$, where we have defined

$$\hat{f}_N(ma) = 18\sqrt{\pi}N^{\frac{3}{2}} \times \begin{cases} \sinh\dfrac{ma}{2}\tanh^{\frac{2N+1}{N}}\dfrac{ma}{2} & \text{if } \ 0 \leq \alpha < \dfrac{\pi}{2}, \\ \left(\dfrac{ma}{2}\right)^{\frac{3N+1}{N}} & \text{if } \ \alpha = \dfrac{\pi}{2}, \\ \sin\dfrac{ma}{2}\tan^{\frac{2N+1}{N}}\dfrac{ma}{2} & \text{if } \ \dfrac{\pi}{2} < \alpha \leq \pi. \end{cases} \tag{2.24}$$

For $0 \leq \alpha \leq \pi/2$ the function $\hat{f}_N(ma)$ satisfies $\hat{f}_N(ma) \to 0^+$ as $N \to 0^+$, whereas for $\pi/2 < \alpha \leq \pi$ it satisfies $\hat{f}_N(ma) \to 0^+$ as $N \to 0^+$ when $0 \leq ma \leq \pi/2$, but $\hat{f}_N(ma) \to \infty$ as $N \to 0^+$ when $\pi/2 < ma \leq \pi$. Furthermore, in the limit $N \to \infty$ we have $f_N(ma) \to f_\infty(ma)$ and, from (2.15),

$$Q \to \frac{f_\infty(ma)}{9m^3}, \tag{2.25}$$

where we have defined

$$f_\infty(ma) = \begin{cases} \dfrac{9}{2}\left(3ma\coth^2 ma - 3\coth ma - ma\right) & \text{if } 0 \le \alpha < \dfrac{\pi}{2}, \\ \dfrac{6(ma)^3}{5} & \text{if } \alpha = \dfrac{\pi}{2}, \\ \dfrac{9}{2}\left(3ma\cot^2 ma - 3\cot ma + ma\right) & \text{if } \dfrac{\pi}{2} < \alpha \le \pi. \end{cases} \tag{2.26}$$

The functions $\hat{f}_N$ and f_∞ given by (2.24) and (2.26) are included in Figure 2.3 as dotted and dashed curves, respectively.

In summary, the solutions for the pressure p and velocity u in the steady unidirectional flow of a thin uniform rivulet are given by (2.7) and (2.11), respectively, in which the free surface profile h is given by (2.9), with the semi-width a to be determined from the flux condition (2.15) with $Q = \bar{Q}$ when N, α and $\bar{Q}$ are prescribed. In the special case of a Newtonian fluid ($N = 1$) equations (2.11)–(2.17) reduce to the solution given by Duffy and Moffatt [31] (albeit presented somewhat differently).

2.1.3 The Special Case of Rivulet Flow Down a Vertical Substrate

The special case of rivulet flow down a vertical substrate (that is, the special case $\alpha = \pi/2$) is of particular interest and hence merits further discussion here. In that case the cross-sectional free surface profile of the rivulet has the simple parabolic form given in (2.9), and equations (2.15) and (2.16) may be solved to give simple explicit solutions for a and hence $h_{\rm m}$, namely

$$a = 2\left(\frac{9\bar{Q}}{\lambda_N}\right)^{\frac{N}{3N+1}}, \quad h_{\rm m} = \left(\frac{9\bar{Q}}{\lambda_N}\right)^{\frac{N}{3N+1}}. \tag{2.27}$$

Figure 2.4 shows a plot of a given by (2.27) as a function of N for various values of $\bar{Q}$, and Figure 2.5 shows a plot of a as a function of $\bar{Q}$ for various values of N.

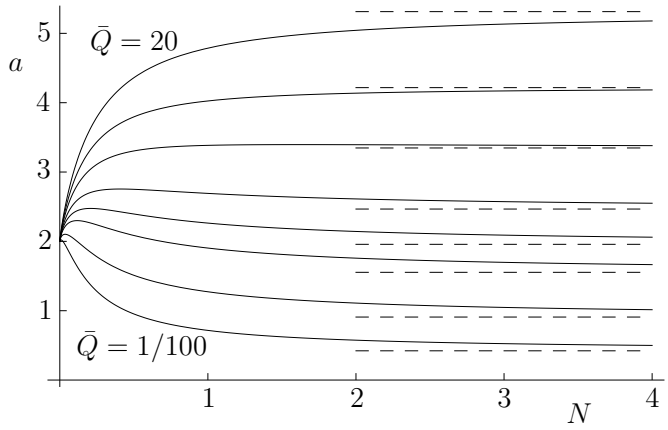

Figure 2.4: Plot of the semi-width a given by (2.27) as a function of N in the special case of a vertical substrate ($\alpha = \pi/2$), for $\bar{Q} = 1/100$, $1/10$, $1/2$, 1, 2, 5, 10 and 20. The dashed lines show the asymptotic solution given by (2.29) in the limit $N \to \infty$.

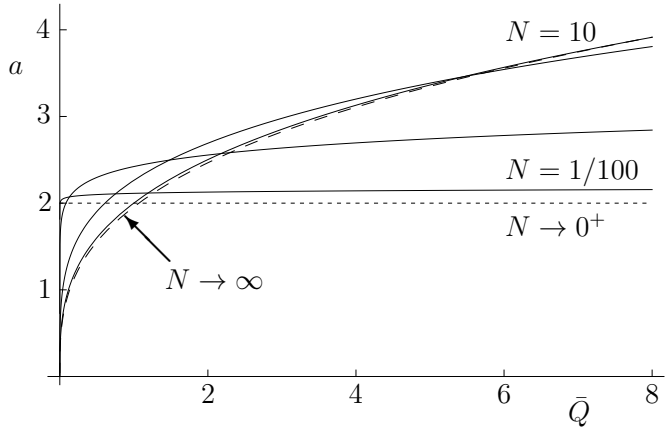

Figure 2.5: Plot of the semi-width a given by (2.27) as a function of $\bar{Q}$ in the special case of a vertical substrate ($\alpha = \pi/2$), for $N = 1/100$, $1/10$, 1 and 10. The dotted line shows the asymptotic solution $a \to 2$ in the limit $N \to 0^+$, and the dashed line shows the asymptotic solution given by (2.29) in the limit $N \to \infty$.

As Figures 2.4 and 2.5 show, for all values of $\bar{Q}$, a is given by (2.27) and satisfies

$$a \sim 2\left(\frac{\bar{Q}}{2\sqrt{\pi}N^{3/2}}\right)^{\frac{N}{3N+1}} \sim 2 + N\log\frac{\bar{Q}^2}{4\pi N^3} \to 2^+ \quad \text{as} \quad N \to 0^+, \tag{2.28}$$

and

$$a \to \frac{15\bar{Q}}{2}^{1/3} \quad \text{as} \quad N \to \infty, \tag{2.29}$$

and takes the value $a = (105\bar{Q}/4)^{1/4}$ when $N = 1$.

As Figure 2.4 illustrates, if $\bar{Q}$ is sufficiently small then a first increases with N to a local maximum and thereafter decreases monotonically. The value of N

at which this maximum occurs increases with $\bar{Q}$, and becomes infinite when $\bar{Q}$ takes a critical value $\bar{Q}_{\rm m}$. To determine $\bar{Q}_{\rm m}$ we therefore let $N \to \infty$ in the equation $da/dN = 0$, where a and λ_N are given in (2.27) and (2.17), respectively; this leads to $\bar{Q}_{\rm m} = 16\exp(\psi(7/2) + \gamma - 1)/15 \simeq 8.21248$, in which $\psi(7/2) = \Gamma'(7/2)/\Gamma(7/2) \simeq 1.10316$ denotes the Digamma function and $\gamma \simeq 0.57722$ denotes Euler's constant. If $\bar{Q}$ is sufficiently large, specifically if $\bar{Q} \geq \bar{Q}_{\rm m}$, then a has no maximum as a function of N, and so simply increases monotonically with N. As Figure 2.4 also shows, whatever the value of $\bar{Q}$ there is only a restricted range of possible values of a, and also that if $\bar{Q} < \bar{Q}_{\rm m}$ then it is possible for two rivulets of fluids with different values of N, with the same value of $\bar{Q}$, to have the same value of a. On the other hand, as Figure 2.5 shows, for a given value of N, a increases monotonically with $\bar{Q}$; in particular, it is immediately apparent from (2.27) that $a \to 0^+$ as $\bar{Q} \to 0^+$ and $a \to \infty$ as $\bar{Q} \to \infty$.

Figure 2.6 shows plots of the velocity profiles $u(y, z)$ given by (2.11) at different positions y across the rivulet, for (a) a strongly shear-thinning fluid with $N = 1/10$ and (b) a strongly shear-thickening fluid with $N = 10$, with $\bar{Q} = 1$ in each case; from (2.27) the corresponding semi-widths and maximum thicknesses are $a \simeq 2.42264$ and $h_{\rm m} \simeq 1.21132$, and $a \simeq 2.00127$ and $h_{\rm m} \simeq 1.00064$, respectively. Figure 2.7 shows contour plots of the velocity corresponding to the cases shown in Figure 2.6; the contour interval is the same in the two parts of the Figure.

For small N (typified by $N = 1/10$) two features of the flow are apparent. The first feature, evident in Figure 2.7(a), is the formation of two regions with $h < 1$, adjacent to the contact lines, in which q is small and so μ is large, leading to a large viscous resistance, and hence almost stationary fluid. Thus the rivulet "self-channels" its flow down a narrow central channel of semi-width

$$\left(2N \log \frac{\bar{Q}^2}{4\pi N^3}\right)^{1/2} (\ll 1) \tag{2.30}$$

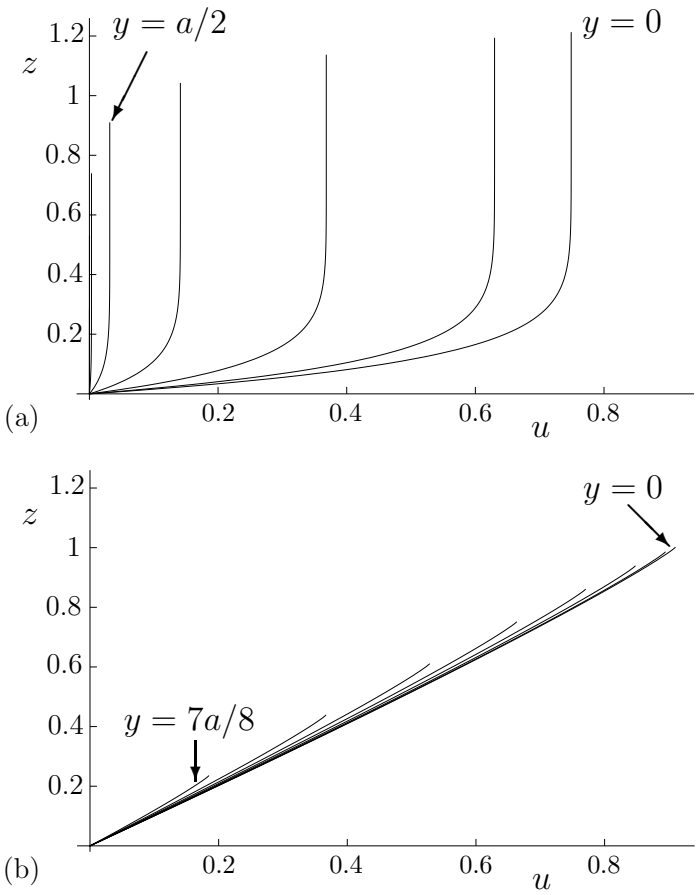

Figure 2.6: Plots of the velocity profiles $u(y, z)$ given by (2.11) at positions $y = 0$, $a/8$, $a/4$, $\ldots$, $7a/8$ across the rivulet in the special case of a vertical substrate ($\alpha = \pi/2$), for (a) $N = 1/10$ and (b) $N = 10$, with $\bar{Q} = 1$ in each case, for which (a) $a \simeq 2.42264$ and $h_{\rm m} \simeq 1.21132$, and (b) $a \simeq 2.00127$ and $h_{\rm m} \simeq 1.00064$.

between two "levées" of slowly moving fluid that form at its sides. In deriving (2.30) we have made use of the results $(2.28)_2$ as $N \to 0$ and the fact that $y = (a^2 - 2a)^{1/2}$ when $h = 1$. These levées are reminiscent of the levées of unyielded (and hence stationary) fluid adjacent to the contact lines of rivulets of viscoplastic fluid as reported by Wilson *et al.* [135] and discussed in Subsection 1.10.6. The second feature is that in the central channel, away from the substrate $z = 0$, the shear rate q is small, and hence the viscosity μ is large; therefore, as is evident in Figure 2.6(a), the velocity profiles have a "plug-like" form at each y position, with most of the fluid moving with a velocity that is independent of z but not of y. Specifically, in the limit $N \to 0$, equations (2.11), $(2.27)_1$ and $(2.9)_2$

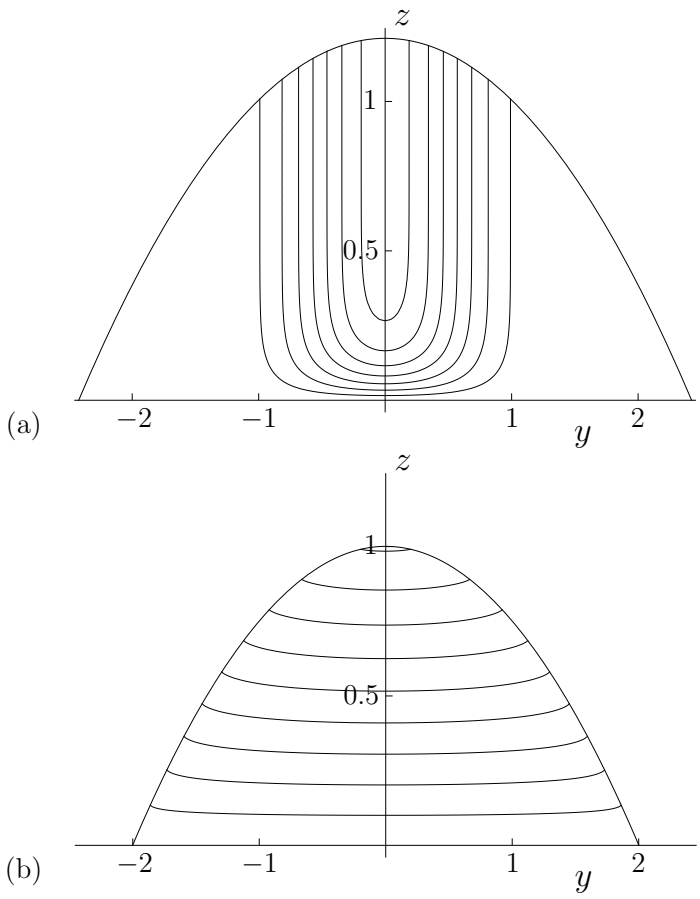

Figure 2.7: Contour plots of the velocity $u(y, z)$ given by (2.11) in the special case of a vertical substrate ($\alpha = \pi/2$), for the same values of N and $\bar{Q}$ as in Figure 2.6, namely (a) $N = 1/10$ and (b) $N = 10$, with $\bar{Q} = 1$ in each case. The contour interval is 0.1 in both parts of the Figure.

with (2.18) and $(2.28)_3$ lead to

$$u \sim Nh^{\frac{N+1}{N}} \sim \frac{\bar{Q}}{2\sqrt{\pi N}} \left(1 - \frac{y^2}{4}\right)^{\frac{N+1}{N}} \quad \text{as} \quad N \to 0^+, \tag{2.31}$$

except in a narrow boundary layer near the substrate (where $u = 0$) in which the shear rate is large. As Figure 2.7(a) illustrates, in this case there are relatively large velocity gradients in the y direction in the middle of the rivulet (where the velocity is not small) as well as large velocity gradients in the z direction near the substrate.

For large N (typified by $N = 10$) the shear rate q is uniform away from the free surface $z = h$ and the viscosity μ decreases linearly with z, and so, as is evident in Figure 2.6(b), the velocity profile is linear in z. Specifically, in the

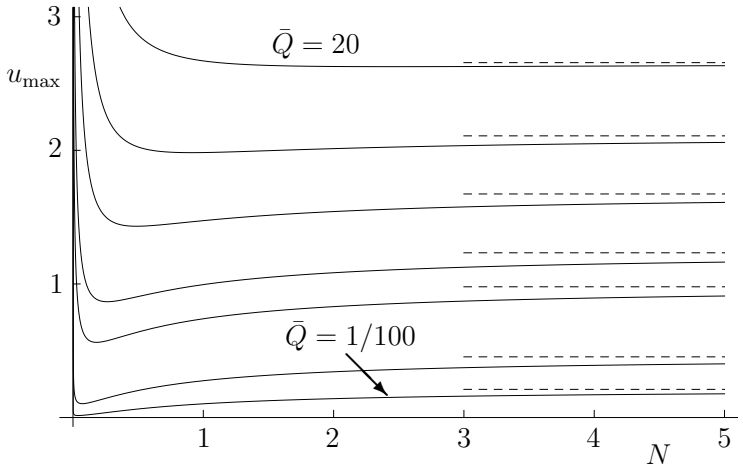

Figure 2.8: Plot of the maximum velocity $u_{\max}$ given by (2.33) as a function of N in the special case of a vertical substrate ($\alpha = \pi/2$), for $\bar{Q} = 1/100$, 1/10, 1, 2, 5, 10 and 20. The dashed lines show the asymptotic solution $u_{\max} = (15\bar{Q}/16)^{1/3}$ in the limit $N \to \infty$.

limit $N \to \infty$, equations (2.11), (2.13) and $(2.27)_1$ with (2.19) and (2.29) lead to

$$q \sim 1, \quad \mu \sim h - z, \quad u \sim z \quad \text{as} \quad N \to \infty, \tag{2.32}$$

except in a narrow boundary layer near the free surface (where $u_z = 0$) in which the gradient of shear is large. As Figure 2.7(b) illustrates, in this case the velocity gradients are almost entirely in the z direction over most of the rivulet.

Figure 2.8 shows a plot of the maximum velocity $u_{\max}$, namely

$$u_{\max} = \frac{N}{N+1}\left(\frac{\bar{Q}}{4\,\mathrm{B}\left(\frac{3}{2}, \frac{2N+1}{N}\right)}\right)^{\frac{N+1}{3N+1}}, \tag{2.33}$$

as a function of N for different values of $\bar{Q}$ (and hence different values of a and h_{m}), showing that $u_{\max}$ decreases from ∞ (specifically, $u_{\max} \sim \bar{Q}(2\sqrt{\pi N})^{-1} \to \infty$ as $N \to 0^+$) to a minimum value, and then increases to $(15\bar{Q}/16)^{1/3}$ as $N \to \infty$, taking the value $u_{\max} = (105\bar{Q})^{1/2}/16$ when $N = 1$.

2.2 Rivulet Flow Down a Slowly Varying Substrate

2.2.1 Flow Around a Large Horizontal Cylinder

Although the solution obtained in Subsection 2.1.2 is for strictly unidirectional flow of a uniform rivulet of fluid of prescribed contact angle down a planar substrate, it also provides the leading order solution for *locally* unidirectional flow down a substrate whose inclination angle α, rather than being constant, varies slowly in the downstream direction; the cross-sectional free surface profile of the rivulet (and in particular, the semi-width a and maximum height $h_{\rm m}$) then varies slowly with position down the substrate. An example is provided by rivulet flow in the azimuthal direction around the outside of a large horizontal circular cylinder, the inclination angle α then varying slowly around the cylinder; in that case the flow corresponds to a prescribed flux of fluid being supplied at the top of the cylinder (where $\alpha = 0$), running around the cylinder under gravity, and falling off at the bottom (where $\alpha = \pi$). Figure 2.9 shows a sketch of such a situation; it is rivulet flow of this type that we describe in the remainder of the present Chapter (although other interpretations, such as, for example, flow down a slowly undulating substrate, are also possible). Specifically, we consider cases where the azimuthal aspect ratio $\epsilon = \ell/R$ and the appropriately defined reduced Reynolds number $Re^* = \beta^4\rho\gamma\ell^2/\bar{\mu}^2 R$, where R is the radius of the cylinder, satisfy $\epsilon \ll \beta$ and $Re^* \ll 1$, the latter implying that inertial effects are negligible. In particular, both of these conditions are satisfied if R is sufficiently large.

Figure 2.10 shows plots of (a) a and (b) $h_{\rm m}$ as functions of α/π for various values of N; thus Figure 2.10(a) shows half of the "footprint" of the rivulet on the cylinder, and Figure 2.10(b) shows the profile of the centreline of the rivulet when the cylinder is viewed "end on" (both of them being "unwrapped" from the cylinder for the purposes of the Figure).

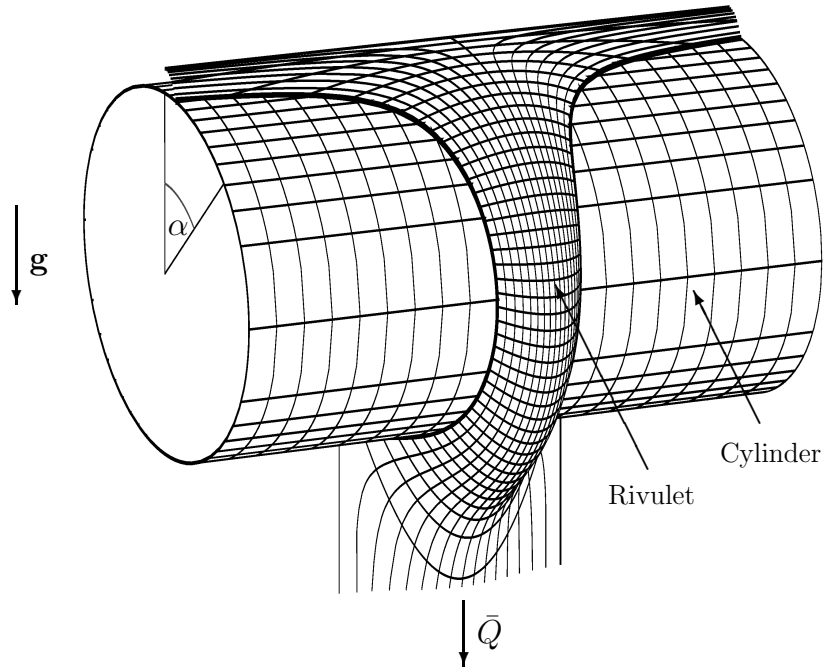

Figure 2.9: Sketch of a slowly varying rivulet of prescribed flux $\bar{Q}$ with constant contact angle and slowly varying semi-width that runs from the top ($\alpha = 0$) to the bottom ($\alpha = \pi$) of a large horizontal circular cylinder.

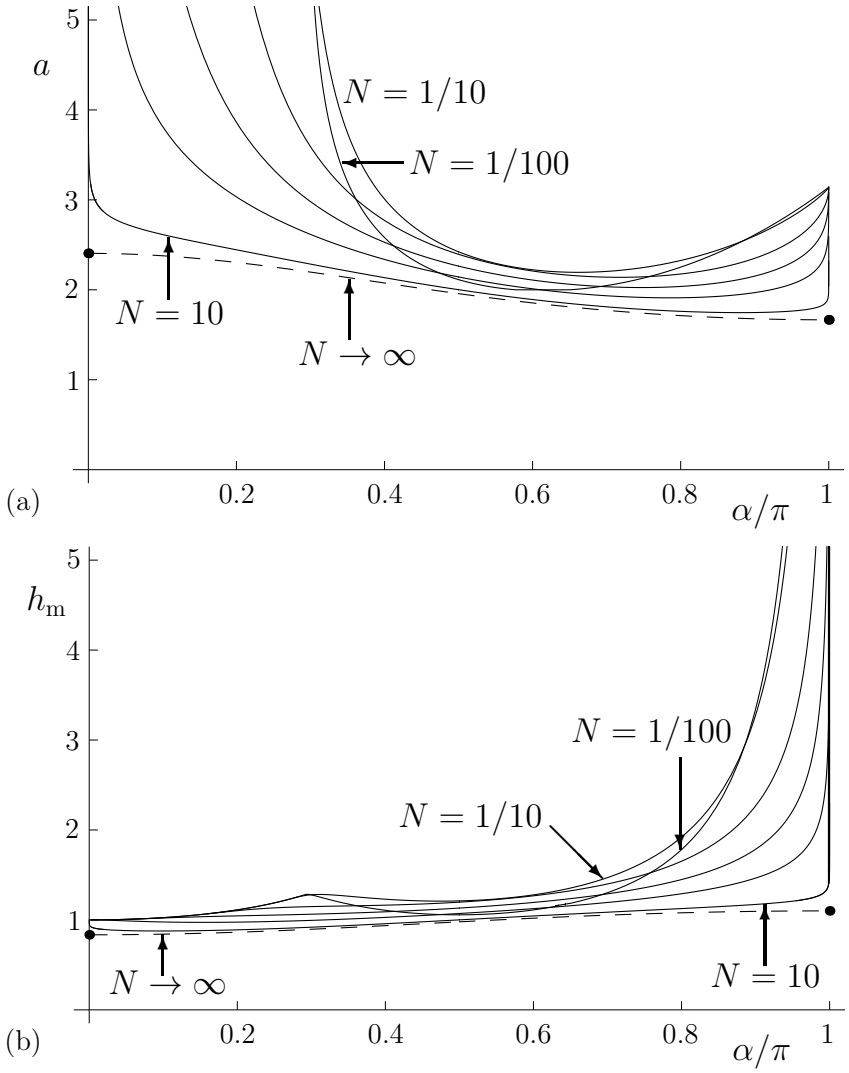

Figure 2.10: Plots of (a) the semi-width a and (b) the maximum thickness $h_{\rm m}$ as functions of α/π in the cases $N = 1/100$, $1/10$, $1/2$, 1, 2 and 10, for $\bar{Q} = 1$. The dashed curves show the leading order asymptotic outer solutions in the limit $N \to \infty$, and the dots denote the values $a \simeq 2.40515$ and $h_{\rm m} \simeq 0.83444$ at $\alpha = 0$ and $a \simeq 1.66639$ and $h_{\rm m} \simeq 1.10047$ at $\alpha = \pi$ on these asymptotic solutions.

Near the top of the cylinder, where the azimuthal component of gravity (proportional to $\sin\alpha$) driving the azimuthal flow is small but the normal component (proportional to $\cos\alpha$) tending to flatten the rivulet is significant, in order to achieve the prescribed flux $\bar{Q}$ the rivulet becomes wide and of finite thickness unity according to

$$a \sim \frac{(2N+1)\bar{Q}}{2N\alpha^{\frac{1}{N}}} \to \infty, \qquad h_{\mathrm{m}} \sim 1 + \frac{\alpha^2}{4} \to 1^+ \tag{2.34}$$

as $\alpha \to 0^+$. In deriving $(2.34)_1$ we have made use of the appropriate limit of (2.15) with $Q = \bar{Q}$, and equation (2.20) together with $\sin\alpha \sim \alpha$ in the limit $\alpha \to 0$. In deriving $(2.34)_2$ we have made use of the equation $(2.10)_1$ together with $m \to 1$ in the limit $\alpha \to 0$.

Near the bottom of the cylinder, where the azimuthal component of gravity is again small and the normal component, now tending to thicken the rivulet, is again significant, the rivulet becomes thick and of finite width π according to

$$a \sim \pi - \frac{2}{\kappa_N}\left(\frac{\pi-\alpha}{\bar{Q}^N}\right)^{\frac{1}{2N+1}} \to \pi^-, \qquad h_{\mathrm{m}} \sim \kappa_N\left(\frac{\bar{Q}^N}{\pi-\alpha}\right)^{\frac{1}{2N+1}} \to \infty \tag{2.35}$$

as $\alpha \to \pi^-$; therefore the thin-film approximation will break down sufficiently near to $\alpha = \pi$. In deriving $(2.35)_1$ we have made use of the appropriate limit of (2.15) with $Q = \bar{Q}$, and equation (2.22) together with $\cos\alpha \to -1$ and $\sin\alpha \sim \pi - \alpha$ in the limit $\alpha \to \pi^-$. In deriving $(2.35)_2$ we have made use of the equation $(2.10)_3$ in the limit $\alpha \to \pi^-$.

At the middle of the cylinder ($\alpha = \pi/2$), where the azimuthal component of gravity is significant but the normal component is zero, the rivulet has finite width and thickness given by (2.27).

As Figure 2.10(a) shows, the rivulet narrows to a minimum width and then widens again as it flows around the cylinder. Its minimum width occurs on the lower half of the cylinder ($\pi/2 < \alpha < \pi$), at a position determined mathematically

by (2.15) and

$$2\csc^2\alpha = N\,\frac{f_N'(ma)ma}{f_N(ma)} - 3N + 1, \tag{2.36}$$

the latter obtained by differentiation of (2.15) with respect to α, with $Q = \bar{Q}$; it may be shown from (2.15) and (2.36) that a has a (unique) stationary point for all values of N and $\bar{Q}$.

On the other hand, as Figure 2.10(b) shows, the nature of the stationary points of $h_{\rm m}$, determined mathematically by (2.15) and

$$2\csc^2\alpha = N\,\frac{f_N'(ma)\sinh ma}{f_N(ma)} - 3N + 1, \tag{2.37}$$

the latter obtained by differentiation of (2.10) and (2.15) with respect to α, depends on the value of $\bar{Q}$. Specifically, it may be shown from (2.15) and (2.37) that there exists a critical (N-dependent) flux $\bar{Q} = \bar{Q}_{\rm c}(N)$ such that if $\bar{Q} < \bar{Q}_{\rm c}$ then $h_{\rm m}$ has two stationary points, and increases from $h_{\rm m} = 1$ at $\alpha = 0$ to a maximum in $0 < \alpha < \pi/2$, decreases to a minimum also in $0 < \alpha < \pi/2$, and then increases monotonically to infinity as $\alpha \to \pi^-$, whereas if $\bar{Q} \geq \bar{Q}_{\rm c}$ then $h_{\rm m}$ has no stationary points, and increases monotonically from $h_{\rm m} = 1$ at $\alpha = 0$ to ∞ as $\alpha \to \pi^-$. Figure 2.11 shows a plot of $\bar{Q}_{\rm c}$ as a function of N, showing that $\bar{Q}_{\rm c}$ decreases from ∞ as $N \to 0^+$ to a minimum value $\bar{Q}_{\rm c} = \bar{Q}_{\rm c,min} \simeq 0.75782$ at $N = N_{\rm min} \simeq 0.67107$, and then increases to ∞ as $N \to \infty$, taking the value $\bar{Q}_{\rm c} \simeq 0.81741$ when $N = 1$. Note also from Figure 2.11 that if $\bar{Q} \leq \bar{Q}_{\rm c,min}$ then $h_{\rm m}$ has two stationary points for any N, whereas if $\bar{Q} > \bar{Q}_{\rm c,min}$ then $h_{\rm m}$ has two stationary points only if N is either sufficiently small or sufficiently large.

As Figure 2.10 also shows, a and $h_{\rm m}$ vary non-monotonically with N, in the sense that at any fixed value of α, both a and $h_{\rm m}$ increase with N up to a maximum, and then decrease monotonically.

Figure 2.10 also includes (as dashed curves) the leading order asymptotic outer solutions (away from $\alpha = 0$ and $\alpha = \pi$) for a and $h_{\rm m}$ in the limit $N \to \infty$,

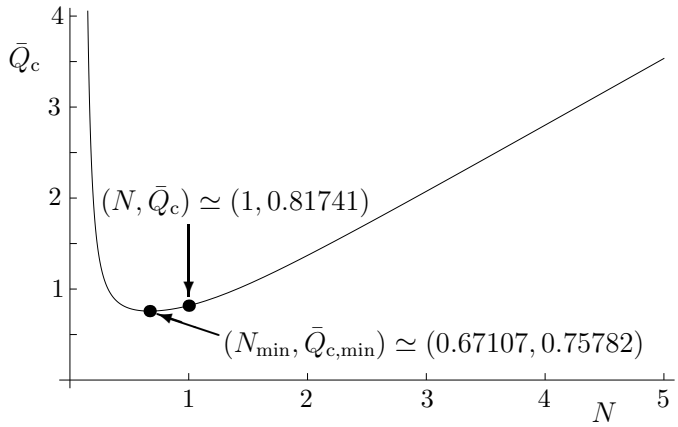

Figure 2.11: Plot of the critical flux $\bar{Q}_c$ as a function of N. The dots denote the minimum value $\bar{Q}_c = \bar{Q}_{c,min} \simeq 0.75782$ at $N = N_{min} \simeq 0.67107$ and the Newtonian value $\bar{Q}_c \simeq 0.81741$ at $N = 1$.

obtained by solving (2.25) with $Q = \bar{Q}$ for a and then using (2.10) for h_m. In particular, Figure 2.10 shows that these outer solutions take finite values at the top and bottom of the cylinder, namely $a \simeq 2.40515$ and $h_m \simeq 0.83444$ at $\alpha = 0$, and $a \simeq 1.66639$ and $h_m \simeq 1.10047$ at $\alpha = \pi$, obtained by solving $\bar{Q} = f_\infty(a)/9$. When N is large but finite there is a thin boundary layer near $\alpha = 0$ in which the solution for a grows without bound and the solution for h_m adjusts to the value $h_m = 1$ given by (2.34) at $\alpha = 0$, and a thin boundary layer near $\alpha = \pi$ in which the solution for h_m grows without bound and the solution for a adjusts to the value $a = \pi$ given by (2.35) at $\alpha = \pi$.

In the limit $N \to 0^+$ the positions of the minimum of a and of the maximum and minimum of h_m approach $\alpha = \pi/2$, while in the limit $N \to \infty$ the position of the minimum of a approaches $\alpha = \pi$ and the positions of the maximum and minimum of h_m approach $\alpha = 0$.

2.2.2 Free Surface Profiles h

Figure 2.12 shows plots of the cross-sectional free surface profile h as a function of y at the stations $\alpha = \pi/20, \pi/10, \ldots, 19\pi/20$ around the cylinder, for $N = 1/2$ and $\bar{Q} = 1$, and Figure 2.13 shows corresponding plots for $N = 2$. As already described, the profiles are wide and of finite thickness near the top of the cylinder,

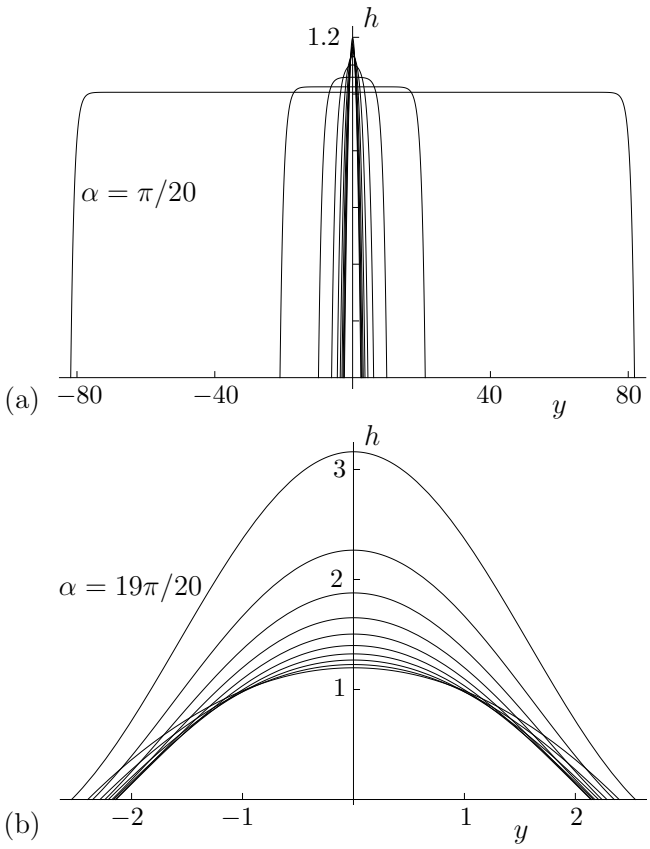

Figure 2.12: Plot of the cross-sectional free surface profile h given by (2.9) as a function of y at the stations (a) $\alpha = \pi/20, \pi/10, \ldots, \pi/2$ on the upper half of cylinder, and (b) $\pi/2, 11\pi/20, \ldots, 19\pi/20$ on the lower half of cylinder, for $N = 1/2$ and $\bar{Q} = 1$. Note the different scales used on the axes in the two parts of the Figure.

but are thick and of finite width near the bottom of the cylinder. The non-monotonic variation of a with α is evident in part (b) of both Figures. Figure 2.12 shows a case for which $\bar{Q} = 1 > \bar{Q}_{\rm c}(1/2) \simeq 0.78818$, and so $h_{\rm m}$ increases monotonically with α in this case, whereas Figure 2.13 shows a case for which $\bar{Q} = 1 < \bar{Q}_{\rm c}(2) \simeq 1.36980$, and so $h_{\rm m}$ varies non-monotonically with α, having a local maximum and a local minimum (both of which are barely discernible in the Figure) on the upper half of the cylinder in this case.

Figure 2.14 shows contour plots of the free surface h in the $(y, \alpha/\pi)$ plane, for several values of N, for $\bar{Q} = 1$. The non-monotonic variation of a with α, evident in all of the cases shown in Figure 2.14, is qualitatively the same for all values of $\bar{Q}$. On the other hand, the form of the variation of h with α depends on $\bar{Q}$. In particular, since at each station α, h has a maximum $h_{\rm m}$ at $y = 0$, if $\bar{Q} < \bar{Q}_{\rm c}$ then

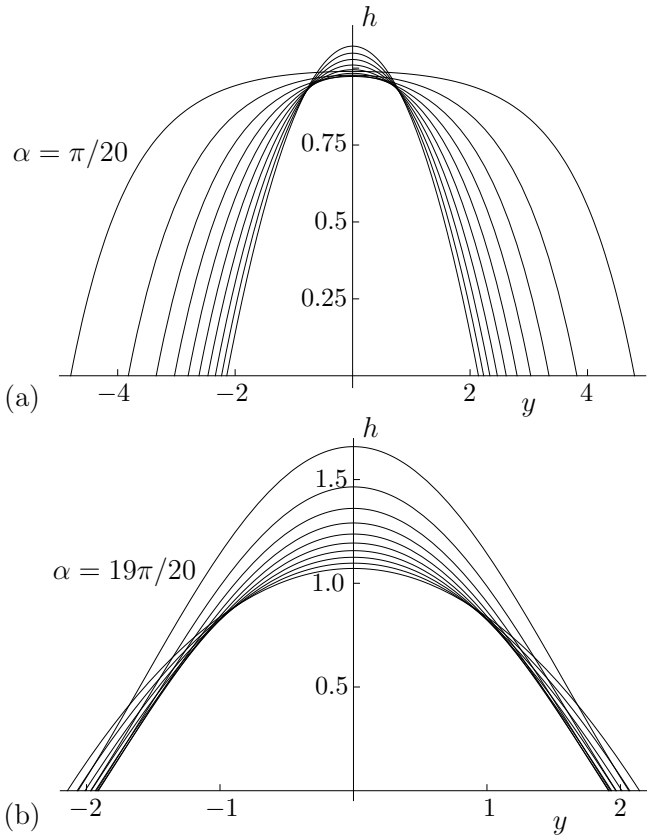

Figure 2.13: As in Figure 2.12, except for $N = 2$.

the maximum of $h_{\rm m}$ (regarded as a function of α) that occurs corresponds to a local maximum of h (regarded as a function of α and y), whereas the minimum of $h_{\rm m}$ corresponds to a saddle point of h; if $\bar{Q} \geq \bar{Q}_{\rm c}$ then $h_{\rm m}$ has no stationary points and so h has no stationary points. Figures 2.14(a) and (c) are for cases with $\bar{Q} = 1 < \bar{Q}_{\rm c}(1/5) \simeq 1.91857$ and $\bar{Q} = 1 < \bar{Q}_{\rm c}(2) \simeq 1.36980$, respectively, so that $h_{\rm m}$ has a local maximum and minimum, and therefore h has a local maximum and a saddle point, at $(y, \alpha/\pi, h_{\rm m}) \simeq (0, 0.30000, 1.24313)$ and $(y, \alpha/\pi, h_{\rm m}) \simeq (0, 0.44011, 1.22739)$ in (a), and at $(y, \alpha/\pi, h_{\rm m}) \simeq (0, 0.00582, 1.00005)$ (very close to the top of the cylinder) and $(y, \alpha/\pi, h_{\rm m}) \simeq (0, 0.15436, 0.97288)$ in (c), all of which are marked with dots; the contour that passes through the saddle point of h is also included in each case. Part (d) shows an enlargement of (c) (with additional contours, shown dashed and dotted) near the top of the cylinder, illustrating more clearly the occurrence of a local maximum in h there. Figure 2.14(b) is for a case

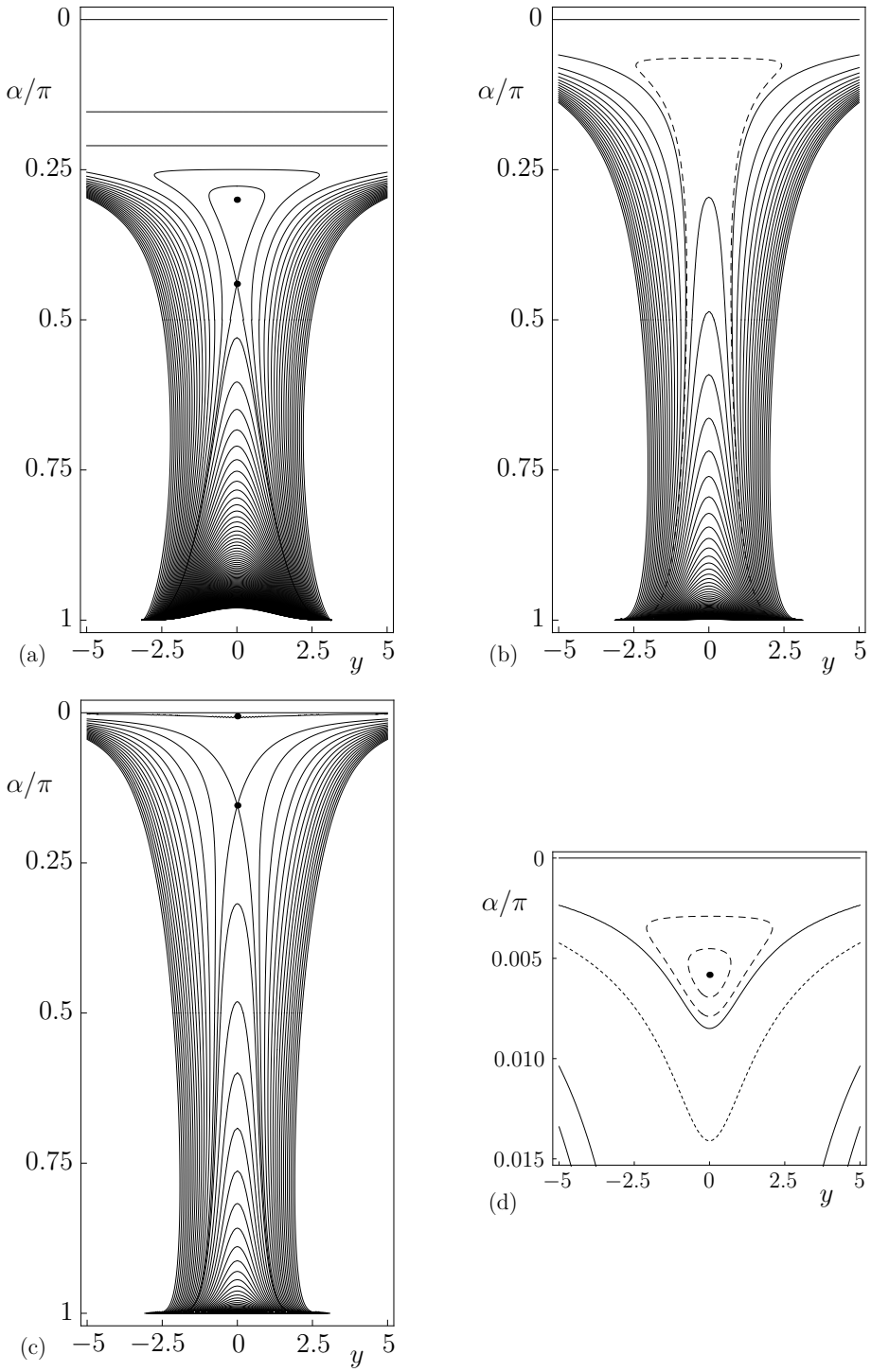

Figure 2.14: Contour plots of the free surface profile h in the $(y, \alpha/\pi)$ plane in the cases (a) $N = 1/5$, (b) $N = 1$, and (c) $N = 2$, for $\bar{Q} = 1$. In each case the contours are drawn at intervals of $1/16$, up to a maximum $h = 8$. The local maximum and the saddle point of h, at $(y, \alpha/\pi, h_{\rm m}) \simeq (0, 0.30000, 1.24313)$ and $(y, \alpha/\pi, h_{\rm m}) \simeq (0, 0.44011, 1.22739)$ in (a), and at $(y, \alpha/\pi, h_{\rm m}) \simeq (0, 0.00582, 1.00005)$ and $(y, \alpha/\pi, h_{\rm m}) \simeq (0, 0.15436, 0.97288)$ in (c), are marked with dots, and the contour that passes through the saddle point is also included. Part (d) shows an enlargement of (c) near the top of the cylinder, with additional contours $h = 1.00002$ and $h = 1.00004$ (shown dashed) and $h = 0.9995$ (shown dotted). In (b), h has no stationary points; an additional contour $h = 1.01$ is included (shown dashed).

with $\bar{Q} = 1 > \bar{Q}_c(1) \simeq 0.81741$, and so h has no stationary points; an additional contour $h = 1.01$ is included (shown dashed) to illustrate the general form of the contours near the top of the cylinder. In all cases, since $h_m \to \infty$ in the limit $\alpha \to \pi^-$, there should, in principle, be infinitely many contours near the bottom of the cylinder, but only contours up to $h = 8$ are plotted. Note also that near the top of the cylinder in Figure 2.14(a) the rivulet is wide and the free surface profile is relatively flat (that is, h varies only slowly with α/π and with y away from the contact lines, as in Figure 2.12(a)), explaining why there are so few contours there.

Velocity profiles and contours of the velocity in cross-sections of the rivulet at different α, as well as the maximum velocity u_{max}, are qualitatively similar to those in the case $\alpha = \pi/2$ shown in Figures 2.6–2.8, and so, for brevity, are not reproduced here.

2.2.3 The Limits of Small and Large Flux $\bar{Q}$

In the limit of small flux, $\bar{Q} \to 0^+$, equations (2.15) with $Q = \bar{Q}$, (2.16), $(2.10)_2$ and (2.20), show that the rivulet becomes narrow and shallow according to

$$a \sim 2h_m \sim 2\left(\frac{9^N \bar{Q}^N}{\lambda_N^N \sin\alpha}\right)^{\frac{1}{3N+1}} = O\left(\bar{Q}^{\frac{N}{3N+1}}\right) \to 0^+; \tag{2.38}$$

also the position of the minimum of a approaches $\alpha = \pi/2^+$, and the positions of the maximum and minimum of h_m approach $\alpha = 0$ and $\alpha = \pi/2^-$, respectively.

In the limit of large flux, $\bar{Q} \to \infty$, equations (2.15) with $Q = \bar{Q}$, (2.16), $(2.10)_1$, and (2.21), show that the rivulet becomes infinitely wide on the upper half of the cylinder and infinitely thick on the lower half of the cylinder according to

$$a \sim \frac{(2N+1)\bar{Q}}{2N}\left(\frac{m^{2N+1}}{\sin\alpha}\right)^{\frac{1}{N}} = O\left(\bar{Q}\right) \to \infty, \qquad h_m \to \frac{1}{m} = O(1) \tag{2.39}$$

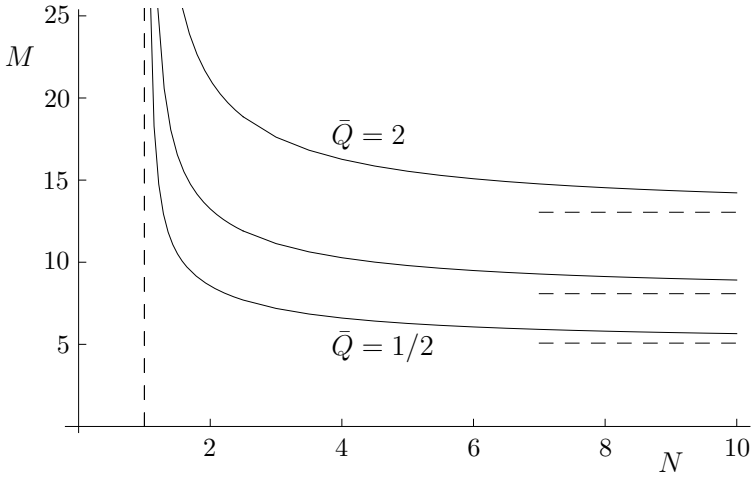

Figure 2.15: Plot of the mass of the rivulet, M, given by (2.42) as a function of N, in the cases $\bar{Q} = 1/2$, 1 and 2. The horizontal dashed lines show the constant asymptotic values in the limit $N \to \infty$. The vertical dashed line shows the value $N = 1$, at and below which the mass is infinite.

for $0 < \alpha < \pi/2$,

$$a = 2h_{\mathrm{m}} = 2\left(\frac{9\bar{Q}}{\lambda_N}\right)^{\frac{N}{3N+1}} = O\left(\bar{Q}^{\frac{N}{3N+1}}\right) \to \infty \tag{2.40}$$

at $\alpha = \pi/2$, and equations (2.15) with $Q = \bar{Q}$, (2.16), $(2.10)_3$, and (2.22), together with h_{m} satisfies $h_{\mathrm{m}} = \tan(ma/2)/m \simeq 2/\pi - a$, lead to

$$a \to \frac{\pi}{m} = O(1), \qquad h_{\mathrm{m}} \sim \kappa_N \left(\frac{m^N \bar{Q}^N}{\sin\alpha}\right)^{\frac{1}{2N+1}} = O\left(\bar{Q}^{\frac{N}{2N+1}}\right) \to \infty \tag{2.41}$$

for $\pi/2 < \alpha < \pi$; also the position of the minimum of a approaches $\alpha = \pi^-$.

2.2.4 The Mass of the Rivulet, M

The mass of the rivulet, denoted by M and non-dimensionalised with $\rho\beta\ell^2 R$, is given by

$$M = \int_0^{\pi}\int_{-a}^{a} h \,\mathrm{d}y \,\mathrm{d}\alpha = \int_0^{\frac{\pi}{2}} \frac{2(ma\coth ma - 1)}{m^2}\,\mathrm{d}\alpha + \int_{\frac{\pi}{2}}^{\pi} \frac{2(1 - ma\cot ma)}{m^2}\,\mathrm{d}\alpha. \tag{2.42}$$

Both of the integrands in (2.42) are finite at $\alpha = \pi/2$. The second integrand is singular like $O((\pi-\alpha)^{-1/(2N+1)})$ as $\alpha \to \pi^-$ (*i.e.* near the bottom of the cylinder) and hence is integrable there; however, the first integrand is singular like $O(\alpha^{-1/N})$ as $\alpha \to 0^+$ (*i.e.* near the top of the cylinder) and so this integral is divergent if $N \leq 1$ but is convergent if $N > 1$, showing that the mass is theoretically infinite in the Newtonian case $N = 1$ and in the shear-thinning case $N < 1$, but that it is finite in the shear-thickening case $N > 1$. In other words, the finite mass in the case $N > 1$ is due to the slower divergence of the width of the rivulet at the top of the cylinder than in the case $N \leq 1$. Figure 2.15 shows a plot of M as a function of N for various values of $\bar{Q}$, confirming this behaviour and showing that M decreases monotonically from ∞ to a (nonzero) $\bar{Q}$-dependent constant asymptotic value (determined by (2.15), (2.26) and (2.42)) in the limit $N \to \infty$.

2.3 Conclusions

In order to begin to rectify the lack of understanding of non-Newtonian rivulet flow, we considered locally unidirectional steady gravity-driven flow of a thin rivulet of a power-law fluid with prescribed volume flux $\bar{Q}$ down a locally planar substrate. In Section 2.1.2 we obtained the solution for unidirectional flow of a uniform rivulet down a planar substrate, and then in Section 2.2 we used it to obtain the solution for a slowly varying rivulet with prescribed constant (nonzero) contact angle β down a slowly varying substrate, specifically flow in the azimuthal direction around the outside of a large horizontal circular cylinder.

As in the special case of a Newtonian fluid, the rivulet is always wide and of finite thickness near the top of the cylinder, but is thick and of finite width near the bottom of the cylinder. In addition, the minimum width of the rivulet always occurs on the lower half of the cylinder, whereas the maximum thickness h_{m} either increases monotonically with the angle α measured around the cylinder

(if $\bar{Q} \geq \bar{Q}_c$), or it has a maximum and then a minimum on the upper half of the cylinder (if $\bar{Q} < \bar{Q}_c$).

The solution was shown to depend strongly on the value of the power-law index of the fluid. For example, as Figures 2.6(a) and 2.7(a) illustrate, a rivulet of strongly shear-thinning fluid self-channels its flow down a narrow central channel between two levées of slowly moving fluid that form at its sides, and in the central channel there is a plug-like flow at each y position except in a boundary layer near the substrate. On the other hand, as Figures 2.6(b) and 2.7(b) illustrate, in a rivulet of a strongly shear-thickening fluid the velocity profile is linear in z except in a boundary layer near the free surface. Another notable qualitative departure from Newtonian behaviour is that, as Figures 2.15 shows, whereas the mass of a rivulet of a Newtonian or a shear-thinning fluid is theoretically infinite, the mass of a rivulet of a shear-thickening fluid is finite.

In the present work we have compared rivulets with the same or different values of the dimensionless prescribed flux $\bar{Q}$. Since the scaling of the volume flux in (2.6) involves N, a prescribed value of $\bar{Q}$ would, in general, correspond to different values of the dimensional prescribed flux for different fluids (that is, for different values of N). However, solutions for rivulets of different power-law fluids with the same prescribed value of the dimensional flux may readily be obtained from the present solution once the values of the parameters ρ, μ_N, γ and β for the different fluids are specified.

As well as being of interest in their own right, the present results provide a benchmark for the study of rivulet flow of more realistic (and hence more mathematically complicated) non-Newtonian fluids.

Chapter 3

Pinning and Depinning of a Rivulet of a Power-Law Fluid Draining Down a Slowly Varying Substrate

In this Chapter we use the solution for unidirectional flow of a thin uniform rivulet of a power-law fluid obtained in Subsection 2.1.2 to describe the flow of a rivulet with prescribed constant semi-width (*i.e.* with pinned contact lines) but slowly varying contact angle down a slowly varying substrate, specifically the flow in the azimuthal direction around the outside of a large horizontal circular cylinder. Pinned contact lines are likely to occur when the substrate is relatively rough, and rivulets with constant width may result from the manner in which the fluid is initially deposited onto the substrate (*e.g.* rapid pouring onto the substrate) and/or the texture of the substrate (*e.g.* a smooth stripe on a rough substrate). The work in this Chapter generalises that of Paterson *et al.* [97] for the case of Newtonian fluid, as described in Sections 1.6 and 1.7.3, to a corresponding analysis for a power-law fluid. In particular, the corresponding solution for a

rivulet of a perfectly wetting fluid, which can never have constant prescribed semi-width, is obtained, and we show that the global behaviour of a rivulet of non-perfectly wetting fluid with prescribed semi-width but slowly varying contact angle is qualitatively very different from that described in Chapter 2.

3.1 Rivulet Flow Down a Planar Substrate

As in Section 2.1, we start by considering briefly unidirectional steady gravity-driven flow of a thin uniform rivulet of a power-law fluid with prescribed volume flux down a planar substrate inclined at an angle α ($0 \leq \alpha \leq \pi$) to the horizontal. The free surface of the rivulet is denoted by $z = h$, the semi-width of the rivulet by a, and the contact angle by β (≥ 0). We adopt the the same setup as in Section 2.1 (see Figure 2.1), but now we non-dimensionalise and scale the variables by writing

$$\begin{gathered} y = \ell y^*, \quad a = \ell a^*, \quad z = \epsilon \ell z^*, \quad h = \epsilon \ell h^*, \quad \beta = \epsilon \beta^*, \\ u = U u^*, \quad p = p_a + \rho g \epsilon \ell p^*, \quad q = \frac{U}{\epsilon \ell} q^*, \quad \mu = \bar{\mu} \mu^*, \quad Q = \epsilon \ell^2 U Q^*, \end{gathered} \tag{3.1}$$

where $\ell = (\gamma/\rho g)^{1/2}$ is the capillary length, in which γ is the coefficient of surface tension of the fluid, ϵ ($\ll 1$) is the transverse aspect ratio, $U = (\rho g \epsilon^{N+1} \ell^{N+1}/\mu_N)^{1/N}$ is the appropriate velocity scale, p_a is the atmospheric pressure, $\bar{\mu} = \mu_N (U/\epsilon\ell)^{N-1} = (\mu_N (\rho g \epsilon \ell)^{N-1})^{1/N}$ is the appropriate viscosity scale, and Q is the volume flux of fluid along the rivulet. In general, there is some freedom in the definition of ϵ. In this Chapter it is most convenient to define ϵ in terms of the prescribed value of the flux, $Q = \bar{Q}$, according to $\epsilon = (\mu_N \bar{Q}^N/\rho g \ell^{3N+1})^{1/(2N+1)}$, in which case $U = (\rho g \bar{Q}^{N+1}/\mu_N \ell^{N+1})^{1/(2N+1)}$, corresponding to taking $\bar{Q}^* = 1$ without loss of generality. In particular, equation (3.1) then shows that the thickness of the rivulet varies with the volume flux according to simply $h \propto \bar{Q}^{N/(2N+1)}$. Note that a different choice of ϵ, namely $\epsilon = \beta$, in which case $U = (\rho g \beta^{N+1} \ell^{N+1}/\mu_N)^{1/N}$,

corresponding to taking $\beta^* = 1$ without loss of generality, was taken in Chapter 2. From now on we use non-dimensional quantities (with the stars omitted, for clarity).

It may be shown straightforwardly that, at leading order in ϵ, the velocity is again due to a longitudinal balance of gravity and viscous effects and is of the form $\mathbf{u} = u(y,z)\mathbf{i}$ given by (2.11), the pressure $p = p(y,z)$ is given by (2.7), and the cross-sectional free surface profile $h = h(y)$ is given by (2.9), where we have defined $m = \sqrt{|\cos\alpha|}$ and a prime denotes differentiation with respect to y. The volume flux of fluid along the rivulet is given by (2.14).

3.2 Rivulet Flow Down a Slowly Varying Substrate

As discussed in Chapter 2, equations (2.11)–(2.14), describing the unidirectional flow of a uniform rivulet down a planar substrate, also provide the leading order description of the locally unidirectional flow of a slowly varying rivulet down a slowly varying substrate. It is rivulets of this type that we consider in this Chapter (although other interpretations are, of course, also possible). Specifically, we again consider the situation in which both the azimuthal aspect ratio, $\ell/R \ll \epsilon$, and the appropriately defined reduced Reynolds number, $\rho\gamma\epsilon^4\ell^2/\bar{\mu}^2 R \ll 1$, are sufficiently small, where R is the radius of the cylinder. Again, both of these conditions are satisfied if the cylinder is sufficiently large.

Figure 3.1 shows a sketch of such a situation, namely a narrow slowly varying rivulet with prescribed flux $Q = \bar{Q}$ $(= 1)$ with prescribed constant semi-width $a = \bar{a}$ $(< \pi)$ and slowly varying contact angle β (> 0) (*i.e.* pinned contact lines all the way around the cylinder) draining from the top $(\alpha = 0)$ to the bottom $(\alpha = \pi)$; it is rivulet flow of this general type that we describe in this Chapter. Figure 3.1, showing a rivulet of fixed width but varying contact angle, may be

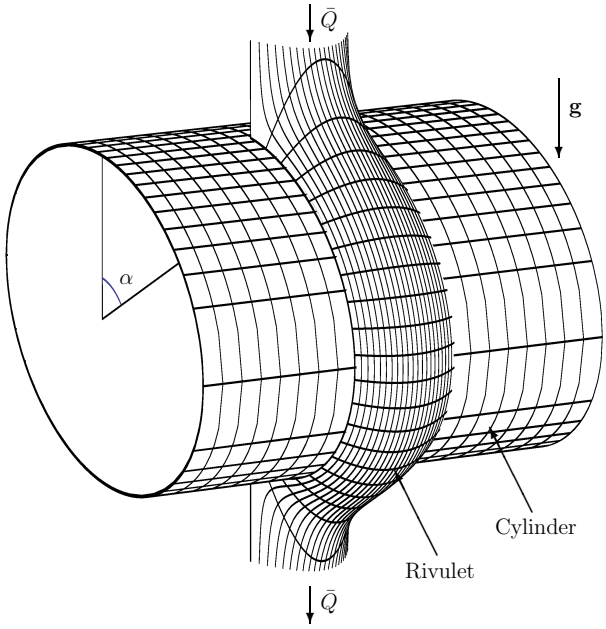

Figure 3.1: Sketch of a narrow slowly varying rivulet with prescribed flux $Q = \bar{Q}$ $(= 1)$ with prescribed constant semi-width $a = \bar{a}$ $(< \pi)$ and slowly varying contact angle β (> 0) draining from the top $(\alpha = 0)$ to the bottom $(\alpha = \pi)$ of a large horizontal cylinder.

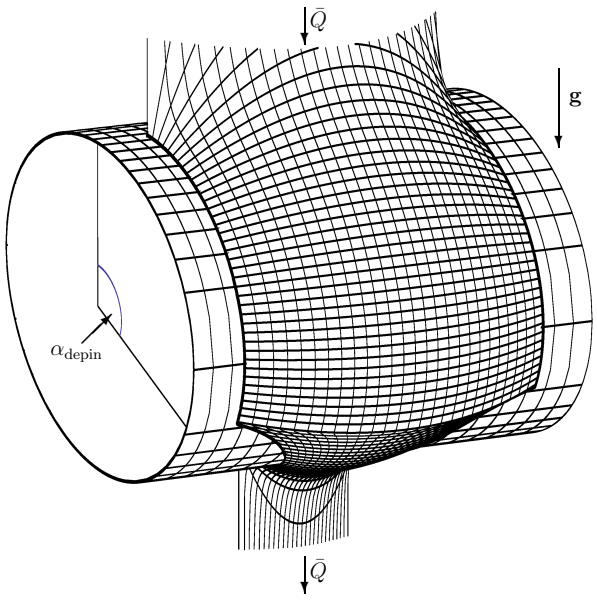

Figure 3.2: As in Figure 3.1, except for a wide rivulet with prescribed constant semi-width $a = \bar{a}$ $(> \pi)$ and slowly varying contact angle β in $0 \leq \alpha \leq \alpha_{\text{depin}}$, but with zero contact angle $\beta = 0$ and slowly varying semi-width $a = \pi/m$ $(\pi \leq a \leq \bar{a})$ in $\alpha_{\text{depin}} \leq \alpha \leq \pi$.

contrasted with Figure 2.9, showing a rivulet of fixed contact angle but varying width.

As discussed in Subsection1.7.3, Paterson *et al.* [97] showed that a rivulet of Newtonian fluid can have constant width all the way around the cylinder only if the rivulet is sufficiently narrow (specifically only if $\bar{a} \leq \pi$), and that for a wider rivulet (specifically for $\bar{a} > \pi$) there is a critical value of α on the lower half of the cylinder, denoted by α_{depin} ($\pi/2 < \alpha_{\text{depin}} < \pi$) and given by

$$\alpha_{\text{depin}} = \cos^{-1}\left(-\frac{\pi^2}{\bar{a}^2}\right) \quad \text{for} \quad \bar{a} > \pi, \tag{3.2}$$

at which the contact angle is equal to zero, $\beta = 0$, and beyond which there is no physically realisable solution with constant width $a = \bar{a}$. For their problem, Paterson *et al.* [97] assumed that the contact lines de-pin at $\alpha = \alpha_{\text{depin}}$ and that thereafter the rivulet drains from $\alpha = \alpha_{\text{depin}}$ to the bottom of the cylinder with zero contact angle $\beta = 0$ and slowly varying semi-width a. [Of course, this behaviour is a special case of the more general scenario in which a rivulet with prescribed constant width de-pins and possibly re-pins at a prescribed non-zero value of the contact angle. This situation was also analysed by Paterson *et al.* [97] for a Newtonian fluid, but for brevity is not pursued here.] Since (3.2) does not depend on viscous effects, it also holds for the present case of a power-law fluid (and indeed, for any generalised Newtonian fluid), and hence the same de-pinning of a wide rivulet occurs in the present problem. Figure 3.2 shows a sketch of such a situation, namely a wide rivulet with prescribed constant semi-width $a = \bar{a}$ ($> \pi$) and slowly varying contact angle β in $0 \leq \alpha \leq \alpha_{\text{depin}}$ (*i.e.* pinned contact lines on the upper part of the cylinder), but with zero contact angle $\beta = 0$ and slowly varying semi-width $a = \pi/m$ ($\pi \leq a \leq \bar{a}$) in $\alpha_{\text{depin}} \leq \alpha \leq \pi$ (*i.e.* de-pinned contact lines on the lower part of the cylinder). Thus in Section 3.3 we obtain the solution for the special case of a rivulet of a perfectly wetting power-law fluid

(*i.e.* a rivulet with zero contact angle, $\beta = 0$), and then in Section 3.4 we use this solution, together with the solution previously obtained in Chapter 2 for the general case of a rivulet of a non-perfectly wetting power-law fluid, to provide the complete description of the rivulets sketched in Figures 3.1 and 3.2.

3.3 A Rivulet of a Perfectly Wetting Fluid ($\beta = 0$)

In the special case of a perfectly wetting fluid ($\beta = 0$) equations (2.8) and (2.4) have no solution for h on the upper half of the cylinder (*i.e.* for $0 \leq \alpha \leq \pi/2$), but on the lower half (*i.e.* for $\pi/2 < \alpha \leq \pi$) they have the simple solution

$$a = \frac{\pi}{m}, \qquad h = \frac{h_{\mathrm{m}}}{2}\left(1 + \cos my\right), \tag{3.3}$$

where h_{m} denotes the (as yet unknown) maximum thickness of the rivulet, which occurs at $y = 0$. In particular, the solution (3.3) shows that the semi-width a varies with α (*i.e.* that a slowly varying rivulet of a perfectly wetting fluid can never have constant semi-width). The maximum velocity, denoted by $u_{\max}$, occurs at $y = 0$ and $z = h_{\mathrm{m}}$ and is again given by (2.12).

To complete the solution we must determine h_{m} appearing in (3.3). Performing the quadrature in (2.14) with h given by (3.3) we find that the flux Q is given by

$$Q = \frac{2\sqrt{\pi}N\,\Gamma\left(\dfrac{5N+2}{2N}\right)}{(2N+1)\Gamma\left(\dfrac{3N+1}{N}\right)}\frac{(\sin\alpha)^{\frac{1}{N}}}{m}h_{\mathrm{m}}^{\frac{2N+1}{N}} = \frac{2N}{2N+1}\,\mathrm{B}\left(\frac{1}{2},\frac{5N+2}{2N}\right)\frac{(\sin\alpha)^{\frac{1}{N}}}{m}h_{\mathrm{m}}^{\frac{2N+1}{N}}, \tag{3.4}$$

where Γ and B again denote Gamma and Beta functions, respectively. Prescribing

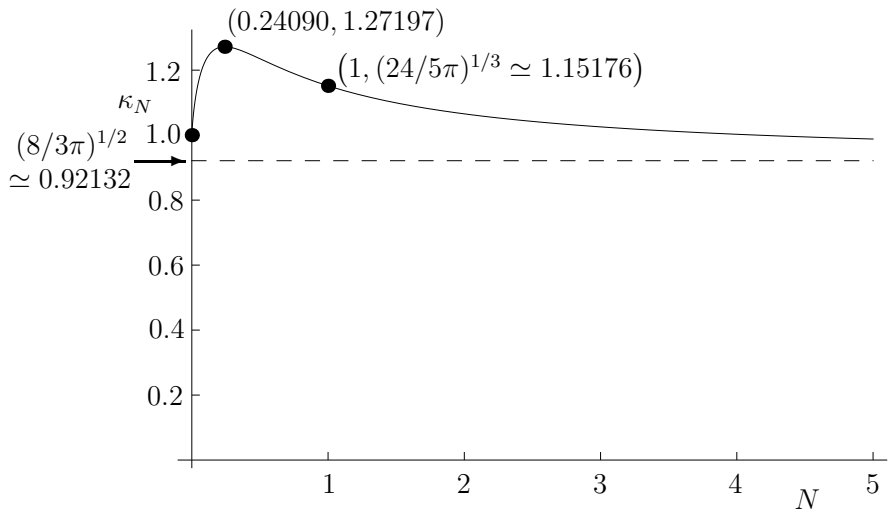

Figure 3.3: Plot of κ_N given by (3.6) as a function of N, together with its asymptotic value $(8/3\pi)^{1/2} \simeq 0.92132$ in the limit $N \to \infty$.

the value of the flux to be $Q = \bar{Q} = 1$ yields

$$h_{\mathrm{m}} = \kappa_N \left(\frac{m^N}{\sin \alpha} \right)^{\frac{1}{2N+1}}, \tag{3.5}$$

where we have introduced κ_N defined by

$$\kappa_N = \left(\frac{(2N+1)\Gamma\left(\dfrac{3N+1}{N}\right)}{2\sqrt{\pi} N \, \Gamma\left(\dfrac{5N+2}{2N}\right)} \right)^{\frac{N}{2N+1}} = \left[\frac{2N}{2N+1} \, \mathrm{B}\left(\frac{1}{2}, \frac{5N+2}{2N} \right) \right]^{-\frac{N}{2N+1}}. \tag{3.6}$$

Equations (3.3) and (3.5) show that, although both a and the form of the cross-sectional free surface profile of the rivulet are independent of N, its size (and, in particular, its maximum thickness h_{m}) depends on N via the flux. Figure 3.3 shows a plot of κ_N given by (3.6) as a function of N, and illustrates that κ_N satisfies

$$\kappa_N = 1 - \frac{1}{2} \log\left(4\pi N^3\right) N + O(N \log N)^2 \to 1^+ \tag{3.7}$$

as $N \to 0^+$, increases to a maximum 1.27197 at $N \simeq 0.24090$, takes the value

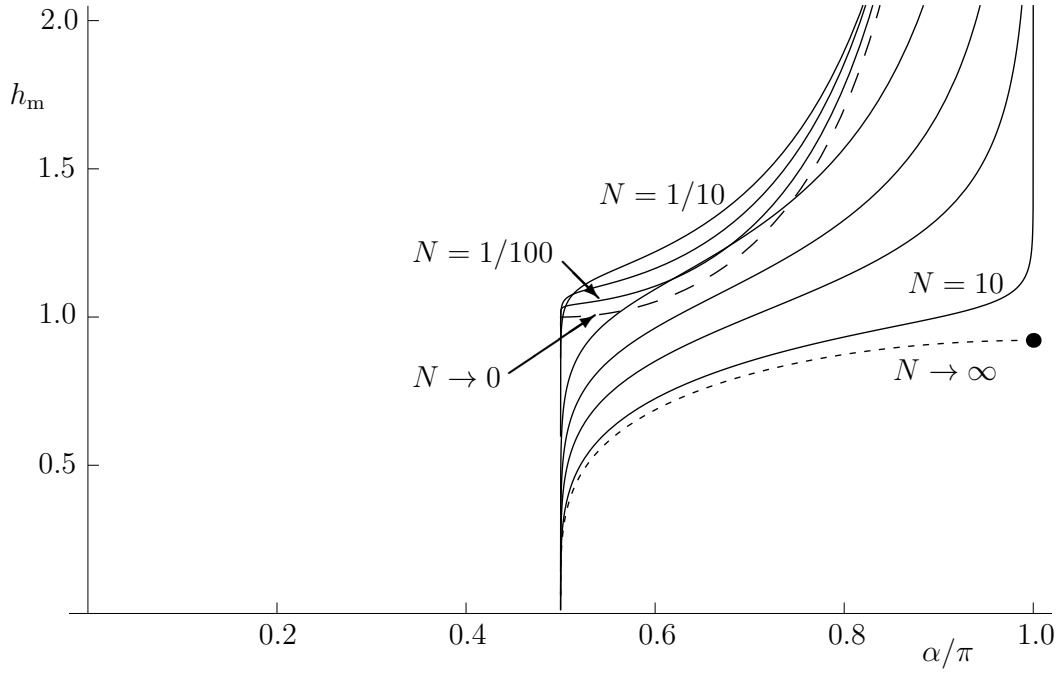

Figure 3.4: Plots of the maximum thickness $h_{\rm m}$ of a rivulet of a perfectly wetting fluid given by (3.5) as a function of α/π for $N = 1/100$, $1/30$, $1/10$, $1/2$, 1, 2 and 10, together with the asymptotic solutions $h_{\rm m} \sim 1/\sin\alpha$ in the limit $N \to 0^+$ (dashed curve), and $h_{\rm m} \sim (8/3\pi)^{1/2}(-\cos\alpha)^{1/4}$ in the limit $N \to \infty$ (dotted curve).

$(24/5\pi)^{1/3} \simeq 1.15176$ at $N = 1$, and thereafter decreases monotonically, satisfying

$$\kappa_N = \left(\frac{8}{3\pi}\right)^{1/2}\left[1 + \frac{3\ln 6\pi - 4}{12N} + O\left(\frac{1}{N^2}\right)\right] \to \left(\frac{8}{3\pi}\right)^{1/2+} \simeq 0.92132^+ \qquad (3.8)$$

as $N \to \infty$. In particular, when $N = 1$ equation (3.5) reduces to the solution in the special case of a Newtonian fluid given by Wilson and Duffy [131], namely $h_{\rm m} = (24m/(5\pi\sin\alpha))^{1/3}$.

Figure 3.4 shows plots of $h_{\rm m}$ given by (3.5) as a function of α/π for a range of values of N, illustrating that in all cases $h_{\rm m}$ increases monotonically with α, and that the rivulet becomes wide and shallow at the middle of the cylinder according to

$$h_{\rm m} \sim \kappa_N\left(\alpha - \frac{\pi}{2}\right)^{\frac{N}{2(2N+1)}} \to 0^+, \qquad a \sim \pi\left(\alpha - \frac{\pi}{2}\right)^{-\frac{1}{2}} \to \infty \qquad (3.9)$$

in the limit $\alpha \to \pi/2^+$, and that it becomes thick and of finite width near the

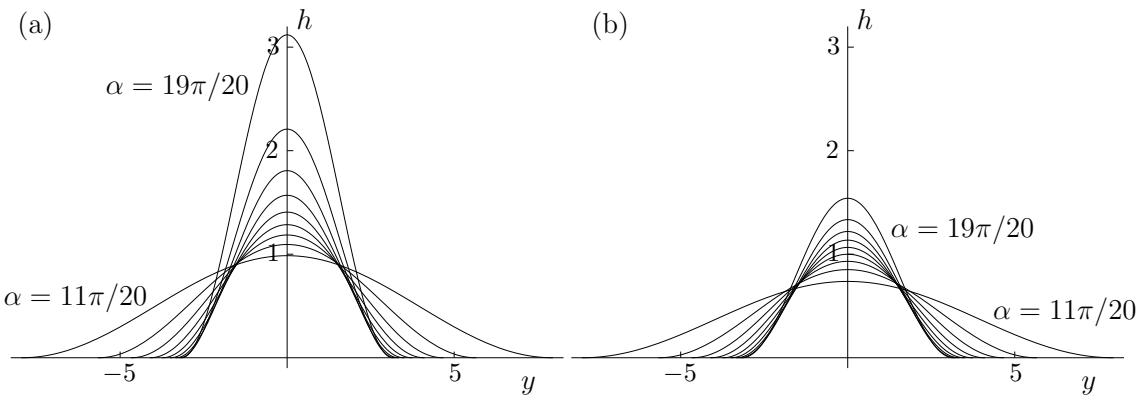

Figure 3.5: Plots of the cross-sectional free surface profile h of a rivulet of a perfectly wetting fluid given by (3.3) as a function of y at $\alpha = 11\pi/20, 12\pi/20, \ldots, 19\pi/20$ for (a) $N = 1/2$ and (b) $N = 2$.

bottom of the cylinder according to

$$h_{\mathrm{m}} \sim \kappa_N \left(\pi - \alpha\right)^{-\frac{1}{2N+1}} \to \infty, \qquad a = \pi + \frac{\pi}{4}\left(\alpha - \pi\right)^2 + O\left(\alpha - \pi\right)^4 \to \pi^+ \quad (3.10)$$

in the limit $\alpha \to \pi^-$. Furthermore, $h_{\mathrm{m}} \sim 1/\sin\alpha$ in the limit of a strongly shear-thinning fluid, $N \to 0^+$, and $h_{\mathrm{m}} \sim (8/3\pi)^{1/2}(-\cos\alpha)^{1/4}$ in the limit of a strongly shear-thickening fluid, $N \to \infty$; these asymptotic solutions are also included in Figure 3.4. Figure 3.4 also shows that the variation of h_{m} is not monotonic in N, in the sense that at any fixed value of α, h_{m} increases with N to a maximum value, and thereafter decreases monotonically with N.

Figure 3.5 shows plots of h given by (3.3) as a function of y at various stations around the cylinder for $N = 1/2$ and $N = 2$, and Figure 3.6 shows contour plots of h in the $(y, \alpha/\pi)$ plane for the same values of N. In particular, Figures 3.5 and 3.6 illustrate that the forms of the rivulets for different values of N are qualitatively similar. Figure 3.6 also shows that there are solutions for h only on the lower half of the cylinder, which is different from Figure 2.14 which shows that those solutions for h are valid from the top to the bottom of the cylinder.

Figure 3.7 shows contour plots of the velocity u given by (2.11) when $\alpha = 3\pi/4$ for $N = 1/10$ and $N = 10$, and shows that in the limits $N \to 0$ and $N \to \infty$ the velocity has the same qualitative behaviour as that described in Chapter 2 for

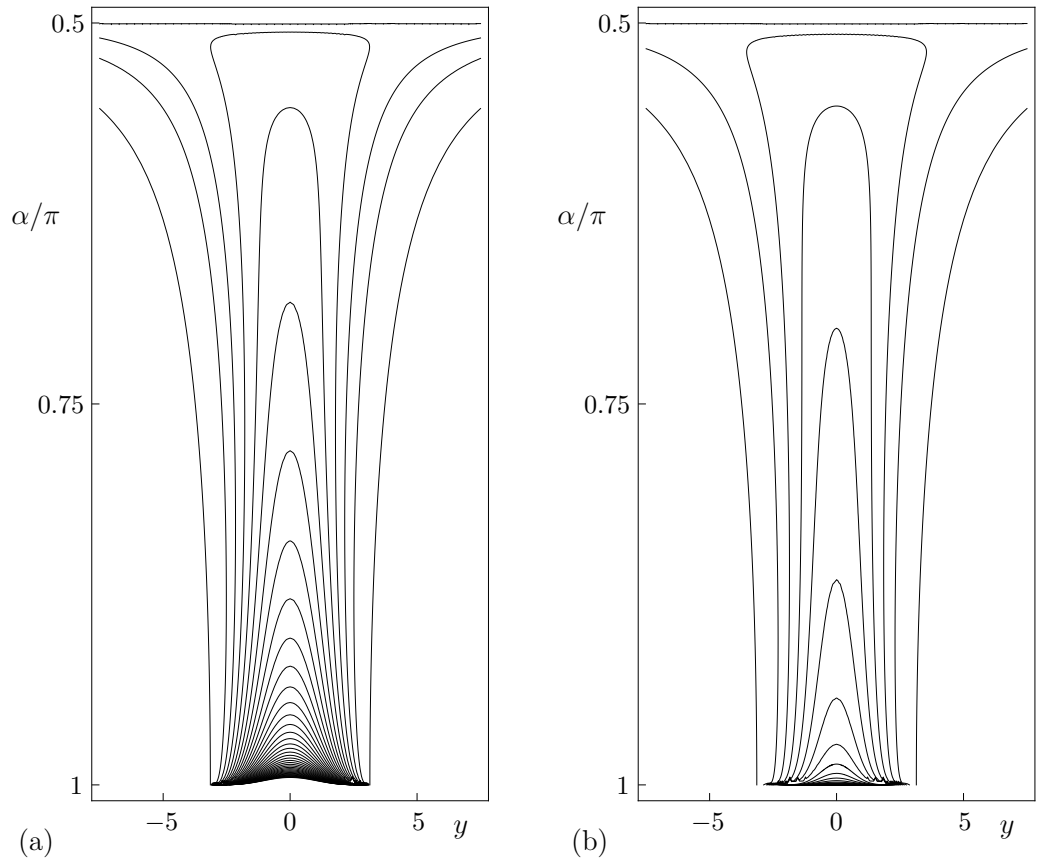

Figure 3.6: Contour plots of the free surface h of a rivulet of a perfectly wetting fluid given by (3.3) in the $(y, \alpha/\pi)$ plane for (a) $N = 1/2$ and (b) $N = 2$. The contours are drawn at intervals of $1/4$ up to a maximum value of $h = 10$ in both cases.

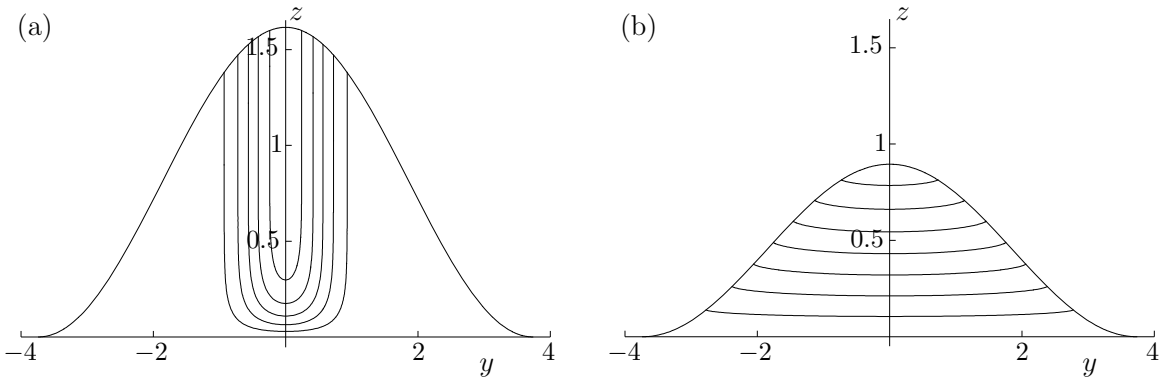

Figure 3.7: Contour plots of the velocity u of a rivulet of a perfectly wetting fluid given by (2.11) when $\alpha = 3\pi/4$ (in which case $a = \pi/m \simeq 3.73600$) for (a) $N = 1/10$ (for which $h_{\mathrm{m}} \simeq 1.61671$) and (b) $N = 10$ (for which $h_{\mathrm{m}} \simeq 0.89530$). The contour interval is 0.1 in both parts of the Figure.

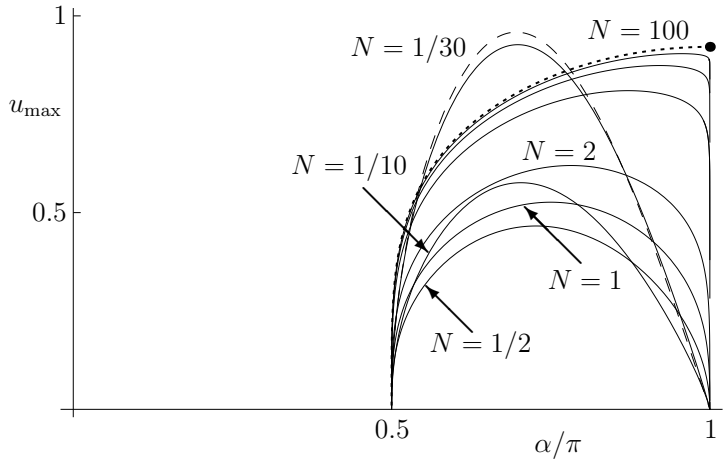

Figure 3.8: Plot of the maximum velocity $u_{\max}$ of a rivulet of a perfectly wetting fluid given by (3.13) as a function of α/π for $N = 1/30$, 1/10, 1/2, 1, 2, 10, 30 and 100, together with the asymptotic solutions $u_{\max} \sim m \sin\alpha/(2\sqrt{\pi N})$ in the limit $N \to 0$, drawn for the case $N = 1/30$ (dashed curve), and $u_{\max} = (8m/3\pi)^{1/2}$ in the limit $N \to \infty$ (dotted curve).

a rivulet of a non-perfectly wetting fluid. In particular, Figure 3.7(a) illustrates that in the limit $N \to 0$ equations (2.11), (3.3), (3.5) and (3.6), with ${\kappa_N}^{(N+1)/N} \sim 1/2\sqrt{\pi N}$, lead to

$$u \sim Nh(h\sin\alpha)^{\frac{1}{N}} \sim \frac{m\sin\alpha}{2\sqrt{\pi N}}\left(\frac{1+\cos my}{2}\right)^{\frac{1+N}{N}} \tag{3.11}$$

except in a narrow boundary layer near the substrate, and hence that the flow "self-channels" down a narrow central channel defined by $h > 1/\sin\alpha$ with semi-width

$$\frac{1}{m}\left(2N\log\frac{m^2\sin^4\alpha}{4\pi N^3}\right)^{\frac{1}{2}} \ (\ll 1) \tag{3.12}$$

between two "levées" of slowly moving fluid. In deriving (3.12) we have made use of the results $h_{\rm m}\sin\alpha \sim 1 + N\log(m\sin^2\alpha/2\sqrt{\pi}N^{3/2})$ and $(h_{\rm m}/2)(1+\cos my) \to 1/\sin\alpha$ in the limit $N \to 0$, so that $1+\cos my$ in (3.11) satisfies $1+\cos my \sim 2 - 2N\log(m\sin^2\alpha/2\sqrt{\pi}N^{3/2})$, together with $\cos my \sim 1 - m^2y^2/2$. In the particular case shown in Figure 3.7(a) the channel is defined by $h > \sqrt{2} \simeq 1.41421$ and has semi-width 0.86475. On the other hand, Figure 3.7(b) illustrates that in the limit $N \to \infty$ there is a simple linear velocity profile $u \sim z$ except in a narrow

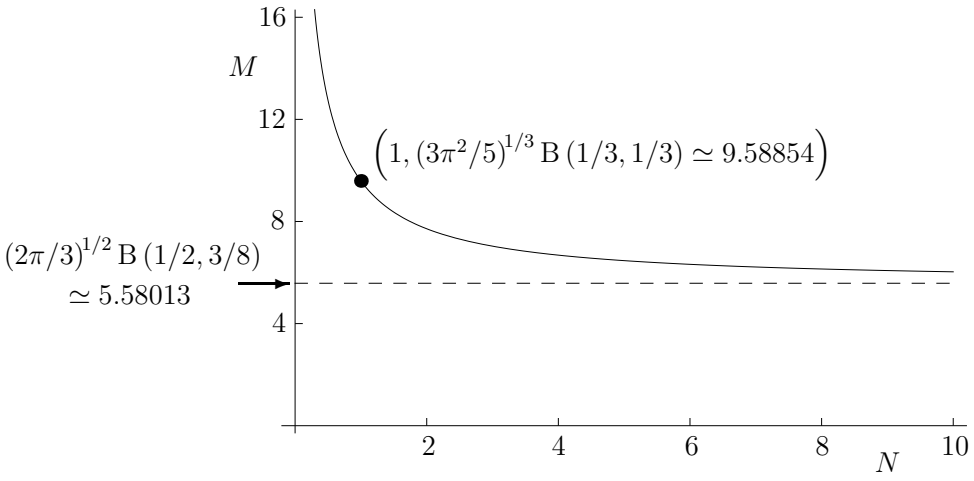

Figure 3.9: Plot of the mass of a rivulet of a perfectly wetting fluid, M, given by (3.15) as a function of N, together with its asymptotic value $(2\pi/3)^{1/2}\,\mathrm{B}(1/2,3/8) \simeq 5.58013$ in the limit $N \to \infty$.

boundary layer near the free surface. Figure 3.8 shows a plot of $u_{\max}$, namely

$$u_{\max} = \frac{N}{N+1}(\sin\alpha)^{\frac{1}{2N+1}}\kappa_N^{\frac{N+1}{N}}\, m^{\frac{N+1}{2N+1}}, \tag{3.13}$$

as a function of α/π for a range of values of N, showing that $u_{\max}$ varies non-monotonically with both α and N. In particular, for any fixed value of N, $u_{\max}$ increases from zero at $\alpha = \pi/2$ to a maximum value, and then decreases back to zero at $\alpha = \pi$, while at any fixed value of α, $u_{\max}$ decreases from ∞ (specifically, $u_{\max} \sim m\sin\alpha/(2\sqrt{\pi N}) \to \infty$ as $N \to 0^+$) to a minimum value, and then increases to $(8m/3\pi)^{1/2}$ as $N \to \infty$, taking the value $u_{\max} = 2(9m^2\sin\alpha/(25\pi^2))^{1/3}$ when $N = 1$; these asymptotic solutions (the former drawn for the case $N = 1/30$) are also included in Figure 3.8.

3.3.1 The Mass of the Rivulet, M

The mass of the rivulet, denoted by M and non-dimensionalised by $\rho\epsilon\ell^2 R$, where R is the radius of the cylinder, is given by

$$M = \int_{\pi/2}^{\pi}\int_{-a}^{a} h\,\mathrm{d}y\,\mathrm{d}\alpha = \int_{\pi/2}^{\pi} \frac{\pi h_{\mathrm{m}}}{m}\,\mathrm{d}\alpha = \pi\kappa_N \int_{\pi/2}^{\pi} \left((-\cos\alpha)^{\frac{N+1}{2}}\sin\alpha\right)^{-\frac{1}{2N+1}}\mathrm{d}\alpha, \tag{3.14}$$

leading to

$$M = \frac{\pi}{2}\kappa_N\,\mathrm{B}\left(\frac{N}{2N+1}, \frac{3N+1}{4(2N+1)}\right). \tag{3.15}$$

Figure 3.9 shows a plot of M as a function of N, illustrating that M decreases monotonically with N, satisfying $M \sim \pi/(2N) \to \infty$ in the limit $N \to 0^+$, $M = (3\pi^2/5)^{1/3}\,\mathrm{B}(1/3,1/3) \simeq 9.58854$ when $N = 1$ (in agreement with equations (9) and (10) of Paterson *et al.* [97]), and $M \to (2\pi/3)^{1/2}\,\mathrm{B}(1/2,3/8)^+ \simeq 5.58013^+$ in the limit $N \to \infty$.

3.4 A Rivulet of a Non-perfectly Wetting Fluid ($\beta > 0$)

In the general case of a non-perfectly wetting fluid ($\beta > 0$) the solution of (2.8) and (2.4) for h

$$h = \beta \times \begin{cases} \dfrac{\cosh ma - \cosh my}{m\sinh ma} & \text{if } \ 0 \le \alpha < \dfrac{\pi}{2}, \\ \dfrac{a^2 - y^2}{2a} & \text{if } \ \alpha = \dfrac{\pi}{2}, \\ \dfrac{\cos my - \cos ma}{m\sin ma} & \text{if } \ \dfrac{\pi}{2} < \alpha \le \pi, \end{cases} \tag{3.16}$$

which differs from (2.9) only by the factor β. The maximum thickness of the rivulet, h_{m}, is obtained by setting $y = 0$ in (3.16) which is given by (1.86). As in the special case of a perfectly wetting fluid described in Section 3.3, although

the form of the cross-sectional free surface profile of the rivulet is independent of N, its size (and, in particular, its contact angle β) depends on N via the flux, which, paralleling (2.14) in Chapter 2, is given by

$$Q = \frac{1}{9}\left(\frac{\sin\alpha\beta^{2N+1}}{m^{3N+1}}\right)^{\frac{1}{N}} f_N\left(ma\right), \tag{3.17}$$

where $f_N(ma)$ is given by (2.16) in which ${}_2F_1$ denotes the hypergeometric function, and where λ_N is given by (2.17).

Unlike in Chapter 2 where we prescribed the values of Q and β to obtain an implicit equation for the semi-width a, in this Chapter we prescribe the values of Q and a to determine the contact angle β. Specifically, setting $Q = \bar{Q} = 1$ and $a = \bar{a}$ in (3.17) yields an *explicit* expression for β, namely

$$\beta = \left(\frac{9^N m^{3N+1}}{f_N(m\bar{a})^N \sin\alpha}\right)^{\frac{1}{2N+1}}, \tag{3.18}$$

and h is then given explicitly by (3.16). We note that β (and hence the rivulet) does not have top-to-bottom symmetry. Note that (3.18) recovers (1.92) in the case $N = 1$.

In the limit $N \to 0^+$ we have

$$\beta \sim \begin{cases} \dfrac{m}{\sin\alpha}\coth\dfrac{m\bar{a}}{2} & \text{if } \ 0 \le \alpha < \dfrac{\pi}{2}, \\ \dfrac{2}{\bar{a}} & \text{if } \ \alpha = \dfrac{\pi}{2}, \\ \dfrac{m}{\sin\alpha}\cot\dfrac{m\bar{a}}{2} & \text{if } \ \dfrac{\pi}{2} < \alpha \le \pi, \end{cases} \tag{3.19}$$

and h_{m} is then given by $h_{\mathrm{m}} \sim 1/\sin\alpha$. On the other hand, in the limit $N \to \infty$ we have $f_N(ma) \to f_\infty(ma)$, where the function $f_\infty(ma)$ is given by (2.26) and hence (3.18) gives

$$\beta \sim 3\left(\frac{m^3}{f_\infty(m\bar{a})}\right)^{\frac{1}{2}}, \tag{3.20}$$

and h_{m} is then given by (1.86).

As we have already described, the behaviour is qualitatively different for a narrow rivulet with $\bar{a} \leq \pi$ and for a wide rivulet with $\bar{a} > \pi$; we shall therefore describe the behaviour of the rivulet in each of these two cases separately in the next two Subsections.

3.4.1 A Narrow Rivulet with $\bar{a} \leq \pi$

As we have already described in Section 3.2, a narrow rivulet with prescribed constant semi-width $\bar{a} \leq \pi$, as sketched in Figure 3.1, can flow all the way from the top to the bottom of the cylinder.

Figure 3.10 shows plots of β and h_{m} for a narrow rivulet with prescribed constant semi-width $\bar{a} = 2$ $(< \pi)$ as functions of α/π for a range of values of N. Figure 3.11 shows plots of h given by (3.16) for a narrow rivulet with prescribed constant semi-width $\bar{a} = 2$ $(< \pi)$ as a function of y at various stations around the cylinder for $N = 1/2$. Figures 3.10 and 3.11 illustrate that the rivulet is thick at the top and bottom of the cylinder, with both β and h_{m} becoming infinite according to

$$\begin{aligned} \beta &\sim \left(\frac{9}{f_N(\bar{a})}\right)^{\frac{N}{2N+1}} \alpha^{-\frac{1}{2N+1}} \to \infty, \\ h_{\mathrm{m}} &\sim \left(\frac{9}{f_N(\bar{a})}\right)^{\frac{N}{2N+1}} \alpha^{-\frac{1}{2N+1}} \tanh\frac{\bar{a}}{2} \to \infty \end{aligned} \tag{3.21}$$

in the limit $\alpha \to 0^+$, and

$$\begin{aligned} \beta &\sim \left(\frac{9}{f_N(\bar{a})}\right)^{\frac{N}{2N+1}} (\pi - \alpha)^{-\frac{1}{2N+1}} \to \infty, \\ h_{\mathrm{m}} &\sim \left(\frac{9}{f_N(\bar{a})}\right)^{\frac{N}{2N+1}} (\pi - \alpha)^{-\frac{1}{2N+1}} \tan\frac{\bar{a}}{2} \to \infty \end{aligned} \tag{3.22}$$

in the limit $\alpha \to \pi^-$, except in the marginal case $\bar{a} = \pi$, in which $\beta = 0$ at $\alpha = \pi$ and the rivulet becomes thick with zero contact angle and finite semi-width π

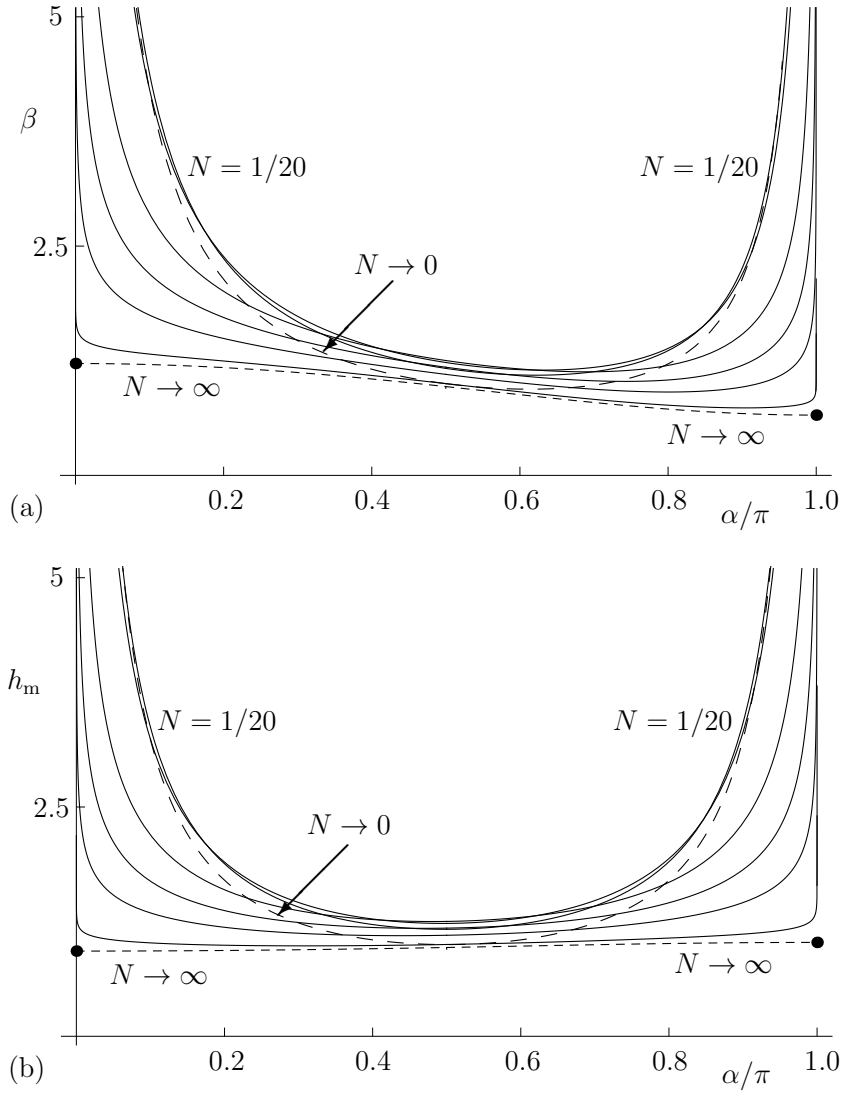

Figure 3.10: Plots of (a) the contact angle β given by (3.18) and (b) the maximum thickness $h_{\rm m}$ given by setting $y = 0$ in (3.16) of a narrow rivulet of a non-perfectly wetting fluid with prescribed constant semi-width $\bar{a} = 2$ ($< \pi$) as functions of α/π for $N = 1/20$, $1/10$, $1/2$, 1, 2 and 10, together with the asymptotic solutions (3.19) in the limit $N \to 0^+$ (dashed curves), and (3.20) in the limit $N \to \infty$ (dotted curves).

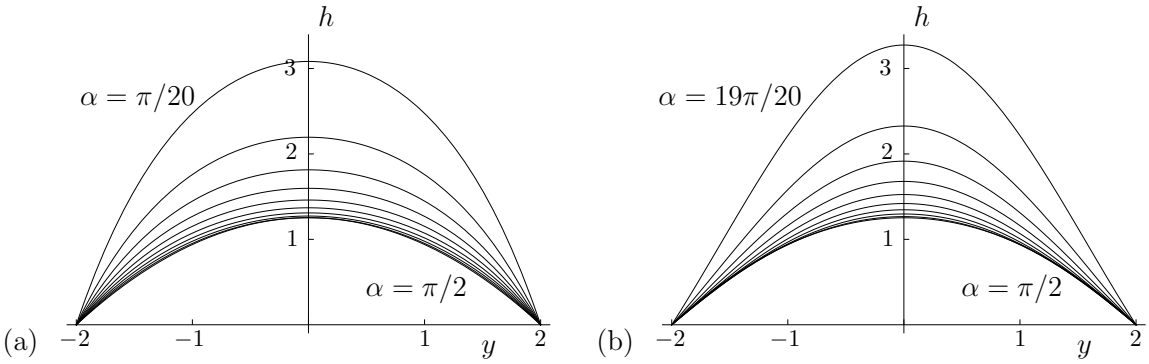

Figure 3.11: Plots of the cross-sectional free surface profile h given by (3.16) for a narrow rivulet of a non-perfectly wetting fluid with prescribed constant semi-width $\bar{a} = 2$ ($< \pi$) as a function of y for $N = 1/2$, at (a) $\alpha = \pi/20$, $\pi/10$, $3\pi/20$, ..., $\pi/2$ on the top half of the cylinder, and (b) $\pi/2$, $11\pi/20$, ..., $19\pi/20$ on the bottom half of the cylinder.

near the bottom of the cylinder according to

$$\beta \sim \frac{\pi\kappa_N}{8}(\pi-\alpha)^{\frac{4N+1}{2N+1}} \to 0^+, \qquad h_{\rm m} \sim \kappa_N(\pi-\alpha)^{-\frac{1}{2N+1}} \to \infty \tag{3.23}$$

in the limit $\alpha \to \pi^-$. In deriving (3.21) and (3.22) we have made use of the appropriate limits of (3.18), (1.86) and (2.22) together with $\sin\alpha \sim \alpha$ and $m \to 1$ in the limit $\alpha \to 0$, and $\sin\alpha \sim \pi - \alpha$ in the limit $\alpha \to \pi^-$, respectively. In deriving (3.23) we have made use of the appropriate limits of (3.18), (3.5) and (2.16) together with $\cos\alpha \to -1$, $\sin\alpha \sim \pi - \alpha$, $m \sim 1 - (\pi-\alpha)^2/2$ and $f_N(m\bar{a}) \sim f_N(\pi\bar{a}) \to \infty$ in the limit $\alpha \to \pi^-$.

Both β and $h_{\rm m}$ are finite in the middle of the cylinder, satisfying

$$\beta \to 2\left(\frac{18^N}{\lambda_N^N \bar{a}^{3N+1}}\right)^{\frac{1}{2N+1}} = O(1), \qquad h_{\rm m} \to \left(\frac{18}{\lambda_N \bar{a}}\right)^{\frac{N}{2N+1}} = O(1) \tag{3.24}$$

in the limit $\alpha \to \pi/2$.

Stationary points of β are determined mathematically by (3.17) and

$$2\csc^2\alpha = N\,\frac{f_N'(ma)ma}{f_N(ma)} - 3N + 1 \tag{3.25}$$

(obtained by differentiation of (3.17) with respect to α) from which it may be

shown that β has a unique minimum value, occurring on the lower half of the cylinder (*i.e.* for $\pi/2 < \alpha < \pi$). On the other hand, stationary points of $h_{\rm m}$ are determined mathematically by (3.17) and

$$2\csc^2\alpha = N\,\frac{f_N'(ma)ma}{f_N(ma)} - (2N+1)\frac{2ma}{\sinh 2ma} + 2 - N \tag{3.26}$$

(obtained by differentiation of (3.16) with $y = 0$) from which it may be shown that $h_{\rm m}$ also has a unique minimum value, but occurring on the upper half of the cylinder (*i.e.* for $0 < \alpha < \pi/2$). Furthermore, Figure 3.10 also shows that, like the variation of $h_{\rm m}$ for a rivulet of a perfectly wetting fluid shown in Figure 3.4, the variation of β and $h_{\rm m}$ is not monotonic in N at any fixed value of α.

In the limit of a very narrow rivulet, $\bar{a} \to 0^+$, the rivulet becomes thick according to

$$\beta \sim 2\left(\frac{18^N}{\lambda_N^N \bar{a}^{3N+1}\sin\alpha}\right)^{\frac{1}{2N+1}} \to \infty, \qquad h_{\rm m} \sim \left(\frac{18^N}{\lambda_N^N \bar{a}^N \sin\alpha}\right)^{\frac{1}{2N+1}} \to \infty. \tag{3.27}$$

3.4.2 A Wide Rivulet with $\bar{a} > \pi$

As we have already described in Section 3.2, a wide rivulet with prescribed constant semi-width $\bar{a} > \pi$, as sketched in Figure 3.2, can flow all the way from the top to the bottom of the cylinder only by flowing from $\alpha = \alpha_{\rm depin}$ ($\pi/2 < \alpha_{\rm depin} < \pi$), where $\alpha_{\rm depin}$ is given by (3.2), to the bottom of the cylinder with de-pinned contact lines and zero contact angle according to the solution for a rivulet of a perfectly wetting fluid described in Section 3.3.

Specifically, at $\alpha = \alpha_{\rm depin}$ the rivulet has zero contact angle $\beta = 0$, semi-width $a = \bar{a}$, and maximum thickness $h_{\rm m} = h_{\rm mdepin}$, where

$$h_{\rm mdepin} = \kappa_N\left(\frac{(-\cos\alpha_{\rm depin})^{\frac{N}{2}}}{\sin\alpha_{\rm depin}}\right)^{\frac{1}{2N+1}} = \kappa_N\left(\frac{\pi^N\bar{a}^{2-N}}{\sqrt{\bar{a}^4-\pi^4}}\right)^{\frac{1}{2N+1}}, \tag{3.28}$$

while for $\alpha_{\rm depin} \leq \alpha \leq \pi$ it has $\beta = 0$, monotonically decreasing slowly varying semi-width $a = \pi/m$ ($\pi \leq a \leq \bar{a}$), and monotonically increasing maximum thickness $h_{\rm m}$ ($\geq h_{\rm mdepin}$) given by (3.5).

In the limit $\alpha \to \alpha_{\rm depin}^-$ we have $a \equiv \bar{a}$, and find that $\beta \to 0^+$ according to

$$\beta = \left(\frac{\pi^N (\bar{a}^4 - \pi^4)^N}{\bar{a}^{3N-1}} \right)^{\frac{1}{2N+1}} \frac{\kappa_N}{4} (\alpha_{\rm depin} - \alpha) + O(\alpha_{\rm depin} - \alpha)^2 \tag{3.29}$$

and $h_{\rm m} \to h_{\rm mdepin}^-$ according to

$$h_{\rm m} = h_{\rm mdepin} + \frac{(N\bar{a}^4 + (2-N)\pi^4) h_{\rm mdepin}}{2\pi^2 \sqrt{\bar{a}^4 - \pi^4}} (\alpha - \alpha_{\rm depin}) + O(\alpha_{\rm depin} - \alpha)^2, \tag{3.30}$$

whereas in the limit $\alpha \to \alpha_{\rm depin}^+$ we have $\beta \equiv 0$, and find that $a \to \bar{a}^-$ according to

$$a = \bar{a} - \frac{\bar{a}\sqrt{\bar{a}^4 - \pi^4}}{2\pi^2} (\alpha - \alpha_{\rm depin}) + O(\alpha_{\rm depin} - \alpha)^2 \tag{3.31}$$

and $h_{\rm m} \to h_{\rm mdepin}^+$ according to (3.30). In particular, the solutions in $\alpha < \alpha_{\rm depin}$ and $\alpha > \alpha_{\rm depin}$ join continuously (but not smoothly) at $\alpha = \alpha_{\rm depin}$.

Figure 3.12 shows plots of a, β and $h_{\rm m}$ for a wide rivulet with prescribed constant semi-width $\bar{a} = 5$ ($> \pi$) in $0 < \alpha \leq \alpha_{\rm depin} \simeq 0.62918\pi$ and slowly varying semi-width $a = \pi/m$ in $\alpha_{\rm depin}/\pi \leq \alpha/\pi \leq 1$ as functions of α/π for a range of values of N. Note that since a takes the constant value $\bar{a}$ for all α when $\bar{a} \leq \pi$ and for $\alpha \leq \alpha_{\rm depin}$ when $\bar{a} > \pi$, and is given by $a = \pi/m$ for $\alpha \geq \alpha_{\rm depin}$ when $\bar{a} > \pi$, the plot of a in Figure 3.12(a) is identical to the corresponding plot for Newtonian fluid given by Figure 6(b) of Paterson *et al.* [97], but is included here for completeness.

Figure 3.13 shows plots of h given by (3.3) and (3.16) for a wide rivulet with prescribed constant semi-width $\bar{a} = 5$ ($> \pi$) as a function of y at various stations around the cylinder, including $\alpha = \alpha_{\rm depin} \simeq 0.62918\pi$, for $N = 1/2$. Figures 3.12 and 3.13 illustrate that the rivulet is again thick at the top of the cylinder with

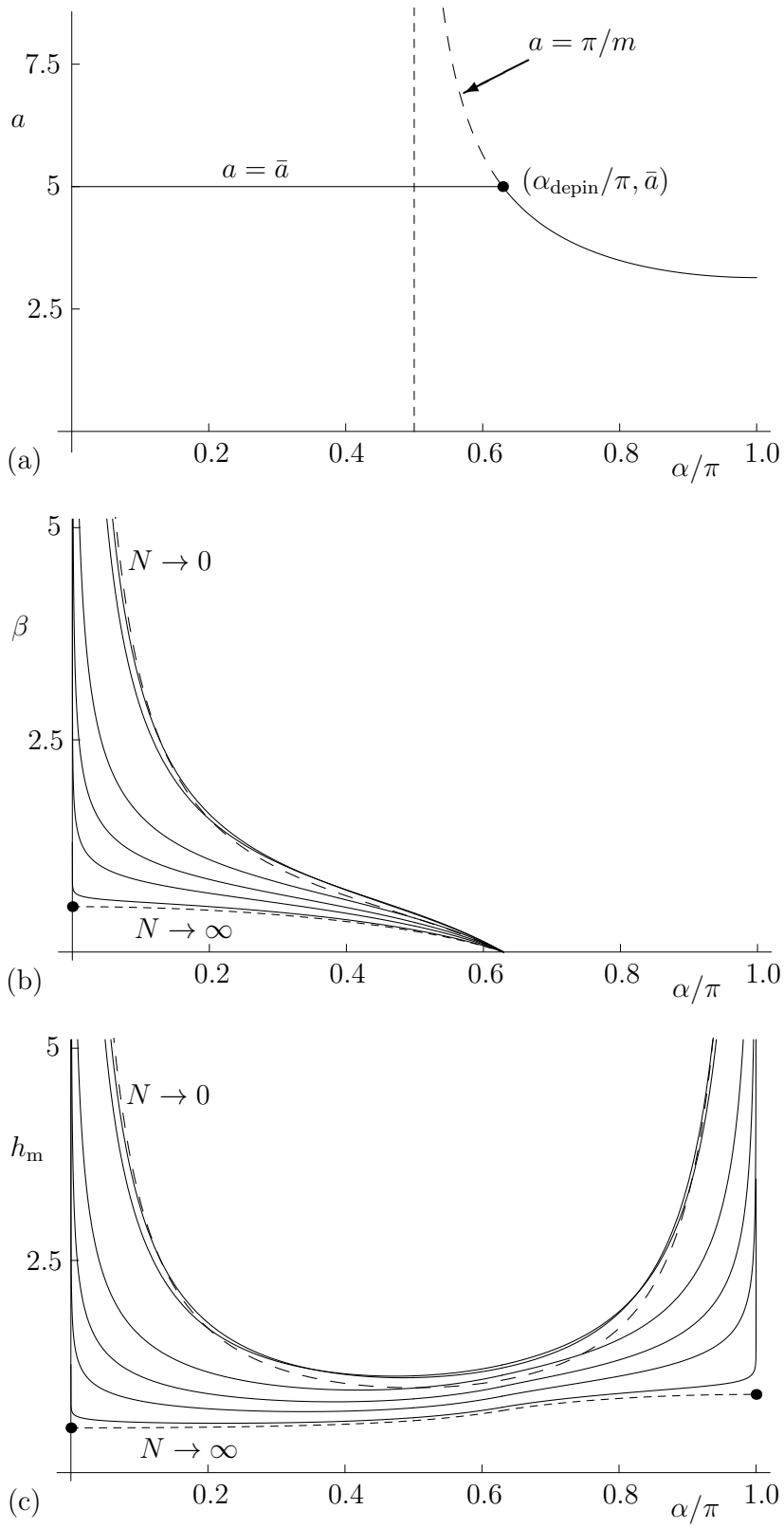

Figure 3.12: Plots of (a) a, (b) β and (c) $h_{\rm m}$ for a wide rivulet of a non-perfectly wetting fluid with prescribed constant semi-width $\bar{a} = 5$ $(> \pi)$ in $0 \leq \alpha/\pi < \alpha_{\rm depin}/\pi \simeq 0.62918$ and slowly varying semi-width $a = \pi/m$ in $\alpha_{\rm depin}/\pi \leq \alpha/\pi \leq 1$ as functions of α/π for $N = 1/20$, $1/10$, $1/2$, 1, 2 and 10, together with the asymptotic solutions (3.19) in the limit $N \to 0^+$ (dashed curves), and (3.20) in the limit $N \to \infty$ (dotted curves).

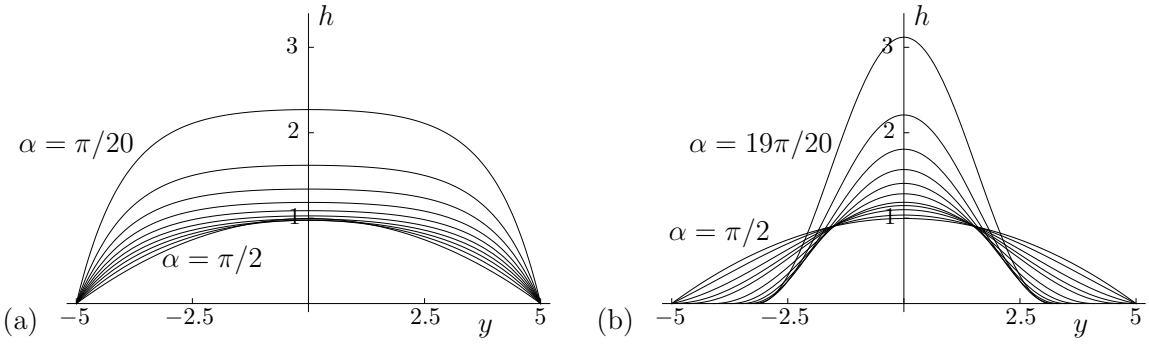

Figure 3.13: Plots of the cross-sectional free surface profile h given by (3.3) and (3.16) for a wide rivulet of a non-perfectly wetting fluid with prescribed constant semi-width $\bar{a} = 5$ ($> \pi$) as a function of y for $N = 1/2$ at (a) $\alpha = \pi/20$, $\pi/10$, $3\pi/20$, ..., $\pi/2$, and (b) $\pi/2$, $11\pi/20$, ..., $19\pi/20$ and $\alpha = \alpha_{\text{depin}} \simeq 0.62918\pi$.

both β and h_{m} becoming infinite according to (3.21) in the limit $\alpha \to 0^+$, and they are again finite in the middle of the cylinder, satisfying (3.24) in the limit $\alpha \to \pi/2$. However, in this case the rivulet becomes thick with zero contact angle and finite semi-width π near the bottom of the cylinder according to (3.10) in the limit $\alpha \to \pi^-$. Furthermore, Figure 3.12 also shows that, like in the case of a narrow rivulet described in Section 3.4.1, the variation of β and h_{m} is not monotonic in N at any fixed value of α.

In the limit of a very wide rivulet, $\bar{a} \to \infty$ (in which $\alpha_{\text{depin}} \to \pi/2^+$), the rivulet becomes flat according to

$$\beta \sim \left(\left(\frac{2N+1}{2N\bar{a}} \right)^N \frac{1}{\sin\alpha} \right)^{\frac{1}{2N+1}} m \to 0^+, \qquad h_{\text{m}} \sim \left(\left(\frac{2N+1}{2N\bar{a}} \right)^N \frac{1}{\sin\alpha} \right)^{\frac{1}{2N+1}} \to 0^+ \tag{3.32}$$

on the upper half of the cylinder and is given by (3.3) on the lower half of the cylinder.

3.4.3 Contour Plots of the Free Surface

Figure 3.14 shows contour plots of h given by (3.3) and (3.16) in the $(y, \alpha/\pi)$ plane for rivulets with prescribed semi-widths $\bar{a} = 2$ and $\bar{a} = 5$ when $N = 2$. In particular, in the latter case the contact lines de-pin at $\alpha/\pi = \alpha_{\text{depin}}/\pi \simeq 0.62918$.

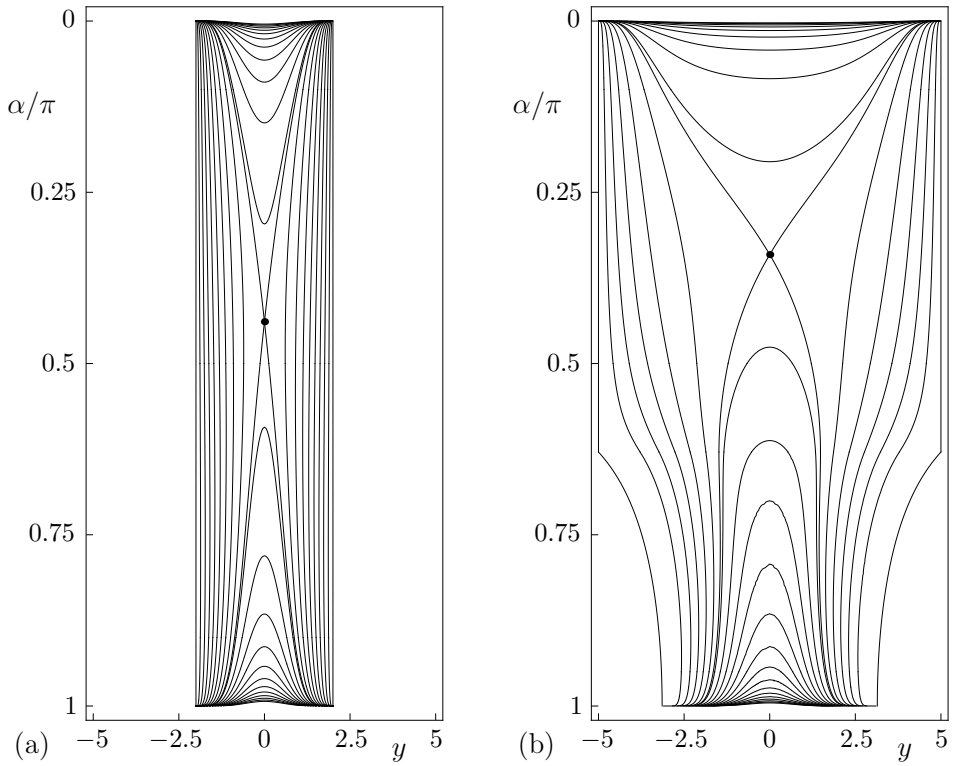

Figure 3.14: Contour plots of the free surface h given by (3.3) and (3.16) in the $(y, \alpha/\pi)$ plane for rivulets of a non-perfectly wetting fluid with prescribed semi-widths (a) $\bar{a} = 2$ and (b) $\bar{a} = 5$ when $N = 2$. In each case the contours are drawn at intervals of $1/8$ up to a maximum $h = 5/2$, together with the contours (a) $h \simeq 1.09701$ and (b) $h \simeq 0.71836$ that pass through the saddle points of h, marked with dots. In (b) the contact lines de-pin at $\alpha/\pi = \alpha_{\text{depin}}/\pi \simeq 0.62918$.

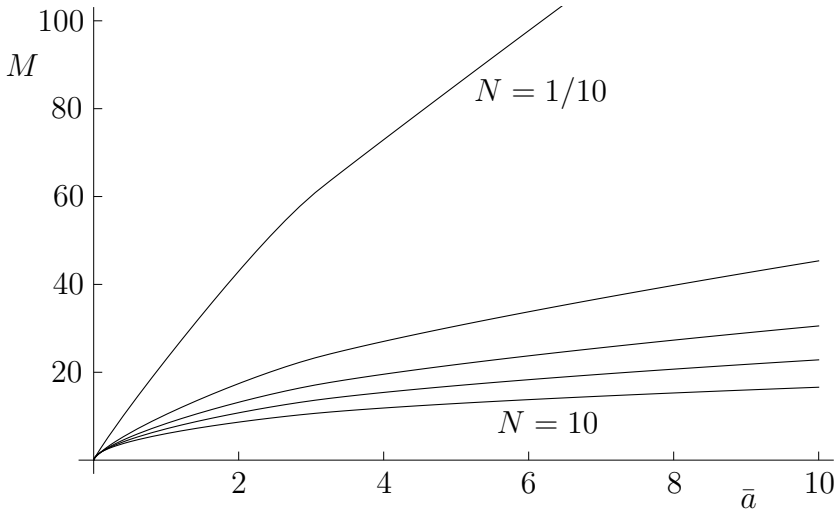

Figure 3.15: Plot of the mass of a rivulet of a non-perfectly wetting fluid, M, given by (3.33) as a function of $\bar{a}$ for $N = 1/10$, $1/2$, 1, 2 and 10.

3.4.4 The Mass of the Rivulet, M

Whatever the value of $\bar{a}$, the mass of the rivulet is given by

$$M = \int_0^{\pi} \int_{-a}^{a} h \, \mathrm{d}y \, \mathrm{d}\alpha = \int_0^{\pi/2} \frac{2\beta(ma \coth ma - 1)}{m^2} \, \mathrm{d}\alpha + \int_{\pi/2}^{\pi} \frac{2\beta(1 - ma \cot ma)}{m^2} \, \mathrm{d}\alpha. \tag{3.33}$$

Both integrands in (3.33) are finite at $\alpha = \pi/2$. When $\bar{a} > \pi$ the second integral is evaluated most easily by splitting it into two integrals, one from $\alpha = \pi/2$ to $\alpha = \alpha_{\mathrm{depin}}$, and one from $\alpha = \alpha_{\mathrm{depin}}$ to $\alpha = \pi$, with the solution for a perfectly wetting fluid (*i.e.* with $\beta = 0$) used in the latter. Figure 3.15 shows a plot of M given by (3.33) as a function of $\bar{a}$ for several values of N, showing that M increases monotonically with $\bar{a}$. In particular, in the limit of a narrow rivulet, $\bar{a} \to 0^+$, $M \to 0^+$ according to

$$M \sim \left(\frac{2^{5N+2} \bar{a}^{N+1}}{3\lambda_N^N} \right)^{\frac{1}{2N+1}} C_N \to 0^+. \tag{3.34}$$

In deriving (3.34) we have made use of equation $(3.21)_1$ together with $m\bar{a} \coth m\bar{a} - 1 \sim (m\bar{a})^2/3$ and $1 - m\bar{a} \cot m\bar{a} \sim (m\bar{a})^2/3$ in limit $\bar{a} \to 0^+$. On the other hand,

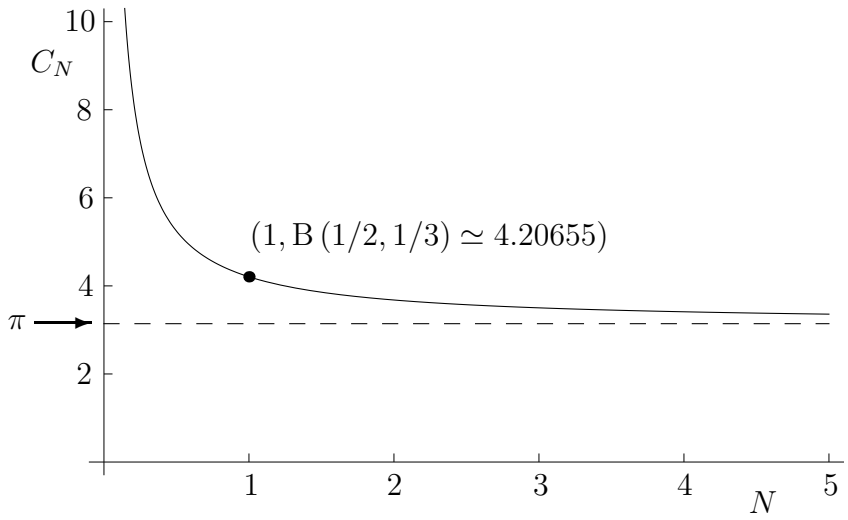

Figure 3.16: Plot of C_N given by (3.36) as a function of N, together with its asymptotic value π in the limit $N \to \infty$.

in the limit of a wide rivulet, $\bar{a} \to \infty$, $M \to \infty$ according to

$$M \sim \left(\frac{(2N+1)^N \bar{a}^{N+1}}{2^N N^N} \right)^{\frac{1}{2N+1}} C_N \to \infty, \tag{3.35}$$

where the constant C_N in both (3.34) and (3.35) is defined by

$$C_N = \int_0^\pi \frac{\mathrm{d}\alpha}{(\sin\alpha)^{\frac{1}{2N+1}}} = \frac{\sqrt{\pi}\,\Gamma\left(\dfrac{N}{2N+1}\right)}{\Gamma\left(\dfrac{4N+1}{2(2N+1)}\right)} = \mathrm{B}\left(\frac{1}{2}, \frac{N}{2N+1}\right). \tag{3.36}$$

In deriving (3.35) we have made use of equations (3.32) and (3.3); also the second integral in (3.33) is evaluated with the solution for a perfectly wetting fluid, since $\alpha_{\mathrm{depin}} \to \pi/2$ in the limit $\bar{a} \to \infty$.

Figure 3.16 shows a plot of C_N given by (3.36) as a function of N, illustrating that C_N decreases monotonically with N, satisfying $C_N \sim 1/N \to \infty$ as $N \to 0$, $C_N = \sqrt{\pi}\,\Gamma(\frac{1}{3})/\Gamma(\frac{5}{6}) \simeq 4.20655$ when $N = 1$ (in agreement with equation (10) of Paterson *et al.* [97]), and $C_N \to \pi^+$ as $N \to \infty$.

Figure 3.17 shows a plot of M given by (3.33) as a function of N for several values of $\bar{a}$, showing that M decreases monotonically with N from ∞ to a

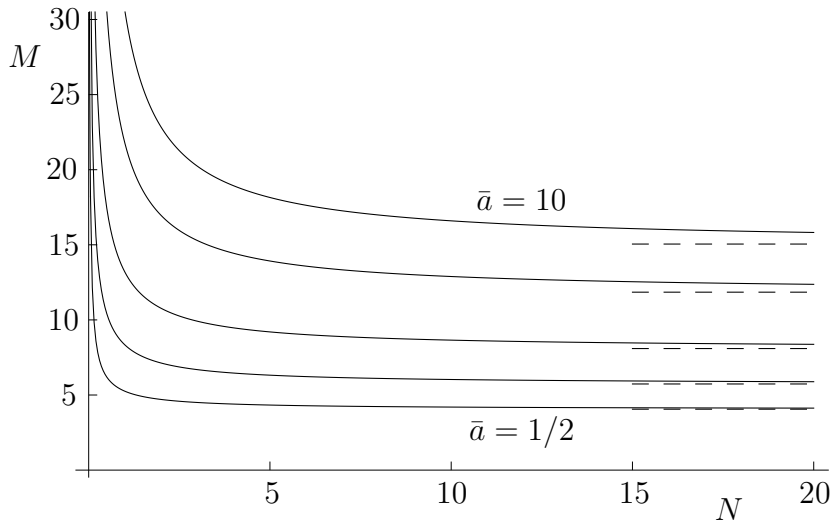

Figure 3.17: Plot of the mass of a rivulet of a non-perfectly wetting fluid, M, given by (3.33) as a function of N for $\bar{a} = 1/2$, 1, 2, 5 and 10. The horizontal dashed lines denote the constant asymptotic values in the limit $N \to \infty$.

(nonzero) $\bar{a}$-dependent constant asymptotic value in the limit $N \to \infty$.

3.5 Conclusions

We described the flow of a slowly varying rivulet of a power-law fluid with prescribed constant semi-width (*i.e.* with pinned contact lines) but slowly varying contact angle down a slowly varying substrate, specifically the flow in the azimuthal direction around the outside of a large horizontal circular cylinder.

We obtained the solution for a perfectly wetting fluid (which can never have pinned contact lines), and showed that, despite having the same local behaviour, the global behaviour of a rivulet of non-perfectly wetting fluid is qualitatively very different from that described in Chapter 2. Specifically, we described how (as sketched in Figure 3.1) the contact lines of a sufficiently narrow rivulet with $\bar{a} \leq \pi$ can remain pinned as it drains all the way from the top to the bottom of the cylinder, but how (as sketched in Figure 3.2) the contact lines of a wider rivulet with $\bar{a} > \pi$ de-pin at $\alpha = \alpha_{\text{depin}}$ on the lower half of the cylinder, and how thereafter it drains to the bottom of the cylinder with zero contact angle $\beta = 0$ and slowly varying semi-width $a = \pi/m$.

How the shape of the rivulet and the velocity within it depend on the power-law index N was described in detail. In particular, we showed that whereas neither h nor u vary monotonically with N at any fixed value of α, its mass is always monotonically increasing in $\bar{a}$ but monotonically decreasing in N.

Despite the limitations of the power-law model, the present results again provide a rare analytical benchmark for the study of rivulet flow of non-Newtonian fluids.

Chapter 4

Rivulet Flow of Generalised Newtonian Fluids

As we discussed in Chapter 1, there is very little work on rivulet flow of fluids with other than the theoretically convenient but highly idealised power-law rheology. Accordingly in this Chapter we consider steady gravity-driven flow of a thin uniform rivulet with more realistic non-Newtonian rheology, namely a generalised Newtonian fluid down a vertical planar substrate. In particular, we obtain general results for *any* generalised Newtonian fluid before giving a detailed account of the behaviour of two popular and widely-used generalised Newtonian fluids, namely a Carreau fluid and an Ellis fluid.

4.1 A generalised Newtonian fluid

In this Chapter we shall be concerned with flow of an incompressible generalised Newtonian fluid with velocity $\mathbf{u}$ and pressure p for which the extra stress $\underline{\underline{\boldsymbol{\sigma}'}}$ is related to the rate of strain $\underline{\underline{\mathbf{e}}} = \frac{1}{2}\left(\nabla\mathbf{u} + (\nabla\mathbf{u})^{\mathrm{T}}\right)$ by $\underline{\underline{\boldsymbol{\sigma}'}} = 2\mu\underline{\underline{\mathbf{e}}}$, where μ is the viscosity function of the specific fluid under consideration.

We shall be concerned primarily with the most commonly occuring kind of generalised Newtonian behaviour, namely shear-thinning fluids (for which μ is a

decreasing function of q), although many of the results obtained are also valid for shear-thickening fluids (for which μ is an increasing function of q).

As described previously in Subsection 1.3.2, an example of a generalised Newtonian fluid is a Carreau fluid, given by

$$\mu = \mu_\infty + \frac{\mu_0 - \mu_\infty}{\left(1 + \lambda^2 q^2\right)^{(1-N)/2}}, \tag{4.1}$$

where $q = \left(2\,\mathrm{tr}(\underline{\underline{\mathbf{e}}}^2)\right)^{1/2}$ is the shear rate, μ_0 and μ_∞ ($\leq \mu_0$) are the viscosities at zero and infinite shear rate, respectively, λ is a (finite) relaxation time, N (≤ 1) is a measure of the shear-thinning behaviour (specifically, the smaller the value of N, the greater the rate of shear thinning). Another example of a generalised Newtonian fluid is an Ellis fluid, given by

$$\mu = \mu_\infty + \frac{\mu_0 - \mu_\infty}{1 + \left(\dfrac{\tau}{\tau_{\mathrm{av}}}\right)^{\alpha-1}}, \tag{4.2}$$

where the measure of the stress, τ, is defined by $\tau = \left(\mathrm{tr}\left(\underline{\underline{\boldsymbol{\sigma}}}'^2\right)/2\right)^{1/2}$, μ_0 and μ_∞ ($\leq \mu_0$) are the viscosities at zero and infinite stress, respectively, $\tau = \mu q$, τ_{av} is the (non-zero) value of the stress τ when μ takes the average value $\mu = \mu_{\mathrm{av}} = (\mu_0+\mu_\infty)/2$, and α (≥ 1) is a measure of the shear-thinning behaviour (specifically, the larger the value of α, the greater the rate of shear thinning). Note that unlike, in the previous Chapters 2 and 3, in this Chapter α is a measure of the shear-thinning behaviour and is not the local slope of the substrate. A conventional Ellis fluid (see, for example, Myers [91]), which has zero viscosity in the limit of infinite stress $\tau \to \infty$, corresponds to the special case $\mu_\infty = 0$.

For the Carreau and Ellis fluids, the stated restrictions on the parameters appearing in the viscosities mean that μ and τ are, respectively, non-increasing and non-decreasing functions of q (that is, $\mathrm{d}\mu/\mathrm{d}q \leq 0$ and $\mathrm{d}\tau/\mathrm{d}q \geq 0$).

Note that each of the limits $\lambda \to 0$, $N \to 1$ and $\mu_\infty \to \mu_0$ for a Carreau

fluid (4.1) and $\tau_{\rm av} \to \infty$ and $\mu_\infty \to \mu_0$ for an Ellis fluid (4.2) corresponds to a Newtonian fluid with constant viscosity $\mu = \mu_0$, and that both of the limits $\lambda \to \infty$ for a Carreau fluid (4.1) and $\tau_{\rm av} \to 0$ for an Ellis fluid (4.2) correspond to a Newtonian fluid with constant viscosity $\mu = \mu_\infty$. Furthermore, the limit $\alpha \to 1$ for an Ellis fluid (4.2) corresponds to a Newtonian fluid with constant viscosity $\mu = \mu_{\rm av}$.

The velocity $\mathbf{u}$ and the pressure p satisfy the mass-conservation and momentum-balance equations for such a fluid, which take the forms

$$\nabla \cdot \mathbf{u} = 0 \qquad \rho \frac{D\mathbf{u}}{Dt} = -\nabla p + \rho \mathbf{g} + \nabla \cdot \underline{\underline{\boldsymbol{\sigma}}}', \tag{4.3}$$

where ρ, $\mathbf{g}$ and t denote the fluid density, acceleration due to gravity, and time,

4.2 Rivulet Flow Down a Vertical Substrate

4.2.1 General Formulation

We consider unidirectional steady gravity-driven flow of a thin uniform rivulet of a generalised Newtonian fluid with semi-width a, contact angle β, and volume flux Q down a vertical planar substrate, as shown in Figure 4.1. We adopt the Cartesian coordinates $Oxyz$, with the z axis normal to the substrate $z = 0$ and the y axis horizontal; the velocity is of the form $\mathbf{u} = u(y, z)\mathbf{i}$ and we denote the free surface profile of the rivulet by $z = h(y)$. We non-dimensionalise and scale the variables according to

$$x = Lx^*, \quad y = Ly^*, \quad a = La^*, \quad z = \epsilon L z^*, \quad h = \epsilon L h^*, \quad \beta = \epsilon \beta^*, \quad u = U u^*,$$
$$p = p_{\rm a} + \frac{\epsilon \gamma}{L} p^*, \quad Q = \epsilon L^2 U Q^*, \quad \mu = \mu_0 \mu^*, \quad \mu_\infty = \mu_0 \mu_\infty^*, \quad q = \frac{U}{\epsilon L} q^*, \quad \tau = \frac{\mu_0 U}{\epsilon L} \tau^*, \tag{4.4}$$

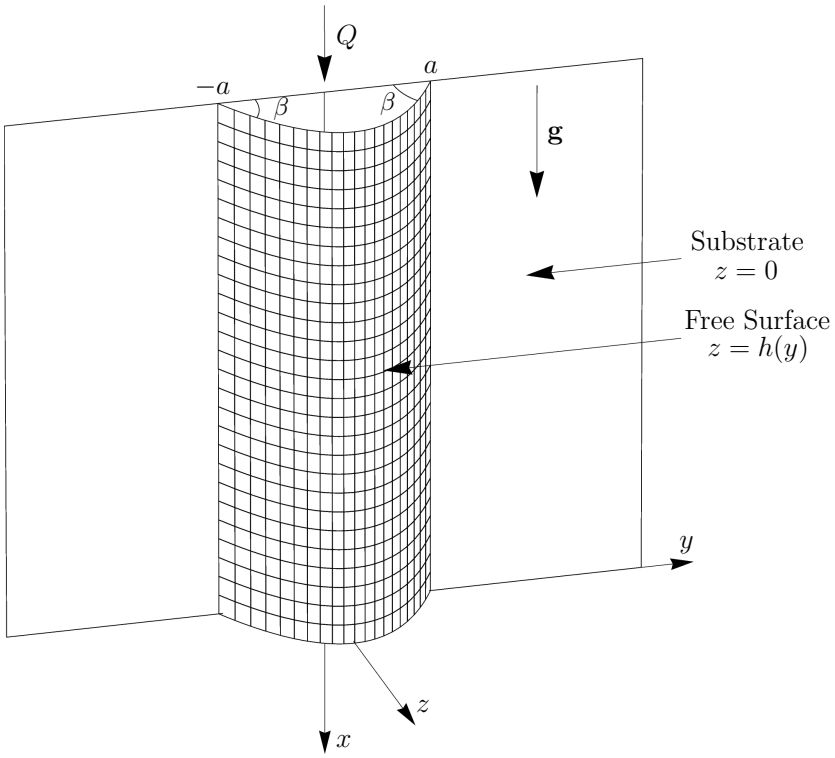

Figure 4.1: Unidirectional steady gravity-driven flow of a thin uniform rivulet of a generalised Newtonian fluid with semi-width a, contact angle β, and volume flux Q down a vertical planar substrate.

where L is an appropriate transverse length scale, $p_{\rm a}$ denotes the constant atmospheric pressure, ϵ ($\ll 1$) is the aspect ratio of the rivulet, γ is the constant coefficient of surface tension of the fluid, and $U = \epsilon^2 \rho g L^2/\mu_0$ is an appropriate velocity scale. There are several equally sensible definitions of L and ϵ, including $L = a$ and $\epsilon = \beta$ (corresponding to taking $a^* = 1$ and $\beta^* = 1$), $L = (\mu_0 Q/\rho g \beta^3)^{1/4}$ and $\epsilon = \beta$ (corresponding to taking $Q^* = 1$ and $\beta^* = 1$), $L = a$ and $\epsilon = (\mu_0 Q/\rho g a^4)^{1/3}$ (corresponding to taking $a^* = 1$ and $Q^* = 1$), and $L = \ell$ and $\epsilon = \beta$, where $\ell = (\gamma/\rho g)^{1/2}$ denotes the capillary length. However, in what follows we leave L and ϵ unspecified in order to keep the subsequent presentation as general as possible. Hereafter all quantities are non-dimensional unless stated otherwise; for clarity we drop the stars superscripts on non-dimensional variables.

As the velocity is of the form $\mathbf{u} = u(y,z)\mathbf{i}$ we have $q = u_z$ at leading order in the thin-film limit $\epsilon \to 0$ (with $u_z \geq 0$ for the type of flow under consideration).

Therefore (4.3) gives

$$0 = -\frac{1}{B}p_x + 1 + (\mu u_z)_z, \qquad 0 = -p_y, \qquad 0 = -p_z, \tag{4.5}$$

where $B = \rho g L^2/\gamma\epsilon$ is an appropriate Bond number. Equation (4.5) is to be integrated subject to the boundary conditions of no slip on the substrate $z = 0$, and balances of normal and tangential stress on the free surface:

$$u = 0 \ \text{ on } \ z = 0, \qquad u_z = 0 \ \text{ and } \ p = -h_{yy} \ \text{ on } \ z = h, \tag{4.6}$$

with h again subject to the contact-line conditions

$$h = 0 \ \text{ and } \ h_y = \mp\beta \ \text{ at } \ y = \pm a. \tag{4.7}$$

The solution for p is $p = -h_{yy}$ with h satisfying $h_{yyy} = 0$, leading to

$$h = h_{\rm m}\left(1 - \frac{y^2}{a^2}\right), \qquad h_{\rm m} = \frac{\beta a}{2}, \qquad p = \frac{\beta}{a}, \tag{4.8}$$

where $h_{\rm m} = h(0)$ denotes the maximum thickness of the rivulet; equation (4.8) shows that, as expected, the free surface of the rivulet has constant curvature, and p is a constant.

From (4.5) and (4.6) the shear stress τ $(= \mu u_z)$ and the shear rate q $(= u_z)$ are given by

$$\tau = \mu q = h - z, \tag{4.9}$$

representing a balance between gravity and viscous effects. In principle, the algebraic equation (4.9) may be solved for q in terms of $h - z$, which may then be integrated with respect to z subject to (4.6) to give u as a function of y and

z. The volume flux of fluid down the rivulet Q is then again given by

$$Q = 2\int_0^a \bar{u}\,\mathrm{d}y, \tag{4.10}$$

where the depth-integrated velocity $\bar{u}$ is given by

$$\bar{u} = \int_0^h u\,\mathrm{d}z. \tag{4.11}$$

In general, there is freedom to prescribe two of the quantities a, β and Q, with the third determined by the algebraic equation (4.10), and with h_m related to a and β by (4.8).

In the case of a Newtonian fluid with constant viscosity $\mu \equiv 1$ the solutions for τ, q, u and Q are simply

$$\tau = q = h - z, \qquad u = \frac{h^2 - (h-z)^2}{2}, \qquad Q = \frac{4\beta^3 a^4}{105}. \tag{4.12}$$

Thus if the values of the contact angle $\beta = \bar{\beta}$ and flux $Q = \bar{Q}$ are prescribed then the semi-width a and maximum thickness h_m are given by $a = (105\bar{Q}/4\bar{\beta}^3)^{1/4}$ and $h_\mathrm{m} = (105\bar{\beta}\bar{Q}/64)^{1/4}$, whereas if the values of the semi-width $a = \bar{a}$ and flux $Q = \bar{Q}$ are prescribed then the contact angle β and maximum thickness h_m are given by $\beta = (105\bar{Q}/4\bar{a}^4)^{1/3}$ and $h_\mathrm{m} = (105\bar{Q}/32\bar{a})^{1/3}$; in both cases the solution with h and p given by (4.8) and u given by (4.12) is then completely determined.

In Section 4.2.2 we obtain the parametric solution u of (4.9) subject to (4.6) for any generalised Newtonian fluid with viscosity function of the form $\mu = \mu(q)$ (including, in particular, for a Carreau fluid), and in Section 4.2.3 we obtain the explicit solution for any generalised Newtonian fluid with viscosity function of the form $\mu = \mu(\tau)$ (including, in particular, for an Ellis fluid).

4.2.2 Viscosity Function of the Form $\mu = \mu(q)$

If the viscosity function is of the form $\mu = \mu(q)$ then, rather than solving (4.9) and integrating $u_z = q$ to obtain u as a function of y and z, we can make more progress analytically by eliminating z in favour of q via (4.9), so that $\mathrm{d}z = -\left(\mathrm{d}(\mu(q)q)/\mathrm{d}q\right)\,\mathrm{d}q$, to obtain u in terms of q :

$$u = \int_q^{q_\mathrm{s}} \tilde{q}\frac{\mathrm{d}\big[\mu(\tilde{q})\tilde{q}\big]}{\mathrm{d}\tilde{q}}\,\mathrm{d}\tilde{q}, \tag{4.13}$$

where $q_\mathrm{s} = q_\mathrm{s}(y) = q|_{z=0}$ is the shear rate at the substrate $z = 0$, to be determined from

$$\tau_\mathrm{s} = \mu(q_\mathrm{s})q_\mathrm{s} = h, \tag{4.14}$$

in which $\tau_\mathrm{s} = \tau_\mathrm{s}(y) = \tau|_{z=0}$ is the stress at the substrate $z = 0$. With an integration by parts, equation (4.13) may be written in the slightly more convenient form

$$u = \mu(q_\mathrm{s})q_\mathrm{s}^2 - \mu(q)q^2 - \int_q^{q_\mathrm{s}} \mu(\tilde{q})\tilde{q}\,\mathrm{d}\tilde{q}. \tag{4.15}$$

Thus (4.9) and (4.15) provide a parametric solution for u as a function of y and z, with the parameter q satisfying $0 \le q \le q_\mathrm{s}$. Although (4.15) involves only quadrature, the q_s that appears must be obtained as a solution of (4.14) for each value of y.

The depth-integrated velocity $\bar{u}$ given by (4.11) may be written

$$\bar{u} = \int_0^h u\,\mathrm{d}z = \big[(z-h)u\big]_0^h - \int_0^h (z-h)u_z\,\mathrm{d}z = \int_0^h (h-z)q\,\mathrm{d}z, \tag{4.16}$$

which with z again eliminated via (4.9) leads to

$$\bar{u} = \int_0^{q_\mathrm{s}} \mu(q)q^2\frac{\mathrm{d}\big[\mu(q)q\big]}{\mathrm{d}q}\,\mathrm{d}q. \tag{4.17}$$

Therefore from (4.10)

$$Q = 2\int_0^a \int_0^{q_\mathrm{s}} \mu(q) q^2 \frac{\mathrm{d}\big[\mu(q)q\big]}{\mathrm{d}q}\,\mathrm{d}q\,\mathrm{d}y, \tag{4.18}$$

and reversing the order of integration we obtain

$$Q = 2a\int_0^{q_\mathrm{m}} \left(1 - \frac{\mu(q)q}{\mu(q_\mathrm{m})q_\mathrm{m}}\right)^{1/2} \mu(q) q^2 \frac{\mathrm{d}\big[\mu(q)q\big]}{\mathrm{d}q}\,\mathrm{d}q, \tag{4.19}$$

where $q_\mathrm{m} = q_\mathrm{s}(0)$ is the maximum shear rate in the rivulet, occurring at $y = 0$, $z = 0$ and satisfying

$$\tau_\mathrm{m} = \mu(q_\mathrm{m})q_\mathrm{m} = h_\mathrm{m}, \tag{4.20}$$

in which $\tau_\mathrm{m} = \tau_\mathrm{s}(0)$ is the maximum stress in the rivulet, occurring at $y = 0$, $z = 0$.

In summary, when $\mu = \mu(q)$ is prescribed, h and p are given by (4.8) and u is given parametrically (with parameter q) by (4.9) and (4.15), with h_m, a, β and Q related by (4.19). If h_m is known then the constant q_m is obtained from (4.20), and then the integral in (4.19) reduces to quadrature; otherwise h_m and q_m are obtained simultaneously from (4.19) and (4.20).

For a Carreau fluid (4.1), with λ scaled by $\mu_0/\epsilon L\rho g$, equations (4.9) and (4.15) give u parametrically as

$$\left.\begin{aligned} h - z &= \left(\mu_\infty + \frac{1-\mu_\infty}{\big(1+\lambda^2 q^2\big)^{(1-N)/2}}\right) q, \\ u &= \frac{\mu_\infty}{2}\left(q_\mathrm{s}^2 - q^2\right) + \frac{1-\mu_\infty}{(1+N)\lambda^2}\left[\frac{1-N\lambda^2 q^2}{(1+\lambda^2 q^2)^{(1-N)/2}} - \frac{1-N\lambda^2 q_\mathrm{s}^2}{(1+\lambda^2 q_\mathrm{s}^2)^{(1-N)/2}}\right]. \end{aligned}\right\} \tag{4.21}$$

However, the integral for Q given in (4.19) cannot, in general, be evaluated in closed form, and so Q must, in general, be evaluated numerically.

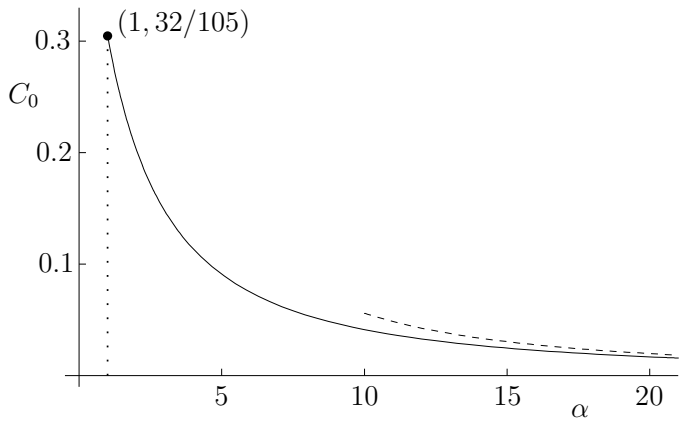

Figure 4.2: Plot of the coefficient C_0 defined in (4.27) as a function of α (≥ 1). The dashed curve shows the leading-order asymptotic behaviour in the limit $\alpha \to \infty$, namely $C_0 \sim \sqrt{\pi}/\alpha^{3/2} \to 0^+$.

4.2.3 Viscosity Function of the Form $\mu = \mu(\tau)$

If the viscosity function is of the form $\mu = \mu(\tau)$ then the solution analogous to (4.15) and (4.19) takes the explicit form

$$u = \int_{h-z}^{h} \frac{\tau}{\mu(\tau)}\,\mathrm{d}\tau, \qquad Q = 2a\int_0^{h_\mathrm{m}} \left(1 - \frac{\tau}{h_\mathrm{m}}\right)^{1/2} \frac{\tau^2}{\mu(\tau)}\,\mathrm{d}\tau, \tag{4.22}$$

with h and h_m satisfying (4.8). Again if h_m is known then the integral for Q reduces to quadrature, but otherwise h_m is obtained from the flux relation in (4.22).

For an Ellis fluid (4.2), with τ_av scaled by $\mu_0 U/\epsilon L$, in the general case $\alpha \neq 1$ and $\mu_\infty \neq 0$ equation (4.22) gives

$$u = \frac{h^2 - (h-z)^2}{2\mu_\infty} - \frac{1-\mu_\infty}{2\mu_\infty}\left[\phi(h) - \phi(h-z)\right], \tag{4.23}$$

where the function $\phi = \phi(\tau)$ is defined by

$$\phi(\tau) = \tau^2\, {}_2F_1\left(1, \frac{2}{\alpha-1}; \frac{\alpha+1}{\alpha-1}; -\mu_\infty\left(\frac{\tau}{\tau_\mathrm{av}}\right)^{\alpha-1}\right), \tag{4.24}$$

in which ${}_2F_1$ denotes a hypergeometric function. However, as for a Carreau fluid, the integral for Q given in (4.22) cannot, in general, be evaluated in closed form,

and so Q must, in general, be evaluated numerically. In the special case $\alpha = 1$, corresponding to a Newtonian fluid with viscosity $\mu = \mu_{\rm av}$, we obtain

$$u = \frac{h^2 - (h-z)^2}{2\mu_{\rm av}}, \qquad Q = \frac{4\beta^3 a^4}{105\mu_{\rm av}}. \tag{4.25}$$

In the special case $\mu_\infty = 0$, corresponding to a conventional Ellis fluid, we obtain

$$u = \frac{h^2 - (h-z)^2}{2} + \frac{h^{\alpha+1} - (h-z)^{\alpha+1}}{(\alpha+1)\tau_{\rm av}^{\alpha-1}}, \qquad Q = \beta^3 a^4 \left[\frac{4}{105} + \frac{C_0}{8}\left(\frac{h_{\rm m}}{\tau_{\rm av}}\right)^{\alpha-1}\right], \tag{4.26}$$

where we have defined the coefficient C_0 by

$$C_0 = \frac{\sqrt{\pi}\,\Gamma(\alpha+2)}{\Gamma(\alpha+\frac{7}{2})} = \frac{\mathrm{B}(\alpha+3,\frac{1}{2})}{\alpha+2}, \tag{4.27}$$

in which Γ and B denote the usual Gamma and Beta functions. Figure 4.2 shows a plot of C_0 as a function of α (≥ 1). In particular, Figure 4.2 shows that C_0 takes the value $C_0 = 32/105$ when $\alpha = 1$, decreases monotonically with α, and satisfies $C_0 \sim \sqrt{\pi}/\alpha^{3/2} \to 0^+$ in the limit $\alpha \to \infty$.

4.3 Comparison of Carreau and Ellis Fluids

Figures 4.3 and 4.4 show plots of the viscosity μ as a function of the shear rate q for a Carreau fluid given by (4.1) for different values of λ, N and μ_∞, and for an Ellis fluid given by (4.2) for different values of $\tau_{\rm av}$, α and μ_∞, respectively, illustrating that in all cases μ decreases from $\mu = 1$ at $q = 0$ and satisfies $\mu \to \mu_\infty^+$ in the limit $q \to \infty$. Moreover, for any given value of q the viscosity μ of a Carreau fluid decreases with λ but increases with N and μ_∞, whereas the viscosity μ of an Ellis fluid increases with $\tau_{\rm av}$ and μ_∞ but increases with α when $q < q_{\rm av} = \tau_{\rm av}/\mu_{\rm av}$, takes the value $\mu_{\rm av}$ for all α when $q = q_{\rm av}$, and decreases with α when $q > q_{\rm av}$. (In Figures 4.3 and 4.4, and in subsequent figures, an arrow across a family of

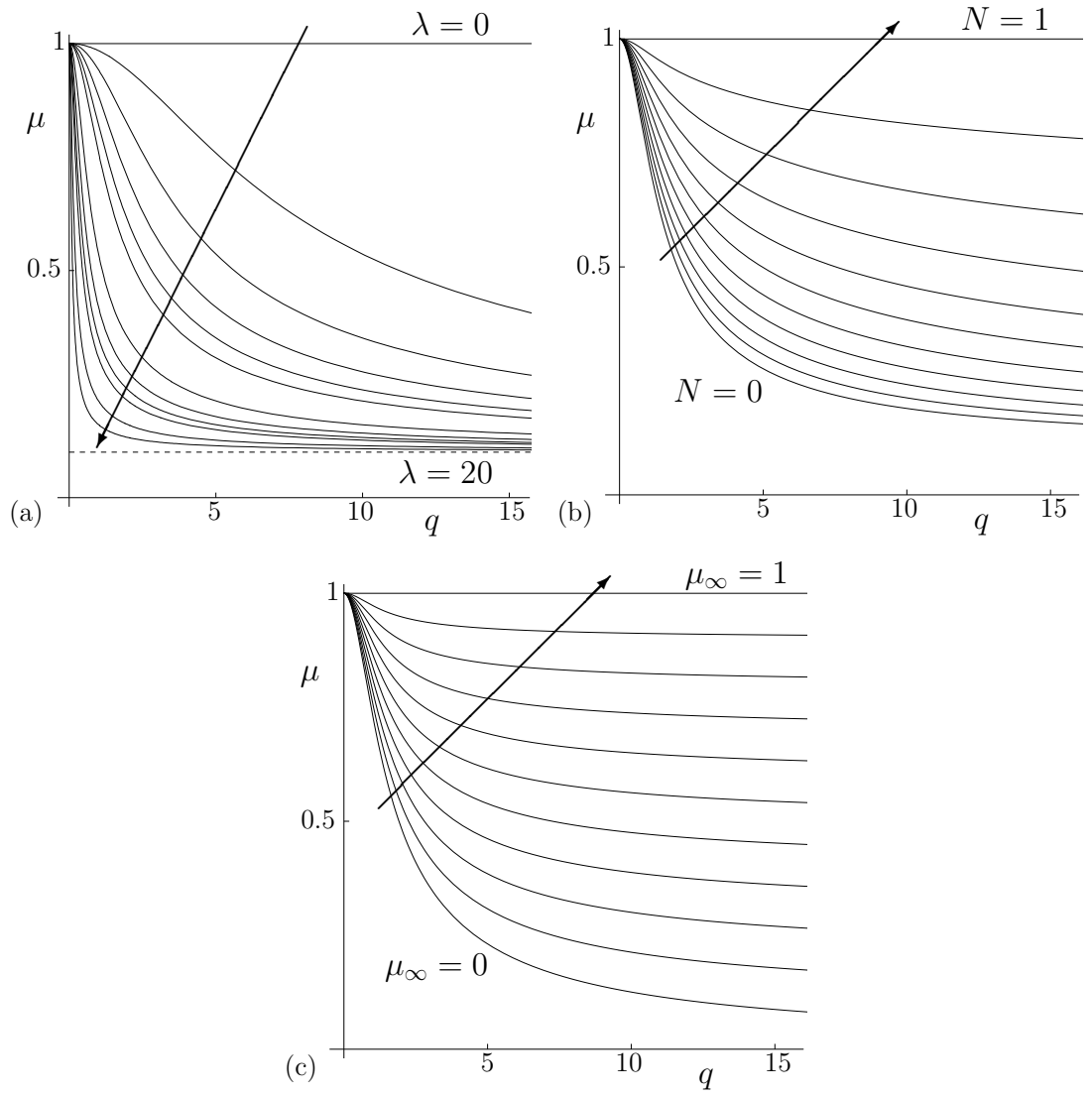

Figure 4.3: Plots of the viscosity μ as a function of the shear rate q for a Carreau fluid given by (4.1) when (a) $\mu_\infty = 1/10$ and $N = 1/10$ for $\lambda = 0$, $1/5$, …, $4/5$, 1, 2, …, 5, 10 and 20, (b) $\mu_\infty = 1/10$ and $\lambda = 1$ for $N = 0$, $1/10$, …, 1, and (c) $N = 1/10$ and $\lambda = 1$ for $\mu_\infty = 0$, $1/10$, …, 1. In part (a) the dashed line shows the asymptotic value in the limit $\lambda \to \infty$, namely $\mu = \mu_\infty = 1/10$.

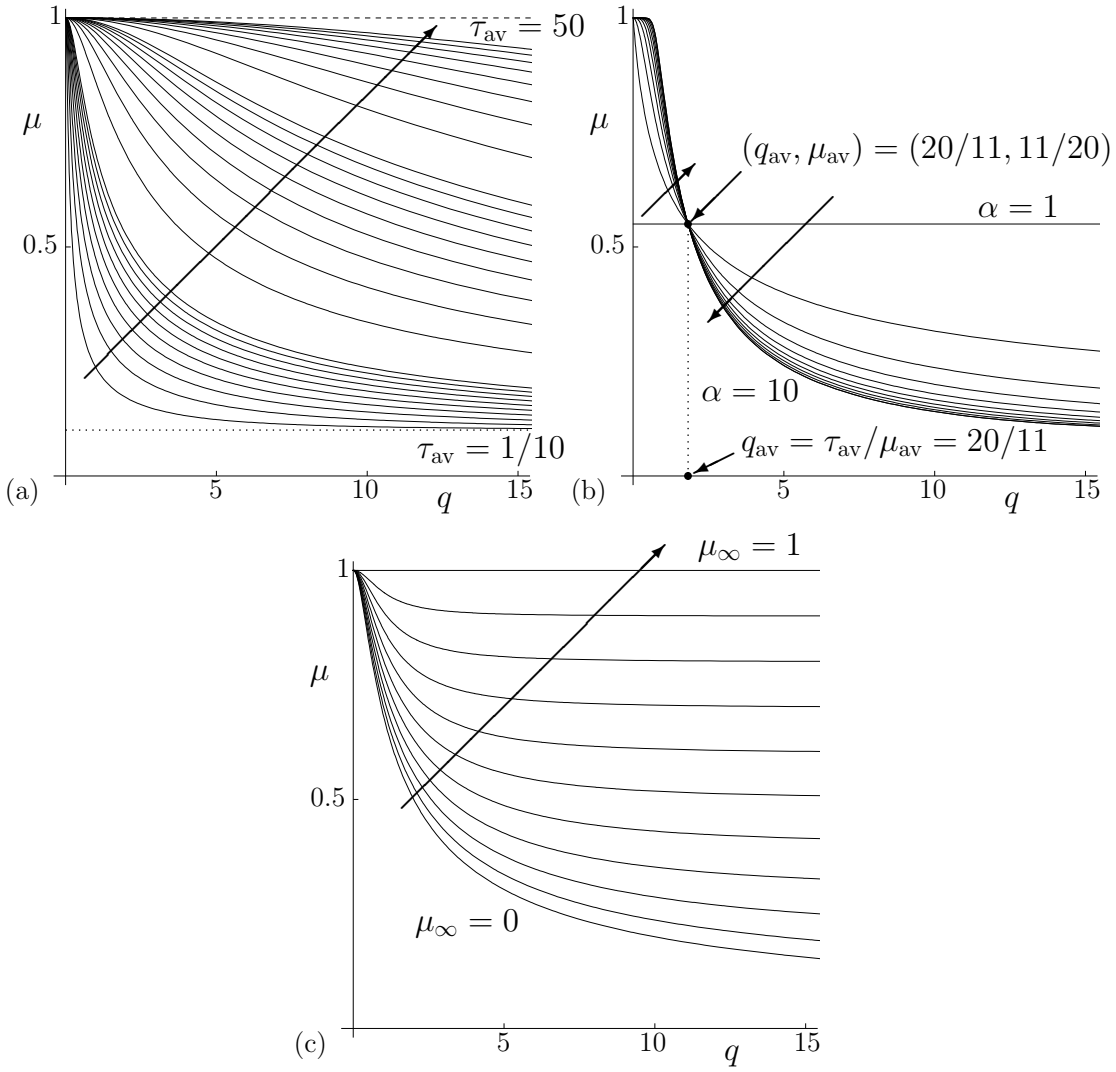

Figure 4.4: Plots of the viscosity μ as a function of the shear rate q for an Ellis fluid given by (4.2) when (a) $\mu_\infty = 1/10$ and $\alpha = 3$ for $\tau_{\rm av} = 1/10$, 1/5, …, 9/10, 1, 2, …, 10, 15, 20, …, 50, (b) $\mu_\infty = 1/10$ and $\tau_{\rm av} = 1$ for $\alpha = 1$, 2, …, 10, and (c) $\alpha = 3$ and $\tau_{\rm av} = 1$ for $\mu_\infty = 0$, 1/10, …, 1. In part (a) the dotted and dashed lines show the asymptotic values in the limits $\tau_{\rm av} \to 0$ and $\tau_{\rm av} \to \infty$, namely $\mu = \mu_\infty = 1/10$ and $\mu = 1$, respectively.

curves denotes the direction of increasing values of the relevant parameter.) As Figure 4.3 also shows, for a Carreau fluid the viscosity gradient $\mathrm{d}\mu/\mathrm{d}q$ at $q = 0$ is always zero, whereas, as Figure 4.4 also shows (although it is a little difficult to discern), for an Ellis fluid it is infinite when $\alpha < 2$, takes the value $-(1-\mu_\infty)/\tau_{\mathrm{av}}$ when $\alpha = 2$, and is zero when $\alpha > 2$.

In Section 4.3.1 we use the exact solution given by (4.19) and (4.21) to describe rivulet flow of a Carreau fluid, and in Section 4.3.2 we use the exact solution given by (4.22) and (4.23) to describe rivulet flow of an Ellis fluid, highlighting the similarities and differences between the behaviour of these two fluids. In particular, we will find that the behaviour of a rivulet of a Carreau fluid and of a rivulet of an Ellis fluid depends on the parameters μ_∞, λ and N and on the parameters μ_∞ and τ_{av}, respectively, in a relatively simple way, reflecting the simple dependence of the viscosities of these fluids on these parameters. However, we will also find that the non-monotonic variation of the viscosity of an Ellis fluid with α leads to a more complicated dependence of the behaviour of the rivulet on α.

4.3.1 A Carreau Fluid

Figure 4.5 shows plots of centreline velocity profiles $u(0, z)$ for a Carreau fluid given by (4.21) for different values of λ, N and μ_∞ with prescribed values of a and β and hence different values of Q, illustrating that $u(0, z)$ increases with λ but decreases with N and μ_∞; this is simply because larger (smaller) values of λ (N and μ_∞) correspond to increased shear thinning, and so to a reduced viscosity and hence to a larger velocity. As discussed in Section 4.1, the cases $\lambda = 0$, $N = 1$ and $\mu_\infty = 1$ and the leading-order behaviour in the limit $\lambda \to \infty$, all of which are included in Figure 4.5, correspond to Newtonian fluids with $\mu = 1$ and $\mu = \mu_\infty$, respectively; in the former cases the solutions for u and Q are given by (4.12),

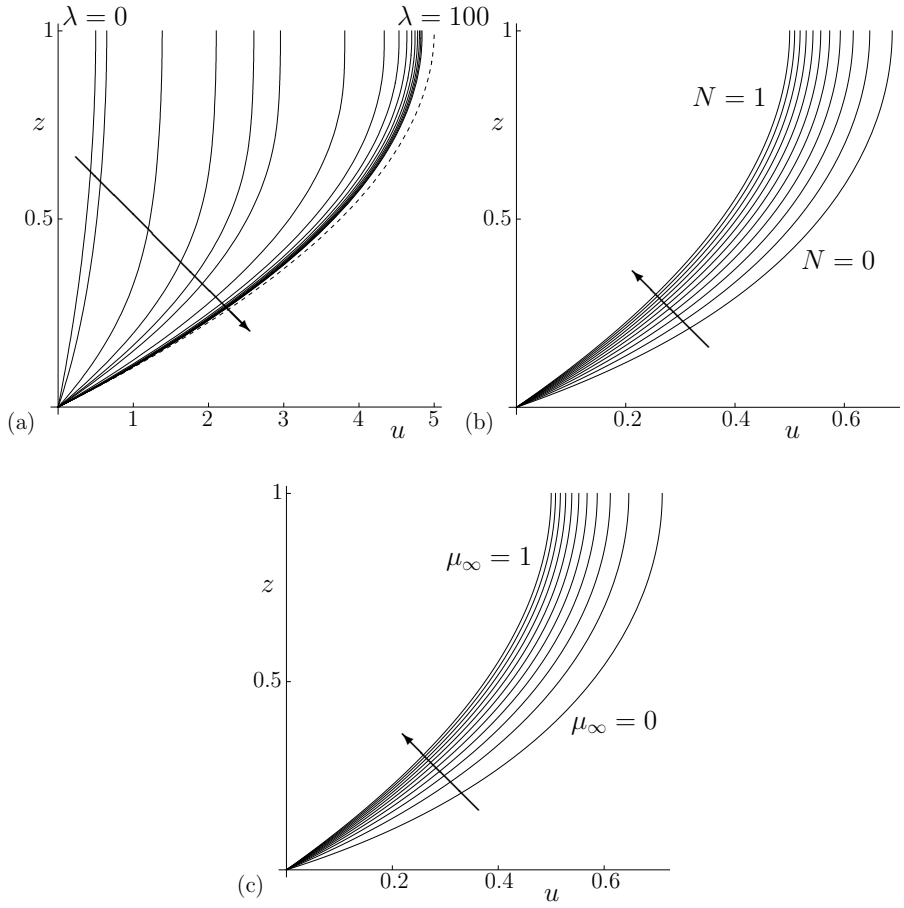

Figure 4.5: Plots of centreline velocity profiles $u(0, z)$ for a Carreau fluid given by (4.21) with $a = 1$ and $\beta = 2$ when (a) $\mu_\infty = 1/10$ and $N = 1/10$ for $\lambda = 0$, 1, ..., 5, 10, 20, ..., 100, (b) $\mu_\infty = 1/10$ and $\lambda = 1$ for $N = 0$, 1/10, ..., 1, and (c) $N = 1/10$ and $\lambda = 1$ for $\mu_\infty = 0$, 1/10, ..., 1. In part (a) the dashed curve shows the leading-order asymptotic solution in the limit $\lambda \to \infty$ given by (4.28).

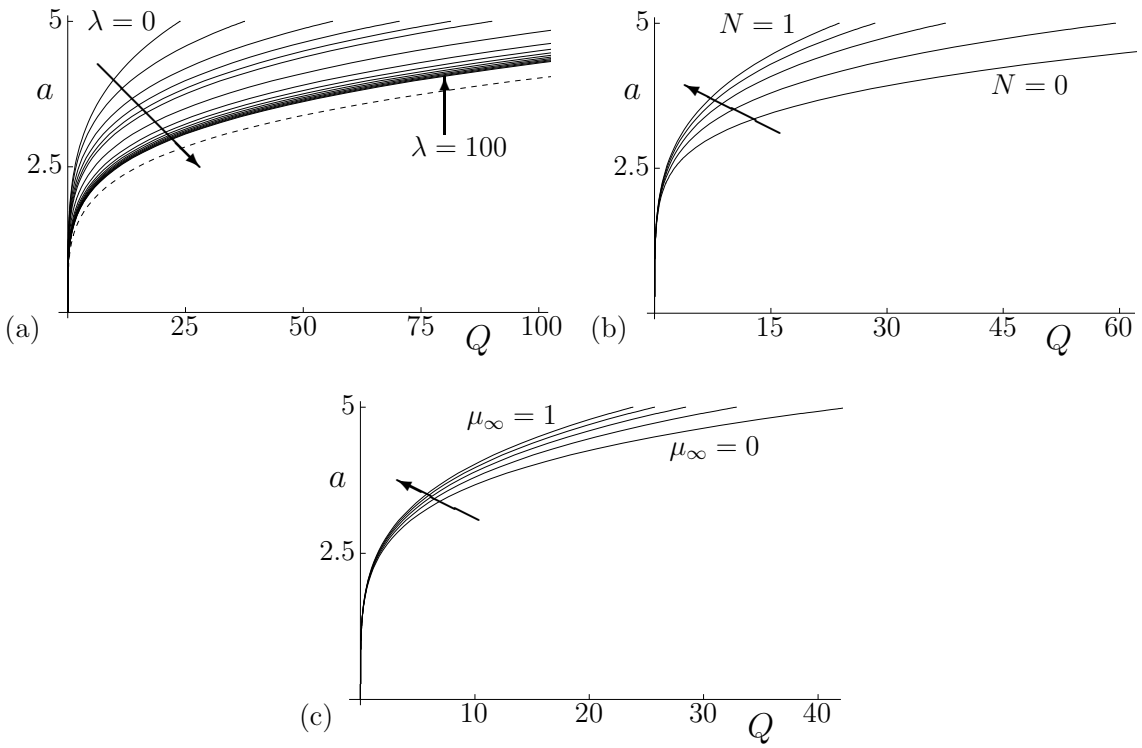

Figure 4.6: Plots of the semi-width a as a function of the flux Q for a Carreau fluid evaluated numerically from (4.19) with $\beta = 1$ when (a) $\mu_\infty = 1/10$ and $N = 1/2$ for $\lambda = 0$, 1, ..., 5, 10, 20, ..., 100, (b) $\mu_\infty = 1/10$ and $\lambda = 1$ for $N = 0$, 1/4, ..., 1, and (c) $N = 1/2$ and $\lambda = 1$ for $\mu_\infty = 0$, 1/4, ..., 1. In part (a) the dashed curve shows the leading-order asymptotic solution in the limit $\lambda \to \infty$ given by (4.28).

and in the latter limit they are given by

$$u = \frac{h^2 - (h-z)^2}{2\mu_\infty}, \qquad Q = \frac{4\beta^3 a^4}{105\mu_\infty}. \tag{4.28}$$

Figure 4.6 shows plots of the semi-width a as a function of the flux Q evaluated numerically from (4.19) for different values of λ, N and μ_∞, illustrating that a always increases with Q. Moreover, for any prescribed flux $Q = \bar{Q}$, a decreases (increases) with λ (N and μ_∞), because an increase (decrease) of λ (N or μ_∞) leads to increased shear thinning, and so a prescribed flux can be achieved with a smaller rivulet. Plots of the contact angle β as a function of the flux Q for different values of λ, N and μ_∞ with a prescribed value of a are qualitatively similar to the plots of a as a function of Q with a prescribed value of β shown in Figure 4.6, and so are omitted for brevity.

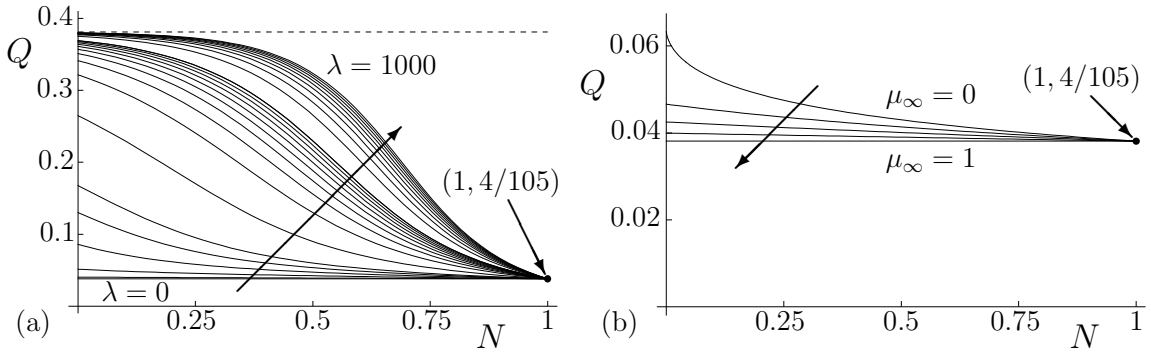

Figure 4.7: Plots of the flux Q as a function of N for a Carreau fluid evaluated numerically from (4.19) with $a = 1$ and $\beta = 1$ when (a) $\mu_\infty = 1/10$ for $\lambda = 0, 1, \ldots, 5, 10, 20, \ldots, 100, 200, \ldots, 1000$, and (b) $\lambda = 2$ for $\mu_\infty = 0, 1/4, \ldots, 1$. In part (a) the dashed line shows the asymptotic value in the limit $\lambda \to \infty$ given by (4.28), namely $Q = 4\beta^3 a^4/105\mu_\infty = 8/21 \simeq 0.3810$.

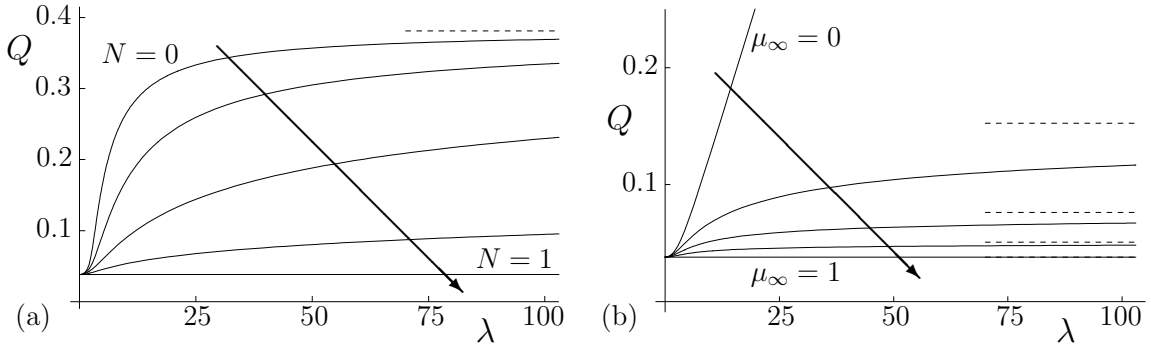

Figure 4.8: Plots of the flux Q as a function of λ for a Carreau fluid evaluated numerically from (4.19) with $a = 1$ and $\beta = 1$ when (a) $\mu_\infty = 1/10$ for $N = 0, 1/4, \ldots, 1$ and (b) $N = 1/2$ for $\mu_\infty = 0, 1/4, \ldots, 1$. The dashed lines show the asymptotic values in the limit $\lambda \to \infty$ given by (4.28).

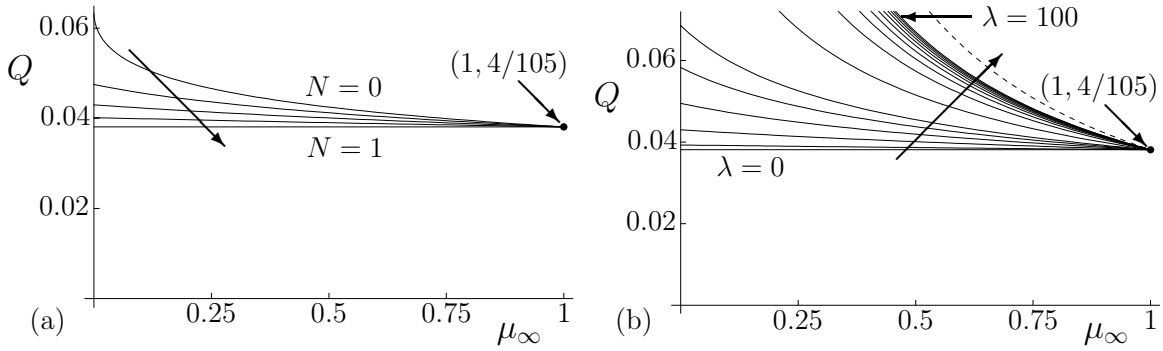

Figure 4.9: Plots of the flux Q as a function of μ_∞ for a Carreau fluid evaluated numerically from (4.19) with $a = 1$ and $\beta = 1$ when (a) $\lambda = 2$ for $N = 0, 1/4, \ldots, 1$, and (b) $N = 1/2$ for $\lambda = 0, 1, \ldots, 5, 10, 20, \ldots, 100$. In part (b) the dashed curve shows the leading-order asymptotic solution in the limit $\lambda \to \infty$ given by (4.28).

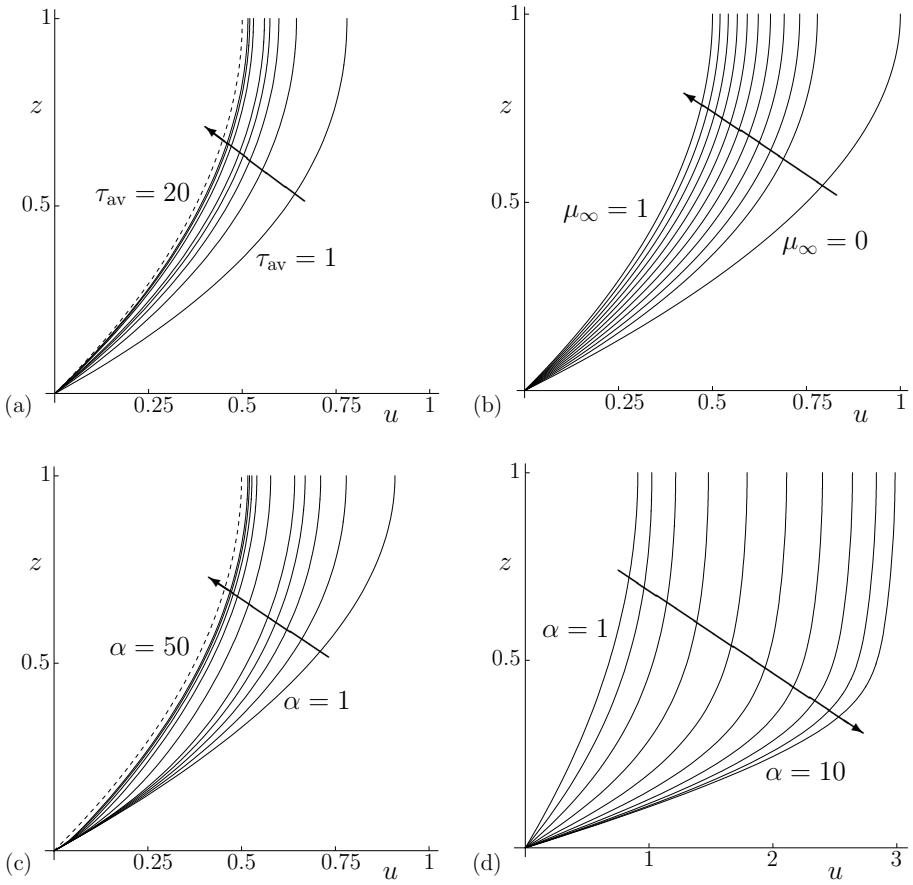

Figure 4.10: Plots of centreline velocity profiles $u(0, z)$ for an Ellis fluid given by (4.23) and (4.25) with $a = 1$ and $\beta = 2$ when (a) $\mu_\infty = 1/10$ and $\alpha = 2$ for $\tau_{\rm av} = 1, 2, \ldots, 5, 10, 15, 20$, (b) $\alpha = 2$ and $\tau_{\rm av} = 1$ for $\mu_\infty = 0, 1/10, \ldots, 1$, (c) $\mu_\infty = 1/10$ and $\tau_{\rm av} = 1$ $\alpha = 1, 2, 3, 4, 5, 10, 20, \ldots, 50$, and (d) $\mu_\infty = 1/10$ and $\tau_{\rm av} = 1/2$ for $\alpha = 1, 2, \ldots, 10$. In parts (a) and (c) the dashed curves show the leading-order asymptotic solution in the limits $\tau_{\rm av} \to \infty$ and $\alpha \to \infty$, respectively, given by (4.12).

Figures 4.7, 4.8 and 4.9 show plots of Q as a function of N evaluated numerically from (4.19) for different values of λ and μ_∞, a function of λ for different values of N and μ_∞, and a function of μ_∞ for different values of N and λ, respectively. In particular, Figures 4.7–4.9 illustrate that Q increases (decreases) with λ (N and μ_∞), that Q takes the value for a Newtonian fluid with $\mu = 1$, namely $Q = 4\beta^3 a^4/105 = 4/105 \simeq 0.0381$, when $N = 1$, $\mu_\infty = 1$ or $\lambda = 0$, that Q approaches the value for a Newtonian fluid with $\mu = \mu_\infty$, namely $Q = 4\beta^3 a^4/105\mu_\infty$, in the limit $\lambda \to \infty$, and that Q takes finite values when $N = 0$ or $\mu_\infty = 0$.

4.3.2 An Ellis Fluid

Figure 4.10 shows plots of centreline velocity profiles $u(0, z)$ for an Ellis fluid given by (4.23) and (4.25) for different values of τ_{av}, μ_∞ and α with prescribed values of a and β and hence different values of Q, illustrating that $u(0, z)$ decreases with τ_{av} and μ_∞, but may either increase or decrease with α. Analogously to a Carreau fluid, the decrease of $u(0, z)$ with τ_{av} and μ_∞ arises simply because larger values of τ_{av} and μ_∞ correspond to decreased shear thinning, and so to an increased viscosity and hence to a smaller velocity. The non-monotonic dependence of $u(0, z)$ on α arises because of the non-monotonic variation of μ with α, shown in Figure 4.4: if q is small over a sufficiently large part of the rivulet then the increase of μ with α leads to a decrease in velocity, as in Figure 4.10(c), whereas if q is large over a sufficiently large part of the rivulet then the decrease of μ with α can lead to an increase in velocity, as in Figure 4.10(d). As discussed in Section 4.1, the case $\mu_\infty = 1$ and the leading-order behaviour in the limit $\tau_{\text{av}} \to \infty$ and the case $\alpha = 1$, all of which are included in Figure 4.10, correspond to Newtonian fluids with $\mu = 1$ and $\mu = \mu_{\text{av}}$, respectively, for which the solutions for u and Q are given by (4.12) and (4.25), respectively.

Figure 4.11 shows plots of the semi-width a as a function of the flux Q for different values of τ_{av}, μ_∞ and α, illustrating that a always increases with Q. Moreover, for any prescribed flux $Q = \bar{Q}$, a increases with τ_{av} and μ_∞, whereas a increases with α for small Q but decreases with α for large Q; the explanation for the latter behaviour is the same as that for the non-monotonicity of $u(0, z)$ with α, discussed above. Analogously to a Carreau fluid, plots of the contact angle β as a function of the flux Q for an Ellis fluid for different values of τ_{av}, μ_∞ and α with a prescribed value of a are qualitatively similar to the plots of a as a function of Q with a prescribed value of β shown in Figure 4.11, and so are again omitted for brevity.

Figure 4.12 shows plots of Q as a function of α for different values of τ_{av} and

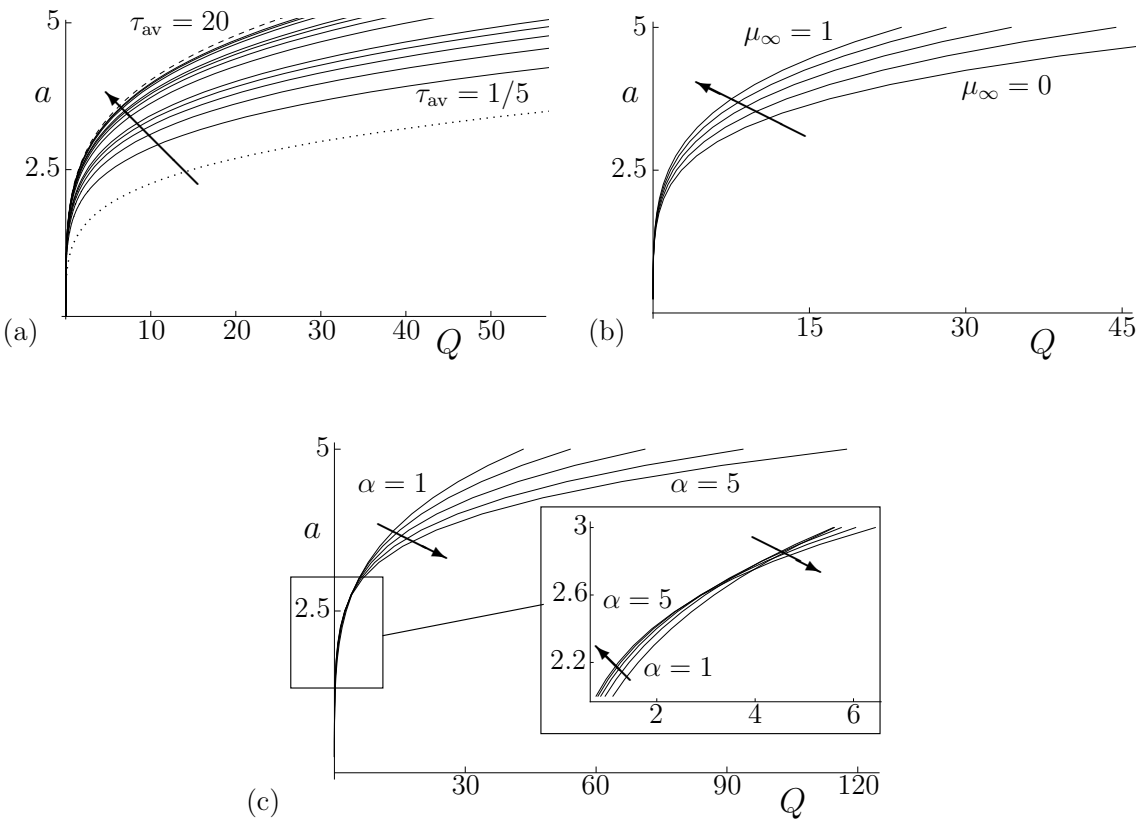

Figure 4.11: Plots of the semi-width a as a function of the flux Q for an Ellis fluid evaluated numerically from (4.22) with $\beta = 1$ when (a) $\mu_\infty = 1/10$ and $\alpha = 2$ for $\tau_{\rm av} = 1/5$, 2/5, 3/5, 4/5, 1, 2, 3, 4, 5, 10, 15, 20, (b) $\alpha = 2$ and $\tau_{\rm av} = 1$ for $\mu_\infty = 0$, 1/4, ..., 1, and (c) $\mu_\infty = 1/10$ and $\tau_{\rm av} = 1$ for $\alpha = 1$, 2, ..., 5. In part (a) the dotted and dashed curves show the leading-order asymptotic solutions in the limits $\tau_{\rm av} \to 0$ and $\tau_{\rm av} \to \infty$ given by (4.28) and (4.12), respectively.

μ_∞. In particular, Figure 4.12(a) shows that Q increases from the value for a Newtonian fluid with $\mu = \mu_{\rm av}$, namely $Q = 4\beta^3 a^4/105\mu_{\rm av} = 16/231 \simeq 0.0693$, at $\alpha = 1$ and tends to the value for a Newtonian fluid with $\mu = \mu_\infty$, namely $Q = 4\beta^3 a^4/105\mu_\infty = 8/21 \simeq 0.3810$, in the limit $\alpha \to \infty$ when $\tau_{\rm av} < \tau_{\rm m} = 1/2$, but decreases and tends to the value for a Newtonian fluid with $\mu = 1$, namely $Q = 4\beta^3 a^4/105 = 4/105 \simeq 0.0381$, in the limit $\alpha \to \infty$ when $\tau_{\rm av} > \tau_{\rm m} = 1/2$. Figure 4.12(b) shows that Q decreases from $Q = 4\beta^3 a^4/105\mu_{\rm av}$ at $\alpha = 1$ and that $Q \to 4\beta^3 a^4/105^+ = 4/105^+$ in the limit $\alpha \to \infty$ when $\tau_{\rm av} > \tau_{\rm m} = 1/2$, whereas Figure 4.12(c) shows that Q increases from $Q = 4\beta^3 a^4/105\mu_{\rm av}$ at $\alpha = 1$ and that $Q \to 4\beta^3 a^4/105\mu_\infty^-$ in the limit $\alpha \to \infty$ when $\tau_{\rm av} < \tau_{\rm m} = 1/2$.

The behaviour of an Ellis fluid in the limit $\alpha \to \infty$ is evidently more complicated than in other cases and will be discussed in detail in Section 4.6.

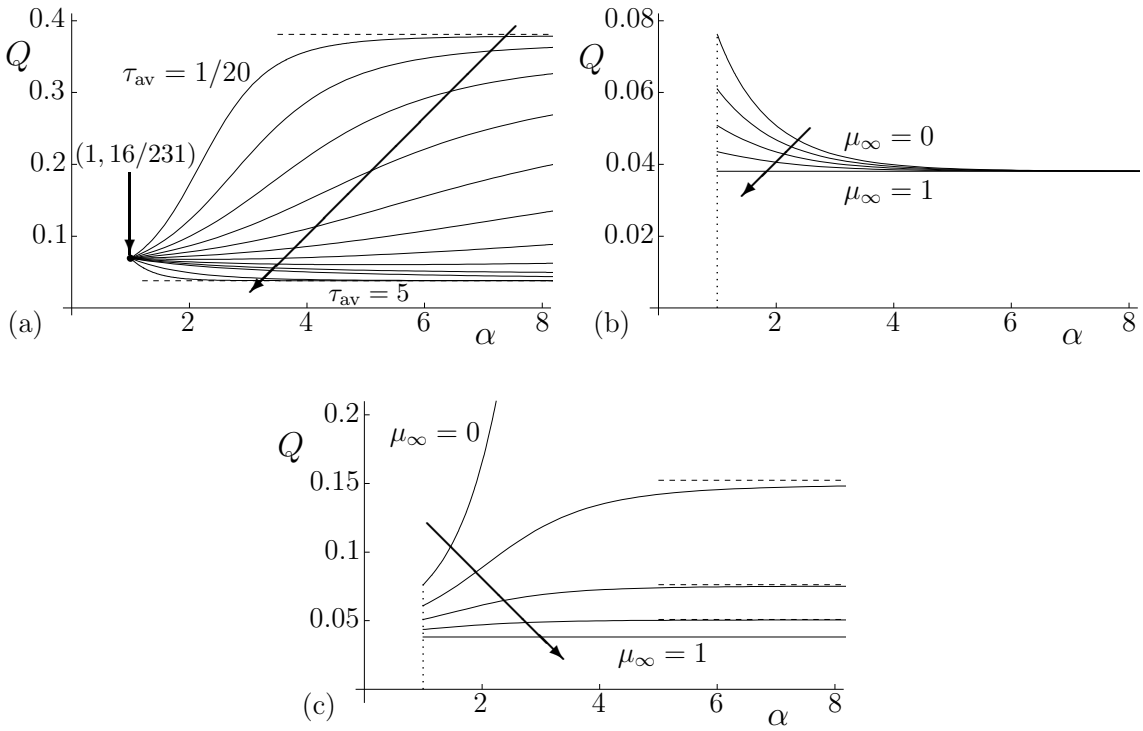

Figure 4.12: Plots of the flux Q as a function of α (≥ 1) for an Ellis fluid evaluated numerically from (4.22) with $a = 1$ and $\beta = 1$ when (a) $\mu_\infty = 1/10$ for $\tau_{\rm av} = 1/20$, $1/10$, ..., $1/4$, 1 and 5, (b) $\tau_{\rm av} = 1 > \tau_{\rm m} = 1/2$ for $\mu_\infty = 0$, $1/4$, ..., 1, and (c) $\tau_{\rm av} = 1/10 < \tau_{\rm m} = 1/2$ for $\mu_\infty = 0$, $1/4$, ..., 1. In parts (a) and (c) the dashed lines show the asymptotic values in the limit $\alpha \to \infty$ given by (4.12) and (4.28), respectively.

Figure 4.13 shows plots of Q as a function of $\tau_{\rm av}$ for different values of α and μ_∞. In particular, Figure 4.13 shows that (except in the special case $\alpha = 1$) Q decreases from $Q = 4\beta^3 a^4/105\mu_\infty$ at $\tau_{\rm av} = 0$, and that $Q \to 4\beta^3 a^4/105^+ = 4/105^+$ in the limit $\tau_{\rm av} \to \infty$.

Figure 4.14 shows plots of Q as a function of μ_∞ for different values of α and $\tau_{\rm av}$. In particular, Figure 4.14 shows that Q decreases from the finite value for a conventional Ellis fluid given by (4.26) at $\mu_\infty = 0$ and takes the value $Q = 4\beta^3 a^4/105 = 4/105$ at $\mu_\infty = 1$.

4.4 Nearly Newtonian Fluids

In this Section we describe the behaviour of rivulets of nearly Newtonian fluids.

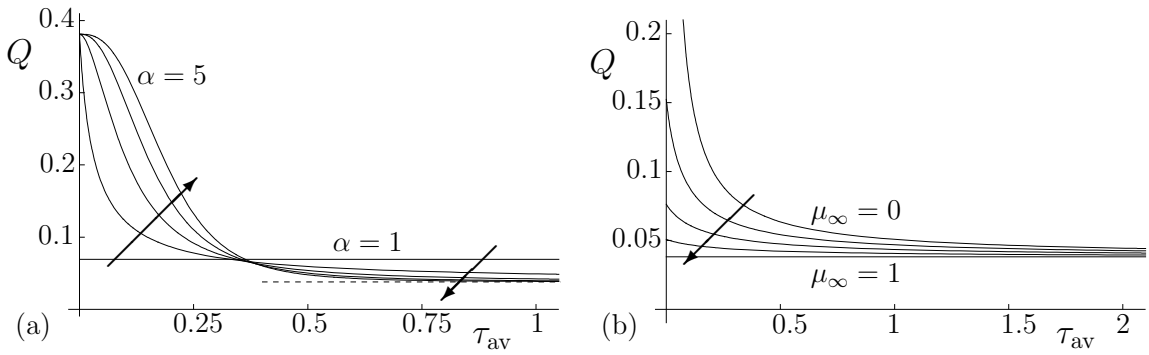

Figure 4.13: Plots of the flux Q as a function of $\tau_{\rm av}$ for an Ellis fluid evaluated numerically from (4.22) with $a = 1$ and $\beta = 1$ when (a) $\mu_\infty = 1/10$ for $\alpha = 1, \ldots, 5$ and (b) $\alpha = 2$ for $\mu_\infty = 0, 1/4, \ldots, 1$. In part (a) the dashed line shows the asymptotic value in the limit $\tau_{\rm av} \to \infty$ given by (4.12), namely $Q \to 4\beta^3 a^4/105 = 4/105$.

4.4.1 General Results

The viscosity of a nearly Newtonian fluid differs only slightly from a constant Newtonian value, and so for a fluid that is nearly Newtonian with viscosity $\mu = 1$ we may write it as

$$\mu = 1 + \mu_1 \delta + O(\delta^2) \tag{4.29}$$

for some $\mu_1 = \mu_1(q)$ or $\mu_1 = \mu_1(\tau)$, where $\delta \ll 1$ is a measure of the small departure from the Newtonian value. In general, this means that the solution for rivulet flow of a nearly Newtonian fluid will differ from that for a Newtonian fluid by an $O(\delta)$ amount, and therefore we expand a as

$$a = a_0 + a_1 \delta + O(\delta^2), \tag{4.30}$$

with corresponding expansions for β, h, u, q, τ and Q, where the leading-order terms (that is, those with suffix 0) correspond to the Newtonian solution (4.12). Thus (4.8) gives

$$h_0 = h_{\rm m0}\left(1 - \frac{y^2}{a_0^2}\right), \qquad h_{\rm m0} = \frac{\beta_0 a_0}{2}, \qquad h_1 = \frac{\beta_0 a_1 \left(a_0^2 + y^2\right) + \beta_1 a_0 \left(a_0^2 - y^2\right)}{2a_0^2}, \tag{4.31}$$

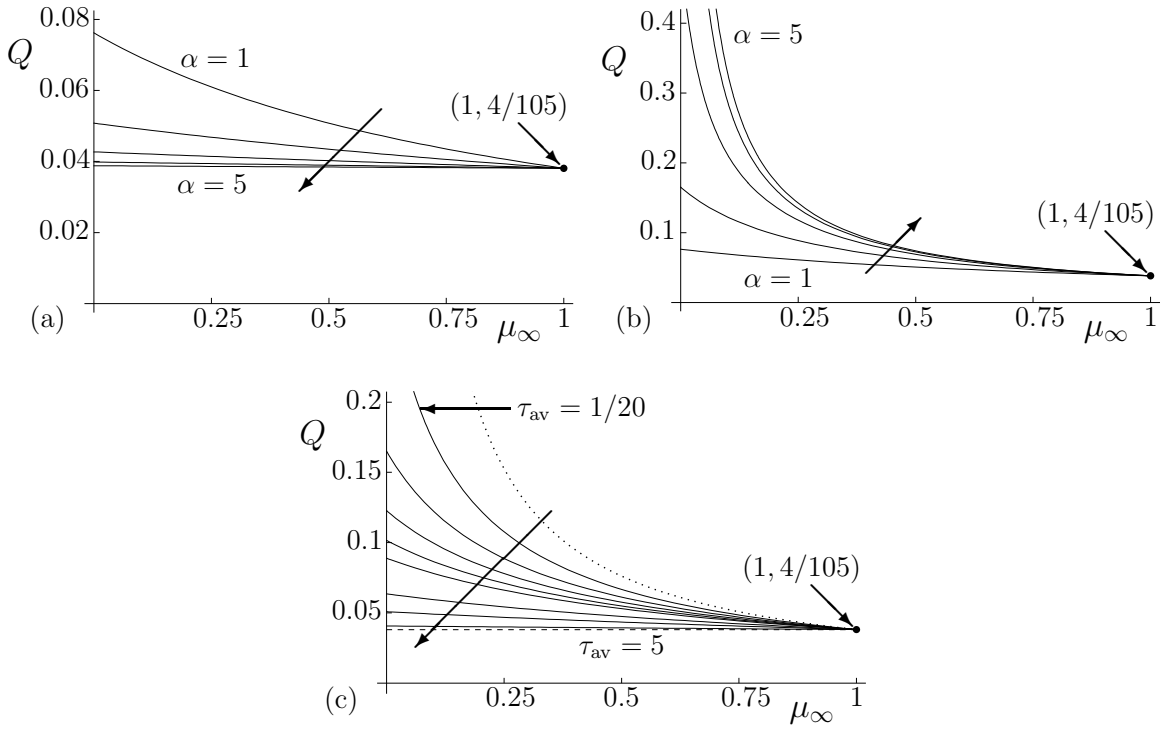

Figure 4.14: Plots of the flux Q as a function of μ_∞ for an Ellis fluid evaluated numerically from (4.22) with $a = 1$ and $\beta = 1$ when (a) $\tau_{\rm av} = 1 > \tau_{\rm m} = 1/2$ for $\alpha = 1, \ldots, 5$, (b) $\tau_{\rm av} = 1/10 < \tau_{\rm m} = 1/2$ for $\alpha = 1, \ldots, 5$, and (c) $\alpha = 2$ for $\tau_{\rm av} = 1/20, 1/10, \ldots, 1/4, 1/2, 1$ and 5. In part (c) the dotted and dashed curves show the leading-order asymptotic solutions in the limits $\tau_{\rm av} \to 0$ and $\tau_{\rm av} \to \infty$ given by (4.28) and (4.12), respectively.

either (4.15) or (4.22) gives

$$u_0 = \frac{h_0^2 - (h_0 - z)^2}{2}, \qquad u_1 = h_1 z - \int_{h_0 - z}^{h_0} \xi \mu_1(\xi)\, \mathrm{d}\xi, \tag{4.32}$$

and either (4.19) or (4.22) gives

$$Q_0 = \frac{4\beta_0^3 a_0^4}{105}, \qquad Q_1 = \frac{4\beta_0^2 a_0^3}{105}(4\beta_0 a_1 + 3\beta_1 a_0) - 2a_0 J_1, \tag{4.33}$$

where we have defined J_1 by

$$J_1 = \int_0^{h_{\rm m0}} \left(1 - \frac{\xi}{h_{\rm m0}}\right)^{1/2} \xi^2 \mu_1(\xi)\, \mathrm{d}\xi, \tag{4.34}$$

with the dummy variable ξ in the integrals in (4.32) and (4.34) corresponding to q in (4.15) and (4.19) and to τ in (4.22). If the contact angle $\beta = \bar{\beta}$ and flux

$Q = \bar{Q}$ are prescribed then $\beta_0 = \bar{\beta}$, $Q_0 = \bar{Q}$, $\beta_1 = 0$ and $Q_1 = 0$, and consequently

$$\begin{aligned} a_0 &= \left(\frac{105\bar{Q}}{4\bar{\beta}^3}\right)^{1/4}, \qquad a_1 = \frac{J_1}{4}\left(\frac{105}{\bar{\beta}^3\bar{Q}}\right)^{1/2}, \\ h_1 &= h_{\mathrm{m1}}\left(1 + \frac{y^2}{a_0^2}\right), \qquad h_{\mathrm{m1}} = \frac{J_1}{8}\left(\frac{105}{\bar{\beta}\bar{Q}}\right)^{1/2}, \end{aligned} \tag{4.35}$$

whereas if the semi-width $a = \bar{a}$ and flux $Q = \bar{Q}$ are prescribed then $a_0 = \bar{a}$, $Q_0 = \bar{Q}$, $a_1 = 0$ and $Q_1 = 0$, and consequently

$$\begin{aligned} \beta_0 &= \left(\frac{105\bar{Q}}{4\bar{a}^4}\right)^{1/3}, \qquad \beta_1 = J_1\left(\frac{70}{9\bar{a}\bar{Q}^2}\right)^{1/3}, \\ h_1 &= h_{\mathrm{m1}}\left(1 - \frac{y^2}{\bar{a}^2}\right), \qquad h_{\mathrm{m1}} = J_1\left(\frac{35\bar{a}^2}{36\bar{Q}^2}\right)^{1/3}. \end{aligned} \tag{4.36}$$

Since, for a shear-thinning fluid, $\mu_1 < 0$ and hence $J_1 < 0$, equations (4.35) and (4.36) show that the effect of weakly non-Newtonian behaviour is always to make the rivulet smaller; in (4.35) it becomes narrower ($a_1 < 0$), whereas in (4.36) its contact angle is reduced ($\beta_1 < 0$), and in both it becomes thinner ($h_{\mathrm{m1}} < 0$). In each case the decrease occurs because the small amount of shear thinning leads to a slight decrease in the viscosity, which means that the velocity is increased slightly and so the prescribed flux $Q = \bar{Q}$ can be achieved with a slightly smaller rivulet.

We now illustrate the above general results with two examples, specifically a Carreau fluid with a small relaxation time λ and an Ellis fluid with a large stress τ_{av}; corresponding results for other limits in which a Carreau fluid and an Ellis fluid are nearly Newtonian with viscosity $\mu = 1$, $\mu = \mu_\infty$ or $\mu = \mu_{\mathrm{av}}$ (as described in Section 4.1) may be obtained in a similar way, but are omitted for brevity.

4.4.2 A Carreau Fluid with a Small Relaxation Time λ

As an example of the general results described in Section 4.4.1 we consider a nearly Newtonian Carreau fluid with a small relaxation time λ. Setting $\delta = \lambda^2 \ll 1$ in

(4.1) we obtain

$$\mu_1 = -kq^2, \qquad \text{where} \quad k = \frac{1}{2}(1-N)(1-\mu_\infty) > 0. \tag{4.37}$$

Then from (4.32) we have

$$u_1 = h_1 z + \frac{k}{4}\left[h_0^4 - (h_0 - z)^4\right] \tag{4.38}$$

and from (4.34) we have

$$J_1 = -\frac{8k}{3465}\beta_0^5 a_0^5, \tag{4.39}$$

and so (4.33) gives

$$Q_1 = \frac{4\beta_0^2 a_0^3}{3465}\left[33(4\beta_0 a_1 + 3\beta_1 a_0) + 4k\beta_0^3 a_0^3\right]. \tag{4.40}$$

If, for example, $\beta_0 = \bar{\beta}$, $Q_0 = \bar{Q}$, $\beta_1 = 0$ and $Q_1 = 0$ then

$$\begin{gathered} a_1 = -\frac{k}{22}\left(\frac{\left(35\bar{Q}\right)^3}{12\bar{\beta}}\right)^{1/4} < 0, \qquad h_1 = h_{\mathrm{m}1}\left(1 + \frac{y^2}{a_0^2}\right), \\ h_{\mathrm{m}1} = -\frac{k}{66}\left(\frac{105\bar{\beta}\bar{Q}}{4}\right)^{3/4} < 0, \end{gathered} \tag{4.41}$$

whereas if $a_0 = \bar{a}$, $Q_0 = \bar{Q}$, $a_1 = 0$ and $Q_1 = 0$ then

$$\beta_1 = -\frac{35k\bar{Q}}{33\bar{a}^2} < 0, \qquad h_1 = h_{\mathrm{m}1}\left(1 - \frac{y^2}{\bar{a}^2}\right), \qquad h_{\mathrm{m}1} = -\frac{35k\bar{Q}}{66\bar{a}} < 0. \tag{4.42}$$

In particular, equations (4.41) and (4.42) confirm that in this case the effect of weakly non-Newtonian behaviour is always to make the rivulet smaller, with a and h_{m} decreasing by amounts proportional to $(\bar{Q}^3/\bar{\beta})^{1/4}$ and $(\bar{\beta}\bar{Q})^{3/4}$, respectively, in (4.41), and with β and h_{m} decreasing by amounts proportional to $\bar{Q}/\bar{a}^2$ and $\bar{Q}/\bar{a}$, respectively, in (4.42).

4.4.3 An Ellis Fluid with a Large Stress $\tau_{\rm av}$

As another example of the general results described in Section 4.4.1 we consider a nearly Newtonian Ellis fluid with a large stress $\tau_{\rm av}$. Setting $\delta = \tau_{\rm av}^{1-\alpha} \ll 1$ in (4.2) we obtain

$$\mu_1 = -(1-\mu_\infty)\tau^{\alpha-1}. \tag{4.43}$$

Then from (4.32) we have

$$u_1 = h_1 z + \frac{1-\mu_\infty}{\alpha+1}\left[h_0^{\alpha+1} - (h_0-z)^{\alpha+1}\right], \tag{4.44}$$

and from (4.34) we have

$$J_1 = -\frac{Ch_{\rm m0}^{\alpha+2}}{2}, \tag{4.45}$$

where the coefficient C is defined by

$$C = \frac{\sqrt{\pi}(1-\mu_\infty)\Gamma(\alpha+2)}{\Gamma\left(\alpha+\frac{7}{2}\right)} = \frac{(1-\mu_\infty)\mathrm{B}(\alpha+3,\frac{1}{2})}{\alpha+2}; \tag{4.46}$$

therefore (4.33) gives

$$Q_1 = a_0 h_{\rm m0}^2\left[\frac{16}{105}\left(4\beta_0 a_1 + 3\beta_1 a_0\right) + Ch_{\rm m0}^{\alpha}\right]. \tag{4.47}$$

If, for example, $\beta_0 = \bar{\beta}$, $Q_0 = \bar{Q}$, $\beta_1 = 0$ and $Q_1 = 0$ then

$$\begin{gathered} a_1 = -\frac{105C}{64\bar{\beta}}\left(\frac{105\bar{\beta}\bar{Q}}{64}\right)^{\alpha/4} < 0, \qquad h_1 = h_{\rm m1}\left(1+\frac{y^2}{a_0^2}\right), \\ h_{\rm m1} = -\frac{105C}{128}\left(\frac{105\bar{\beta}\bar{Q}}{64}\right)^{\alpha/4} < 0, \end{gathered} \tag{4.48}$$

whereas if $a_0 = \bar{a}$, $Q_0 = \bar{Q}$, $a_1 = 0$ and $Q_1 = 0$ then

$$\beta_1 = -\frac{35C}{16\bar{a}}\left(\frac{105\bar{Q}}{32\bar{a}}\right)^{\alpha/3} < 0, \qquad h_1 = h_{\mathrm{m}1}\left(1 - \frac{y^2}{\bar{a}^2}\right), \\ h_{\mathrm{m}1} = -\frac{35C}{32}\left(\frac{105\bar{Q}}{32\bar{a}}\right)^{\alpha/3} < 0. \tag{4.49}$$

In particular, equations (4.48) and (4.49) confirm again that the effect of weakly non-Newtonian behaviour is always to make the rivulet smaller, with a and h_{m} now decreasing by amounts proportional to $(\bar{\beta}\bar{Q})^{\alpha/4}/\bar{\beta}$ and $(\bar{\beta}\bar{Q})^{\alpha/4}$, respectively, in (4.48), and with β and h_{m} decreasing by amounts proportional to $(\bar{Q}/\bar{a})^{\alpha/3}$ and $\bar{a}(\bar{Q}/\bar{a})^{\alpha/3}$, respectively, in (4.49).

4.5 Rivulets with Small or Large Prescribed Flux

In this Section we describe the behaviour of rivulets with small or large prescribed flux $Q = \bar{Q}$. For brevity, details are given only for the case of a viscosity function of the form $\mu = \mu(\tau)$, but the final results are also valid for the case of a viscosity function of the form $\mu = \mu(q)$.

It is convenient first to note that the substitution $\tau = h_{\mathrm{m}}t$ $(0 \le t \le 1)$ together with $(4.8)_2$ allows the flux Q in (4.22) to be expressed (without approximation) in the equivalent forms

$$Q = 2ah_{\mathrm{m}}^3 I = \frac{4h_{\mathrm{m}}^4}{\beta} I = \frac{\beta^3 a^4}{4} I, \tag{4.50}$$

where we have defined the integral I by

$$I = \int_0^1 \frac{(1-t)^{1/2}t^2}{\mu(h_{\mathrm{m}}t)}\,\mathrm{d}t. \tag{4.51}$$

Since μ satisfies $0 \le \mu_\infty < \mu(h_{\mathrm{m}}t) \le 1$, it is clear that I is finite and nonzero.

In the limit of small prescribed flux, $\bar{Q} \to 0$, the rivulet thins $(h_{\mathrm{m}} \to 0)$, and

$\mu(h_{\mathrm{m}}t) \to 1$ throughout the rivulet, leading to $I \to 16/105$. Thus if $\beta = \bar{\beta}$ is prescribed then $h_{\mathrm{m}} \sim (105\bar{\beta}\bar{Q}/64)^{1/4} \to 0$ and $a \sim (105\bar{Q}/4\bar{\beta}^3)^{1/4} \to 0$, whereas if $a = \bar{a}$ is prescribed then $h_{\mathrm{m}} \sim (105\bar{Q}/32\bar{a})^{1/3} \to 0$ and $\beta \sim (105\bar{Q}/4\bar{a}^4)^{1/3} \to 0$. In both cases the stress τ and shear rate q (both of which are zero on the free surface) are small everywhere, and the fluid behaves like a Newtonian fluid with $\mu = 1$.

In the limit of large prescribed flux, $\bar{Q} \to \infty$, the rivulet thickens ($h_{\mathrm{m}} \to \infty$), and $\mu(h_{\mathrm{m}}t) \to \mu_\infty$ except in a thin boundary layer near the free surface at which $\tau = 0$; the dominant contribution to I given by (4.51) is from outside the boundary layer, leading to $I \to 16/(105\mu_\infty)$ in the limit $h_{\mathrm{m}} \to \infty$ (provided that $\mu_\infty \neq 0$). Thus if $\beta = \bar{\beta}$ is prescribed then $h_{\mathrm{m}} \sim (105\mu_\infty\bar{\beta}\bar{Q}/64)^{1/4} \to \infty$ and $a \sim (105\mu_\infty\bar{Q}/4\bar{\beta}^3)^{1/4} \to \infty$, whereas if $a = \bar{a}$ is prescribed then $h_{\mathrm{m}} \sim (105\mu_\infty\bar{Q}/32\bar{a})^{1/3} \to \infty$ and $\beta \sim (105\mu_\infty\bar{Q}/4\bar{a}^4)^{1/3} \to \infty$. In both cases the stress τ and shear rate q are large everywhere except in the boundary layer, and the fluid behaves like a Newtonian fluid with $\mu = \mu_\infty$.

In the case of a viscosity function of the form $\mu = \mu(q)$, the relation $\tau = \mu q$ implies that $\tau \sim q$ in the limit $q \to 0$, and that $\tau \sim \mu_\infty q$ in the limit $q \to \infty$, and so the above results concerning h_{m}, a and β again hold in the limits $\bar{Q} \to 0$ and $\bar{Q} \to \infty$, respectively.

The results obtained thus far are for the general case $\mu_\infty \neq 0$. In the special case $\mu_\infty = 0$ the behaviour of a rivulet when $\bar{Q}$ is small is as described above, but the behaviour when $\bar{Q}$ is large will depend on the asymptotic behaviour of μ for large q or τ, and so it is impossible to give useful general results. For example, for a rivulet of a conventional Ellis fluid (4.2) in the limit $\bar{Q} \to \infty$, equation (4.26) gives

$$a \sim \left[\frac{8\bar{Q}}{C_0\bar{\beta}^3}\left(\frac{2\tau_{\mathrm{av}}}{\bar{\beta}}\right)^{\alpha-1}\right]^{1/(\alpha+3)} \to \infty, \qquad h_{\mathrm{m}} = \frac{\bar{\beta}a}{2} \to \infty, \qquad u \sim \frac{h^{\alpha+1} - (h-z)^{\alpha+1}}{(\alpha+1)\tau_{\mathrm{av}}^{\alpha-1}} \tag{4.52}$$

if $\beta = \bar{\beta}$ is prescribed, and

$$\beta \sim \left[\frac{8\bar{Q}}{C_0\bar{a}^4}\left(\frac{2\tau_{\rm av}}{\bar{a}}\right)^{\alpha-1}\right]^{1/(\alpha+2)} \to \infty, \qquad h_{\rm m} = \frac{\beta\bar{a}}{2} \to \infty, \qquad u \sim \frac{h^{\alpha+1} - (h-z)^{\alpha+1}}{(\alpha+1)\tau_{\rm av}^{\alpha-1}} \tag{4.53}$$

if $a = \bar{a}$ is prescribed. In both (4.52) and (4.53) the large flux is achieved by a combination of the rivulet becoming thick ($h_{\rm m} \to \infty$) and the velocity becoming large ($u \to \infty$ except in a thin boundary layer near the substrate).

4.6 Strongly Shear-thinning Fluids

In this Section we describe strongly shear-thinning Carreau and Ellis fluids, and, in particular, the behaviour of rivulets of such fluids.

A Carreau fluid given by (4.1) is strongly shear thinning in the limits $\lambda \to \infty$ and $N \to -\infty$; at leading order in both limits it behaves like a Newtonian fluid with $\mu = \mu_\infty$ except where q is small. Thus a rivulet of such a fluid behaves like a rivulet of a Newtonian fluid with $\mu = \mu_\infty$ except in a thin boundary layer near the free surface, and so at leading order the solutions for u and Q are given simply by (4.28).

An Ellis fluid given by (4.2) is strongly shear thinning in the limits $\tau_{\rm av} \to 0$ and $\alpha \to \infty$; at leading order in the former limit the behaviour is the same as for a Carreau fluid described above, but, as mentioned earlier, the behaviour in the latter limit is more complicated and is described in Sections 4.6.1 and 4.6.2 below.

4.6.1 A Strongly Shear-thinning Ellis Fluid

At leading order in the strongly shear-thinning limit $\alpha \to \infty$ the viscosity of an Ellis fluid (4.2) with $\mu_\infty \neq 0$ takes the form

$$\mu \sim \begin{cases} 1 & \text{if } \tau < \tau_{\rm av}, \\ \mu_{\rm av} & \text{if } \tau = \tau_{\rm av}, \\ \mu_\infty & \text{if } \tau > \tau_{\rm av}, \end{cases} \tag{4.54}$$

or, in terms of q,

$$\mu \sim \begin{cases} 1 & \text{if } q < \tau_{\rm av}, \\ \dfrac{\tau_{\rm av}}{q} & \text{if } \tau_{\rm av} \le q \le \dfrac{\tau_{\rm av}}{\mu_\infty}, \\ \mu_\infty & \text{if } q > \dfrac{\tau_{\rm av}}{\mu_\infty} \end{cases} \tag{4.55}$$

(which, in particular, satisfies $\mu = \mu_{\rm av}$ when $q = q_{\rm av} = \tau_{\rm av}/\mu_{\rm av}$). Thus for $\tau < \tau_{\rm av}$ the fluid behaves like a Newtonian fluid with $\mu = 1$, but, unlike a biviscosity fluid (1.25), for $\tau > \tau_{\rm av}$ it behaves like a Newtonian fluid with $\mu = \mu_\infty$, there being a transition from one viscosity to the other across any surface on which $\tau = \tau_{\rm av}$.

Note that μ is discontinuous at $\tau = \tau_{\rm av}$ in the limit $\alpha \to \infty$ when it is regarded as a function of τ, given by (4.54), but is continuous when it is regarded as a function of q, given by (4.55), the change in μ from $\mu = 1$ to $\mu = \mu_\infty$ in the latter case occurring over the $O(1)$ change $\tau_{\rm av}(1 - \mu_\infty)/\mu_\infty$ in q.

Figure 4.15 shows plots of the viscosity of an Ellis fluid (4.2) as a function of τ and as a function of q for several large values of α, together with the leading-order asymptotic expressions (4.54) and (4.55), shown with dashed curves.

If the shear rate q and hence the stress τ are sufficiently small everywhere, specifically if $\tau \le \tau_{\rm av}$, which requires that $\tau_{\rm av} \ge \tau_{\rm m}$ $(= h_{\rm m})$, then the fluid behaves like a Newtonian fluid with $\mu = 1$, and the solutions for u and Q are given simply by (4.12).

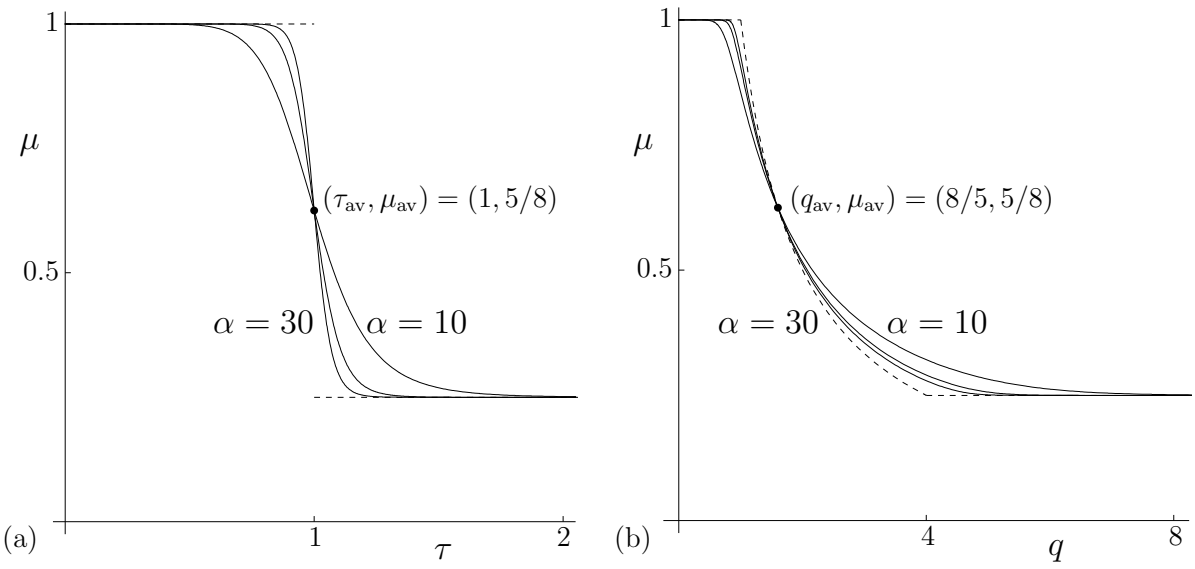

Figure 4.15: Plots of the viscosity of an Ellis fluid given by (4.2) with $\tau_{\rm av} = 1$ and $\mu_\infty = 1/4$: (a) as a function of τ and (b) as a function of q, for $\alpha = 10$, 20 and 30. In parts (a) and (b) the dashed curves show the leading-order asymptotic expressions in the limit $\alpha \to \infty$ given by (4.54) and (4.55), respectively.

On the other hand, if q and hence τ become larger, specifically if τ exceeds $\tau_{\rm av}$ somewhere, which requires that $\tau_{\rm av} < \tau_{\rm m}$ $(= h_{\rm m})$, then, as the sketch of the cross-section of a rivulet shown in Figure 4.16 illustrates, the rivulet comprises two regions, one (shown shaded) adjacent to the free surface with viscosity $\mu = 1$, and the other (shown unshaded) away from the free surface with viscosity $\mu = \mu_\infty$. These two regions are separated from each other by the surface on which $\tau = \tau_{\rm av}$, that is, the surface $z = H(y)$, where

$$H = h - \tau_{\rm av} = h_{\rm m}\left(1 - \frac{y^2}{a^2}\right) - \tau_{\rm av}. \tag{4.56}$$

This surface intersects the substrate $z = 0$ at $y = \pm b$, where b, given by

$$b = a\left(1 - \frac{\tau_{\rm av}}{h_{\rm m}}\right)^{1/2}, \tag{4.57}$$

denotes the semi-width of the region with viscosity $\mu = \mu_\infty$; the maximum thickness of this region is denoted by $H_{\rm m} = H(0) = h_{\rm m} - \tau_{\rm av}$. As Figure 4.16 also shows, the region with viscosity $\mu = 1$ comprises three subregions, two of them

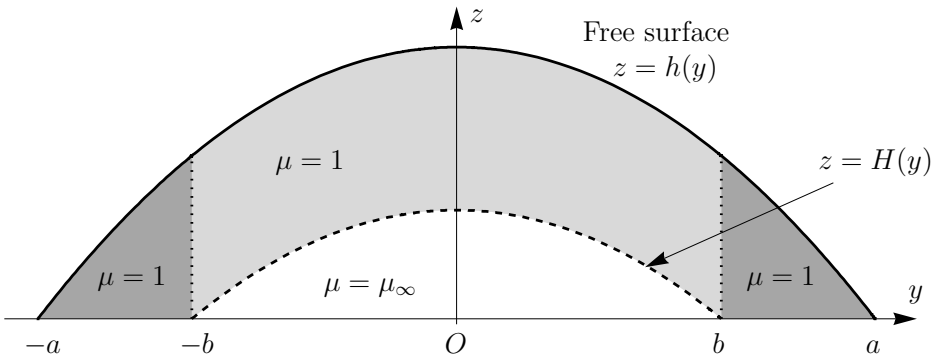

Figure 4.16: Sketch of a cross-section of a rivulet of a strongly shear-thinning Ellis fluid in the limit $\alpha \to \infty$ when $\tau_{\rm av} < \tau_{\rm m}$. The shading denotes the region with viscosity $\mu = 1$, and no shading denotes the region with viscosity $\mu = \mu_\infty$; these regions are separated from each other by the surface $z = H(y) = h(y) - \tau_{\rm av}$, shown with a dashed line. Within the shaded region, the darker shading denotes the two subregions in which the fluid moves with a relatively small velocity, and the lighter shading denotes the subregion in which the fluid moves with a relatively large velocity.

(shown with darker shading) at the sides of the rivulet, in $b < |y| < a$, in which the fluid moves with a relatively small velocity u given by (4.12), and a third one (shown with lighter shading) in the middle of the rivulet, in $H < z < h$ for $|y| < b$, in which the fluid moves with a relatively large velocity, namely

$$u \sim \frac{\tau_{\rm av}^2 - (h-z)^2}{2} + \frac{h^2 - \tau_{\rm av}^2}{2\mu_\infty}, \tag{4.58}$$

because it is lubricated by the fluid with $\mu = \mu_\infty$ in $0 < z < H$ for $|y| < b$ and moving with the velocity given in (4.28). Note that u is continuous across the surface $z = H$, whereas $q = u_z$ changes discontinuously across it because of the discontinuous change in viscosity there. The leading-order flux Q in this case is given by

$$Q \sim \frac{4\beta^3 a^4}{105} + \frac{2\,(1-\mu_\infty)\,(2\beta^2 a^2 + 6\beta a \tau_{\rm av} + 15\tau_{\rm av}^2)\beta b^3}{105\mu_\infty a}, \tag{4.59}$$

and we note that a, β, $h_{\rm m}$, b and Q, as well as the velocity u, are $O(1)$ in the limit $\alpha \to \infty$. The structure of the flow in this case is somewhat similar to that of rivulet flow of a biviscosity fluid, as described by Wilson *et al.* [135] and discussed in Subsection 1.10.6.

Figure 4.17 shows contour plots of the velocity u for two values of $\tau_{\rm av}$ with

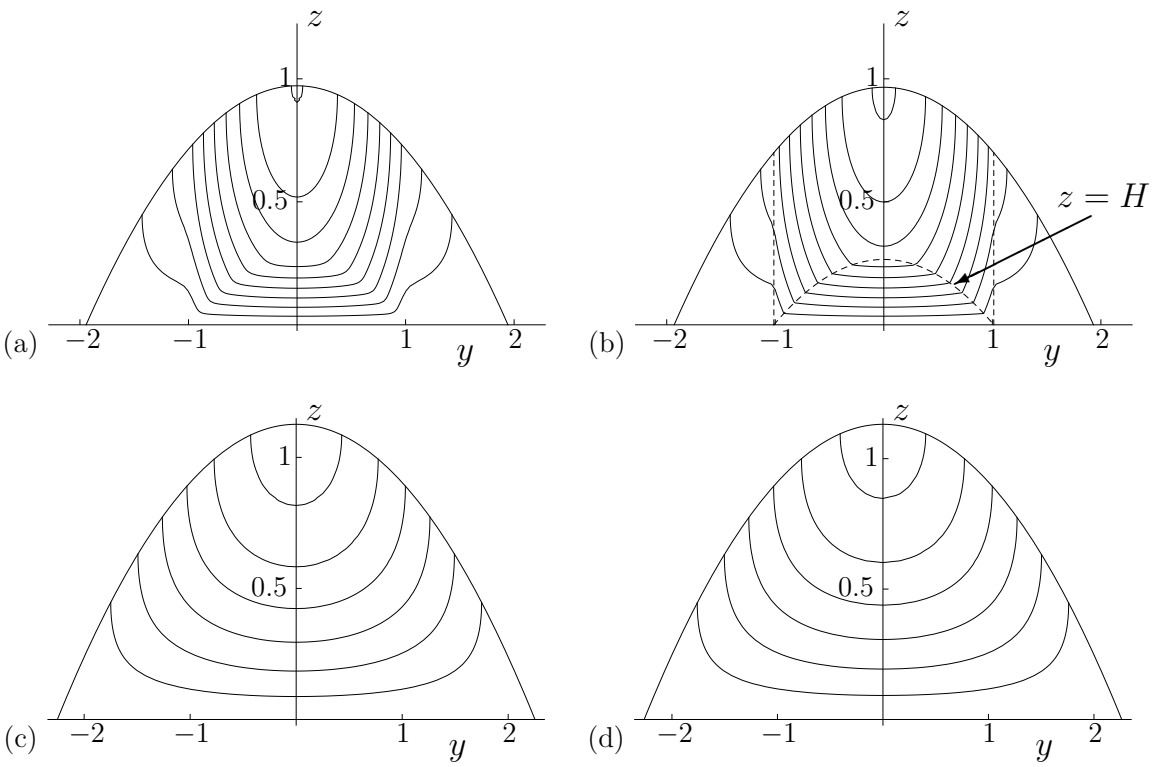

Figure 4.17: Contour plots of the velocity u for an Ellis fluid with $\mu_\infty = 1/3$, $\beta = 1$ and $Q = 1$: (a) the exact solution (4.23) for $\alpha = 50$ and $\tau_{\rm av} = 7/10$ ($< \tau_{\rm m} \simeq 0.9717$), for which $a \simeq 1.9433$, (b) the leading-order asymptotic solution in the limit $\alpha \to \infty$ given by (4.12), (4.28) and (4.58) for $\tau_{\rm av} = 7/10$ ($< \tau_{\rm m} \simeq 0.9657$), for which $a \simeq 1.9313$, $b \simeq 1.0130$ and $H_{\rm m} \simeq 0.2657$, (c) the exact solution (4.23) for $\alpha = 5$ and $\tau_{\rm av} = 2$ ($> \tau_{\rm m} \simeq 1.1263$), for which $a \simeq 2.2525$, and (d) the leading-order asymptotic solution in the limit $\alpha \to \infty$ given by (4.12) for $\tau_{\rm av} = 2$ ($> \tau_{\rm m} \simeq 1.1318$), for which $a \simeq 2.2635$. In part (b) the surfaces $z = H$ and $y = \pm b$ are shown with dashed lines. In all parts the contours are drawn at intervals of 1/10.

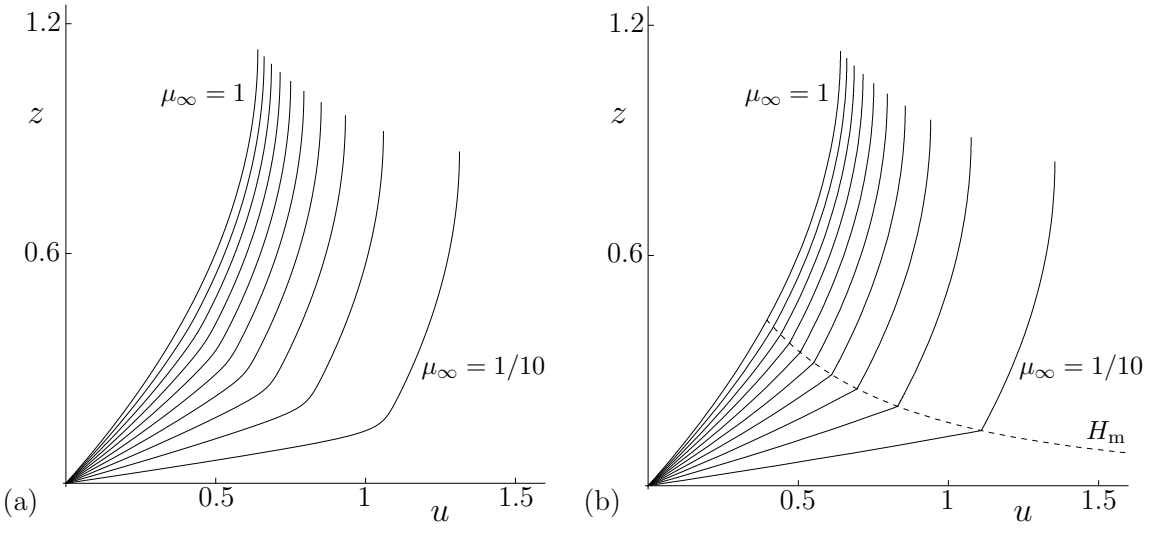

Figure 4.18: Plots of centreline velocity profiles $u(0, z)$ for an Ellis fluid with $\beta = 1$, $Q = 1$ and $\tau_{\rm av} = 7/10$ ($< \tau_{\rm m}$), for $\mu_\infty = 1/10, 1/5, \ldots, 1$: (a) the exact solution (4.23) for $\alpha = 50$, and (b) the leading-order asymptotic solution in the limit $\alpha \to \infty$ given by (4.28) and (4.58). In part (b) the maximum thickness of the region with viscosity $\mu = \mu_\infty$, namely $z = H_{\rm m}$, is shown with a dashed curve.

$\mu_\infty = 1/3$, $\beta = 1$ and $Q = 1$. Figure 4.17(a) shows the exact solution (4.23) for $\alpha = 50$ and $\tau_{\rm av} = 7/10$ ($< \tau_{\rm m} \simeq 0.9717$), with a obtained from (4.22), and Figure 4.17(b) shows the leading-order asymptotic solution given by (4.12), (4.28) and (4.58) for $\tau_{\rm av} = 7/10$ ($< \tau_{\rm m} \simeq 0.9657$), with a obtained from (4.59). Figure 4.17(b) also includes the surfaces $z = H$ and $y = \pm b$ separating the subregions sketched in Figure 4.16, shown with dashed lines. The contours in Figure 4.17(a) are smooth, whereas those in Figure 4.17(b), although continuous, have the expected discontinuities in slope across $z = H$. Figure 4.17(c) shows the exact solution (4.23) for $\alpha = 5$ and $\tau_{\rm av} = 2$ ($> \tau_{\rm m} \simeq 1.1263$), with a obtained from (4.22), and Figure 4.17(d) shows the leading-order asymptotic solution given by (4.12) for $\tau_{\rm av} = 2$ ($> \tau_{\rm m} \simeq 1.1318$), demonstrating the good agreement between them for a relatively modest value of α.

Figure 4.18 shows plots of centreline velocity profiles $u(0, z)$ for several values of μ_∞ with $\beta = 1$, $Q = 1$ and $\tau_{\rm av} = 7/10$ ($< \tau_{\rm m}$). Figure 4.18(a) shows the exact solution (4.23) for $\alpha = 50$, and Figure 4.18(b) shows the leading-order asymptotic solution given by (4.28) and (4.58). In particular, Figure 4.18(b) illustrates the discontinuity in $q = u_z$ across $z = H_{\rm m}$ in the leading-order asymptotic solution.

4.6.2 A Strongly Shear-thinning Conventional Ellis Fluid

The behaviour in the special case of a conventional Ellis fluid is also of interest, and while some features of the behaviour are similar to those in the case of an Ellis fluid described in Section 4.6.1, there are also some significant differences.

At leading order in the strongly shear-thinning limit $\alpha \to \infty$ the viscosity of

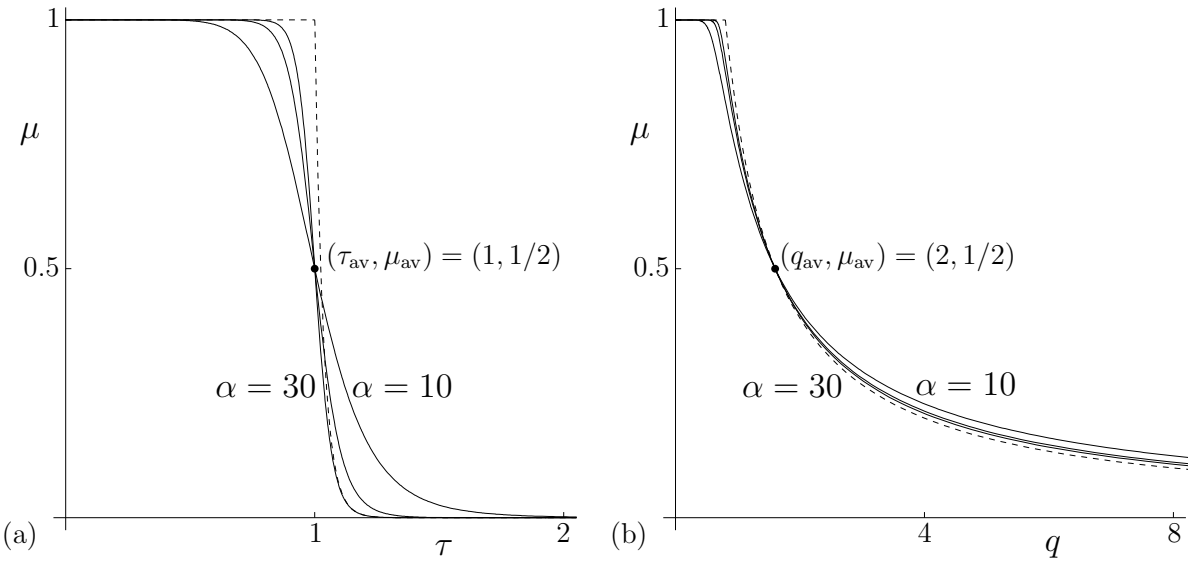

Figure 4.19: Plots of the viscosity of a conventional Ellis fluid given by (4.2) with $\tau_{\rm av} = 1$ and $\mu_\infty = 0$: (a) as a function of τ and (b) as a function of q, for $\alpha = 10$, 20 and 30. In parts (a) and (b) the dashed curves show the leading-order asymptotic expressions in the limit $\alpha \to \infty$ given by (4.60) with $\alpha = 30$ and (4.61), respectively.

a conventional Ellis fluid with $\mu_\infty = 0$ takes the form

$$\mu \sim \begin{cases} 1 & \text{if } \tau < \tau_{\rm av}, \\ \dfrac{1}{2} & \text{if } \tau = \tau_{\rm av}, \\ \left(\dfrac{\tau_{\rm av}}{\tau}\right)^{\alpha-1} \to 0 & \text{if } \tau > \tau_{\rm av}, \end{cases} \tag{4.60}$$

or, in terms of q,

$$\mu \sim \begin{cases} 1 & \text{if } q < \tau_{\rm av}, \\ \dfrac{\tau_{\rm av}}{q} & \text{if } q \geq \tau_{\rm av} \end{cases} \tag{4.61}$$

(which, in particular, satisfies $\mu = \mu_{\rm av} = 1/2$ when $q = q_{\rm av} = \tau_{\rm av}/\mu_{\rm av} = 2\tau_{\rm av}$). Thus for $\tau < \tau_{\rm av}$ the fluid behaves like a Newtonian fluid with $\mu = 1$, whereas, unlike for an Ellis fluid, for $\tau > \tau_{\rm av}$ it behaves like a power-law fluid with non-constant viscosity $\tau_{\rm av} q^{-1}$ with consistency parameter $\tau_{\rm av}$ and power-law index zero, there again being a transition from one viscosity to the other across any surface on which $\tau = \tau_{\rm av}$. Note that (4.60), but not (4.61), depends on α.

Figure 4.19 shows plots of the viscosity of a conventional Ellis fluid (4.2) as a

function of τ and as a function of q for several large values of α, together with the leading-order asymptotic expressions (4.60) with $\alpha = 30$ and (4.61), shown with dashed curves.

If $\tau_{\rm av} \geq \tau_{\rm m}$ $(= h_{\rm m})$ then the fluid behaves like a Newtonian fluid with $\mu = 1$, and the solutions for u and Q are again given simply by (4.12).

On the other hand, if $\tau_{\rm av} < \tau_{\rm m}$ $(= h_{\rm m})$ then the rivulet comprises two regions with different viscosities, somewhat similar to those sketched in Figure 4.16 (with the label $\mu = \mu_\infty$ replaced with $\mu = (\tau_{\rm av}/\tau)^{\alpha-1}$), but with the major difference that, as we shall show below, in the present case the semi-width of the region with viscosity $\mu = (\tau_{\rm av}/\tau)^{\alpha-1}$ is asymptotically small, *i.e.* $b \ll 1$. Thus almost all of the rivulet has viscosity $\mu = 1$, and the region with viscosity $\mu = (\tau_{\rm av}/\tau)^{\alpha-1}$ is thin and narrow. These two regions are again separated from each other by the surface $z = H(y)$ given by (6.7). Over most of the rivulet the velocity u is given by (4.12), but in the narrow central region $|y| < b$ it is given to $O(1)$ by

$$u \sim \frac{h^{\alpha+1} - (h-z)^{\alpha+1}}{\alpha \tau_{\rm av}^{\alpha-1}} + \frac{h^2 - (h-z)^2}{2}. \tag{4.62}$$

Note that (4.62) is uniformly valid across the entire central region, *i.e.* in both $0 < z < H$ and $H < z < h$. The leading-order flux Q in this case is therefore given by

$$Q \sim \beta^3 a^4 \left[\frac{4}{105} + \frac{\sqrt{\pi}}{8\alpha^{3/2}} \left(\frac{h_{\rm m}}{\tau_{\rm av}} \right)^{\alpha-1} \right], \tag{4.63}$$

from which it may be shown that

$$\begin{gathered} h_{\rm m} \sim \tau_{\rm av} \left[1 + \frac{\log(k\alpha^{3/2})}{\alpha} \right] \to \tau_{\rm av}^+, \qquad H_{\rm m} \sim \tau_{\rm av} \frac{\log(k\alpha^{3/2})}{\alpha} \to 0^+, \\ b \sim a \left(\frac{\log(k\alpha^{3/2})}{\alpha} \right)^{1/2} \to 0^+, \end{gathered} \tag{4.64}$$

where the coefficient k (> 0) is found from (4.63) to be given by

$$k = \frac{105\bar{Q} - 32\tau_{\rm av}^3\bar{a}}{105\sqrt{\pi}\tau_{\rm av}^3\bar{a}} \qquad \text{or} \qquad k = \frac{105\bar{\beta}\bar{Q} - 64\tau_{\rm av}^4}{210\sqrt{\pi}\tau_{\rm av}^4} \tag{4.65}$$

when $a = \bar{a}$ or $\beta = \bar{\beta}$, respectively, is prescribed. In deriving (4.64) we have made use of the result $\big(1+\log(k\alpha^{3/2})/\alpha\big)^{\alpha-1} \sim k\alpha^{3/2}$ in the limit $\alpha \to \infty$, so that $h_{\rm m}$ in (4.64) satisfies $(h_{\rm m}/\tau_{\rm av})^{\alpha-1} \sim k\alpha^{3/2}$. The velocity (4.62) has a "plug-like" profile with magnitude $u \sim k\tau_{\rm av}^2\alpha^{1/2} = O(\alpha^{1/2}) \to \infty$ except in a thin boundary layer of thickness $O(\alpha^{-1})$ near the substrate. Note that the leading-order flux Q given in (4.63) has two $O(1)$ contributions, one from the $O(1)$ velocity (4.12) over most of the rivulet, and one from the large $O(\alpha^{1/2}) \gg 1$ velocity (4.62) in the narrow central region $|y| < b$ of semi-width $O((\log\alpha/\alpha)^{1/2}) \ll 1$. The structure of the flow in this case is somewhat similar to that of rivulet flow of a power-law fluid in the strongly shear-thinning limit, as described in Chapters 2 and 3.

Figure 4.20 shows contour plots of the velocity u for two pairs of values of α and $\tau_{\rm av}$ with $\beta = 1$ and $Q = 1$. Figure 4.20(a) shows the exact solution (4.26) for $\alpha = 20$ and $\tau_{\rm av} = 7/10$ ($< \tau_{\rm m} \simeq 0.8488$), and Figure 4.20(b) shows the asymptotic solution given by (4.12), (4.62) and (4.63) for $\alpha = 20$ and $\tau_{\rm av} = 7/10$ ($< \tau_{\rm m} \simeq 0.8574$). Figure 4.20(b) also includes the surfaces $z = H$ and $y = \pm b$ separating the subregions described above, shown with dashed lines. Figure 4.20(c) shows the exact solution (4.26) for $\alpha = 5$ and $\tau_{\rm av} = 2$ ($> \tau_{\rm m} \simeq 1.1235$), and Figure 4.20(d) shows the leading-order asymptotic solution given by (4.12) for $\tau_{\rm av} = 2$ ($> \tau_{\rm m} \simeq 1.1318$), again demonstrating the good agreement between them for a relatively modest value of α.

Figure 4.21 shows plots of scaled centreline velocity profiles $u(0,z)/\alpha^{1/2}$ for several values of α with $\beta = 1$, $Q = 1$ and $\tau_{\rm av} = 1/10$ ($< \tau_{\rm m}$), together with the leading-order asymptotic solution in the limit $\alpha \to \infty$, namely $u(0,z)/\alpha^{1/2} \to k\tau_{\rm av}^{2-} \simeq 28.2078^-$, shown with a dashed line. In particular, Figure 4.21 illustrates

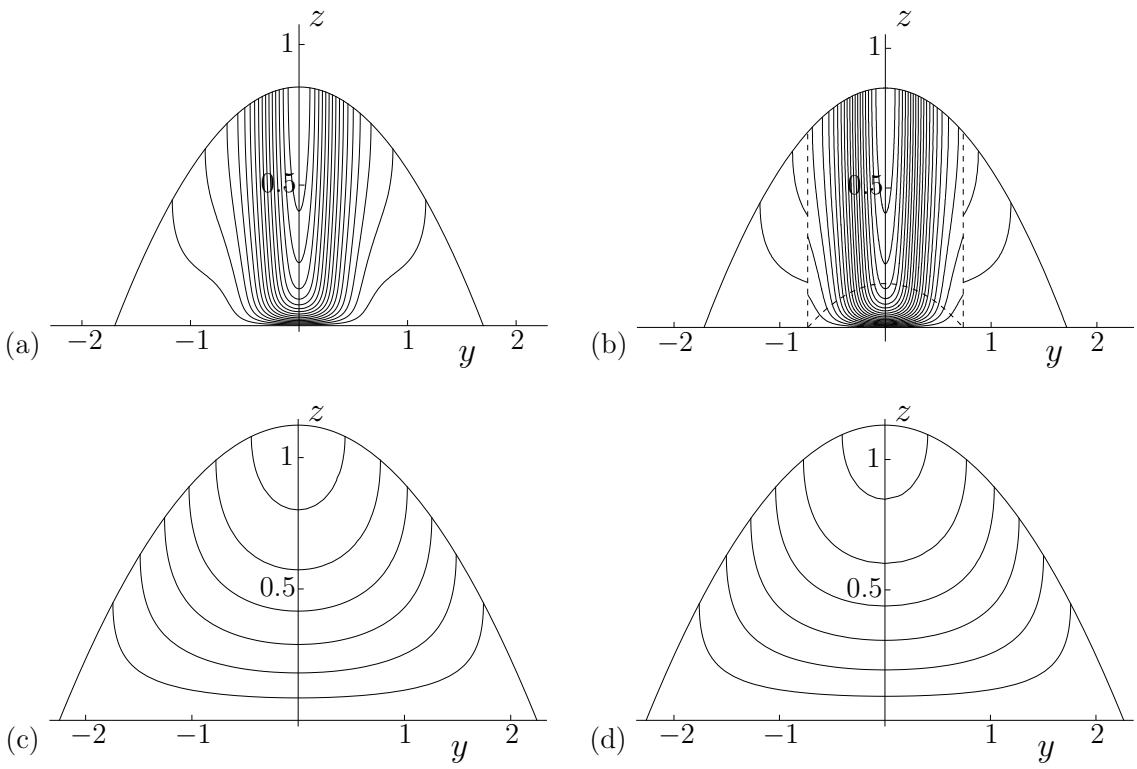

Figure 4.20: Contour plots of the velocity u for a conventional Ellis fluid with $\mu_\infty = 0$, $\beta = 1$ and $Q = 1$: (a) the exact solution (4.26) for $\alpha = 20$ and $\tau_{\rm av} = 7/10$ ($< \tau_{\rm m} \simeq 0.8488$), for which $a \simeq 1.6977$, (b) the asymptotic solution in the limit $\alpha \to \infty$ given by (4.12), (4.62) and (4.63) for $\alpha = 20$ and $\tau_{\rm av} = 7/10$ ($< \tau_{\rm m} \simeq 0.8574$), for which $a \simeq 1.7148$ and $b \simeq 0.8131$, (c) the exact solution (4.26) for $\alpha = 5$ and $\tau_{\rm av} = 2$ ($> \tau_{\rm m} \simeq 1.1235$), for which $a \simeq 2.2470$, and (d) the leading-order asymptotic solution in the limit $\alpha \to \infty$ given by (4.12) for $\tau_{\rm av} = 2$ ($> \tau_{\rm m} \simeq 1.1318$), for which $a \simeq 2.2635$. In part (b) the surfaces $z = H$ and $y = \pm b$ are shown with dashed lines. In all parts the contours are drawn at intervals of 1/10.

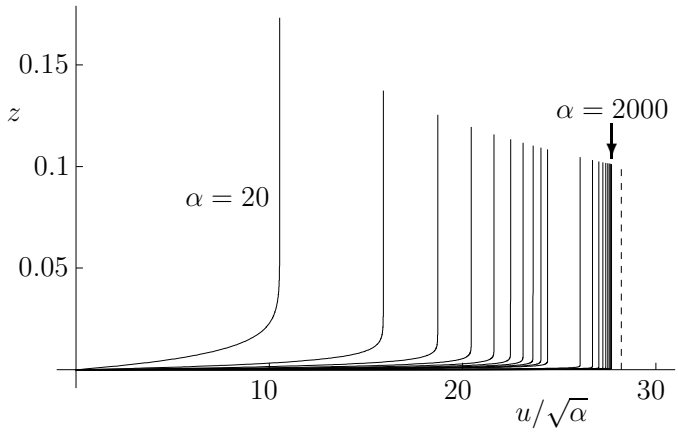

Figure 4.21: Plots of scaled centreline velocity profiles $u(0,z)/\alpha^{1/2}$ for a conventional Ellis fluid with $\mu_\infty = 0$ when $\beta = 1$, $Q = 1$ and $\tau_{\rm av} = 1/10$ ($< \tau_{\rm m}$) for $\alpha = 20$, 40, ..., 200, 400, 600, ..., 2000. The dashed line shows the asymptotic value in the limit $\alpha \to \infty$, namely $u(0,z)/\alpha^{1/2} \to k\tau_{\rm av}^{2-} \simeq 28.2078^-$.

the thin boundary layer near the substrate, the plug-like velocity profile outside the boundary layer, and the convergence of the scaled profiles in the limit $\alpha \to \infty$.

4.7 Conclusions

We considered steady gravity-driven flow of a thin uniform rivulet of a generalised Newtonian fluid down a vertical planar substrate. In Section 4.2.1 we obtained the parametric solution for the velocity u and volume flux Q given by (4.15) and (4.19) for any generalised Newtonian fluid whose viscosity is of the form $\mu = \mu(q)$ (including, in particular, the solution for a Carreau fluid), and the explicit solution given by (4.22) for any generalised Newtonian fluid whose viscosity is of the form $\mu = \mu(\tau)$ (including, in particular, the solutions for an Ellis fluid). In Section 4.3 we used these solutions to describe rivulet flow of a Carreau fluid and of an Ellis fluid, highlighting the similarities and differences between the behaviour of these two fluids. In addition, we described the behaviour of rivulets of nearly Newtonian fluids (Section 4.4), rivulets with small or large prescribed flux (Section 4.5), and rivulets of strongly shear-thinning Carreau and Ellis fluids (Section 4.6).

In addition to a number of general results for rivulet flow of *any* generalised Newtonian fluid, the main conclusion of this chapter is that any increase of shear

thinning leads to an increase in Q if the semi-width a and the contact angle β are prescribed, or to a decrease in a or β if Q is prescribed. It was found that the behaviour of a rivulet of a Carreau fluid and of a rivulet of an Ellis fluid depends on the parameters μ_∞, λ and N and on the parameters μ_∞ and $\tau_{\rm av}$, respectively, in a relatively simple way, reflecting the simple dependence of the viscosities of these fluids on these parameters shown in Figures 4.3 and 4.4(a,b). However, the non-monotonic variation of the viscosity of an Ellis fluid with α shown in Figure 4.4(c) leads to a more complicated dependence of the behaviour of the rivulet on α. In particular, if q is sufficiently small (large) then μ increases (decreases) with α, causing a decrease (an increase) in the velocity of the rivulet. Furthermore, a rivulet of a strongly shear-thinning Ellis fluid for which $\tau_{\rm av} < \tau_{\rm m}$ comprises two regions with different viscosities, as sketched in Figure 4.16, leading to the rather complicated velocity profiles illustrated in Figures 4.17 and 4.18 for an Ellis fluid and Figures 4.20 and 4.21 for a conventional Ellis fluid. In particular, in the latter case the velocity has a plug-like profile with large magnitude $O(\alpha^{1/2}) \gg 1$ in a narrow central region of the rivulet of semi-width $O((\log\alpha/\alpha)^{1/2}) \ll 1$.

Chapter 5

Advection and Taylor–Aris Dispersion in a Semi-circular Rivulet

In this Chapter we consider advection and Taylor–Aris dispersion of a passive solute in steady unidirectional flow of a uniform non-thin rivulet of Newtonian fluid down a vertical planar substrate when the flow is driven by gravity and/or a uniform shear stress on its free surface. We consider only the case in which the contact angle of the rivulet has the prescribed value $\pi/2$; we refer to such a rivulet simply as a "semi-circular rivulet". In Section 5.1 we derive the exact solution for the velocity within a semi-circular rivulet by solving either the appropriate Poisson equation or, when gravity is neglected, Laplace's equation in the domain defined by the cross-section of the rivulet, via the method of separation of variables, as used by Perazzo and Gratton [100] for gravity-driven flow. In Sections 5.3 and 5.4 we consider the processes of (short-time) advection and of (long-time) Taylor–Aris dispersion, respectively, of a passive solute injected into the rivulet.

5.1 Exact Solutions for Flow in a Semi-circular Rivulet

5.1.1 Purely Gravity-driven Case

Consider steady unidirectional gravity-driven flow of a uniform non-thin rivulet of incompressible Newtonian fluid down a planar substrate inclined at an angle α ($0 \leq \alpha \leq \pi$) to the horizontal. We adopt Cartesian coordinates $Oxyz$, with the x axis down the line of greatest slope, the y axis horizontal and the z axis normal to the substrate $z = 0$. The fluid velocity is of the form $\mathbf{u} = u(y, z)\mathbf{i}$, with u and the fluid pressure p satisfying the governing Navier–Stokes equation

$$\mu\nabla^2 u = p_x - \rho g \sin\alpha, \qquad p_y = 0, \qquad p_z = -\rho g \cos\alpha, \tag{5.1}$$

to be solved subject to the no-slip condition on the substrate and the stress-balance condition at the free surface:

$$\begin{gathered} u = 0 \quad \text{on} \quad z = 0, \\ \mu\mathbf{n}\cdot\nabla u = 0 \quad \text{and} \quad p = p_a - \frac{\gamma h''}{(1+h'^2)^{3/2}} \quad \text{on} \quad z = h, \end{gathered} \tag{5.2}$$

where μ and ρ are the constant viscosity and the density of the fluid, respectively, g is the gravitational acceleration, $z = h(y)$ denotes the cross-sectional free surface profile of the rivulet, which has mean curvature $h''(1+h'^2)^{-3/2}$ and outward unit normal $\mathbf{n} = (0, -h', 1)/(1+h'^2)^{1/2}$, γ is the coefficient of surface tension of the fluid, p_a is atmospheric pressure, a prime denotes differentiation with respect to argument, and ∇^2 denotes the two-dimensional Laplacian operator given by

$$\nabla^2 = \frac{\partial^2}{\partial y^2} + \frac{\partial^2}{\partial z^2}. \tag{5.3}$$

We assume that the rivulet is symmetric about its centreline $y = 0$, and that its maximum thickness $h_{\rm m} = h(0)$ occurs at $y = 0$, and we denote its semi-width by a. The contact lines are at $y = \pm a$, at which h satisfies the conditions

$$h = 0 \quad \text{and} \quad h' = \mp \tan\beta \quad \text{at} \quad y = \pm a, \tag{5.4}$$

where β (> 0) denotes the contact angle. The volume flux of fluid along the rivulet, Q, the cross-sectional area of the rivulet, A, and the mean velocity over the cross-section of the rivulet, $\bar{u}$, are given by

$$Q = \int_{-a}^{a}\int_{0}^{h} u \,\mathrm{d}z\,\mathrm{d}y, \qquad A = \int_{-a}^{+a} h \,\mathrm{d}y, \qquad \bar{u} = \frac{Q}{A}, \tag{5.5}$$

respectively.

Integrating $(5.1)_3$ subject to $(5.2)_3$ gives

$$p = \rho g \cos\alpha\,(h - z) - \frac{\gamma h''}{(1 + h'^2)^{3/2}}, \tag{5.6}$$

from which, with equation $(5.1)_2$, we obtain a third order differential equation for the free surface, namely

$$\left(\rho g \cos\alpha\, h - \frac{\gamma h''}{(1 + h'^2)^{3/2}}\right)' = 0, \tag{5.7}$$

representing a transverse balance between gravity and surface-tension effects.

We scale and non-dimensionalise the variables appropriately by writing

$$\begin{aligned} &y = \ell y^*, \quad z = \ell z^*, \quad h = \ell h^*, \quad a = \ell a^*, \quad u = U u^*, \\ &p = p_a + \rho g \ell p^*, \quad \bar{u} = U\bar{u}^*, \quad Q = U\ell^2 Q^*, \quad A = \ell^2 A^*, \end{aligned} \tag{5.8}$$

where $\ell = (\gamma/\rho g)^{1/2}$ is the capillary length, and $U = \rho g \ell^2/\mu$ is an appropriate velocity scale for gravity-driven flow. From now on we use non-dimensional quan-

tities (omitting the star superscripts, for clarity); the governing Navier–Stokes equation and the boundary conditions for u, (5.1) and (5.2), become

$$\nabla^2 u = -\sin\alpha, \qquad u = 0 \quad \text{on} \quad z = 0, \qquad \frac{\partial u}{\partial z} - h'\frac{\partial u}{\partial y} = 0 \quad \text{on} \quad z = h. \tag{5.9}$$

In addition, the non-dimensional form of equation (5.7) is

$$\left(\cos\alpha\, h - \frac{h''}{(1+h'^2)^{3/2}}\right)' = 0, \tag{5.10}$$

and the boundary conditions (5.4) for h still hold; also the volume flux Q, the cross-sectional area A, and mean velocity $\bar{u}$ are still given by (5.5). The problem (5.9) for u, with h determined (in terms of elliptic integrals) by (5.10) subject to (5.4), cannot, in general, be solved in closed form, and so u must, in general, be evaluated numerically.

In the case of flow down a vertical substrate ($\alpha = \pi/2$), surface tension alone determines the cross-sectional shape of the rivulet in (5.10), and the free surface of the rivulet therefore has constant curvature (that is, it is part of a circle), and p is constant. Although with this simplification it may be possible to solve (5.9) analytically for u (using, for example, bipolar coordinates) for any value of the contact angle β, for simplicity we shall restrict our attention entirely to a situation where a relatively simple closed-form solution can be obtained, namely the case when the contact angle β takes the value $\beta = \pi/2$. In this case equation (5.10) may be integrated subject to (5.4) to yield the semi-circular cross-sectional free surface profile of the rivulet:

$$h = \sqrt{a^2 - y^2}. \tag{5.11}$$

For convenience, hereafter we refer to this rivulet simply as a “semi-circular

rivulet". In this case the problem (5.9) reduces to

$$\nabla^2 u = -1, \qquad u = 0 \quad \text{on} \quad z = 0, \qquad \frac{\partial u}{\partial z} - h' \frac{\partial u}{\partial y} = 0 \quad \text{on} \quad z = h. \tag{5.12}$$

The Poisson equation for u in (5.12) may be reduced to Laplace's equation by means of the algebraic substitution

$$u = v - \frac{z^2}{2}, \tag{5.13}$$

leading to the problem

$$\nabla^2 v = 0, \qquad v = 0 \quad \text{on} \quad z = 0, \qquad \frac{\partial v}{\partial z} - h' \frac{\partial v}{\partial y} = h \quad \text{on} \quad z = h. \tag{5.14}$$

In order to solve the problem (5.14) we use cylindrical polar coordinates (r, θ, x) with $y = r\cos\theta$ and $z = r\sin\theta$. The boundary conditions in (5.14) then become

$$v = 0 \quad \text{on} \quad \theta = 0, \pi \quad \text{for} \quad 0 \leq r \leq a, \tag{5.15}$$

$$\frac{\partial v}{\partial r} = a\sin^2\theta \quad \text{on} \quad r = a \quad \text{for} \quad 0 \leq \theta \leq \pi. \tag{5.16}$$

The problem (5.14) is solved using separation of variables in the semi-circular domain Ω given by $0 \leq r \leq a$ and $0 \leq \theta \leq \pi$. Setting $v = R(r)\Theta(\theta)$ leads to

$$\Theta'' + \lambda^2 \Theta = 0, \quad r^2 R'' + rR' - \lambda^2 R = 0, \tag{5.17}$$

where λ is a separation constant. Subject to (5.15) and regularity at the origin $r = 0$, (5.17) leads to the Fourier series solution

$$v = \sum_{m=1}^{\infty} A_m \left(\frac{r}{a}\right)^m \sin m\theta, \tag{5.18}$$

where the coefficients of the Fourier series, A_m, are determined by the boundary

condition (5.16):

$$A_m = \begin{cases} 0 & \text{if } m \text{ is even,} \\ -\dfrac{8}{\pi m^2(m^2-4)} & \text{if } m \text{ is odd.} \end{cases} \tag{5.19}$$

Therefore, the solution for v is given by

$$v = -\frac{8}{\pi}\sum_{n=0}^{\infty} \frac{r^{2n+1}\sin(2n+1)\theta}{(2n+1)^2\left[(2n+1)^2-4\right]a^{2n+1}}. \tag{5.20}$$

From the solution (5.20) and the relation (5.13), the solution for u is given by

$$u = -\frac{8}{\pi}\sum_{n=0}^{\infty} \frac{r^{2n+1}\sin(2n+1)\theta}{(2n+1)^2\left[(2n+1)^2-4\right]a^{2n+1}} - \frac{z^2}{2}, \tag{5.21}$$

which, in order to more readily evaluate this solution numerically, we may alternatively express it in terms of the Lerch transcendent, Φ, via the relation

$$\Phi\left(\frac{r^2\mathrm{e}^{2i\theta}}{a^2}, 2, \frac{1}{2}\right) = \sum_{n=0}^{\infty} \frac{r^{2n}\mathrm{e}^{2ni\theta}}{a^{2n}(\frac{1}{2}+n)^2}, \tag{5.22}$$

(see, for example, Gradshteyn and Ryzhik [49]), to give

$$\begin{aligned} u = \frac{a^2}{2\pi}\mathrm{Im}\Bigg\{ &\frac{r\mathrm{e}^{i\theta}}{a} - \frac{a}{r\mathrm{e}^{i\theta}} - \left(\frac{r^2\mathrm{e}^{2i\theta}}{a^2} - \frac{a^2}{r^2\mathrm{e}^{2i\theta}}\right)\tanh^{-1}\left(\frac{r\mathrm{e}^{i\theta}}{a}\right) \\ &+ \frac{r\mathrm{e}^{i\theta}}{a}\Phi\left(\frac{r^2\mathrm{e}^{2i\theta}}{a^2}, 2, \frac{1}{2}\right)\Bigg\} - \frac{z^2}{2}. \end{aligned} \tag{5.23}$$

The maximum velocity, $u_{\max}$, occurs at $r = a$ and $\theta = \pi/2$, and is given by

$$u_{\max} = \frac{(2+4G-\pi)a^2}{2\pi} \simeq 0.401432a^2, \tag{5.24}$$

where G is Catalan's constant, defined by

$$G = \sum_{n=0}^{\infty} \frac{(-1)^n}{(2n+1)^2} \simeq 0.915966, \tag{5.25}$$

(see, for example, Gradshteyn and Ryzhik [49]). From (5.5) the flux of fluid along the rivulet, Q, may be written

$$Q = \int_0^{\pi} \int_0^{a} ru \, \mathrm{d}r \, \mathrm{d}\theta = \frac{(6 - \pi^2 + 7\zeta(3))a^4}{4\pi} \simeq 0.361663a^4, \tag{5.26}$$

where ζ denotes the Riemann Zeta function, defined by

$$\zeta(s) = \frac{1}{\Gamma(s)} \int_0^{\infty} \frac{t^{s-1}}{1 - \mathrm{e}^{-t}} \, \mathrm{d}t, \tag{5.27}$$

where Γ denotes the Gamma function (see, for example, Gradshteyn and Ryzhik [49]). Also from (5.5) the cross-sectional area of the rivulet, A, and the mean velocity over the cross-section of the rivulet, $\bar{u}$, are given by

$$A = \frac{\pi a^2}{2}, \qquad \bar{u} = \frac{2}{\pi a^2} \int_0^{\pi} \int_0^{a} ru \, \mathrm{d}r \, \mathrm{d}\theta = \frac{2Q}{\pi a^2} \simeq 0.230242a^2, \tag{5.28}$$

respectively. The present solution for the velocity (5.21) was first obtained by Perazzo and Gratton [100]. Note that, however, Perazzo and Gratton [100] did not provide our expression (5.23).

Our aim now is to validate the accuracy and the reliability of the numerical procedure that we will use for deriving the effective diffusivity D_{eff} for Taylor–Aris dispersion in Section 5.4. In order to do this we compare the exact solution and the numerical solution for $\bar{u}$ over the semi-circular domain Ω. Thus, we solved the problem for the velocity u in (5.12) numerically with the mathematical software package MATHEMATICA, using a finite element method over Ω, implemented via NDSolve. The domain was discretised using triangular mesh

Mesh size	$\bar{u}$	Global Error
0.2	0.2302408196	$1.13018494 \times 10^{-6}$
0.02	0.2302426978	$7.480166668 \times 10^{-7}$
0.002	0.2302419725	$2.277267364 \times 10^{-8}$
0.0005	0.2302419514	$1.659569799 \times 10^{-9}$
0.00025	0.2302419503	$5.903413176 \times 10^{-10}$
0.0001	0.2302419499	$1.152373632 \times 10^{-10}$
0.00001	0.2302419498	$1.857082063 \times 10^{-11}$

Table 5.1: Numerical values of the mean velocity $\bar{u}$ and the global error (defined as the modulus of the difference between the exact and the numerical solutions for $\bar{u}$) in gravity-driven flow of a semi-circular rivulet draining down a vertical substrate ($\alpha = \pi/2$) in the case $a = 1$ for a range of mesh sizes.

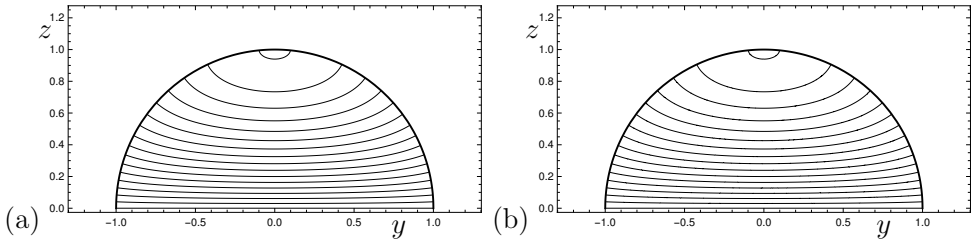

Figure 5.1: Contour plots of the velocity u of gravity-driven flow of a semi-circular rivulet draining down a vertical substrate in the case $a = 1$: (a) the exact solution given by (5.23), and (b) the numerical solution of (5.12). In both parts the contours are drawn at intervals of 1/40.

elements and then this mesh was refined appropriately to increase the accuracy and the precision of the solution. Computations with a finer mesh involved more computational time, and therefore the number of mesh elements was selected appropriately in order to achieve a balance between the accuracy of the solution and the computational effort required; therefore we took the mesh size to be 0.0005.

Table 5.1 shows numerical values of the mean velocity $\bar{u}$ for range of values of the mesh size, confirming that as the mesh size decreases the global error (defined as the modulus of the difference between the exact and the numerical solutions for $\bar{u}$) also decreases.

Figure 5.1 shows contour plots of the velocity u in the case $a = 1$; the contour interval is the same in both parts of the figure. Figure 5.1(a) shows the exact solution given by (5.23), and Figure 5.1(b) shows the numerical solution of (5.12), which is in excellent agreement with the exact solution. Figure 5.1 illustrates that, as expected, there are larger velocity gradients in the z direction near the

substrate, and the contours of u meet the free surface perpendicularly.

5.1.2 Purely Shear-stress-driven Case

The analysis in Subsection 5.1.1 concerns gravity-driven flow of a semi-circular rivulet draining down a vertical planar substrate, but a similar analysis can be performed for another, closely related, problem, namely, flow of a rivulet of fluid on a vertical planar substrate driven by a uniform longitudinal surface shear stress τ, hereafter referred to simply as a shear-stress-driven rivulet.

We consider the case in which the contribution to the velocity due to gravity is negligible in comparison with that due to the surface shear stress, τ, so that the terms p_x, $\rho g \sin\alpha$ and $\rho g \cos\alpha$ in (5.1) may be neglected. Then the fluid velocity is again of the form $\mathbf{u} = u(y,z)\mathbf{i}$, with u and the fluid pressure p satisfying the governing Navier–Stokes equation

$$\nabla^2 u = 0, \qquad p_y = 0, \qquad p_z = 0, \tag{5.29}$$

to be solved subject to the boundary conditions

$$\begin{gathered} u = 0 \quad \text{on} \quad z = 0, \\ \mu \mathbf{n}\cdot\nabla u = \tau \quad \text{and} \quad p = p_a - \frac{\gamma h''}{(1+h'^2)^{3/2}} \quad \text{on} \quad z = h, \end{gathered} \tag{5.30}$$

where ∇^2 again denotes the two-dimensional Laplacian operator given by (5.3). Also h again satisfies the conditions (5.4). The volume flux of fluid along the rivulet, Q, the cross-sectional area of the rivulet, A, and the mean velocity over a cross-section, $\bar{u}$, are again given by (5.5). In this case we scale and nondimensionalise the variables appropriately according to (5.8), but now with $U = \tau\ell/\mu$ as an appropriate velocity scale for shear-stress-driven flow, where ℓ is again the capillary length. For clarity we immediately drop the star superscripts on nondimensional variables, and so the governing Navier–Stokes equation and boundary

conditions for u, (5.29) and (5.30), become

$$\nabla^2 u = 0, \qquad u = 0 \quad \text{on} \quad z = 0, \qquad \frac{\partial u}{\partial z} - h' \frac{\partial u}{\partial y} = 1 \quad \text{on} \quad z = h, \tag{5.31}$$

which, as in the case of the gravity-driven problem discussed in Subsection 5.1.1, cannot, in general, be solved in closed form, and so u must, in general, be evaluated numerically.

Again in this case surface tension alone determines the cross-sectional shape of the rivulet. As in Subsection 5.1.1, we shall consider only the particular case in which the contact angle β has the prescribed value $\beta = \pi/2$, and so the cross-sectional free surface profile of the rivulet is again semi-circular, and h is again given by (5.11).

In order to solve the problem (5.31) we again use cylindrical polar coordinates (r, θ, x) with $y = r\cos\theta$ and $z = r\sin\theta$. The boundary conditions in (5.31) then become

$$u = 0 \quad \text{on} \quad \theta = 0, \pi \quad \text{for} \quad 0 \leq r \leq a, \tag{5.32}$$

$$\frac{\partial u}{\partial r} = 1 \quad \text{on} \quad r = a \quad \text{for} \quad 0 \leq \theta \leq \pi. \tag{5.33}$$

The problem (5.31) is again solved using separation of variables in the semi-circular domain Ω given by $0 \leq r \leq a$ and $0 \leq \theta \leq \pi$; setting $u = R(r)\Theta(\theta)$ again leads to (5.17), which, subject to (5.32) and regularity at the origin $r = 0$, leads to the Fourier series solution

$$u = \sum_{m=1}^{\infty} A_m \left(\frac{r}{a}\right)^m \sin m\theta, \tag{5.34}$$

where the coefficients of the Fourier series, A_m, are determined by the boundary

condition (5.33):

$$A_m = \begin{cases} 0 & \text{if } m \text{ is even,} \\ \dfrac{4}{\pi m^2} & \text{if } m \text{ is odd.} \end{cases} \tag{5.35}$$

Therefore, the solution for u is given by

$$u = \frac{4}{\pi} \sum_{n=0}^{\infty} \frac{r^{2n+1} \sin(2n+1)\theta}{(2n+1)^2 a^{2n+1}}, \tag{5.36}$$

which, may alternatively be expressed in terms of the Lerch transcendent via the relation (5.22) to give

$$u = \frac{a}{\pi} \mathrm{Im} \left\{ \frac{r\,\mathrm{e}^{i\theta}}{a} \Phi \left(\frac{r^2 \mathrm{e}^{2i\theta}}{a^2}, 2, \frac{1}{2} \right) \right\}. \tag{5.37}$$

Note that the velocity given by (5.34) and (5.37) is always in the direction of the applied shear stress. The maximum velocity, $u_{\max}$, occurs at $r = a$ and $\theta = \pi/2$, and is given by

$$u_{\max} = \frac{4aG}{\pi} \simeq 1.166244a, \tag{5.38}$$

where $G \simeq 0.915966$ is Catalan's constant, given by (5.25). From (5.5) the flux of fluid along the rivulet, Q, may be written

$$Q = \int_0^{\pi} \int_0^{a} ru \,\mathrm{d}r \,\mathrm{d}\theta = \frac{(4 - \pi^2 + 14\zeta(3))a^3}{4\pi} \simeq 0.872105a^3, \tag{5.39}$$

where ζ denotes the Riemann Zeta function, given by (5.27). Also from (5.5) the mean velocity over the cross-section of the rivulet, $\bar{u}$, is given by

$$\bar{u} = \frac{2Q}{\pi a^2} \simeq 0.555199a. \tag{5.40}$$

Figure 5.2 shows contour plots of the velocity u in the case $a = 1$; the contour

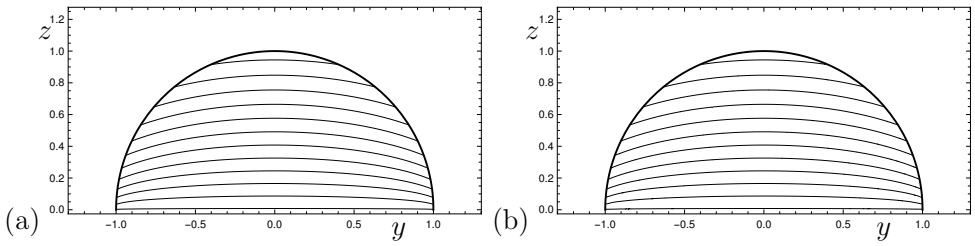

Figure 5.2: Contour plots of the velocity u of shear-stress-driven flow of a semi-circular rivulet draining down a vertical substrate in the case $a = 1$: (a) the exact solution given by (5.37), and (b) the numerical solution of (5.31). In both parts the contours are drawn at intervals of 1/10.

interval is the same in both parts of the figure. Figure 5.2(a) shows the exact solution given by (5.37), and Figure 5.2(b) shows the numerical solution of (5.31), which is again in excellent agreement with the exact solution.

5.1.3 Gravity- and Shear-stress-driven Case

In this Subsection we analyse the problem of a flow of a uniform rivulet down a vertical substrate, the flow being driven by both gravity and a uniform longitudinal shear stress τ. The fluid velocity is again of the form $\mathbf{u} = u(y, z)\mathbf{i}$, with u and the fluid pressure p again satisfying the equations (5.1) with $\alpha = \pi/2$, which are to be solved subject to the boundary conditions (5.30). Again h satisfies the conditions (5.4). The flux of fluid along the rivulet, Q, the cross-sectional area of the rivulet, A, and the mean velocity over the cross-section, $\bar{u}$, are again given by (5.5). We scale and nondimensionalise the variables according to

$$\begin{gathered} y = \ell y^*, \quad z = \ell z^*, \quad h = \ell h^*, \quad a = \ell a^*, \quad u = U u^*, \\ p = p_a + \rho g \ell p^*, \quad \bar{u} = U \bar{u}^*, \quad \tau = \rho g \ell \tau^*, \quad Q = U \ell^2 Q^*, \quad A = \ell^2 A^*, \end{gathered} \tag{5.41}$$

where ℓ is again the capillary length, and $U = \rho g \ell^2/\mu$ is again an appropriate velocity scale associated with gravity-driven flow.

From now on we use non-dimensional quantities (omitting the star superscripts, for clarity); the governing Navier–Stokes equation and boundary condi-

tions for u, (5.1) and (5.2), become

$$\nabla^2 u = -1, \qquad u = 0 \quad \text{on} \quad z = 0, \qquad \frac{\partial u}{\partial z} - h' \frac{\partial u}{\partial y} = \tau \quad \text{on} \quad z = h(y), \tag{5.42}$$

and again we consider only the case of the prescribed contact angle $\beta = \pi/2$.

As in both Subsections 5.1.1 and 5.1.2, the cross-sectional shape of the rivulet is again semi-circular, and h is again given by (5.11). Since the problem (5.42) is linear we can solve it by simply superposing the solutions for the velocity u for the cases of purely gravity-driven and purely shear-stress-driven flow of a semi-circular rivulet obtained previously. Therefore from (5.23) and (5.37) we have the solution

$$\begin{aligned} u = \frac{a^2}{2\pi} \mathrm{Im} \Bigg\{ & \frac{r\,\mathrm{e}^{i\theta}}{a} - \frac{a}{r\,\mathrm{e}^{i\theta}} - \left(\frac{r^2 \mathrm{e}^{2i\theta}}{a^2} - \frac{a^2}{r^2 \mathrm{e}^{2i\theta}} \right) \tanh^{-1} \left(\frac{r\,\mathrm{e}^{i\theta}}{a} \right) \\ & + \left(1 + \frac{2\tau}{a} \right) \frac{r\,\mathrm{e}^{i\theta}}{a} \Phi \left(\frac{r^2 \mathrm{e}^{2i\theta}}{a^2}, 2, \frac{1}{2} \right) \Bigg\} - \frac{z^2}{2}. \end{aligned} \tag{5.43}$$

From (5.26) and (5.39) the volume flux of fluid along the rivulet, Q, is given by

$$Q = \frac{a^3}{4\pi} \Big[a \left(6 - \pi^2 + 7\zeta(3) \right) + \left(4 - \pi^2 + 14\zeta(3) \right) \tau \Big]. \tag{5.44}$$

Inspection of (5.44) reveals that for $\tau \geq 0$ the flux Q is a monotonically increasing function of a, but that for $\tau < 0$ it initially decreases to a minimum value $Q = Q_{\min}$ at $a = a_{\min}$, where

$$\begin{aligned} Q_{\min} &= -\frac{27 \left(4 - \pi^2 + 14\zeta(3) \right)^4 \tau^4}{1024\pi \left(6 - \pi^2 + 7\zeta(3) \right)^3} \simeq -1.28969\tau^4 < 0 \\ a_{\min} &= -\frac{3 \left(4 - \pi^2 + 14\zeta(3) \right) \tau}{4 \left(6 - \pi^2 + 7\zeta(3) \right)} \simeq -1.80853\tau < 0, \end{aligned} \tag{5.45}$$

then increases monotonically, taking the value $Q = 0$ at $a = a_0$, where

$$a_0 = -\frac{(4 - \pi^2 + 14\zeta(3))\,\tau}{6 - \pi^2 + 7\zeta(3)} \simeq -2.41137\tau. \tag{5.46}$$

Note also that $Q = 0$ and hence $\bar{u} = 0$ when τ takes the critical value

$$\tau_{\rm c} = -\frac{(6 - \pi^2 + 7\zeta(3))\,a}{4 - \pi^2 + 14\zeta(3)} \simeq -0.414702a. \tag{5.47}$$

Figure 5.3 shows a plot of the flux Q as a function of a given by (5.44) for various values of τ, illustrating that Q increases monotonically with a when $\tau = 1$ and $\tau = 0$, but that when $\tau = -1$ it decreases to a minimum value $Q = Q_{\rm min} \simeq -1.28969$ at $a = a_{\rm min} \simeq 1.80853$, taking the value $Q = 0$ at $a = a_0 \simeq 2.41137$, and then increases to ∞. Figure 5.3 is qualitatively the same as Figure 2 of Wilson and Duffy [132] (see Figure 1.14), who studied the corresponding problem for the case of a thin rivulet on a vertical substrate; the main results of Wilson and Duffy [132] were summarised in Section 1.8. Wilson and Duffy [132] also categorised and analysed all of the five possible flow patterns that can occur in the case of a thin rivulet. In order to perform a similar analysis for the present problem and, in particular, to determine whether there are also only five flow patterns in this case we would need to calculate where $u = 0$. This cannot be done analytically; however, numerical calculations of the velocity u given by (5.43) suggest that this is indeed the case.

Figure 5.4 shows examples of contour plots of the velocity u given by (5.43), showing the five different types of cross-sectional flow pattern, in the cases (a) $\tau = -1/5$, (b) $\tau = -32/100$, (c) $\tau \simeq -0.344209$, (d) $\tau = -2/5$, and (e) $\tau = -2/3$. In Figure 5.4 regions of downwards flow (*i.e.* regions with $u > 0$) are shaded, and regions of upwards flow (*i.e.* regions with $u < 0$) are unshaded. Figure 5.4 is qualitatively the same as Figure 1 of Wilson and Duffy [132].

As Figure 5.4 illustrates, when $\tau \geq 0$ (*i.e.* the prescribed shear stress acts in

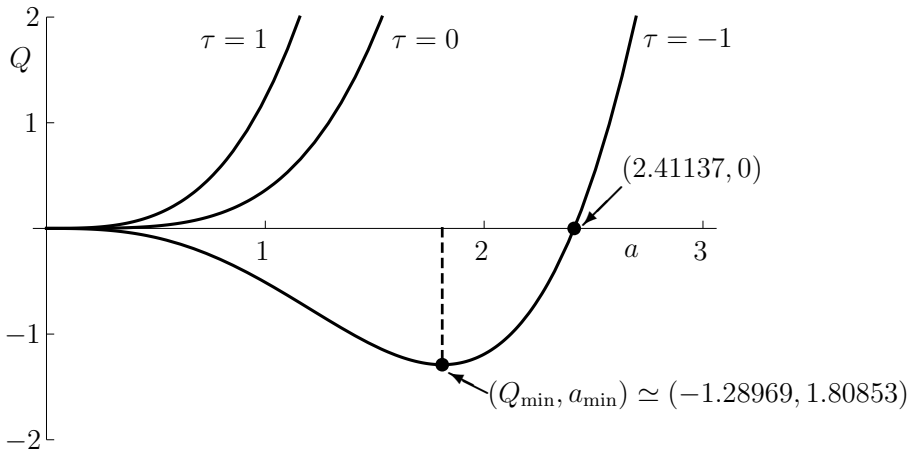

Figure 5.3: Plot of the flux Q given by (5.44) as a function of a in gravity- and shear-stress-driven flow in a semi-circular rivulet on a vertical substrate in the cases $\tau = -1$, 0, and 1. The dots indicate, for the case $\tau = -1$, the minimum value $Q = Q_{\min} \simeq -1.28969$ at $a = a_{\min} \simeq 1.80853$ and the value $Q = 0$ at $a = a_0 \simeq 2.41137$.

cooperation with the effect of gravity), the velocity is downwards throughout the rivulet (*i.e.* $u \geq 0$), but in contrast, when $\tau < 0$ (*i.e.* the prescribed shear stress acts in opposition to the effect of gravity) the velocity is upwards near the edge of the rivulet, but it can be downwards elsewhere.

5.2 Dispersion of a Passive Solute in a Semi-circular Rivulet

As discussed in Section 1.11, in general, when a passive solute is injected into a unidirectional flow such as the rivulet flow described in Section 5.1 it disperses because of a combination of advection and diffusion effects, and so the evolution of its concentration $c = c(x, y, z, t)$ is governed by the (dimensional) advection–diffusion equation

$$c_t + uc_x = D(c_{xx} + \nabla^2 c), \tag{5.48}$$

where t denotes time, D is the diffusion coefficient of the solute, and ∇^2 again denotes the two-dimensional Laplacian operator given by (5.3), to be solved subject to the no-flux conditions on the boundary of the fluid (comprising both the

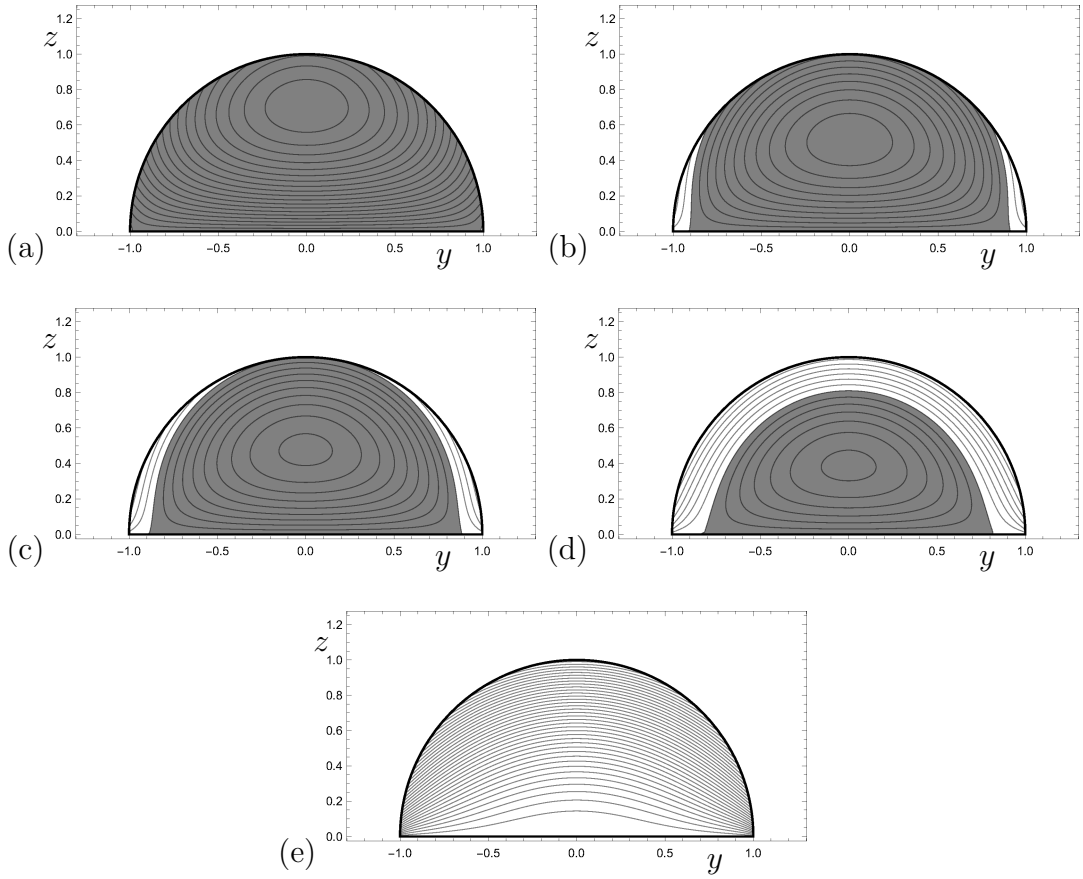

Figure 5.4: Contour plots of the velocity u given by (5.43) in gravity- and shear-stress driven flow in a semi-circular rivulet on a vertical substrate in the case $a = 1$: (a) $\tau = -1/5$, (b) $\tau = -32/100$, (c) $\tau \simeq -0.344209$, (d) $\tau = -2/5$, and (e) $\tau = -2/3$. In each part regions of downwards flow (*i.e.* $u > 0$) are shaded in grey while regions of upwards flow (*i.e.* $u < 0$) are unshaded. The contours are drawn at intervals of 1/100 in each part of the figure.

substrate and the free surface of the rivulet),

$$\mathbf{n} \cdot \nabla c = 0 \quad \text{on} \quad z = 0 \quad \text{and} \quad z = h, \tag{5.49}$$

where $\mathbf{n}$ denotes the unit outward normal to the boundary of the fluid. In addition, we shall assume that the solute is injected at some initial instant $t = 0$ with a prescribed initial concentration $c(x, y, z, 0)$ that is localised over a possibly infinite portion $x_1 \leq x \leq x_2$ of the rivulet, with x_1 and x_2 prescribed.

A key quantity of interest is the mean concentration over the cross-section, which we denote by $\bar{c} = \bar{c}(x, t)$, and which is defined by

$$\bar{c} = \frac{1}{A} \int_{-a}^{a} \int_{0}^{h} c \, \mathrm{d}z \, \mathrm{d}y. \tag{5.50}$$

In addition, we denote the mean of the initial concentration of c over the rivulet by the constant $\overline{C}_0$, defined by

$$\overline{C}_0 = \frac{1}{A(x_2 - x_1)} \int_{x_1}^{x_2} \int_{-a}^{a} \int_{0}^{h} c(x, y, z, 0) \, \mathrm{d}z \, \mathrm{d}y \, \mathrm{d}x, \tag{5.51}$$

in which the integral is interpreted as an appropriate limit if $x_2 - x_1$ is infinite.

5.3 Advection of a Passive Solute in a Semi-circular Rivulet

In this Section we consider the short-time advection of a slug of a passive solute injected into steady unidirectional flow of a semi-circular rivulet of Newtonian fluid on a vertical planar substrate when the flow is driven either purely by gravity or purely by a uniform surface shear stress on its free surface. For simplicity we will not consider the case when gravity and surface shear stress act simultaneously.

At sufficiently small times after the solute is injected, specifically for $t \ll \ell^2/D$,

the process of advection will dominate over that of diffusion, and so the effects of diffusion may be ignored. In that case the governing equation (5.48) for c reduces simply to the advection equation

$$c_t + uc_x = 0, \tag{5.52}$$

which has general solution

$$c(x, y, z, t) = c\big(x - u(y, z)t, y, z, 0\big). \tag{5.53}$$

The solution (5.53) simply reflects the fact that the particle of solute that is at $\mathbf{x} = \mathbf{x_0}$ at $t = 0$ is at

$$\mathbf{x} = \mathbf{x_0} + u(y, z)t\mathbf{i} \tag{5.54}$$

at time t.

Note that the behaviour of u described in both Subsections 5.1.1 and 5.1.2 means that all of the solute is advected downwards.

5.3.1 An Initially Semi-infinite Slug of Solute in Purely Gravity-driven Flow

We first consider an initially semi-infinite slug of solute of uniform concentration $c = c_0$ in $x \leq 0$, with $c = 0$ in $x > 0$ at time $t = 0$, where c_0 is a constant.

We scale and nondimensionalise the variables as in (5.8), together with

$$x = \ell x^*, \quad t = \frac{\ell}{U}t^*, \quad c = \overline{C}_0 c^*, \quad \bar{c} = \overline{C}_0 \bar{c}^*, \tag{5.55}$$

and for clarity we again drop the stars superscripts on non-dimensional variables.

Thus, with $\overline{C}_0 = c_0$, c satisfies the initial condition

$$c = \begin{cases} 1 & \text{if } x \leq 0, \\ 0 & \text{if } x > 0, \end{cases} \tag{5.56}$$

at time $t = 0$, and the solution for c at time t is given by

$$c = \begin{cases} 1 & \text{if } x \leq ut, \\ 0 & \text{if } x > ut, \end{cases} \tag{5.57}$$

the slug having a front at $x = ut$ which is planar at time $t = 0$ but is curved for $t > 0$. Because of the no-slip condition at the substrate, the base of the front at $x = 0$, $z = 0$ remains stationary for all t. From the definition (5.50), the value of $\bar{c}$ at any station x and any time t is the fraction of the cross-sectional area of the rivulet for which $u(y, z) \geq x/t$, which is of the self-similar form

$$\bar{c} = \begin{cases} 1 & \text{if } x \leq 0, \\ f(\xi) & \text{if } 0 \leq x \leq u_{\max} t, \\ 0 & \text{if } x > u_{\max} t, \end{cases} \tag{5.58}$$

where $\xi = x/u_{\max} t$, in which $u_{\max}$ is the maximum velocity of the fluid given by (5.24), and the function $f(\xi)$ is to be obtained from (5.50). In this case, the condition $u \geq x/t$ for any value of x satisfying $0 \leq x \leq u_{\max} t$ is equivalent to the condition $H \leq z \leq h$, where $z = H$ $(0 \leq H \leq h)$ is the curve on which $u = x/t$. We note that the curve $z = H$ is one of the velocity contours, namely the one on which $u = x/t$; the curve $z = H$ is the location of the front of the slug at the position x at time t. If we denote the positions where the curve $z = H$ intersects

the free surface $z = h$ by $y = \pm b$, then the function $f(\xi)$ in (5.58) is given by

$$f = \int_{-b}^{b} \int_{H}^{h} \mathrm{d}z \, \mathrm{d}y = \int_{-b}^{b} (h - H) \, \mathrm{d}y, \tag{5.59}$$

which satisfies $0 \leq f(x/u_{\max}t) \leq 1$, with $f(0) = 1$ and $f(u_{\max}t) = 0$. Note that this result may not be true in situations with both downwards and upwards flow, since in such cases the curve defined by $u = x/t$ may be multiple-valued and/or may comprise disjoint segments. However, if the flow is either entirely downwards or entirely upwards, then the curve $z = H$ is single-valued; we obtain the function $f(\xi)$ in these cases. In order to do this we first determined H and b by solving the equation $u = x/t$ numerically for z, for given values of x, y and t, with u and $u_{\max}$ given by (5.23) and (5.24), respectively; this provides $z = H$ as a set of points, from which an interpolated function for H, comprising cubic polynomial curves between successive data points, was obtained. Then we performed a numerical integration to determine the area between the free surface $z = h(y)$ and the interpolated function for $z = H$.

Figure 5.5 shows contour plots of the velocity u of gravity-driven flow of a semi-circular rivulet on a vertical substrate given by (5.23) in the case $a = 1$. Figure 5.5(a) shows a comparison between the calculated points for H and the exact velocity contours, and Figure 5.5(b) shows a comparison between the interpolated function for H and the exact velocity contours. These figures illustrate that our numerical evaluations of H, and hence b, are accurate.

Figure 5.6 shows the solution (5.58) for the mean concentration $\bar{c}$ in gravity-driven flow of a semi-circular rivulet on a vertical substrate plotted as a function of x at times $u_{\max}t = 1/4$, $1/2$, $\ldots$ and 2 with $a = 1$, for an initially semi-infinite slug of uniform concentration, illustrating the advection of the solute by the flow, and including the initial condition for $\bar{c}$ at $t = 0$ as a dashed line. Note that because of the self-similar form of (5.58), plots of $\bar{c}$ at any other times $t > 0$ will

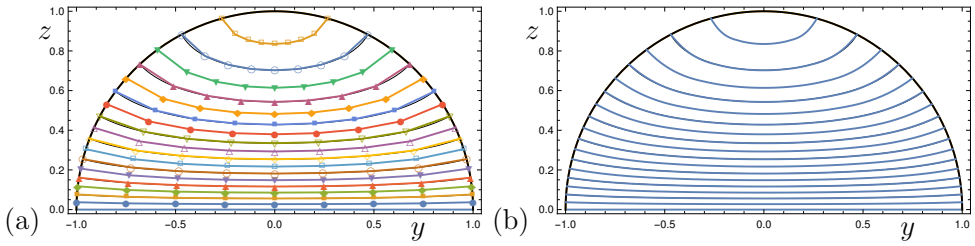

Figure 5.5: Contour plots of the velocity u in gravity-driven flow of a semi-circular rivulet on a vertical substrate given by (5.23) in the case $a = 1$: (a) comparison between the calculated points for H and the exact velocity contours, and (b) comparison between the interpolated function for H and the exact velocity contours.

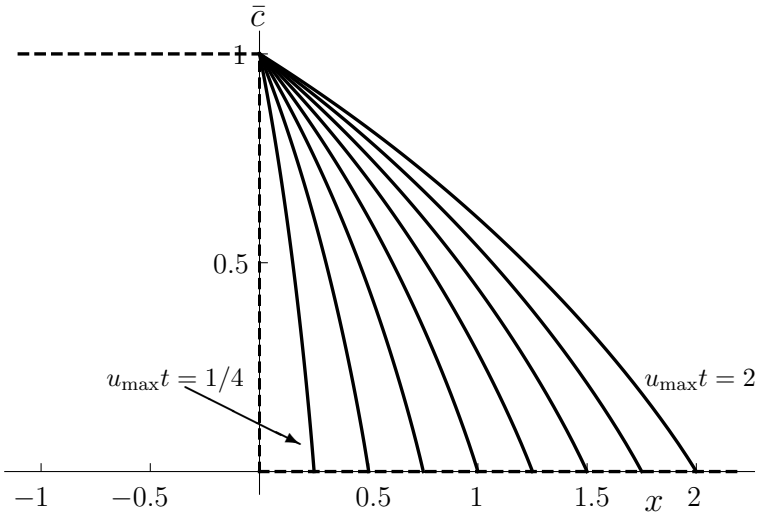

Figure 5.6: Plot of the mean concentration $\bar{c}$ due to advection in gravity-driven flow of a semi-circular rivulet on a vertical substrate, in the case when the solute initially takes the form of a semi-infinite slug of uniform concentration $c = 1$ in $x \leq 0$, with $c = 0$ in $x > 0$, given by (5.58), as a function of x satisfying $0 \leq x \leq u_{\max}t$ at times t given by $u_{\max}t = 0$, $1/4$, $1/2$, ... and 2, with $a = 1$. The initial condition for $\bar{c}$ is shown as a dashed line.

be the same as the one for $u_{\max}t = 1$ in Figure 5.6 except that in each case the x coordinate is either stretched or shrunk by the amount $u_{\max}t$. Figure 5.6 also shows that the function $f(\xi)$ decreases monotonically from the value 1 at $x = 0$ to the value 0 at $x = u_{\max}t$. Note that the solute is always advected downwards, and therefore $c = 1$ and $\bar{c} = 1$ for $x \leq 0$ for all values of t, which, in particular, explains why all the curves in Figure 5.6 pass through $x = 0$ and $\bar{c} = 1$.

5.3.2 An Initially Finite Slug of Solute in Purely Gravity-driven Flow

We now consider an initially finite-width slug of solute of uniform concentration $c = c_0$ in $0 \leq x \leq \Delta$ with $c = 0$ in $x < 0$ and $x > \Delta$ at $t = 0$, where both c_0 and the length of the slug Δ (> 0) are constants.

Thus, with $\overline{C}_0 = c_0$ again, c satisfies the initial condition

$$c = \begin{cases} 0 & \text{if } x \leq 0, \\ 1 & \text{if } 0 < x \leq \Delta, \\ 0 & \text{if } x > \Delta, \end{cases} \tag{5.60}$$

at time $t = 0$, and so the solution for c at time t is given by

$$c = \begin{cases} 0 & \text{if } x \leq ut, \\ 1 & \text{if } 0 < x \leq ut + \Delta, \\ 0 & \text{if } x > \Delta + ut. \end{cases} \tag{5.61}$$

In this case the slug of solute has a front at $x = ut + \Delta$ and a back at $x = ut$. From the definition (5.50) the value of $\bar{c}$ at any station x and any time t is again the fraction of the cross-sectional area of the rivulet for which $u(y, z) \geq x/t$. The solution for $\bar{c}$ at time $t \geq 0$ is of the (non-self-similar) form

$$\bar{c} = \begin{cases} 0 & \text{if } x \leq 0, \\ 1 - f\left(\dfrac{x}{u_{\max} t}\right) & \text{if } 0 < x \leq u_{\max} t, \\ 1 & \text{if } u_{\max} t < x \leq 1, \\ f\left(\dfrac{x - \Delta}{u_{\max} t}\right) & \text{if } \Delta < x \leq \Delta + u_{\max} t, \\ 0 & \text{if } x > \Delta + u_{\max} t, \end{cases} \tag{5.62}$$

when $0 \leq t \leq \Delta/u_{\max}$ (that is, until the solute particle initially at the apex of the rivulet at $x = 0$ reaches $x = \Delta$), and is of the form

$$\bar{c} = \begin{cases} 0 & \text{if } x \leq 0, \\ 1 - f\left(\dfrac{x}{u_{\max}t}\right) & \text{if } 0 < x \leq \Delta, \\ f\left(\dfrac{x-\Delta}{u_{\max}t}\right) - f\left(\dfrac{x}{u_{\max}t}\right) & \text{if } \Delta < x \leq u_{\max}t, \\ f\left(\dfrac{x-\Delta}{u_{\max}t}\right) & \text{if } u_{\max}t < x \leq \Delta + u_{\max}t, \\ 0 & \text{if } x > \Delta + u_{\max}t, \end{cases} \tag{5.63}$$

when $t > \Delta/u_{\max}$, where $u_{\max}$ is given by (5.24). In both cases the function f appearing in the solutions (5.62) and (5.63), is the same as that appearing previously in (5.58), and hence the previously calculated approximation to f may be used here.

Up to the instant $t = \Delta/u_{\max}$, $\bar{c}$ increases monotonically with x up to its maximum value 1, which is its value on a decreasing interval lying within the interval $0 \leq x \leq \Delta$, and decreases monotonically with x in $x > \Delta$. At $t = \Delta/u_{\max}$ the interval has shrunk to the point $x = u_{\max}\Delta$, and thereafter $\bar{c} < 1$ for all x.

Figure 5.7 shows the solution (5.62) and (5.63) for the mean concentration $\bar{c}$ in gravity-driven flow of a semi-circular rivulet on a vertical substrate plotted as a function of x/Δ at times $u_{\max}t/\Delta = 1/4,\ 1/2,\ \ldots$ and 3, with $a = 1$, for an initially finite slug of uniform concentration, illustrating the advection of the solute by the flow, and including the initial condition for $\bar{c}$ at $t = 0$ as a dashed line. Figure 5.7 also shows for $x/\Delta \geq 1$ the locus of the corner in $\bar{c}$ as a dotted curve; the same curve also gives the envelope of the solution curves $\bar{c}$.

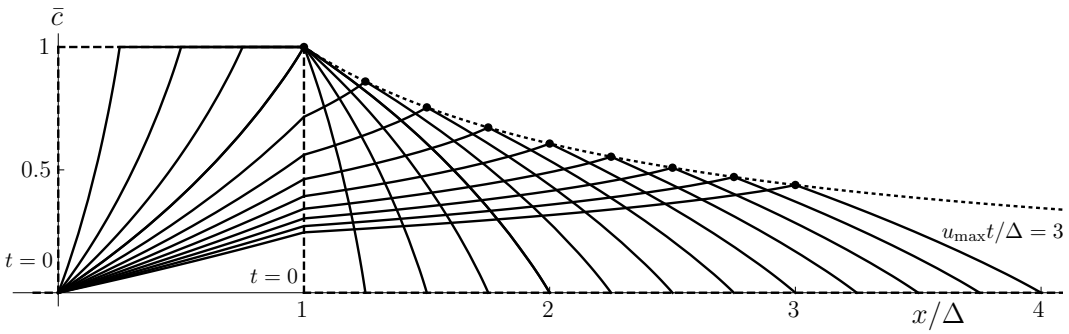

Figure 5.7: Plot of the mean concentration $\bar{c}$ due to advection in gravity-driven flow of a semi-circular rivulet on a vertical substrate, in the case when the solute initially takes the form of a finite slug of uniform concentration $c = 1$ in $0 \leq x \leq \Delta$, with $c = 0$ in $x < 0$ and $x > \Delta$, given by (5.62) and (5.63), as a function of x/Δ at times t given by $u_{\max}t/\Delta = 1/4,\ 1/2,\ \ldots$ and 3, with $a = 1$. The initial condition for $\bar{c}$ is shown as a dashed line. For $x/\Delta \geq 1$ the locus of the corner in $\bar{c}$ and the envelope of the solution curves $\bar{c}$ are shown as a dotted curve.

5.3.3 An Initially Semi-infinite Slug of Solute in Purely Shear-stress-driven Flow

We now consider an initially semi-infinite slug of solute of uniform concentration c_0, with its front located at $x = 0$ at time $t = 0$, for which the concentration takes the form $c = c_0$ in $x \leq 0$ and $c = 0$ in $x > 0$ at time $t = 0$. The mean concentration over the cross-section, $\bar{c}$, is again defined by (5.50). In this case we scale and non-dimensionalise the variables appropriately according to (5.8) together with (5.55) but now with $U = \tau\ell/\mu$; we again drop the stars superscripts on non-dimensional variables, for clarity. With $\overline{C}_0 = c_0$, the solution for $\bar{c}$ at time $t \geq 0$ is again given by (5.58), with $u_{\max}$ again given by (5.38).

As in Subsection 5.3.1, the curve $z = H$ was again evaluated numerically as a set of points by solving the equation $u = x/t$ numerically for z, for given x, y and t, with u and $u_{\max}$ given by (5.37) and (5.38), respectively. The area between $z = h$ and the interpolated function for H was calculated (by numerical integration) in order to determine the function f in (5.59).

Figure 5.8 shows contour plots of the velocity u of shear-stress-driven flow of a semi-circular rivulet on a vertical substrate given by (5.37) with $a = 1$. Figure 5.8(a) shows a comparison between the calculated points for H and the exact

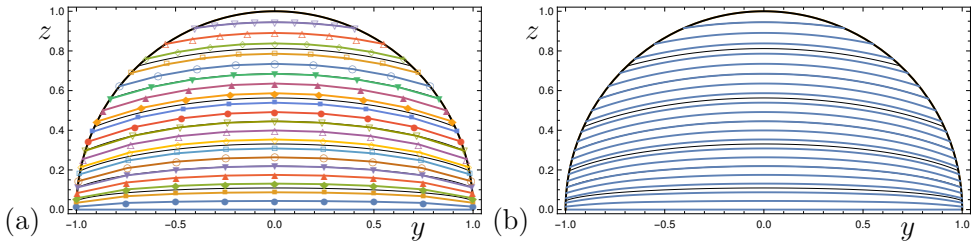

Figure 5.8: Contour plots of the velocity u of shear-stress-driven flow of a semi-circular rivulet on a vertical substrate given by (5.37) in the case $a = 1$: (a) comparison between the calculated points for H and the exact velocity contours, and (b) comparison between the interpolated function for H and the exact velocity contours.

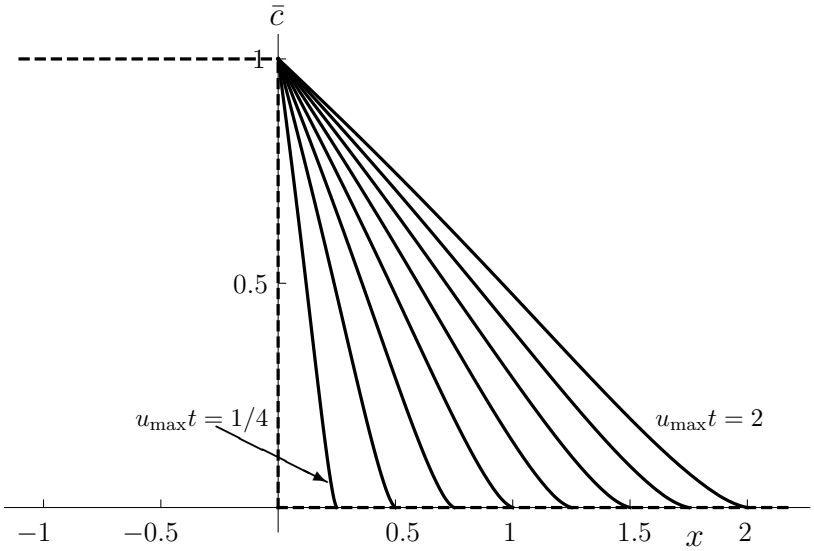

Figure 5.9: Plot of the mean concentration $\bar{c}$ due to advection in shear-stress-driven flow of a semi-circular rivulet on a vertical substrate, in the case when the solute initially takes the form of a semi-infinite slug of uniform concentration $c = 1$ in $x \leq 0$, with $c = 0$ in $x > 0$, given by (5.58), as a function of x satisfying $0 \leq x \leq u_{\max}t$ at times t given by $u_{\max}t = 0$, $1/4$, $1/2$, $\ldots$ and 2, with $a = 1$. The initial condition for $\bar{c}$ is shown as dashed line.

velocity contours, and Figure 5.8(b) shows a comparison between the interpolated function for H and the exact velocity contours. These figures illustrate that our numerical evaluations of H, and hence b, are again accurate.

Figure 5.9 shows the solution (5.58) for the mean concentration $\bar{c}$ in shear-stress-driven flow of a semi-circular rivulet on a vertical substrate plotted as a function of x at times $u_{\max}t = 1/4$, $1/2$, $\ldots$ and 2 with $a = 1$, for an initially semi-infinite slug of uniform concentration, illustrating the advection of the solute by the flow, and including the initial condition for $\bar{c}$ at $t = 0$ as a dashed line. Figure 5.9 also shows that the function $f(\xi)$ decreases monotonically from the

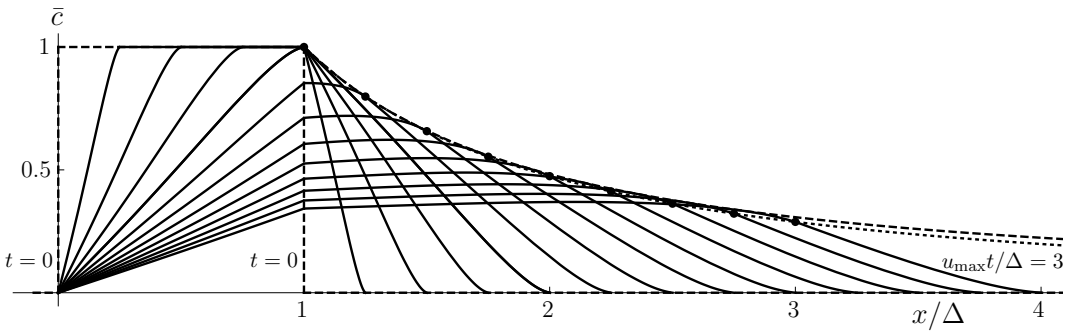

Figure 5.10: Plot of the mean concentration $\bar{c}$ due to advection in shear-stress-driven flow of a semi-circular rivulet on a vertical substrate, in the case when the solute initially takes the form of a finite slug of uniform concentration $c = 1$ in $0 \leq x \leq \Delta$, with $c = 0$ in $x < 0$ and $x > \Delta$, given by (5.62) and (5.63), as a function of x/Δ at times t given by $u_{\max}t/\Delta = 1/4$, $1/2$, ... and 3, with $a = 1$. The initial condition of $\bar{c}$ is shown as a dashed line. For $x/\Delta \geq 1$ the locus of the corner in $\bar{c}$ is shown as a dotted curve, and the envelope of the solution curves $\bar{c}$ is shown as a dashed curve.

value 1 at $x = 0$ to the value 0 at $x = u_{\max}t$.

5.3.4 An Initially Finite Slug of Solute in Purely Shear-stress-driven Flow

In this case the solution for $\bar{c}$ at time $t \geq 0$ is again given by (5.62) and (5.63), in which the function f was previously determined numerically, with $u_{\max}$ again given by (5.38). Figure 5.10 shows the solution (5.62) and (5.63) for the mean concentration $\bar{c}$ in shear-stress-driven flow of a semi-circular rivulet on a vertical substrate plotted as a function of x/Δ at times $u_{\max}t/\Delta = 1/4$, $1/2$, ... and 3, with $a = 1$, for an initially finite slug of uniform concentration, illustrating the advection of the solute by the flow, and including the initial condition of $\bar{c}$ at $t = 0$ as a dashed line. Figure 5.10 also shows for $x/\Delta \geq 1$ the locus of the corners in $\bar{c}$ as a dotted curve and the envelope of the solution curves $\bar{c}$ as a dashed curve.

5.4 Taylor–Aris Dispersion of a Passive Solute in a Semi-circular Rivulet

In this Section we consider the long-time Taylor–Aris dispersion of a slug of a passive solute injected into steady unidirectional flow of a semi-circular rivulet of Newtonian fluid on a vertical planar substrate. We consider the problem when gravity and a uniform surface shear stress τ on the free surface of the rivulet act simultaneously.

At sufficiently large times after the solute is injected, specifically for $t \gg \ell^2/D$, the effects of diffusion of the solute cannot be ignored. In this case the governing equation and the boundary conditions for the concentration of the solute, c, are (5.48) and (5.49), respectively. In this section we will derive the effective diffusivity D_{eff} for the present rivulet flow analogous to that for flow in a pipe or channel, as introduced in Section 1.11.

Consider Taylor–Aris dispersion of a solute in a semi-circular rivulet with the cross-section $\mathcal{D}$ bounded by the closed curve $\partial\mathcal{D}$ (comprising both $z = 0$ and $z = h$). Note that in this Chapter $\mathcal{D} = \Omega$, in which Ω is again the semi-circular domain of such a rivulet given by $0 \leq r \leq a$ and $0 \leq \theta \leq \pi$.

We consider a situation in which the solute initially takes the form of a finite slug of non-uniform concentration $c(x, y, z, 0)$ in $0 \leq x \leq \Delta$, where Δ is a constant, with $c = 0$ in $x < 0$ and $x > \Delta$. The mean concentration over the cross-section, $\bar{c}$, is again defined by (5.50). In addition, we now denote the mean of the initial concentration of c by the constant $\overline{C}_0$, defined by

$$\overline{C}_0 = \frac{1}{A\Delta} \int_0^{\Delta} \int_{-a}^{a} \int_0^{h} c(x, y, z, 0) \, \mathrm{d}z \, \mathrm{d}y \, \mathrm{d}x, \tag{5.64}$$

where $A = \pi a^2/2$ again denotes the cross-sectional area of the rivulet. We scale

and nondimensionalise variables according to (5.41), together with

$$x = Lx^*, \qquad t = \frac{L}{U}t^*, \qquad c = \overline{C_0}c^*, \qquad D_{\text{eff}} = DD^*_{\text{eff}}, \tag{5.65}$$

where L is a downstream lengthscale over which there is an appreciable change in the concentration. For clarity we immediately drop the star superscripts on non-dimensional variables, and so the governing equation and boundary conditions for c, (5.48) and (5.49), become

$$\delta \,\text{Pe}\left(\frac{\partial c}{\partial t} + u(y,z)\frac{\partial c}{\partial x}\right) = \delta^2\frac{\partial^2 c}{\partial x^2} + \nabla^2 c, \tag{5.66}$$

$$\mathbf{n}\cdot\nabla c = 0 \quad \text{on} \quad z = 0 \quad \text{and} \quad z = h, \tag{5.67}$$

where $\delta = \ell/L$ is a longitudinal aspect ratio of the solute, and

$$\text{Pe} = \frac{U\ell}{D} \tag{5.68}$$

is the appropriate Péclet number, which is a ratio of advective effects and diffusive effects. We assume that the lengthscale over which Taylor–Aris dispersion of the solute takes place is such that $\delta \ll 1$, and we seek the leading order behaviour of D_{eff} in the limit $\delta \to 0$ with $\text{Pe} = O(1)$.

For convenience, we rewrite the problem (5.66) and (5.67) in terms of a frame of reference moving with the mean velocity of the flow, $\bar{u}$, and so we introduce a coordinate ξ and time T defined by $\xi = x - \bar{u}t$ and $T = t$, so that

$$(x,t) \to (\xi, T), \quad \frac{\partial}{\partial x} \to \frac{\partial}{\partial \xi} \quad \text{and} \quad \frac{\partial}{\partial t} \to \frac{\partial}{\partial T} - \frac{\partial}{\partial \xi}. \tag{5.69}$$

Then the problem (5.66) and (5.67) becomes

$$\delta \mathrm{Pe}\left(\frac{\partial c}{\partial T}+\widetilde{u}\,\frac{\partial c}{\partial \xi}\right)=\delta^2\frac{\partial^2 c}{\partial \xi^2}+\nabla^2 c, \tag{5.70}$$

$$\mathbf{n}\cdot\nabla c=0 \quad \text{on} \quad z=0 \quad \text{and} \quad z=h, \tag{5.71}$$

where we denote the deviation of u from the mean velocity by $\widetilde{u}=u-\overline{u}$, so that $\widetilde{u}$ has zero mean, *i.e.*

$$\int_{-a}^{a}\int_{0}^{h}\widetilde{u}\,\mathrm{d}z\,\mathrm{d}y=0. \tag{5.72}$$

We use the method of multiple scales (see, for example, Bender and Orszag [14]), with times T_n ($n=0,\,1,\,2,\,\ldots$) defined by $T_n=\delta^n T$, so that

$$\frac{\partial}{\partial T}=\frac{\partial}{\partial T_0}+\delta\frac{\partial}{\partial T_1}+\delta^2\frac{\partial}{\partial T_2}+\ldots, \tag{5.73}$$

and hence (5.70) gives

$$\delta \mathrm{Pe}\left(\frac{\partial c}{\partial T_0}+\delta\frac{\partial c}{\partial T_1}+\delta^2\frac{\partial c}{\partial T_2}+\cdots+\widetilde{u}\,\frac{\partial c}{\partial \xi}\right)=\delta^2\frac{\partial^2 c}{\partial \xi^2}+\nabla^2 c. \tag{5.74}$$

We expand c as an asymptotic series in powers of δ:

$$c=c_0+\delta c_1+\delta^2 c_2+\ldots, \tag{5.75}$$

where $c_n=c_n(\xi,y,z,T_0,T_1,\ldots)$, and substitute (5.75) into (5.74) to obtain equations for the leading-order, the first-order and the second-order terms of c, namely

$$\nabla^2 c_0=0, \tag{5.76}$$

$$\mathrm{Pe}\left(\frac{\partial c_0}{\partial T_0}+\widetilde{u}\,\frac{\partial c_0}{\partial \xi}\right)=\nabla^2 c_1, \tag{5.77}$$

$$\mathrm{Pe}\left(\frac{\partial c_1}{\partial T_0}+\frac{\partial c_0}{\partial T_1}+\widetilde{u}\,\frac{\partial c_1}{\partial \xi}\right)=\frac{\partial^2 c_0}{\partial \xi^2}+\nabla^2 c_2, \tag{5.78}$$

subject to the corresponding boundary conditions obtained from (5.71), namely

$$\mathbf{n}\cdot\nabla c_n = 0 \quad \text{on} \quad z=0 \quad \text{and} \quad z=h, \qquad n=0,1,2,\ldots. \tag{5.79}$$

Integration of (5.76) over $\mathcal{D}$ yields

$$\begin{aligned} 0 &= \iint_{\mathcal{D}} c_0\nabla^2 c_0 \,\mathrm{d}S \\ &= \iint_{\mathcal{D}} \big(\nabla\cdot(c_0\nabla c_0) - (\nabla c_0\cdot\nabla c_0)\big)\,\mathrm{d}S \qquad \text{(by the product rule)} \\ &= \frac{1}{A}\oint_{\partial\mathcal{D}} c_0\nabla c_0\cdot\mathbf{n}\,\mathrm{d}s - \iint_{\mathcal{D}} \left|\nabla c_0\right|^2 \mathrm{d}S \qquad \text{(by Green's theorem)} \\ &= -\iint_{\mathcal{D}} \left|\nabla c_0\right|^2 \mathrm{d}S, \qquad \text{(by (5.79) with } n=0) \end{aligned} \tag{5.80}$$

where s denotes arc length along $\partial\mathcal{D}$. Hence we have $|\nabla c_0|^2 = 0$, so that $\partial c_0/\partial y = \partial c_0/\partial z = 0$, and hence c_0 is independent of y and z.

Integration of (5.77) over $\mathcal{D}$ and use of (5.72) gives

$$\iint_{\mathcal{D}} \nabla^2 c_1 \,\mathrm{d}S = A\mathrm{Pe}\,\frac{\partial c_0}{\partial T_0}. \tag{5.81}$$

Using Green's theorem and then (5.79) with $n=1$ we have

$$\iint_{\mathcal{D}} \nabla^2 c_1 \,\mathrm{d}S = \oint_{\partial\mathcal{D}} \nabla c_1\cdot\mathbf{n}\,\mathrm{d}s = 0, \tag{5.82}$$

so that (5.81) shows that $\partial c_0/\partial T_0 = 0$, and hence that c_0 is independent of T_0. Hence, we deduce that c_0 depends only on ξ, T_1, T_2, …, and, from (5.77), that c_1 therefore satisfies

$$\nabla^2 c_1 = \mathrm{Pe}\,\widetilde{u}\,\frac{\partial c_0}{\partial \xi}. \tag{5.83}$$

We define $C_1 = C_1(\xi, y, z, T_0, T_1, \ldots)$ by the substitution

$$c_1 = \mathrm{Pe}\,\frac{\partial c_0}{\partial \xi} C_1; \tag{5.84}$$

then C_1 satisfies the Neumann problem

$$\nabla^2 C_1 = \widetilde{u} \quad \text{in} \quad \mathcal{D}, \qquad \mathbf{n}\cdot\nabla C_1 = 0 \quad \text{on} \quad \partial\mathcal{D}. \tag{5.85}$$

The function C_1 is determined only up to an additive function of ξ, T_0, T_1, ..., that is, if $C_1 = \phi_1(y,z)$ is one solution of (5.85) then so is $C_1 = \phi_1(y,z) + \psi_1(\xi, T_0, T_1, \dots)$, with ψ_1 an arbitrary function. In fact, the final expression for the effective diffusivity will be shown to be independent of the choice of ψ_1, but for definiteness and convenience we choose ψ_1 to be

$$\psi_1 = -\frac{1}{A}\iint_{\mathcal{D}} \phi_1(y,z)\,\mathrm{d}A, \tag{5.86}$$

which is a constant, independent of ξ, y, z, T_0 and T_1; then C_1 depends on y and z only, and

$$\iint_{\mathcal{D}} C_1\,\mathrm{d}S = 0, \tag{5.87}$$

with which (5.85) determines C_1 uniquely.

Integration of (5.78) over $\mathcal{D}$ gives

$$\mathrm{Pe}\left[\iint_{\mathcal{D}} \frac{\partial c_1}{\partial T_0}\,\mathrm{d}S + A\frac{\partial c_0}{\partial T_1} + \iint_{\mathcal{D}} \widetilde{u}\,\frac{\partial c_1}{\partial \xi}\,\mathrm{d}S\right] = A\frac{\partial^2 c_0}{\partial \xi^2} + \iint_{\mathcal{D}} \nabla^2 c_2\,\mathrm{d}S, \tag{5.88}$$

which with (5.84) and Green's theorem may be written in the form

$$\begin{aligned}\mathrm{Pe}\left[\mathrm{Pe}\,\frac{\partial c_0}{\partial \xi}\frac{\partial}{\partial T_0}\iint_{\mathcal{D}} C_1\,\mathrm{d}S + A\frac{\partial c_0}{\partial T_1} + \mathrm{Pe}\,\frac{\partial}{\partial \xi}\left(\frac{\partial c_0}{\partial \xi}\iint_{\mathcal{D}} \widetilde{u}\,C_1\,\mathrm{d}S\right)\right] \\ = A\frac{\partial^2 c_0}{\partial \xi^2} + \oint_{\partial\mathcal{D}} \nabla c_2\cdot\mathbf{n}\,\mathrm{d}s.\end{aligned} \tag{5.89}$$

Use of (5.79) and (5.87) then yields

$$\mathrm{Pe}\,A\frac{\partial c_0}{\partial T_1} + \mathrm{Pe}^2\frac{\partial^2 c_0}{\partial \xi^2}\iint_{\mathcal{D}} \widetilde{u}\,C_1\,\mathrm{d}S = A\frac{\partial^2 c_0}{\partial \xi^2}, \tag{5.90}$$

leading to the main result, namely the governing equation for the leading-order concentration c_0 in the moving frame of reference:

$$\frac{\partial c_0}{\partial T_1} = \frac{D_{\text{eff}}}{\text{Pe}} \frac{\partial^2 c_0}{\partial \xi^2}, \qquad D_{\text{eff}} = 1 + \kappa \text{Pe}^2, \qquad \kappa = -\frac{1}{A} \iint_{\mathcal{D}} \widetilde{u}\, C_1 \, \mathrm{d}S, \tag{5.91}$$

where C_1 is the solution of (5.85) and (5.87).

Moreover,

$$\begin{aligned} \iint_{\mathcal{D}} \widetilde{u}\, C_1 \, \mathrm{d}S &= \iint_{\mathcal{D}} C_1 \nabla^2 C_1 \, \mathrm{d}S && \text{(by (5.85))} \\ &= \iint_{\mathcal{D}} \left(\nabla \cdot (C_1 \nabla C_1) - (\nabla C_1 \cdot \nabla C_1) \right) \mathrm{d}S && \text{(by the product rule)} \\ &= \oint_{\partial \mathcal{D}} C_1 \nabla C_1 \cdot \mathbf{n} \, \mathrm{d}s - \iint_{\mathcal{D}} \left| \nabla C_1 \right|^2 \mathrm{d}S && \text{(by Green's theorem)} \\ &= - \iint_{\mathcal{D}} \left| \nabla C_1 \right|^2 \mathrm{d}S, && \text{(by (5.85))} \end{aligned} \tag{5.92}$$

so that D_{eff} in (5.91) may be written in the alternative form

$$D_{\text{eff}} = 1 + \kappa \text{Pe}^2, \qquad \kappa = \frac{1}{A} \iint_{\mathcal{D}} |\nabla C_1|^2 \, \mathrm{d}S, \tag{5.93}$$

which, in particular, shows that $D_{\text{eff}} > 1$.

The corresponding equation for c_0 relative to a fixed frame of reference may be written in terms of the original variables as

$$\frac{\partial c_0}{\partial t} + \overline{u} \frac{\partial c_0}{\partial x} = D_{\text{eff}} \frac{\partial^2 c_0}{\partial x^2}, \qquad D_{\text{eff}} = D\left(1 + \kappa \text{Pe}^2\right), \qquad \kappa = -\frac{1}{A} \iint_{\mathcal{D}} \frac{\widetilde{u}}{U} C_1 \, \mathrm{d}S, \tag{5.94}$$

showing that at leading order in δ the solute moves with the velocity $\overline{u}$ and diffuses with the effective diffusivity D_{eff}, and C_1 is again the solution of (5.85) and (5.87), namely (again in dimensional terms)

$$\ell^2 \nabla^2 C_1 = \frac{\widetilde{u}}{U} \quad \text{in} \quad \mathcal{D}, \qquad \mathbf{n} \cdot \nabla C_1 = 0 \quad \text{on} \quad \partial \mathcal{D}, \qquad \iint_{\mathcal{D}} C_1 \, \mathrm{d}S = 0. \tag{5.95}$$

We note that at leading order in δ, $\bar{c} = c_0$, and so equation $(5.94)_1$ may alternatively be expressed in the form

$$\frac{\partial \bar{c}}{\partial t} + \overline{u}\frac{\partial \bar{c}}{\partial x} = D_{\text{eff}}\,\frac{\partial^2 \bar{c}}{\partial x^2}. \tag{5.96}$$

As discussed in Section 1.11, for Taylor–Aris dispersion of a passive solute in, for example, steady unidirectional flow in a channel of arbitrary cross-section $\mathcal{D}$ driven by a prescribed pressure gradient $G = -\mathrm{d}p/\mathrm{d}x$, equation (5.66) leads to (5.96) at leading order in δ, in which the effective diffusivity D_{eff} takes the (dimensional) form

$$D_{\text{eff}} = D\left(1 + \kappa_{\text{con}}\,\mathrm{Pe}_{\text{con}}^2\right), \qquad \kappa_{\text{con}} = \frac{1}{A}\iint_{\mathcal{D}} \frac{\widetilde{u}}{\overline{u}}\, C_{1\,\text{con}}\,\mathrm{d}S, \tag{5.97}$$

where Pe_{con} denotes the "conventional" Péclet number often used in studies of Taylor–Aris dispersion and defined in terms of $\overline{u}$ by

$$\mathrm{Pe}_{\text{con}} = \frac{\overline{u}\mathcal{L}}{D}, \tag{5.98}$$

where $\mathcal{L}$ denotes a typical diameter of $\mathcal{D}$, and $C_{1\,\text{con}}$ is the solution of the Neumann problem

$$\mathcal{L}^2\nabla^2 C_{1\,\text{con}} = \frac{\widetilde{u}}{\overline{u}} \quad \text{in} \quad \mathcal{D}, \quad \mathbf{n}\cdot\nabla C_{1\,\text{con}} = 0 \quad \text{on} \quad \partial\mathcal{D}, \quad \iint_{\mathcal{D}} C_{1\,\text{con}}\,\mathrm{d}S = 0, \tag{5.99}$$

in which $\partial\mathcal{D}$ is the closed curve bounding $\mathcal{D}$. We may, of course, choose to regard the quantities κ, Pe and C_1 as being related to the corresponding conventional quantities κ_{con}, Pe_{con} and $C_{1\,\text{con}}$ by

$$\kappa_{\text{con}} = \left(\frac{U\ell}{\overline{u}\mathcal{L}}\right)^2 \kappa, \qquad \mathrm{Pe}_{\text{con}} = \frac{\overline{u}\mathcal{L}}{U\ell}\mathrm{Pe}, \qquad C_{1\,\text{con}} = -\frac{U\ell^2}{\overline{u}\mathcal{L}^2}C_1 \tag{5.100}$$

(so that, in particular, $\kappa_{\text{con}}\,\mathrm{Pe}_{\text{con}}^2 = \kappa\,\mathrm{Pe}^2$). However, when values of D_{eff} in dif-

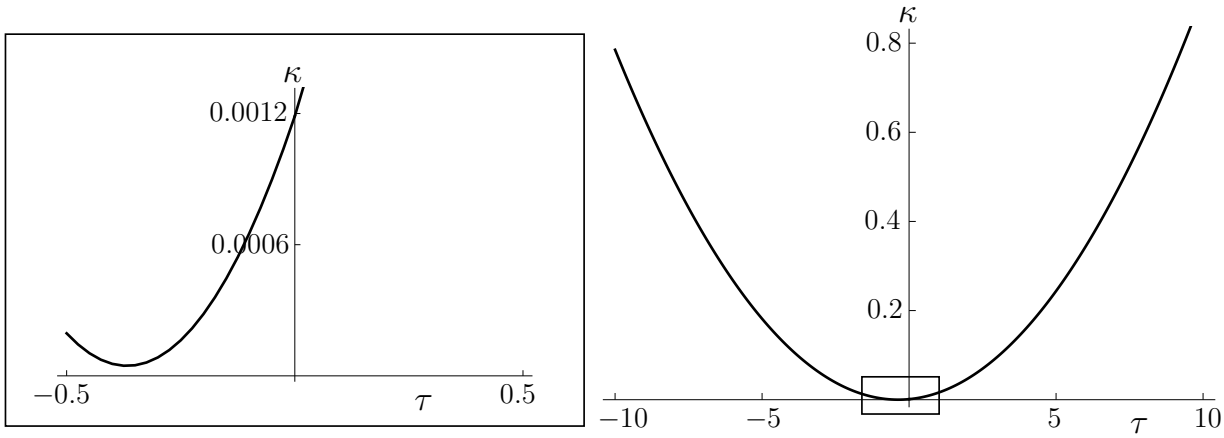

Figure 5.11: Plot of κ as a function of τ for gravity- and shear-stress-driven flow in a semi-circular rivulet on a vertical substrate, in the case $a = 1$. The insert shows an enlargement for small values of κ, also showing that κ is always positive.

ferent rivulet flows with different values of τ are to be compared, the conventional formulation (5.97)–(5.99) is inconvenient, since both $\mathrm{Pe}_{\mathrm{con}}$ and κ_{con} depend on the value of τ (through their dependence on $\overline{u}$), whereas in the present formulation (5.94)–(5.95) Pe is independent of τ, and so the dependence of D_{eff} given by (5.91) on τ is isolated in just one parameter, namely κ. In addition, in the special case in which τ takes the critical value τ_{c} given by (5.47) for which $\overline{u} = 0$, not only is the problem (5.99) for $C_{1\,\mathrm{con}}$ singular, but also $\mathrm{Pe}_{\mathrm{con}}$ is zero and κ_{con} is infinite (with $\kappa_{\mathrm{con}}\mathrm{Pe}_{\mathrm{con}}^2$ finite), which means that it is necessary to define D_{eff} via an appropriate limiting process; the present formulation avoids this. Furthermore, if $\tau < \tau_{\mathrm{c}}$ then $\overline{u} < 0$ and so, slightly confusingly, $\mathrm{Pe}_{\mathrm{con}}$ is negative; again the present formulation, in which Pe is always positive, avoids this complication.

We now use the result (5.94)–(5.95) to analyse Taylor–Aris dispersion in a semi-circular rivulet. We solve the problem for C_1 in (5.85) numerically with u in (5.43), again using a finite element method over the semi-circular domain Ω. Once the solution for C_1 is obtained, κ is computed via numerical integration of $C_1\tilde{u}$. Figure 5.11 shows a plot of κ as a function of τ in the case $a = 1$; note that the value of Q varies along this curve. The insert in Figure 5.11 shows an enlargement for small values of τ, illustrating that κ is always positive.

Mesh size	κ_{con} using the exact solutions for $\bar{u}$ and u
0.3	0.0223940769
0.03	0.0224077627
0.003	0.0224137318
0.0003	0.0224138089
0.00025	0.0224138096
0.0002	0.0224138096
0.00015	0.0224138099
0.0001	0.0224138099
0.00005	0.0224138098
0.00001	0.0224138098

Table 5.2: Numerical values of κ_{con} in purely gravity-driven flow of a semi-circular rivulet on a vertical substrate using the exact solutions for $\bar{u}$ and u given by (5.28) and (5.23), respectively, with $a = 1$ for a range of mesh sizes.

5.4.1 Purely Gravity-driven Flow

For purely gravity-driven flow, in which case $\tau = 0$, Table 5.2 shows κ_{con} calculated from (5.100) with $\bar{u}$ given by (5.28) in the case $a = 1$ using the exact solution for u given by (5.23) for a range of values of mesh size, illustrating that κ_{con} is indeed converging to a value $\kappa_{\text{con}} = \kappa_{\text{GD}}$, where

$$\kappa_{\text{GD}} \simeq 0.0224138, \tag{5.101}$$

or equivalently

$$\kappa_{\text{GD}} \simeq 0.4553362\bar{u}^2. \tag{5.102}$$

5.4.2 Purely Shear-stress-driven Flow

For purely shear-stress-driven flow, we obtain the value of κ_{con} again calculated from (5.100) with $\bar{u}$ given by (5.40) in the case $a = 1$ using the exact solution for u given by (5.37), namely $\kappa_{\text{con}} = \kappa_{\text{SD}}$, where

$$\kappa_{\text{SD}} \simeq 0.0274506, \tag{5.103}$$

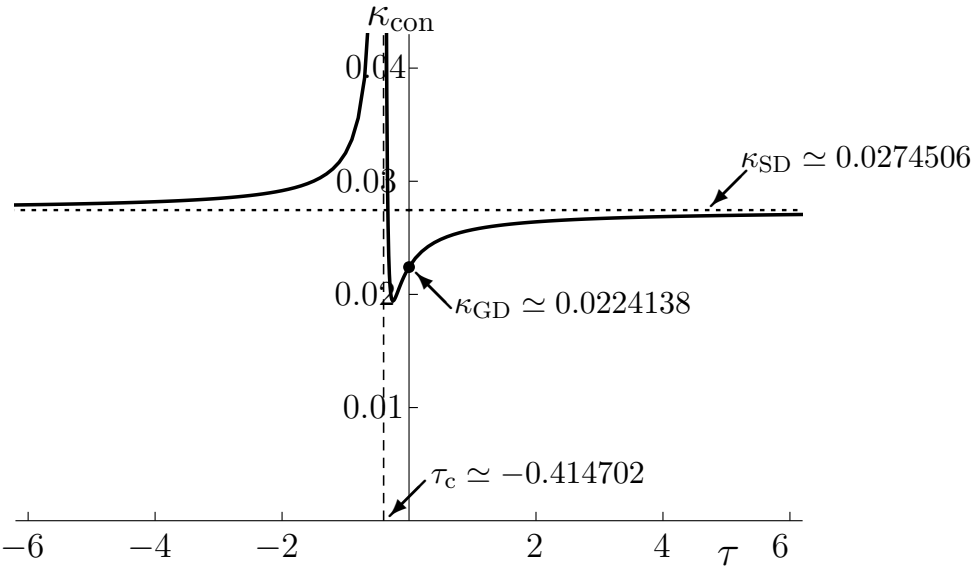

Figure 5.12: Plot of $\kappa_{\rm con}$ as a function of τ for gravity- and shear-stress-driven flow in a semi-circular rivulet on a vertical substrate, in the case $a = 1$. The vertical dashed line is the value $\tau_{\rm c} \simeq -0.414702$ at which $\kappa_{\rm con}$ becomes infinite. The dot indicates the case $\kappa_{\rm con} = \kappa_{\rm GD} \simeq 0.0224138$ when $\tau = 0$. The horizontal dotted line is the asymptotic value $\kappa_{\rm con} = \kappa_{\rm SD} \simeq 0.0274506$ in the limit $\tau \to \pm\infty$.

or equivalently

$$\kappa_{\rm SD} \simeq 0.0890542\bar{u}^2. \tag{5.104}$$

5.4.3 Gravity- and Shear-stress-driven Flow

Figure 5.12 shows a plot of $\kappa_{\rm con}$ as a function of τ in the case $a = 1$; note again that the value of Q varies along this curve. As Figure 5.12 shows, $\kappa_{\rm con}$ is infinite when $\bar{u} = 0$ (that is, when $\tau_{\rm c} \simeq -0.414702$), that $\kappa_{\rm con} = \kappa_{\rm GD}$ when $\tau = 0$, and that $\kappa_{\rm con}$ approaches the value $\kappa_{\rm con} = \kappa_{\rm SD}$ in the limit $\tau \to \pm\infty$. Clearly an artificial singularity occurs in the conventional formulation (5.97)–(5.99) when $\bar{u} = 0$, as shown in Figure 5.12, whereas the present formulation (5.94)–(5.95) is well behaved, as shown in Figure 5.11.

5.5 Conclusions

In this Chapter we considered dispersion of a passive solute in steady unidirectional flow of a uniform non-thin rivulet of Newtonian fluid on a vertical planar substrate when the flow is driven by gravity and/or a uniform shear stress on its free surface. We considered only the case in which the contact angle of the rivulet has the prescribed value $\pi/2$, the cross-section of the rivulet then being semi-circular.

In Section 5.1 we obtained the exact solution for the velocity within a semi-circular rivulet by solving either the appropriate Poisson equation or, when gravity is neglected, Laplace's equation in the domain defined by the cross-section of the rivulet.

In Section 5.3 we considered the short-time advection of a slug of a passive solute injected at time $t = 0$ into the semi-circular rivulet on a vertical planar substrate when the flow is driven either purely by gravity or purely by a uniform surface shear stress τ at its free surface. In particular, we presented the general form of the mean concentration $\bar{c}$ at small times, and we used this result to describe the advection of both an initially semi-infinite slug and an initially finite slug of solute. We used the fact that $\bar{c}$ at any station x and any time t is the fraction of the cross-sectional area of the rivulet for which $u(y, z) \geq x/t$ to find the form of $\bar{c}$.

In Section 5.4 we described the long-time Taylor–Aris dispersion of an initially finite slug of solute. In particular, we used the method of multiple scales to show that well-known results concerning Taylor–Aris dispersion of a solute of non-uniform concentration at large times in flow in a channel of arbitrary cross-section essentially hold for Taylor–Aris dispersion in a semi-circular rivulet flow. We avoided an artificial singularity that occurs in the conventional formulation (5.97)–(5.99) when $\bar{u} = 0$, as shown in Figure 5.12, by using the formulation (5.94)–(5.95). In particular, we obtained the form of the effective diffusivity D_{eff},

given by (5.94), for Taylor–Aris dispersion in a semi-circular rivulet.

Chapter 6

Advection and Taylor–Aris Dispersion in a Thin Rivulet

In this Chapter we consider advection and Taylor–Aris dispersion of a passive solute in steady unidirectional flow of a uniform thin rivulet of Newtonian fluid on a vertical planar substrate when the flow is driven by gravity and/or a uniform shear stress on its free surface. The problems for Chapters 5 and 6 are the same, but because the rivulet is now thin it is possible to make more progress analytically. Aspects of this flow problem were summarised in Section 1.8, but for convenience in Section 6.1 we revisit the main results of Wilson and Duffy [132] who considered steady flow of a thin uniform rivulet of non-perfectly wetting fluid on a vertical substrate subject to a uniform shear stress τ. In Sections 6.2 and 6.3 we consider the processes of (short-time) advection and of (long-time) Taylor–Aris dispersion, respectively, of a passive solute injected into the rivulet.

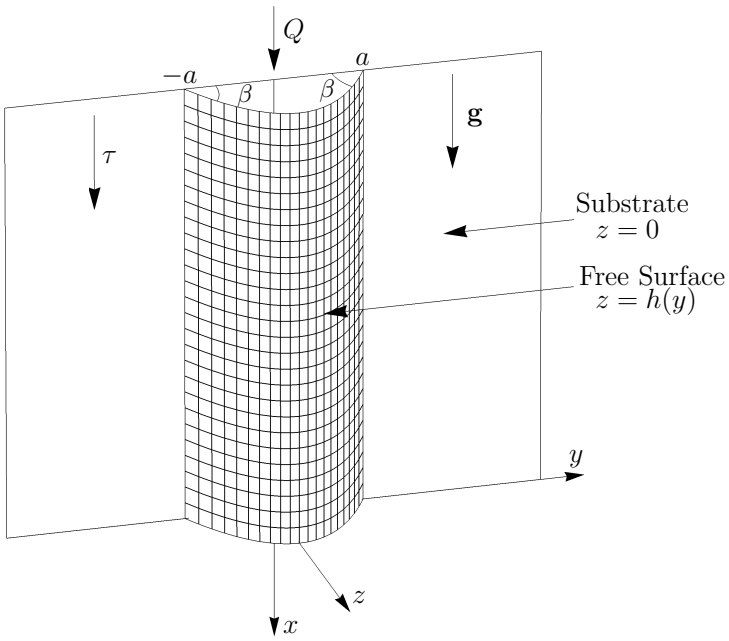

Figure 6.1: Sketch of the unidirectional steady flow of a thin uniform rivulet of a Newtonian fluid with semi-width a, contact angle β, and volume flux Q on a vertical planar substrate subject to a uniform shear stress τ on its free surface.

6.1 Summary of the Solution for the Flow of the Rivulet

Consider steady unidirectional flow of a thin uniform rivulet of a Newtonian fluid with constant viscosity μ, density ρ and coefficient of surface tension γ down a vertical substrate, the flow being driven by both gravity and a uniform longitudinal shear stress τ on its free surface. We refer the description to a Cartesian coordinates $Oxyz$ with, Ox down the line of greatest slope, Oy horizontal, Oz normal to the substrate at $z = 0$, and the origin on the substrate at the center of the rivulet, as shown in Figure 6.1. The free surface of the rivulet is again denoted by $z = h(y)$, the maximum thickness of the rivulet at its middle by $h_{\rm m} = h(0)$, the semi-width of the rivulet by a, the contact angle by β (> 0), the cross-sectional area of the rivulet by A, the volume flux of fluid along the rivulet by Q, and the mean velocity over the cross-section by $\bar{u}$.

In dimensional variables the velocity $\mathbf{u} = u(y, z)\mathbf{i}$ and the pressure $p = p(y, z)$

satisfy the familiar Navier–Stokes equation and mass-conservation equations subject to the normal stress balance $p = -h''$ (the dash means differentiation with respect to y), the tangential stress balance $u_z = \tau$ and the kinematic condition at the free surface $z = h(y)$, the no-slip condition $u = 0$ at $z = 0$, and the condition at the contact lines (*i.e.* $h'(\pm a) = \mp\beta$). We scale and nondimensionalise y and a with ℓ, z, h and h_m with $\epsilon\ell$, β with ϵ, A with $\epsilon\ell^2$, u and $\bar{u}$ with $U = \epsilon^2\rho g\ell^2/\mu$, Q with $\epsilon U\ell^2$, p with $p_a + \epsilon\rho g\ell$, τ with $\epsilon\rho g\ell$, where g is the gravitational acceleration, $\ell = (\gamma/\rho g)^{1/2}$ is the capillary length, and ϵ ($\ll 1$) is the aspect ratio of the cross-section of the rivulet. At leading order in the limit of small aspect ratio $\epsilon \to 0$ (*i.e.* for a thin rivulet) the governing equations are readily solved to yield the solutions for u and p, namely

$$u = \frac{2hz - z^2}{2} + \tau z, \qquad p = \frac{\beta}{a}, \tag{6.1}$$

and the free surface h is simply the parabolic profile

$$h = h_\mathrm{m}\left(1 - \frac{y^2}{a^2}\right), \qquad \text{where} \quad h_\mathrm{m} = \frac{\beta a}{2}. \tag{6.2}$$

The flux of fluid down the rivulet, Q, the cross-sectional area of the rivulet, A, and the mean velocity over cross-section, $\overline{u}$, are given by

$$Q = \frac{32ah_\mathrm{m}^3}{105} + \frac{8\tau a h_\mathrm{m}^2}{15}, \qquad A = \frac{4ah_\mathrm{m}}{3}, \qquad \overline{u} = \frac{8h_\mathrm{m}^2}{35} + \frac{2\tau h_\mathrm{m}}{5}. \tag{6.3}$$

In general, for a given value of τ there is freedom to prescribe any two of the three quantities $a = \bar{a}$, $\beta = \bar{\beta}$ and $Q = \bar{Q}$, with the third determined by the algebraic equation $(6.3)_1$, and with h_m related to a and β by (6.2).

We denote the minimum and maximum fluid velocities over the rivulet by u_min and u_max, respectively, which satisfy $u_\mathrm{min} \le 0$ and $u_\mathrm{max} \ge 0$. In the case of purely gravity-driven flow the solution for the velocity u is simply given by (6.1)

with $\tau = 0$, and hence

$$u_{\min} = 0, \qquad u_{\max} = \frac{h_{\mathrm{m}}^2}{2}, \tag{6.4}$$

occurring at the substrate $z = 0$ and the apex $y = 0$, $z = h_{\mathrm{m}}$ of the rivulet, respectively. In the case of purely shear-stress-driven flow, we may obtain the solution for the velocity u by taking the limit $|\tau| \to \infty$ in (6.1) with u rescaled as $u = \tau\widehat{u}$ to yield $\widehat{u} = z$; then the rescaled flux $\widehat{Q} = Q/\tau$ satisfies $\widehat{Q} = 8ah_{\mathrm{m}}^2/15$, and the rescaled minimum and maximum velocities are $\widehat{u}_{\min} = u_{\min}/\tau = 0$ and $\widehat{u}_{\max} = u_{\max}/\tau = h_{\mathrm{m}}$.

For future reference note that the flux Q (and hence the mean velocity $\bar{u}$) are positive for $\tau > \tau_{\mathrm{c}}$, zero for $\tau = \tau_{\mathrm{c}}$ and negative for $\tau < \tau_{\mathrm{c}}$, where the critical value $\tau = \tau_{\mathrm{c}}$ (< 0) corresponding to no net flow is given by

$$\tau_{\mathrm{c}} = -\frac{4h_{\mathrm{m}}}{7}. \tag{6.5}$$

In the case when $\tau \geq 0$ the velocity is downwards throughout the rivulet (i.e. $u \geq 0$), and the maximum velocity $u_{\max} = a\beta(a\beta + 4\tau)/8$ occurs at the apex of the rivulet at $y = 0$ and $z = h_{\mathrm{m}}$ (type I), but when $\tau < 0$ the velocity is upwards near the edges of the rivulet (*i.e.* $u < 0$), but it can be downwards elsewhere. In the latter case, when $a\beta \leq -2\tau$ the velocity is upwards throughout the rivulet, and the minimum velocity $u_{\min} = a\beta(a\beta + 4\tau)/8$ occurs at the apex (type V), but when $-a\beta/2 < \tau < 0$ there is a region of downwards flow in the centre of the rivulet, and the maximum velocity $u_{\max} = (a\beta + 2\tau)^2/8$ occurs within the rivulet at $y = 0$, $z = (a\beta + 2\tau)/2$ and the minimum velocity $u_{\min} = \tau^2/2$ occurs on the free surface at $y = \pm(a(a\beta + 2\tau)/\beta)^{1/2}$, $z = -\tau$ and $\tau_{\mathrm{c}} = -2a\beta/7$.

As in Chapter 5, we again denote the mean concentration over the cross-section of the rivulet by $\bar{c} = \bar{c}(x, t)$, which is again given by (5.50).

6.2 Advection of a Passive Solute in a Thin Rivulet

In this Section we consider a slug of a passive solute injected at time $t = 0$ into a thin rivulet of Newtonian fluid undergoing steady unidirectional flow on a vertical planar substrate, in the case when gravity and the surface shear stress act simultaneously. As in Section 5.3, at sufficiently small times after the solute is injected (specifically for $t \ll \ell^2/D$), the process of advection will dominate over that of diffusion, and so the effect of diffusion may be ignored. In that case the governing equation (5.48) for c again reduces simply to the advection equation (5.52) which has general solution given by (5.53).

Note that the behaviour of u described in Section 6.1 means that when $\tau \geq 0$ all of the solute is advected downwards, whereas when $\tau < 0$ some or all of it is advected upwards.

We scale and nondimensionalise the variables as described in Section 6.1 together with (5.55), where $\overline{C}_0$ again denotes the mean initial concentration given in (5.51); for clarity we again drop the stars superscripts on non-dimensional variables.

6.2.1 An Initially Semi-infinite Slug of Solute

We consider an initially semi-infinite slug of solute of uniform concentration $c = c_0$ in $x \leq 0$ with $c = 0$ in $x > 0$ at time $t = 0$, where c_0 is a constant. In this case $\overline{C}_0 = c_0$ in $x \leq 0$, and the solution for c at time t is given by (5.57). As in Section 5.3, using the definition (5.50), the value of $\bar{c}$ at any station x and time t is the fraction of the cross-sectional area for which $u(y, z) \geq x/t$, which is of the self-similar form

$$\bar{c} = \begin{cases} 1 & \text{if } \; x < u_{\min} t, \\ f(\xi) & \text{if } \; u_{\min} t \leq x \leq u_{\max} t, \\ 0 & \text{if } \; x > u_{\max} t, \end{cases} \tag{6.6}$$

where $\xi = x/u_{\mathrm{m}}t$, in which we have defined u_{m} by $u_{\mathrm{m}} = u_{\max} - u_{\min}$ (> 0), and the function f, which is determined by (5.50), satisfies $0 \leq f(x/u_{\mathrm{m}}t) \leq 1$, with $f(u_{\min}/u_{\mathrm{m}}) = 1$ and $f(u_{\max}/u_{\mathrm{m}}) = 0$.

Figure 6.2 shows plots of the front of the solute for advection in a rivulet in the case of an initially semi-infinite slug of uniform initial concentration at times $t > 0$. Figure 6.2(a) is for purely gravity-driven flow, and Figure 6.2(b) is for purely shear-stress-driven flow, both of which illustrate that the solute is always advected downwards. In both parts regions of uniform concentration are shaded in brown.

Figure 6.3 shows plots of the mean concentration $\bar{c}$ as a function of x for an initially semi-infinite slug of uniform concentration, given by (6.6) for advection in gravity- and shear-stress-driven flow in the rivulet for various values of τ at time $t = 1$ when $a = 1$ and $\beta = 1$, illustrating the advection of the solute by the flow for both positive and negative values of τ. In particular, when $\tau \leq -\beta a/2 = -1/2$ all the solute is advected upwards everywhere, and therefore $c = 0$ and $\bar{c} = 0$ for $x \geq 0$ for all t, which explains why the curves for such cases in Figure 6.3 all pass through $x = 0$ and $\bar{c} = 0$. On the other hand, when $\tau \geq 0$ all the solute is advected downwards everywhere, and therefore $c = 1$ and $\bar{c} = 1$ for $x \leq 0$ for all t, which explains why the curves for such cases in Figure 6.3 all pass through $x = 0$ and $\bar{c} = 1$. Note that because of the self-similar form of (6.6), plots of $\bar{c}$ at any other time $t > 0$ will be the same as those in Figure 6.3 except that in each case the x coordinate must be either stretched or shrunken by the amount $u_{\mathrm{m}}t$. Figure 6.3 also includes a curve for the critical value $\tau = \tau_{\mathrm{c}} = -2/7$ (shown dotted) for which the net advection is zero.

Figure 6.4 shows plots of the front of the solute for advection in gravity- and shear-stress-driven flow in the rivulet in the case of an initially semi-infinite slug of uniform initial concentration at times $t > 0$, and illustrates the advection of the solute by the flow for various values of τ. Recall that in Section 6.1 we

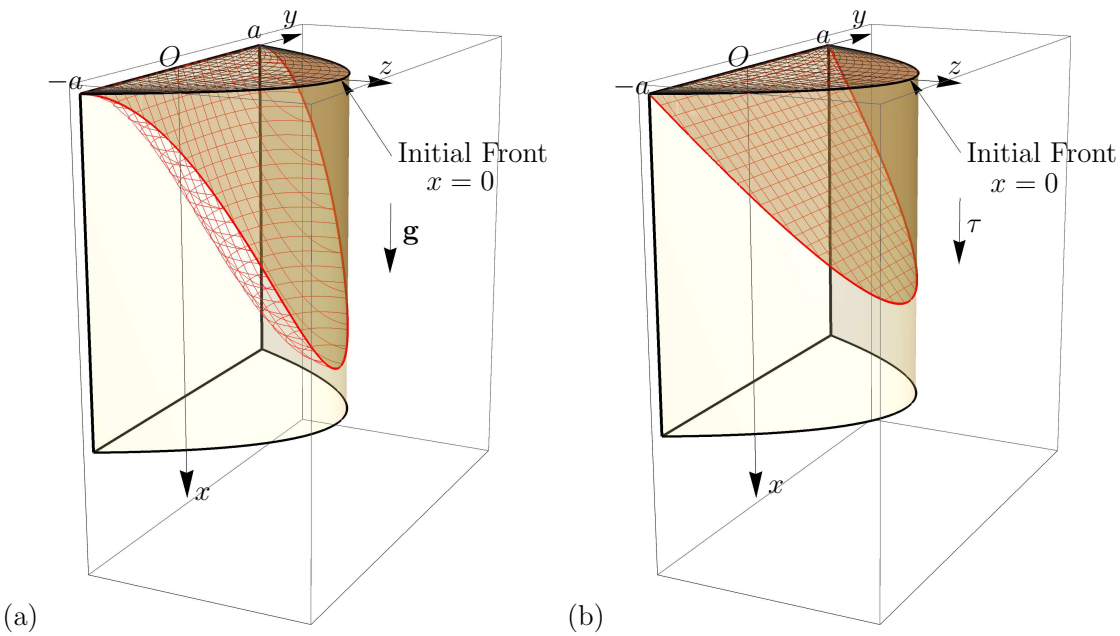

Figure 6.2: Plots of the front of the solute due to advection in a thin rivulet on a vertical substrate at time $t > 0$, in the case of an initially semi-infinite slug of uniform initial concentration in the cases (a) purely gravity-driven flow with $a = 1$ and $\beta = 1$, and (b) purely shear-stress-driven flow with $a = 1$, $\beta = 1$ and $\tau = 1/5$. In both parts regions of uniform concentration are shaded in brown.

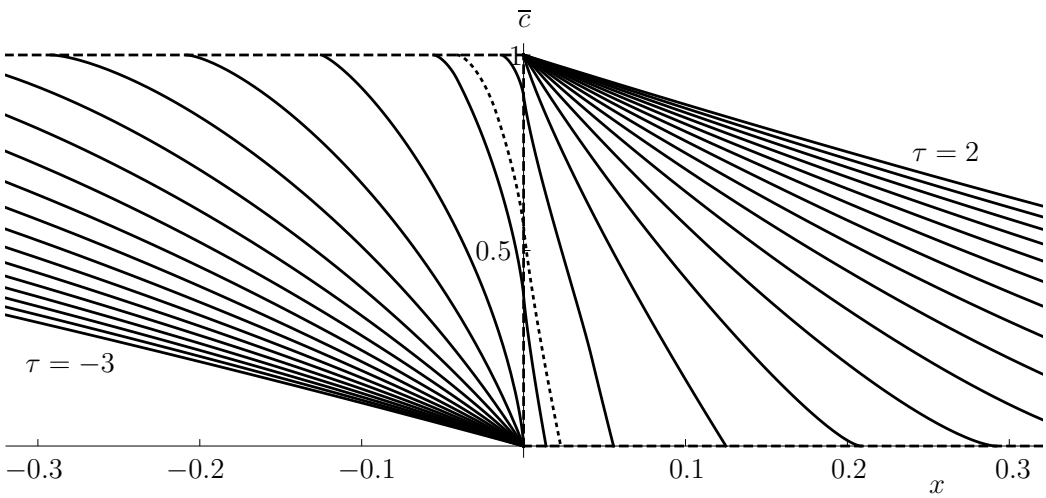

Figure 6.3: Plot of the mean concentration $\bar{c}$ due to advection in gravity- and shear-stress-driven flow of a thin rivulet on a vertical substrate, in the case when the solute initially takes the form of a semi-infinite slug of uniform concentration $c = 1$ in $x \leq 0$ with $c = 0$ in $x > 0$, given by (6.6), as a function of x satisfying $u_{\min} t \leq x \leq u_{\max} t$, for $\tau = -3, -17/6, \ldots, 2$, and $\tau_c = -2/7$ (shown dotted) at time $t = 1$, with $a = 1$ and $\beta = 1$ in each case. The initial condition for $\bar{c}$ is shown as a dashed line.

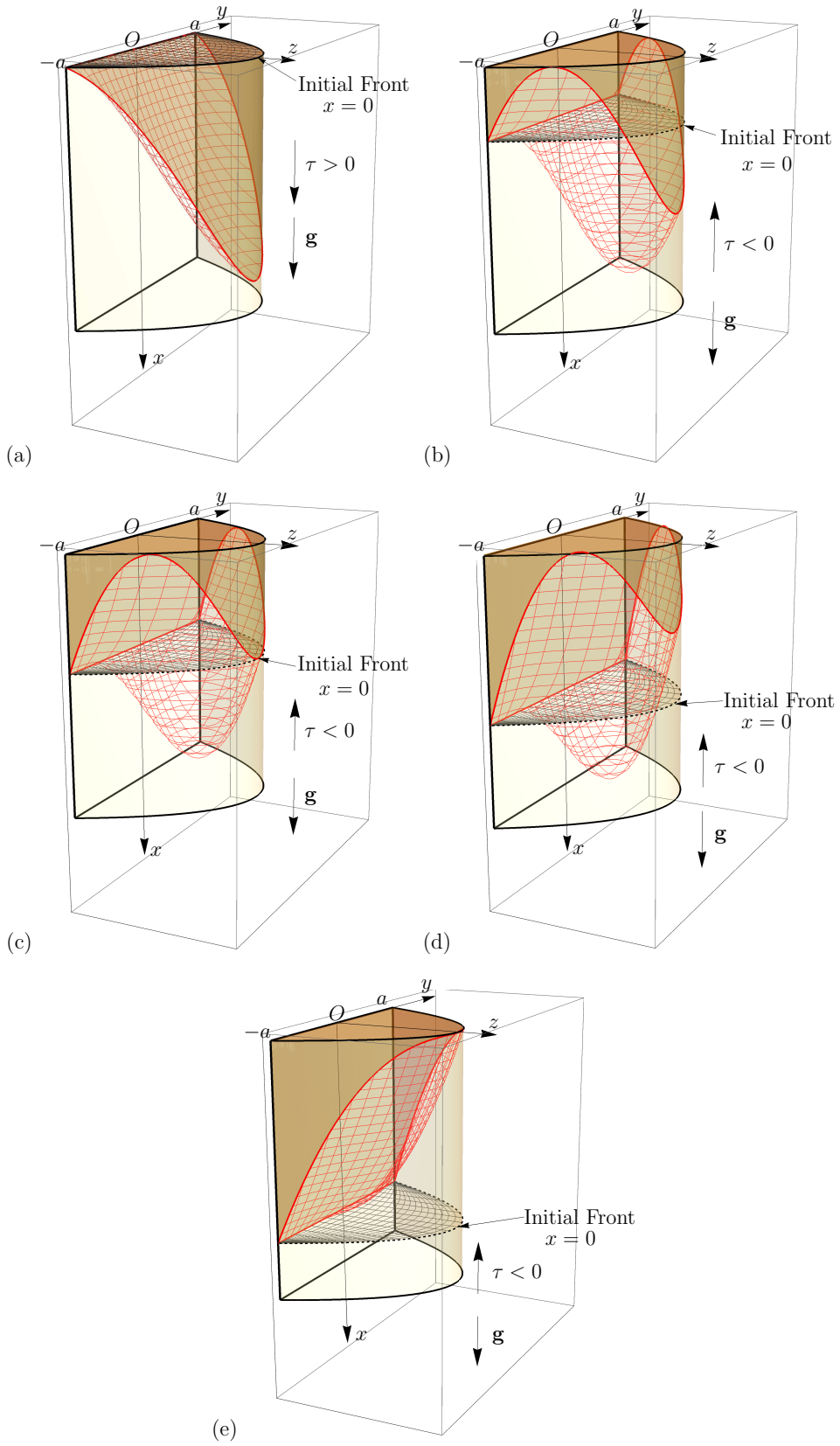

Figure 6.4: Plots of the front of the solute due to advection in gravity- and shear-stress-driven flow in a thin rivulet on a vertical substrate at time $t > 0$, in the case of an initially semi-infinite slug of uniform initial concentration for the five different types of cross-sectional flow pattern with $\beta = 1$, namely (a) type I with $a = 1$ and $\tau = 1/10$, (b) type II with $a = 1$ and $\tau = -1/5$, (c) type III with $a = 1$ and $\tau = -1/4$, (d) type IV with $a \simeq 8.7103$ and $\tau = -5/2$, and (e) type V with $a \simeq 1.5383$ and $\tau = -4/5$. In all parts regions of uniform concentration are shaded in brown.

described the five flow patterns that may occur in the rivulet. In particular, for a type I flow pattern the solute is always advected downwards, as shown in Figure 6.4(a), for type II–IV flow patterns some of the solute is advected upwards, as shown in Figure 6.4(b)–(d), and for a type V flow pattern the solute is always advected upwards, as shown in Figure 6.4(e). In Figure 6.4 regions of uniform concentration are again shaded in brown.

In general, a complete list of the forms that the function f in (6.6) takes for different values of τ could be constructed, but it would be unwieldy, partly because when $\tau < 0$ several different forms of the velocity contour $u = x/t$ must be considered, each of which leads to a different form for f, and partly because it seems that, in general, the integral in (5.50) is not available in closed form. However, we can obtain explicit expressions for f in the special cases $\tau \geq 0$ and of purely shear-stress-driven flow, as described in the next two Subsections 6.2.2 and 6.2.3.

6.2.2 Flow Driven by a Positive Shear Stress $\tau \geq 0$

For positive values of τ we have $u_{\min} = 0$ and $u_{\mathrm{m}} = u_{\max} = (h_{\mathrm{m}}^2/2) + \tau h_{\mathrm{m}}$, and the condition $u \geq x/t$ for any value of x satisfying $0 \leq x \leq u_{\max} t$ is equivalent to the condition $H \leq z \leq h$, where $z = H$ $(0 \leq H \leq h)$ is the curve on which $u = x/t$, so that from (6.1)

$$H = h + \tau - \left[(h + \tau)^2 - \frac{2x}{t} \right]^{1/2}. \tag{6.7}$$

The curve (6.7) intersects the free surface $z = h$ at $y = \pm b$, where

$$b = a \left[1 + \frac{\tau}{h_{\mathrm{m}}} - \left(\frac{\tau^2}{h_{\mathrm{m}}^2} + \frac{2x}{h_{\mathrm{m}}^2 t} \right)^{1/2} \right]^{1/2}, \tag{6.8}$$

and the function f in (6.6) is given by (5.59), which leads to

$$f = \left[1 + \frac{\tau}{h_\mathrm{m}} + \left(\frac{2x}{h_\mathrm{m}^2 t}\right)^{1/2}\right]^{1/2} \left[\left(1 + \frac{\tau}{h_\mathrm{m}}\right) E(\phi|m) - \left(\frac{2x}{h_\mathrm{m}^2 t}\right)^{1/2} F(\phi|m)\right] - \frac{\tau}{h_\mathrm{m}} \left[1 + \frac{\tau}{h_\mathrm{m}} - \left(\frac{\tau^2}{h_\mathrm{m}^2} + \frac{2x}{h_\mathrm{m}^2 t}\right)^{1/2}\right]^{1/2}, \tag{6.9}$$

where $F(\phi|m)$ and $E(\phi|m)$ denote incomplete elliptic integrals of the first and second kinds, respectively, with

$$\phi = \sin^{-1}\left[\left(\frac{1 + \frac{\tau}{h_\mathrm{m}} - \left(\frac{\tau^2}{h_\mathrm{m}^2} + \frac{2x}{h_\mathrm{m}^2 t}\right)^{1/2}}{1 + \frac{\tau}{h_\mathrm{m}} - \left(\frac{2x}{h_\mathrm{m}^2 t}\right)^{1/2}}\right)^{1/2}\right], \qquad m = \frac{1 + \frac{\tau}{h_\mathrm{m}} - \left(\frac{2x}{h_\mathrm{m}^2 t}\right)^{1/2}}{1 + \frac{\tau}{h_\mathrm{m}} + \left(\frac{2x}{h_\mathrm{m}^2 t}\right)^{1/2}}, \tag{6.10}$$

where, $F(\phi|m)$ and $E(\phi|m)$ are defined by

$$F(\phi|m) = \int_0^{\sin\phi} \frac{\mathrm{d}x}{\sqrt{(1-x^2)(1-m^2x^2)}}, \quad E(\phi|m) = \int_0^{\sin\phi} \frac{\sqrt{1-m^2x^2}}{\sqrt{1-x^2}}\,\mathrm{d}x, \tag{6.11}$$

(see, for example, Gradshteyn and Ryzhik [49]). From (6.9) we have

$$\frac{\partial f}{\partial x} = -\frac{3F(\phi|m)}{2h_\mathrm{m}^2 t\left[1 + \frac{\tau}{h_\mathrm{m}} + \left(\frac{2x}{h_\mathrm{m}^2 t}\right)^{1/2}\right]^{1/2}}, \tag{6.12}$$

showing that $\partial f/\partial x < 0$ for $0 \le x \le u_{\max} t$, that is, f decreases monotonically with x.

In particular, in the case of purely gravity-driven flow (so that $\tau = 0$) we have

$\phi = \pi/2$ and equations (6.9) and (6.10) reduce to

$$f = \left[1 + \left(\frac{2x}{h_{\rm m}^2 t}\right)^{1/2}\right]^{1/2} \left[E(m) - \left(\frac{2x}{h_{\rm m}^2 t}\right)^{1/2} K(m)\right], \qquad m = \frac{1 - \left(\frac{2x}{h_{\rm m}^2 t}\right)^{1/2}}{1 + \left(\frac{2x}{h_{\rm m}^2 t}\right)^{1/2}}, \tag{6.13}$$

where $K(m) = F(\pi/2|m)$ and $E(m) = E(\pi/2|m)$ denote complete elliptic integrals of the first and second kinds, respectively. In Figure 6.3 the curves for $\tau \geq 1/6$ and the curve for $\tau = 0$ correspond to (6.9) and (6.13), respectively.

6.2.3 Purely Shear-stress-driven Flow

For purely shear-stress-driven flow, we have $u = \tau z$, $u_{\rm min} = 0$ and $u_{\rm max} = \tau h_{\rm m}$, and an analogous analysis to that described in Subsection 6.2.2 reveals that the corresponding forms for H and b are given by

$$H = \frac{x}{\tau t} \qquad \text{and} \qquad b = a\left(1 - \frac{x}{\tau h_{\rm m} t}\right)^{1/2}. \tag{6.14}$$

Then from (5.50) the function f in (6.6) is given explicitly by

$$f = \left(1 - \frac{x}{\tau h_{\rm m} t}\right)^{3/2} \tag{6.15}$$

for $0 \leq x \leq \tau h_{\rm m} t$. From (6.15) we have

$$\frac{\partial f}{\partial x} = -\frac{3}{2\tau h_{\rm m} t}\left(1 - \frac{x}{\tau h_{\rm m} t}\right)^{1/2}, \tag{6.16}$$

showing again that $\partial f/\partial x < 0$ for $0 \leq x \leq u_{\rm max} t$, that is, f again decreases monotonically with x.

Figure 6.5 shows plots of two examples of the mean concentration $\bar{c}$ in the rivulet as a function of x for an initially semi-infinite slug of uniform concentration, given by (6.6) when $a = 1$ and $h_{\rm m} = 1$ at several times t in the cases (a)

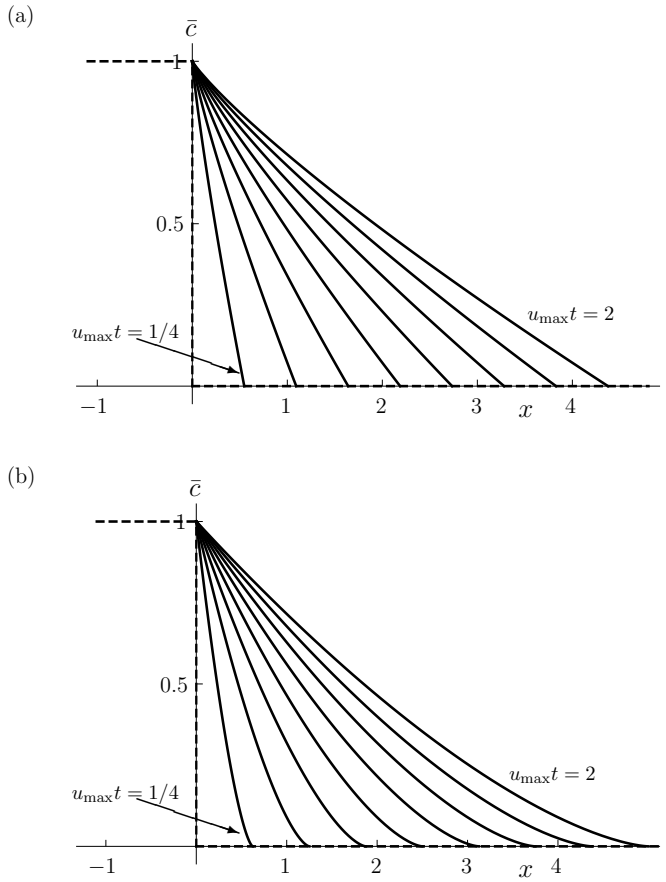

Figure 6.5: Plots of the mean concentration $\bar{c}$ due to advection in a rivulet on a vertical substrate, in the case when the solute initially takes the form a semi-infinite slug of uniform concentration, given by (6.6), as a function of x satisfying $0 \le x \le u_{\max}t$ at times $u_{\max}t = 1/4$, $1/2$, ..., and 2, in the cases (a) purely gravity-driven flow, given by (6.13) for which $u_{\max} = 35/16$ and (b) purely shear-stress-driven flow, given by (6.15) for which $u_{\max} = 5/2$, with $a = 1$ and $h_{\rm m} = 1$ in both cases. In both parts the initial condition for $\bar{c}$ is shown as a dashed line.

purely gravity-driven flow, given by (6.13) for which $u_{\min} = 0$ and $u_{\max} = 35/16$ and (b) purely shear-stress-driven flow, given by (6.15) for which $u_{\min} = 0$ and $u_{\max} = 5/2$. Figure 6.5 also shows that the function $f(\xi)$ decreases monotonically from the value 1 at $x = 0$ to the value 0 at $x = u_{\max}t$. Note that because of the self-similar form of (6.6), plots of $\bar{c}$ at any other time $t > 0$ would again be the same as the one for $u_{\max}t = 1$ in Figure 6.5 except that in each case the x coordinate must be either stretched or shrunk by the amount $u_{\max}t$.

6.2.4 An Initially Finite Slug of Solute

Now we consider when the solute initially takes the form of a finite slug of uniform concentration c_0 in $0 \leq x \leq \Delta$ with $c = 0$ in $x < 0$ and $x > \Delta$, where both c_0 and the length of the slug Δ (> 0) are constants. In this case $\overline{C}_0 = c_0$ again, the solution for c at time t is given by (5.61), and the solution for $\bar{c}$ at time t is given by

$$\bar{c} = \begin{cases} 0 & \text{if } \; x \leq u_{\min} t, \\ 1 - f\left(\dfrac{x}{u_{\mathrm{m}} t}\right) & \text{if } \; u_{\min} t < x \leq u_{\max} t, \\ 1 & \text{if } \; u_{\max} t < x \leq \Delta + u_{\min} t, \\ f\left(\dfrac{x - \Delta}{u_{\mathrm{m}} t}\right) & \text{if } \; \Delta + u_{\min} t < x \leq \Delta + u_{\max} t, \\ 0 & \text{if } \; x > \Delta + u_{\max} t \end{cases} \tag{6.17}$$

when $t \leq \Delta / u_{\mathrm{m}}$ (that is, up to the instant when the point of the rear of the slug at which the velocity is a maximum and the point of the front of the slug at which the velocity is a minimum first reach the same x value), and by

$$\bar{c} = \begin{cases} 0 & \text{if } \; x \leq u_{\min} t, \\ 1 - f\left(\dfrac{x}{u_{\mathrm{m}} t}\right) & \text{if } \; u_{\min} t < x \leq \Delta + u_{\min} t, \\ f\left(\dfrac{x - \Delta}{u_{\mathrm{m}} t}\right) - f\left(\dfrac{x}{u_{\mathrm{m}} t}\right) & \text{if } \; \Delta + u_{\min} t < x \leq u_{\max} t, \\ f\left(\dfrac{x - \Delta}{u_{\mathrm{m}} t}\right) & \text{if } \; u_{\max} t < x \leq \Delta + u_{\max} t, \\ 0 & \text{if } \; x > \Delta + u_{\max} t \end{cases} \tag{6.18}$$

when $t > \Delta / u_{\mathrm{m}}$. In both cases the function f in (6.17) and (6.18) is the same as in (6.6).

Up to the instant $t = \Delta / u_{\mathrm{m}}$, $\bar{c}$ increases monotonically with x up to its maximum value 1 on a decreasing interval that lies within $0 \leq x \leq \Delta$, and

decreases monotonically with x to the right of this interval. At $t = \Delta/u_{\rm m}$ the interval has shrunk to a point at $x = (u_{\rm max}/u_{\rm m})\Delta$, and thereafter $\bar{c}$ satisfies $\bar{c} < 1$ everywhere, and can develop additional non-monotonic dependence on x beyond what it inherits in an obvious way from the initial distribution of c. In addition, $\bar{c}$ at $x = 0$ takes the constant value $1 - f(0)$ for $t \leq -\Delta/u_{\rm min}$, but (if $u_{\rm min} \neq 0$) decreases thereafter, whereas $\bar{c}$ at $x = \Delta$ takes the constant value $f(0)$ for $t \leq \Delta/u_{\rm max}$, but (if $u_{\rm max} \neq 0$) decreases thereafter.

Figure 6.6 shows three examples of the solution (6.17) and (6.18) for the mean concentration $\bar{c}$ in gravity- and shear-stress- driven flow of the rivulet plotted as a function of x/Δ at times $u_{\rm m}t/\Delta = 1/4,\ 1/2,\ \ldots,\ 5$, with $a = 1$ and $\beta = 1$, for an initially finite slug of uniform concentration, illustrating the advection of the solute by the flow, in the cases (a) $\tau = -2/3$ (for which $u_{\rm min} = -5/24$ and $u_{\rm max} = 0$), (b) $\tau = -1/3$ (for which $u_{\rm min} = -1/18$ and $u_{\rm max} = 1/72$), and (c) $\tau = -1/6$ (for which $u_{\rm min} = -1/72$ and $u_{\rm max} = 1/18$) and including the initial condition for $\bar{c}$ at $t = 0$ as a dashed line in each case. In cases (b) and (c) we have $-1/2 = -\beta a/2 < \tau < 0$, and so there is both upward and downward flow, with consequent upward and downward advection of solute by the flow, whereas in case (a) we have $\tau < -\beta a/2 = -1/2$ and so the advection of the solute is upward everywhere. In Figure 6.6(c), non-monotonic dependence of $\bar{c}$ on x of the kind mentioned earlier is evident in $x > \Delta$ when $t > \Delta/u_{\rm max}$. Figure 6.6(c) also shows, for $x/\Delta \geq 1$, the envelope of the solution curves $\bar{c}$ as a dotted curve.

Figure 6.7 shows two examples of the mean concentration $\bar{c}$ plotted as a function of x/Δ given by (6.17) and (6.18) due to advection in the case of an initially finite slug of uniform concentration at several times t when $a = 1$ and $h_{\rm m} = 1$. Figure 6.7(a) is for purely gravity-driven flow, given by (6.13) (for which $u_{\rm min} = 0$ and $u_{\rm max} = 35/16$), at times t given by $u_{\rm max}t/\Delta = 4/35,\ 6/35,\ \ldots,\ 34/35$, and Figure 6.7(b) is for purely shear-stress-driven flow, given by (6.15), at times t given by $u_{\rm max}t/\Delta = 1/10,\ 1/5,\ \ldots,\ 3/2$ (for which $u_{\rm min} = 0$ and $u_{\rm max} = 5/2$).

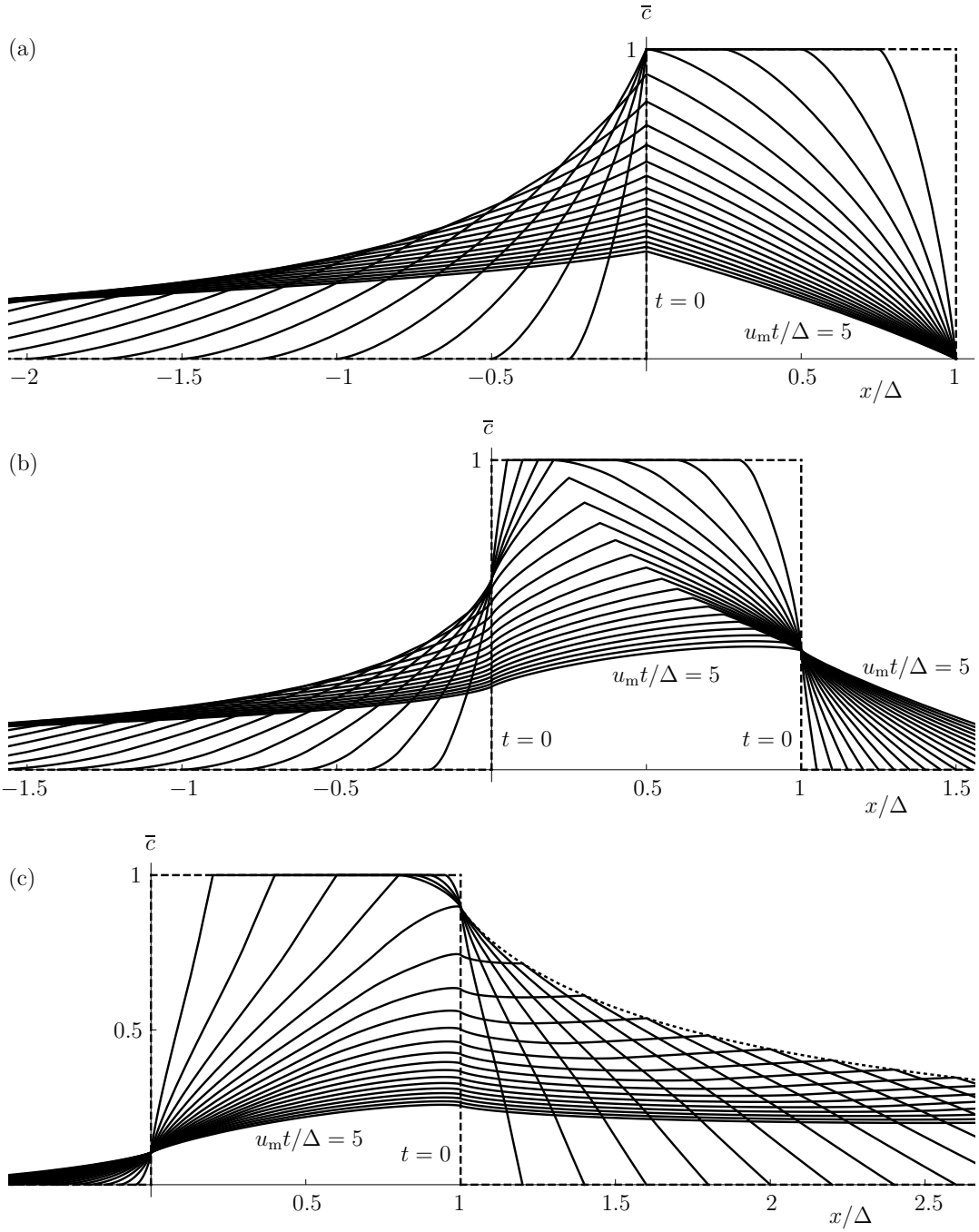

Figure 6.6: Plots of the mean concentration $\bar{c}$ due to advection in gravity- and shear-stress-driven flow of a thin rivulet on a vertical substrate in the case when the solute initially takes the form of a finite slug of uniform concentration $c = 1$ in $0 \le x \le \Delta$ with $c = 0$ in $x < 0$ and $x > \Delta$, given by (6.17) and (6.18), as a function of x/Δ at times t given by $u_{\rm m}t/\Delta = 0$, 1/4, 1/2, …, 5, for (a) $\tau = -2/3$, (b) $\tau = -1/3$, and (c) $\tau = -1/6$ with $a = 1$ and $\beta = 1$ in each case (so that $u_{\rm m} = 5/24$, 5/72, and 5/72, respectively). In each part the initial condition for $\bar{c}$ is shown as a dashed line, and in part (c) the envelope of the solution curves $\bar{c}$ in $x/\Delta \ge 1$ is shown as a dotted curve.

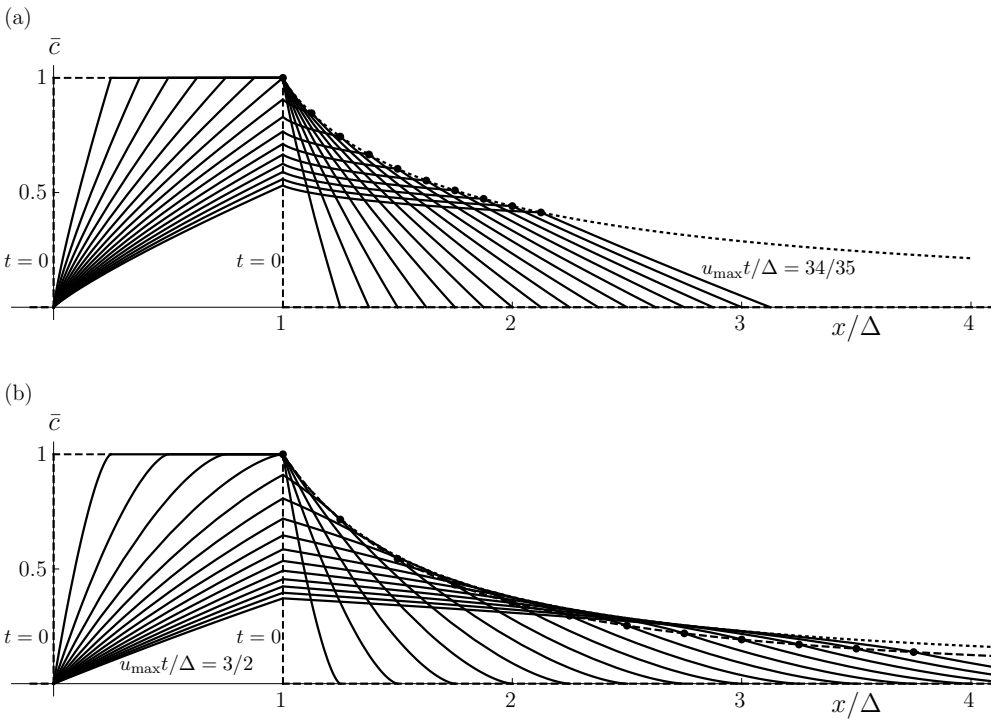

Figure 6.7: Plots of the mean concentration $\bar{c}$ due to advection in a thin rivulet on a vertical substrate in the case when the solute initially takes the form of a finite slug of uniform concentration $c = 1$ in $0 \le x \le \Delta$ with $c = 0$ in $x < 0$ and $x > \Delta$, as a function of x/Δ in (a) purely gravity-driven flow, given by (6.13), at times $u_{\max}t/\Delta = 4/35, 6/35, \ldots, 34/35$, and (b) purely shear-stress-driven flow, given by (6.15), at times $u_{\max}t/\Delta = 1/10, 1/5, \ldots, 3/2$, with $a = 1$ and $h_{\mathrm{m}} = 1$ in both cases (so that $u_{\max} = 35/16$ and $u_{\max} = 5/2$, respectively). For $x/\Delta \ge 1$ in part (a) the locus of the corner in $\bar{c}$ is shown as a dotted curve, and in part (b) the locus of the corners in $\bar{c}$ is shown as a dashed curve and the envelope of the solution curves $\bar{c}$ is shown as a dotted curve. In both parts the initial condition for $\bar{c}$ is shown as a dashed line.

In both cases there is downward flow everywhere, with consequent downward advection of the solute as sketched in Figure 6.2. Figure 6.7(a) also shows, for $x/\Delta \ge 1$, the locus of the corner in the solution for $\bar{c}$ as a dotted curve; in this case the same curve also gives the envelope of the solution curves $\bar{c}$. Figure 6.7(b) also shows that, for $x/\Delta \ge 1$, the locus of the corner in the solution for $\bar{c}$ as a dashed curve and the envelope of the solution curves $\bar{c}$ as a dotted curve.

6.3 Taylor–Aris Dispersion of a Passive Solute in a Thin Rivulet

In this Section we consider the long-time Taylor–Aris dispersion of a passive solute injected into steady unidirectional flow of a thin rivulet of fluid on a vertical planar substrate.

As in Section 5.4 of Chapter 5, at sufficiently large times (specifically for $t \gg \ell^2/D$), the effect of diffusion of the solute cannot be ignored. In this case the governing equation and the boundary conditions for the concentration of solute, c, are again given by (5.48) and (5.49), respectively. In this Section, we will derive the effective diffusivity D_{eff}, for the present flow of a thin rivulet.

In Section 5.4 we used the method of multiple scales to show that the known results concerning Taylor–Aris dispersion of a passive solute at large times in flow in a channel of arbitrary cross-section essentially hold true for Taylor–Aris dispersion in rivulet flow. In Section 6.4 we use the results (5.94) and (5.95) to analyse Taylor–Aris dispersion in a thin rivulet; this analysis is somewhat similar to the corresponding discussion of Guell *et al.* [53] for pressure-driven flow in a thin channel, as discussed in Section 1.11.

6.4 Taylor–Aris Dispersion in a Thin Rivulet on a Vertical Substrate

In this Section we use the results (5.94) and (5.95) to obtain the effective diffusivity, D_{eff}, for Taylor–Aris dispersion in a thin rivulet on a vertical substrate.

With the scalings (5.65) the problem (5.95) becomes

$$C_{1yy} + \frac{1}{\epsilon^2} C_{1zz} = \epsilon^2 (u - \overline{u}), \quad C_{1z} = 0 \quad \text{on} \quad z = 0, \quad C_{1z} = \epsilon^2 C_{1y} h' \quad \text{on} \quad z = h, \tag{6.19}$$

and we seek a solution of C_1 in the form

$$C_1 = \epsilon^2 \left(C_{10} + \epsilon^2 C_{12} + \epsilon^4 C_{14} + \dots \right). \tag{6.20}$$

Then at leading order in ϵ^2

$$C_{10zz} = 0, \qquad C_{10z} = 0 \quad \text{on} \quad z = 0, \qquad C_{10z} = 0 \quad \text{on} \quad z = h, \tag{6.21}$$

so that $C_{10} = C_{10}(y)$. At first order in ϵ^2

$$C_{10}'' + C_{12zz} = u - \overline{u}, \qquad C_{12z} = 0 \quad \text{on} \quad z = 0, \qquad C_{12z} = C_{10}' h' \quad \text{on} \quad z = h. \tag{6.22}$$

Since the contact angle is nonzero, consistency of the boundary conditions in (6.22) at $y = \pm a$ requires that

$$C_{10}' = 0 \quad \text{at} \quad y = \pm a. \tag{6.23}$$

From (6.22) we have

$$C_{12} = -\frac{z^4}{24} + \frac{(h+\tau)z^3}{6} - (\overline{u} + C_{10}'')\frac{z^2}{2} + B \tag{6.24}$$

for some arbitrary function $B = B(y)$, which with $(6.22)_3$ gives

$$-\frac{h^3}{6} + \frac{(h+\tau)h^2}{2} - (\overline{u} + C_{10}'')h = C_{10}' h', \tag{6.25}$$

that is,

$$(hC_{10}')' = R, \tag{6.26}$$

where for convenience we have written

$$R = R(y) = \frac{h^2(2h+3\tau)}{6} - \overline{u}h. \tag{6.27}$$

Integrating equation (6.26) once yields

$$C'_{10} = \frac{1}{h}\int_{-a}^{y} R(\tilde{y})\,\mathrm{d}\tilde{y}, \tag{6.28}$$

and hence C_{10} is given by

$$C_{10} = \int_{-a}^{y} \frac{1}{h(\hat{y})}\int_{-a}^{\hat{y}} R(\tilde{y})\,\mathrm{d}\tilde{y}\,\mathrm{d}\hat{y}, \tag{6.29}$$

which is determined only up to an irrelevant additive constant.

The leading order term in the limit $\epsilon \to 0$ of the problem (5.95) gives the main result for dispersion in a thin rivulet, namely that the effective diffusivity D_{eff} is given by

$$D_{\text{eff}} = 1 + \kappa_0 \mathrm{Pe}^2, \tag{6.30}$$

where Pe is given by (5.68), and the dispersion coefficient κ_0 is given by

$$\kappa_0 = \frac{1}{A}\int_{-a}^{a} hC'^2_{10}\,\mathrm{d}y = \frac{1}{A}\int_{-a}^{a}\frac{1}{h}\left(\int_{-a}^{y} R(\tilde{y})\,\mathrm{d}\tilde{y}\right)^2 \mathrm{d}y, \tag{6.31}$$

in which the cross-sectional profile of the rivulet h is given by (6.2). Evaluating equation (6.29) yields an explicit solution for C_{10}, namely

$$C_{10} = \frac{h_{\mathrm{m}}(a^2-y^2)^2\left[20h_{\mathrm{m}}y^2 - 7a^2(8h_{\mathrm{m}}+9\tau)\right]}{2520a^4}, \tag{6.32}$$

and evaluating equation (6.31) leads to an explicit expression for κ_0, namely

$$\kappa_0 = \frac{\beta^2 a^4\left(13388\beta^2a^2 + 57876\beta a\tau + 63063\tau^2\right)}{331080750}. \tag{6.33}$$

If the values of the contact angle $\beta = \bar{\beta}$ and the semi-width $a = \bar{a}$ are prescribed (in which case h is determined explicitly) then clearly κ_0 in (6.33) is simply quadratic in τ; however, if $Q = \bar{Q}$ is one of the prescribed quantities, along with

either a or β (in which case h depends on τ via the flux relation $(6.3)_1$), then the dependence of κ_0 on τ is rather more complicated. Thus, the interpretation of κ_0 as τ varies depends on which two of the parameters Q, a and β are prescribed, as described in the following Subsections.

6.4.1 Purely Gravity-driven Flow

For purely gravity-driven flow (so that $\tau = 0$) equation (6.33) leads to $\kappa_0 = \kappa_{\rm GD}$, where

$$\kappa_{\rm GD} = \frac{6694\beta^4 a^6}{165540375} \simeq 4.0437 \times 10^{-5}\beta^4 a^6, \tag{6.34}$$

which may be written in the equivalent form

$$\kappa_{\rm GD} = \frac{3347 a^2 \overline{u}^2}{270270} \simeq 0.0124 a^2 \overline{u}^2, \tag{6.35}$$

where $\overline{u} = 2\beta^2 a^2/35$. The result (6.35) can be recognised as being identical to the result for dispersion in pressure-driven flow in a thin channel of parabolic cross-section (see, for example, Ajdari et al [2], whose corresponding result for κ_0 has an extra factor of 1/4 arising from their definition of the Péclet number, namely ${\rm Pe}_{\rm con} = 2a\overline{u}/D$, and whose equation (7) contains a minor typographical error, namely a missing opening square bracket before the second integral sign; however, after these differences are accounted for, our result (6.35) is in exact agreement with their result for $D_{\rm eff}$ and κ_0, namely their equations (9) and (7), respectively). In this case $Q = 4\beta^3 a^4/105$, and so equation (6.34), which provides the most useful form of κ_0 if β and a are prescribed, may alternatively be written in the equivalent forms

$$\kappa_{\rm GD} = \frac{3347}{60060}\left(\frac{\bar{Q}^3}{105\bar{\beta}}\right)^{1/2} \simeq 0.0054\left(\frac{\bar{Q}^3}{\bar{\beta}}\right)^{1/2}, \tag{6.36}$$

$$\kappa_{\rm GD} = \frac{3347}{30030}\left(\frac{\bar{Q}^2\bar{a}}{210}\right)^{2/3} \simeq 0.0032(\bar{Q}^2\bar{a})^{2/3}, \tag{6.37}$$

which are most useful if either β and Q are prescribed or a and Q are prescribed, respectively.

6.4.2 Purely Shear-stress-driven Flow

We may obtain from (6.33) the form of κ_0, with κ_0 rescaled as $\kappa_0 = \tau^2\kappa_{\rm SD}$, corresponding to dispersion in purely shear-stress-driven flow in the limits $\tau \to \pm\infty$, namely

$$\kappa_{\rm SD} = \frac{\beta^2 a^4}{5250} \simeq 0.0002 a^2\beta^2 a^4, \tag{6.38}$$

or equivalently,

$$\kappa_{\rm SD} = \frac{a^2\overline{u}_{\rm SD}^2}{210} \simeq 0.0048 a^2\overline{u}^2, \tag{6.39}$$

in which $\overline{u}_{\rm SD} = \overline{u}/\tau = \beta a/5$. In this case $\hat{Q} = Q/\tau = 2\tau\beta^2 a^3/15$, and so equation (6.38), which provides the most useful form of κ_0 if β and a are prescribed, may alternatively be written in the equivalent forms

$$\widehat{\kappa_{\rm SD}} = \frac{1}{140}\left(\frac{\sqrt{3}\bar{Q}^2}{5\sqrt{2}\bar{\beta}}\right)^{2/3} \simeq 0.0028\left(\frac{\bar{Q}^2}{\bar{\beta}}\right)^{2/3}, \tag{6.40}$$

$$\widehat{\widehat{\kappa_{\rm SD}}} = \frac{\bar{Q}\bar{a}}{700} \simeq 0.0014\bar{Q}\bar{a}, \tag{6.41}$$

in which κ_0 has been rescaled as $\kappa_0 = \tau^{2/3}\widehat{\kappa_{\rm SD}}$ and $\kappa_0 = \tau\widehat{\widehat{\kappa_{\rm SD}}}$, respectively, and which are most useful if either β and Q are prescribed or a and Q are prescribed, respectively.

6.4.3 A Rivulet with Prescribed $\beta = \bar{\beta}$ and $a = \bar{a}$

When $\beta = \bar{\beta}$ and $a = \bar{a}$ are prescribed then κ_0 in (6.33) is simply quadratic in τ. Figure 6.8 shows a plot of κ_0 given by (6.33) as a function of τ for different values of $\bar{a}$, with $\bar{\beta} = 1$ in each case; note that whereas $\bar{\beta}$ and $\bar{a}$ are constants on each curve, the value of Q varies along the curves. The insert in Figure 6.8 shows an

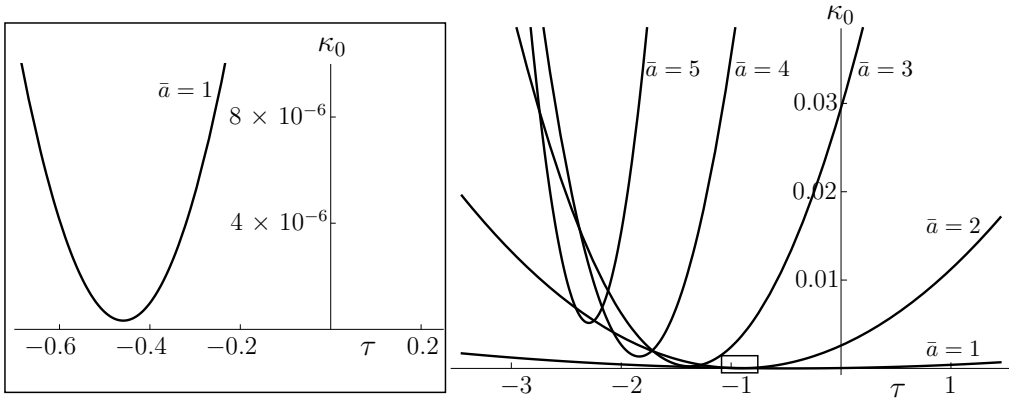

Figure 6.8: Plot of κ_0 given by (6.33) as a function of τ for gravity- and shear-stress-driven flow in a thin rivulet on a vertical substrate, for a range of values of the prescribed semi-width $\bar{a}$, namely $\bar{a} = 1$, 2, 3, 4 and 5, with $\bar{\beta} = 1$ in each case. The inset shows an enlargement for small values of κ_0, also showing that κ_0 is always positive.

enlargement of κ_0 for small values of τ, and illustrates that κ_0 is always positive. The minimum value of κ_0 on a given curve is $\kappa_0 = \kappa_{0\min}$ at $\tau = \tau_{\min}$, where

$$\kappa_{0\min} = \frac{8\bar{\beta}^4\bar{a}^4}{24279255} \simeq 3.2950 \times 10^{-7}\bar{\beta}^4\bar{a}^4, \tag{6.42}$$

$$\tau_{\min} = -\frac{106\bar{\beta}\bar{a}}{231} \simeq -0.4589\bar{\beta}\bar{a}, \tag{6.43}$$

corresponding to the value

$$Q = -\frac{16\bar{\beta}^3\bar{a}^4}{693} \simeq -0.0231\bar{\beta}^3\bar{a}^4, \tag{6.44}$$

for given values of $\bar{\beta}$ and $\bar{a}$; values of κ_0 below $\kappa_{0\min}$ are not achievable for any value of τ. Note also that for $\kappa_0 > \kappa_{0\min}$ there are always two different values of τ, and hence two rivulets with different fluxes Q (but with the same values of $\bar{\beta}$ and $\bar{a}$), with the same value of κ_0; for example, when $\bar{a} = 2$ and $\bar{\beta} = 1$, the value $\kappa_0 = 0.01$ is attained with $\tau \simeq -2.7273$ (for which $Q \simeq -2.2996$) and with $\tau \simeq 0.8918$ (for which $Q \simeq 1.5607$).

6.4.4 A Rivulet with Prescribed $\beta = \bar{\beta}$ and $Q = \bar{Q}$

When $\beta = \bar{\beta}$ and $Q = \bar{Q}$ are prescribed then κ_0 is given parametrically as a function of τ (with parameter a) by (6.33), (6.2) and (6.3), specifically τ and κ_0 are given explicitly by

$$\tau = \frac{15\bar{Q}}{8ah_{\mathrm{m}}^2} - \frac{4h_{\mathrm{m}}}{7}, \qquad \kappa_0 = \frac{8a^6\bar{\beta}^4}{1324323} + \frac{3\bar{Q}^2}{280a^2\bar{\beta}^2} + \frac{4a^2\bar{\beta}\bar{Q}}{8085}. \tag{6.45}$$

In particular, κ_0 has branches satisfying

$$\kappa_0 = \frac{1}{140}\left(\frac{3\bar{Q}^4\tau^2}{50\bar{\beta}^2}\right)^{1/3} + \frac{31}{2695}\left(\frac{\bar{Q}^5}{60\bar{\beta}\tau^2}\right)^{1/3} + O\left(\frac{1}{\tau}\right) \to \infty \tag{6.46}$$

in the limits $\tau \to \pm\infty$ (corresponding to $a \to 0^+$), and a branch in $\tau < 0$ satisfying

$$\kappa_0 = \frac{343\tau^6}{30888\bar{\beta}^2} + \frac{38\bar{Q}\tau^2}{2145\bar{\beta}} + O(\tau) \to \infty \tag{6.47}$$

in the limit $\tau \to -\infty$ (corresponding to $a \to +\infty$). In the special case $Q = 0$ (which, for a nontrivial flow, is possible only if $\tau < 0$, and there is a single solution for the rivulet) we have $h_{\mathrm{m}} = -7\tau/4$, and κ_0 is given by the leading order term in (6.47), that is,

$$\kappa_0 = \frac{343\tau^6}{30888\bar{\beta}^2} \simeq 0.0111\left(\frac{\tau^3}{\bar{\beta}}\right)^2 \qquad \text{for} \quad \tau < 0. \tag{6.48}$$

Figure 6.9 shows a plot of κ_0 given by (6.45) as a function of τ for different values of $\bar{Q}$ with $\bar{\beta} = 1$ in each case, including the leading order asymptotic results (6.46) and (6.47). Note that whereas $\bar{\beta}$ and $\bar{Q}$ are constants on each curve, the value of a varies along the curves.

When $\bar{Q} > 0$ there is a unique value of κ_0 for all values of τ, but when $\bar{Q}$ satisfies $Q_{\min} = -3087\tau^4/5120\bar{\beta} < \bar{Q} < 0$ there are two values of κ_0 for all values of $\tau < 0$. The latter non-uniqueness arises because, as described in

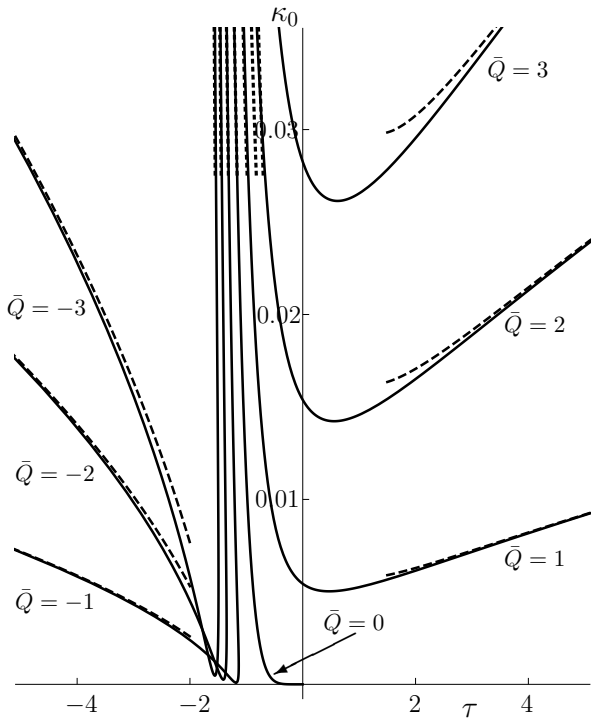

Figure 6.9: Plot of κ_0 given by (6.45) as a function of τ for gravity- and shear-stress-driven flow in a thin rivulet on a vertical substrate, for a range of values of the prescribed flux $\bar{Q}$, namely $\bar{Q} = -3, -2, -1, \ldots, 3$, with $\bar{\beta} = 1$ in each case. The dashed and dotted curves show the leading order asymptotic results (6.46) and (6.47), respectively.

Section 1.8, and as shown in Figure 1.14, when $\tau < 0$ there are two possible values of a (and hence two possible rivulets, a narrower one and a wider one) that correspond to the same value of Q; these two rivulets are associated with the smaller and larger values of κ_0, respectively. Also there is no rivulet solution when Q satisfies $\bar{Q} < Q_{\min} = -3087\tau^4/5120\bar{\beta}$, or equivalently, when $\tau > \tau_{\max}$ where $\tau_{\max} = -(-5120\bar{\beta}\bar{Q}/3087)^{1/4}$ for $Q < 0$; this is consistent with the fact the curves for $Q < 0$ in Figure 6.9 lie entirely in $\tau \leq \tau_{\max}$.

As Figure 6.9 shows, when $Q \neq 0$ then κ_0 again has a minimum value; an analogous analysis to that described in the previous Subsection 6.4.3 reveals that the minimum value $\kappa_0 = \kappa_{0\min}$ occurs at $\tau = \tau_{\min}$, where

$$\begin{aligned} \kappa_{0\min} &= \frac{1}{1155}\left(\frac{2(11518 + 217\sqrt{2821}\sigma)\bar{Q}^3}{1365\bar{\beta}}\right)^{1/2} \\ &\simeq 0.0050\left(\frac{\bar{Q}^3}{\bar{\beta}}\right)^{1/2} \quad \text{or} \quad 0.0001\left(-\frac{\bar{Q}^3}{\bar{\beta}}\right)^{1/2}, \end{aligned} \tag{6.49}$$

and

$$\begin{aligned}\tau_{\min} &= \sigma\left(\frac{2(32874353\sqrt{2821}\sigma - 1662451778)\bar{\beta}\bar{Q}}{3471933465}\right)^{1/4} \\ &\simeq 0.4685(\bar{\beta}\bar{Q})^{1/4} \quad \text{or} \quad -1.1837(-\bar{\beta}\bar{Q})^{1/4},\end{aligned} \tag{6.50}$$

corresponding to

$$\begin{aligned}a &= \left(\frac{21(\sqrt{2821}\sigma - 26)\bar{Q}}{40\bar{\beta}^3}\right)^{1/4} \\ &\simeq 1.9424\left(\frac{\bar{Q}}{\bar{\beta}^3}\right)^{1/4} \quad \text{or} \quad 2.5386\left(-\frac{\bar{Q}}{\bar{\beta}^3}\right)^{1/4},\end{aligned} \tag{6.51}$$

where we have introduced the notation $\sigma = \text{sgn}(Q) = \pm 1$, and the decimal approximations are valid for $\bar{Q} > 0$ and $\bar{Q} < 0$, respectively. For given values of $\bar{\beta}$ and $\bar{Q}$, values of κ_0 satisfying $\kappa_0 < \kappa_{0\min}$ are not achievable for any value of τ. In addition, except when $\bar{Q} = 0$, each value of $\kappa_0 > \kappa_{0\min}$ is achieved with two different values of τ, and hence in this case two different rivulets will lead to the same value of κ_0.

6.4.5 A Rivulet with Prescribed $a = \bar{a}$ and $Q = \bar{Q}$

When $a = \bar{a}$ and $Q = \bar{Q}$ are prescribed then κ_0 as a function of τ is again given parametrically by (6.45), but is now parameterised by β (rather than by a). Qualitatively the behaviour in this case is similar to that in the case of prescribed β and Q described in Subsection 6.4.4. In particular, κ_0 has branches satisfying

$$\kappa_0 = \frac{\bar{Q}\bar{a}\tau}{700} + \frac{73}{5390}\left(\frac{\bar{Q}^3\bar{a}}{30\tau}\right)^{1/2} + O\left(\frac{1}{\tau}\right) \to \infty \tag{6.52}$$

in the limits $\tau \to \pm\infty$ (corresponding to $\beta \to 0^+$), and a branch in $\tau < 0$ satisfying

$$\kappa_0 = \frac{7\bar{a}^2\tau^4}{7722} - \frac{178\bar{Q}\bar{a}\tau}{45045} + O(1) \to \infty \tag{6.53}$$

in the limit $\tau \to -\infty$ (corresponding to $\beta \to +\infty$). In the special case $Q = 0$ then κ_0 is simply given by

$$\kappa_0 = \frac{7\bar{a}^2\tau^4}{7722} \simeq 0.0009(\bar{a}\tau^2)^2 \qquad \text{for} \quad \tau < 0. \tag{6.54}$$

Figure 6.10 shows a plot of κ_0 given by (6.33), (6.2) and (6.3) as a function of τ for different values of $\bar{Q}$ with $\bar{a} = 1$ in each case, including the leading order asymptotic results (6.52) and (6.53). Note that whereas $\bar{a}$ and $\bar{Q}$ are constants on each curve, the value of β varies along the curves.

Like in the case of prescribed β and Q discussed in Subsection 6.4.4, when $\bar{Q} > 0$ there is a unique value of κ_0 for all values of τ, but when $\bar{Q}$ satisfies $Q_{\min} = 98\bar{a}\tau^3/405 < \bar{Q} < 0$ there are two values of κ_0 for all values of $\tau < 0$, associated with two rivulets that have the same values of $\bar{a}$ and $\bar{Q}$ but different values of β. Also, the curves for $Q < 0$ in Figure 6.10 lie entirely in $\tau \leq \tau_{\max}$, where now $\tau_{\max} = (405\bar{Q}/98\bar{a})^{1/3}$.

As Figure 6.10 shows, when $Q \neq 0$ then κ_0 again has a minimum value $\kappa_0 = \kappa_{0\min}$, occurring at $\tau = \tau_{\min}$, where

$$\begin{aligned} \kappa_{0\min} &= \frac{3}{770}\left(\frac{(3279 + 82\sqrt{1599}\sigma)\bar{Q}^4\bar{a}^2}{14^2 \times 65}\right)^{1/3} \\ &\simeq 0.0031(\bar{Q}^2\bar{a})^{2/3} \quad \text{or} \quad 0.00005(\bar{Q}^2\bar{a})^{2/3}, \end{aligned} \tag{6.55}$$

and

$$\begin{aligned} \tau_{\min} &= \left(\frac{(4872223 - 121471\sqrt{1599}\sigma)\bar{Q}}{77^2 \times 390\bar{a}}\right)^{1/3} \\ &\simeq 0.1861\left(\frac{\bar{Q}}{\bar{a}}\right)^{1/3} \quad \text{or} \quad 1.6144\left(\frac{\bar{Q}}{\bar{a}}\right)^{1/3}, \end{aligned} \tag{6.56}$$

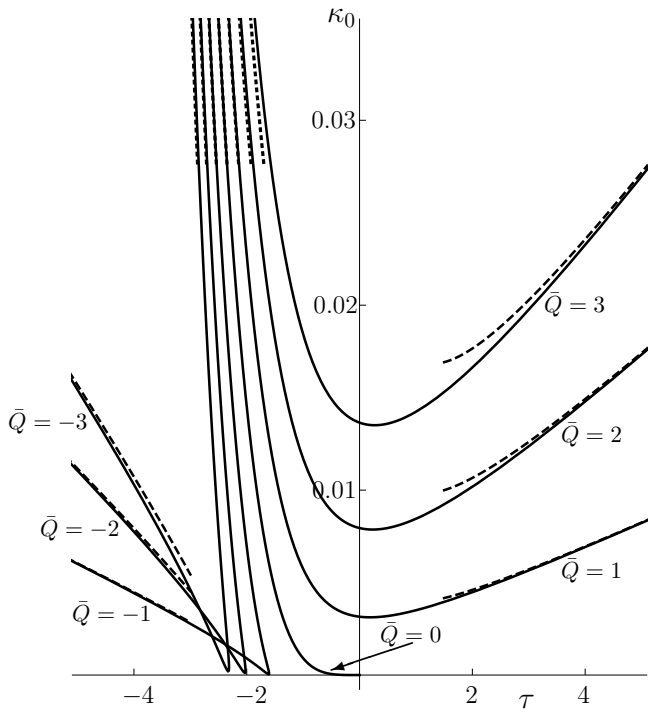

Figure 6.10: Plot of κ_0 given by (6.45) as a function of τ for for gravity- and shear-stress-driven flow in a thin rivulet on a vertical substrate, for a range of values of the prescribed flux $\bar{Q}$, namely $\bar{Q} = -3, -2, -1, \ldots, 3$, with $\bar{a} = 1$ in each case. The dashed and dotted curves show the leading order asymptotic results (6.52) and (6.53), respectively.

corresponding to

$$\begin{aligned} \beta &= \left(\frac{63(\sqrt{1599}\sigma - 13)\bar{Q}}{80\bar{a}^4} \right)^{1/3} \\ &\simeq 2.7700 \left(\frac{\bar{Q}}{\bar{a}^4} \right)^{1/3} \quad \text{or} \quad -3.4685 \left(\frac{\bar{Q}}{\bar{a}^4} \right)^{1/3}, \end{aligned} \tag{6.57}$$

and, once again, for given values of $\bar{a}$ and $\bar{Q}$, values of κ_0 satisfying $\kappa_0 < \kappa_{0\min}$ are not achievable for any value of τ. In addition, except when $\bar{Q} = 0$, each value of $\kappa_0 > \kappa_{0\min}$ is achieved with two different values of τ, and hence in this case two different rivulets will lead to the same value of κ_0.

6.5 Conclusions

In this Chapter we considered dispersion of a passive solute in steady unidirectional flow of a uniform thin rivulet of Newtonian fluid on a vertical planar

substrate when the flow is driven by both gravity and a uniform shear stress on its free surface.

In Section 6.2 we considered the short-time advection of a slug of a passive solute injected at time $t = 0$ into the rivulet on a vertical planar substrate; in particular, we presented the general form of the mean concentration $\bar{c}$ given by (5.50) at small times, and we used this result to describe advection of both an initially semi-infinite slug and an initially finite slug of solute. It was found that, in general it is difficult to obtain the function f in (6.6) in closed form; however, we derived it in the special cases $\tau \geq 0$ and of purely shear-stress-driven flow, as described in Subsections 6.2.2 and 6.2.3.

In Section 6.3 we described the long-time Taylor–Aris dispersion of an initially finite slug of solute, and in Section 6.4 we used the results (5.94) and (5.95) to obtain our main result, namely the general expression for the effective diffusivity, D_{eff}, in a thin rivulet, given by equations (6.30) and (6.33). As discussed in Chapter 5, care was taken to formulate the problem in such a way as to avoid the complication that arises when $\bar{u} \leq 0$ (*i.e.* when $Q \leq 0$) when using the conventional formulation of the problem given by (5.97)–(5.99). In addition, we discussed in detail the different interpretations of (6.33) depending on which two of the three parameters β, a and Q are prescribed. In all three situations considered, we found that, except in the special case of no net flow, $Q = 0$, the coefficient κ_0 always has a strictly positive global minimum as a function of τ (*i.e.* that D_{eff} is always strictly greater than D) and that any value of κ_0 above its minimum value can be achieved with two different values of τ (*i.e.* two different rivulets will lead to the same value of κ_0).

Chapter 7

Conclusions and Future Work

7.1 Conclusions

This thesis considered two different aspects of rivulet flow, namely non-Newtonian rheology and transport of a passive solute.

In Chapter 2 we obtained the solution for the steady gravity-driven unidirectional flow of a thin parallel-sided rivulet of a power-law fluid with prescribed volume flux Q down a planar substrate, and then showed how this solution can be used to describe the locally unidirectional steady gravity-driven flow of a thin rivulet with prescribed constant (nonzero) contact angle β but slowly varying semi-width a down a slowly varying substrate, such as the flow in the azimuthal direction around the outside of a large horizontal circular cylinder. In Chapter 3 we considered the converse situation of a rivulet of a power-law fluid with prescribed constant semi-width a (*i.e.* pinned contact lines) but slowly varying contact angle β.

In Chapter 2 we demonstrated how the features of the solution are strongly influenced by the shear-dependence of the viscosity. For example, rivulet flow of a strongly shear-thinning fluid self-channels down a narrow central channel between two levées of slowly moving fluid that form at the sides of the rivulet,

and in the central channel there is a plug-like flow except in a boundary layer near the substrate, as shown in Figures 2.6(a) and 5.1(a). On the other hand, in rivulet flow of a strongly shear-thickening fluid, the velocity profile is linear except in a boundary layer near the free surface, as shown in Figures 2.6(b) and 5.1(b).

Like the analysis of the corresponding situation for a Newtonian fluid studied by Paterson *et al.* [97], in Chapter 3 we found that the global behaviour of a rivulet with prescribed semi-width is qualitatively very different from that of a rivulet with prescribed contact angle described in Chapter 2. Specifically, we found that a rivulet with pinned contact lines can flow all the way from the top to the bottom of the cylinder only when it is sufficiently narrow; however, when it is sufficiently wide, the contact angle reaches its minimum physically realisable value of zero at some location on the lower half of the cylinder. We then discussed a possible scenario in which the contact lines de-pin at this location, and the rivulet flows to the bottom of the cylinder with zero contact angle and slowly varying semi-width. How the shape of the rivulet and the velocity within it depend on the power-law index N was described in detail. In particular, we showed that whereas neither the free surface of the rivulet h nor the velocity u vary monotonically with N at any fixed value of the angle of inclination of the substrate α, its mass is always monotonically increasing as a function of prescribed constant $\bar{a}$ but is monotonically decreasing in N.

Results obtained in Chapters 2 and 3 concerning rivulet flow of a power-law fluid provide a rare analytical description for the study of rivulet flow of non-Newtonian fluids, and are a useful benchmark for the studies of rivulet flow of more realistic non-Newtonian fluids. In Chapter 4 we focused on non-Newtonian effects in unidirectional rivulet flow of more realistic generalised Newtonian fluids, such as a Carreau fluid and an Ellis fluid. Specifically, we considered gravity-driven flow of a thin uniform rivulet of a generalised Newtonian fluid down a

vertical planar substrate. We derived the parametric solution for the velocity and for the volume flux for any generalised Newtonian fluid whose viscosity is specified as a function of the shear rate (including, in particular, the solution for a Carreau fluid), and the explicit solution for any generalised Newtonian fluid whose viscosity is specified as a function of the shear stress (including, in particular, the solution for an Ellis fluid). These solutions were then used to describe rivulet flow of a Carreau fluid and of an Ellis fluid, and to highlight the similarities and differences between the behaviour of these two fluids. We found that the behaviour of a rivulet of a Carreau fluid and of a rivulet of an Ellis fluid depends on the parameters μ_∞, λ and N and on the parameters μ_∞ and $\tau_{\rm av}$, respectively, in a relatively simple way, reflecting the simple dependence of the viscosities of these fluids on these parameters, as shown in Figures 4.3 and 4.4(a,b). We found that any increase of shear thinning leads to an increase in the volume flux of the rivulet if the semi-width a and the contact angle β are prescribed, or to a decrease in a or β if the flux Q is prescribed. The behaviour of rivulets of nearly Newtonian fluids was also investigated. In particular, we showed that the effect of weakly non-Newtonian shear-thinning behaviour is always to make the rivulet of prescribed flux smaller. The non-monotonic variation of the viscosity of an Ellis fluid with α leads to a more complicated dependence of the behaviour of the rivulet on this parameter than on the other parameters in the Careau and Ellis models. In particular, a rivulet of a strongly shear-thinning Ellis fluid can comprise two regions with different viscosities, with the velocity having a plug-like profile with large magnitude in a narrow central region of the rivulet. The structure of the flow in this case is somewhat similar to that of rivulet flow of a power-law fluid in the strongly shear-thinning limit, as described in Chapters 2 and 3.

In Chapters 5 and 6 we considered advection and Taylor–Aris dispersion of a passive solute in uniform non-thin and thin rivulets, respectively, of Newtonian

fluid undergoing steady unidirectional flow driven by gravity and/or a prescribed uniform shear stress τ on their free surfaces on a vertical planar substrate. The problems considered in Chapters 5 and 6 are the same, but because in Chapter 6 the rivulet was taken to be thin it was possible to make more progress analytically.

In Chapter 5, we considered only the case in which the contact angle of the rivulet has the prescribed value $\pi/2$; in this case it was possible to obtain a closed-form solution for the velocity, the cross-sectional free surface profile of the rivulet then being semi-circular. We presented the general form of the mean concentration $\bar{c}$ at small times $t \ll \ell^2/D$ during which the effect of advection dominates over that of diffusion, and we used this result to describe advection of both an initially semi-infinite slug and an initially finite slug of solute. We used the fact that $\bar{c}$ at any station x and any time t is the fraction of the cross-sectional area of the rivulet for which $u(y, z) \geq x/t$ to find the form of $\bar{c}$. In addition, we showed by using the method of multiple scales that well-known results concerning Taylor–Aris dispersion of a solute at large times $t \gg \ell^2/D$ in flow in a channel of arbitrary cross-section essentially hold for Taylor–Aris dispersion in flow in a semi-circular rivulet. In particular, we obtained the general expression for the effective diffusivity D_{eff}, given by (5.94), for Taylor–Aris dispersion in a semi-circular rivulet. Care had to be taken when considering the conventional formulation (5.97)–(5.99) in which velocities are scaled with $\bar{u}$, in order to avoid an artificial singularity when $\bar{u} = 0$, as shown in Figure 5.12.

In Chapter 6 we presented the general form of $\bar{c}$ at small times in a thin rivulet, and we used this result to describe advection of both an initially semi-infinite slug and an initially finite slug of solute. We presented examples showing both upward and downward advection, and highlighting the fact that $\bar{c}$ may eventually exhibit additional non-monotonic variation in x beyond what it inherits in an obvious way from the initial distribution of c, as shown in Figure 6.6(c). We found that, in general, it is difficult to obtain the function f in (6.6) in closed form; however,

we derived it in the special cases in which $\tau \geq 0$ everywhere and of purely shear-stress-driven flow. In addition, by using the results (5.94) and (5.95) we obtained the explicit form of the effective diffusivity, D_{eff}, for Taylor–Aris dispersion in a thin rivulet. Specifically, by using the results (5.94) and (5.95) we obtained the explicit expression form for D_{eff} given by (6.33) for Taylor–Aris dispersion in the special case of a thin rivulet on a vertical substrate, and discussed in detail its different interpretations depending on which two of the three parameters β, a and Q are prescribed. In all of the three situations considered we found that, except in the special case of no net flow, $Q = 0$, the coefficient κ_0 always has a strictly positive global minimum as a function of τ (*i.e.* that D_{eff} is always strictly greater than D) and that any value of κ_0 above its minimum value can be achieved with two different values of τ (*i.e.* two different rivulets will lead to the same value of κ_0).

7.2 Future Work

There are many directions in which the work presented in this thesis could be extended.

In Chapter 3 we considered gravity-driven rivulets of power-law fluid with pinned contact lines (*i.e.* prescribed semi-width) but variable contact angle on a large stationary horizontal cylinder. This could be extended to discuss the general scenario in which the contact lines de-pin and possibly re-pin at a prescribed nonzero value of the contact angle, and the rivulet flows to the bottom of the cylinder with nonzero contact angle and slowly varying semi-width. This situation was analysed by Paterson *et al.* [97] for a Newtonian fluid, but the corresponding analysis for a power-law fluid has yet to be done.

In Chapter 4 we considered rivulet flow of more realistic generalised Newtonian fluids, such as a Carreau fluid and an Ellis fluid, down a vertical planar substrate.

It would be of considerable interest to examine the combined effects of gravity and surface shear stress on such a flow. It should also be possible to generalise the solution obtained in Chapter 4 to the case of steady rivulet flow of a Carreau fluid and an Ellis fluid on a large stationary horizontal cylinder, such as that considered in Chapters 2 and 3.

Chapters 5 and 6 considered transport of a passive solute in rivulet flow. Future work could focus on the effect of a non-passive solute on the flow. Chemical reactions of the solute with the solvent can affect the effective diffusivity D_{eff}; Balakotaiah and Chang [10] investigated this using the centre-manifold theorem. Another extension could be to consider rivulets of fluids with suspended particles that could affect the viscosity, diffusivity and/or density of the fluid, so that μ, D and/or ρ depend on the particle concentration c, as investigated by, for example, Espín and Kumar [39]. Smith [115] showed the buoyancy of a contaminant in flow in a slowly varying channels could lead to a considerable reduction in the dispersion.

The inclusion of thermal effects on rivulet flow would also be of interest. In this case the temperature, $T = T(x, y, z, t)$, satisfies an advection–diffusion equation with an appropriate thermal diffusivity D_T, and in the simplest case the boundary conditions will consist of a fixed temperature at the substrate and Newton's law of cooling at the free surface of the rivulet, namely

$$-k_{\text{th}} \nabla T \cdot \mathbf{n} = \alpha_{\text{th}} (T - T_\infty), \tag{7.1}$$

where k_{th} is the thermal conductivity of the fluid, α_{th} is the coefficient of heat transfer at the free surface (which is a measure of the ratio of the heat flux to the temperature difference across the free surface), and T_∞ is the temperature of the surrounding atmosphere. (The condition (7.1) is applicable to cases where the heat transfer at the free surface is dominated by convective heat transfer, as is

commonly the case at a liquid-gas boundary.) For example, the problem of axial dispersion of heat from an initially hot "slug" of fluid in the rivulet (analogous to the initial slug of solute considered in Chapters 5 and 6) could be considered, and, in particular, the dependence of D_{eff} on α_{th} investigated; a problem of this type was considered by Lungu and Moffatt [74] for the case of Poiseuille flow in a circular pipe.

Another interesting extensions to all of the work in this thesis would be to include inertial terms in the analysis; this may be important for some applications, but also would allow unsteady flows to be considered, which would be necessary to address the question of the stability of steady flows, and also to validate the analysis against experimental investigations.

Fan and Hwang [42], and Prenosil and Jarvis [101], Zhang and Frigaard [143], and Dutta *et al.* [34] considered the effects of non-Newtonian rheology on Taylor–Aris dispersion in flow in a pipe, in a channel and down an inclined substrate, respectively; another natural extension would be to consider the effect of a non-Newtonian rheology on Taylor–Aris dispersion in rivulet flow. This would bring together the two main themes of this thesis, namely non-Newtonian effects in rivulets and dispersion in rivulets.

We believe that the results described in the present thesis provide a useful contribution to the comparatively small body of work on rivulet flow of Newtonian and non-Newtonian fluids; nonetheless the previously mentioned open challenges and possible extensions show that much research still remains to be done.

Bibliography

[1] A. Adrover and S. Cerbelli. Laminar dispersion at low and high Peclet numbers in finite-length patterned microtubes. *Phys. Fluids*, 29:062005, 2017.

[2] A. Ajdari, N. Bontoux, and H. A. Stone. Hydrodynamic dispersion in shallow microchannels: the effect of cross-sectional shape. *Anal. Chem.*, 78:387–392, 2006.

[3] S. V. Alekseenko, S. P. Aktershev, A. V. Bobylev, S. M. Kharlamov, and D. M. Markovich. Nonlinear forced waves in a vertical rivulet flow. *J. Fluid Mech.*, 770:350–373, 2015.

[4] S. V. Alekseenko, A. V. Bobylev, V. V. Guzanov, D. M. Markovich, and S. M. Kharlamov. Regular waves on vertical falling rivulets at different wetting contact angles. *Thermophys. Aeromech.*, 17:345–357, 2010.

[5] S. V. Alekseenko, A. V. Bobylev, and D. M. Markovich. Rivulet flow on the outer surface of an inclined cylinder. *J. Eng. Thermophys.*, 17:259–272, 2008.

[6] S. V. Alekseenko, P. I. Gesheva, and P. A. Kuibin. Free-boundary fluid flow on an inclined cylinder. *Phys.-Doklady*, 42:269–272, 1997.

[7] S. V. Alekseenko, D. M. Markovich, and S. I. Shtork. Wave flow of rivulets on the outer surface of an inclined cylinder. *Phys. Fluids*, 8:3288–3299, 1996.

[8] R. F. Allen and C. M. Biggin. Longitudinal flow of a lenticular liquid filament down an inclined plane. *Phys. Fluids*, 17:287–291, 1974.

[9] R. Aris. On the dispersion of a solute in a fluid flowing through a tube. *Proc. Roy. Soc. London A*, 235:67–77, 1956.

[10] V. Balakotaiah and H.-C. Chang. Dispersion of chemical solutes in chromatographs and reactors. *Phil. Trans. Roy. Soc. London A*, 351:39–75, 1995.

[11] N. J. Balmforth, R. V. Craster, and R. Sassi. Shallow viscoplastic flow on an inclined plane. *J. Fluid Mech.*, 470:1–29, 2002.

[12] H. Barnes. The yield stress—a review or "$\pi\alpha\nu\tau\alpha\ \rho\varepsilon\iota$"—everything flows? *J. Non-Newt. Fluid Mech.*, 81:133–178, 1999.

[13] H. A. Barnes, J. F. Hutton, and K. Walters. *An Introduction to Rheology.* Elsevier, 1989.

[14] C. M. Bender and S. A. Orszag. Advanced mathematical methods for scientists and engineers I: Asymptotic methods and perturbation theory., 1999.

[15] E. S. Benilov. On the stability of shallow rivulets. *J. Fluid Mech.*, 636:455–474, 2009.

[16] M. Bentwich, D. Glasser, J. Kern, and D. Williams. Analysis of rectilinear rivulet flow. *A. I. Ch. E. J.*, 22:772–779, 1976.

[17] R. B. Bird, G. C. Dai, and B. J. Yarusso. The rheology and flow of viscoplastic materials. *Rev. Chem. Eng.*, 1:1–70, 1983.

[18] B. Birnir, K. Mertens, V. Putkaradze, and P. Vorobieff. Morphology of a stream flowing down an inclined plane. Part 2. Meandering. *J. Fluid Mech.*, 607:401–411, 2008.

[19] D. V. Boger and K. Walters. *Rheological Phenomena in Focus*. Elsevier, 2012.

[20] P. C. Chatwin. The approach to normality of the concentration distribution of a solute in a solvent flowing along a straight pipe. *J. Fluid Mech.*, 43:321–352, 1970.

[21] P. C. Chatwin and P. J. Sullivan. The effect of aspect ratio on longitudinal diffusivity in rectangular channels. *J. Fluid Mech.*, 120:347–358, 1982.

[22] P. Colinet, H. Kaya, S. Rossomme, and B. Scheid. Some advances in lubrication-type theories. *Europ. Phys. J. Special Topics*, 146:377–389, 2007.

[23] P. Coussot. *Mudflow Rheology and Dynamics*. Balkema, 1997.

[24] R. V. Craster and O. K. Matar. Dynamics and stability of thin liquid films. *Rev. Mod. Phys.*, 81:1131–1198, 2009.

[25] A. Daerr, J. Eggers, L. Limat, and N. Valade. General mechanism for the meandering instability of rivulets of Newtonian fluids. *Phys. Rev. Letters*, 106:184501, 2011.

[26] A. A. Darhuber, J. Z. Chen, J. M. Davis, and S. M. Troian. A study of mixing in thermocapillary flows on micropatterned surfaces. *Phil. Trans. Roy. Soc. London A*, 362:1037–1058, 2004.

[27] A. A. Darhuber, J. M. Davis, S. M. Troian, and W. W. Reisner. Thermocapillary actuation of liquid flow on chemically patterned surfaces. *Phys. Fluids*, 15:1295–1304, 2003.

[28] A. A. Darhuber and S. M. Troian. Principles of microfluidic actuation by modulation of surface stresses. *Annu. Rev. Fluid Mech.*, 37:425–455, 2005.

[29] J. A. Diez, A. G. González, and L. Kondic. On the breakup of fluid rivulets. *Phys. Fluids*, 21:082105, 2009.

[30] J. A. Diez, A. G. González, and L. Kondic. Instability of a transverse liquid rivulet on an inclined plane. *Phys. Fluids*, 24:032104, 2012.

[31] B. R. Duffy and H. K. Moffatt. Flow of a viscous trickle on a slowly varying incline. *Chem. Eng. J.*, 60:141–146, 1995.

[32] B. R. Duffy and H. K. Moffatt. A similarity solution for viscous source flow on a vertical plane. *Europ. J. Appl. Math.*, 8:37–47, 1997.

[33] B. R. Duffy and S. K. Wilson. A rivulet of perfectly wetting fluid with temperature-dependent viscosity draining down a uniformly heated or cooled slowly varying substrate. *Phys. Fluids*, 15:3236–3239, 2003.

[34] B. K. Dutta, P. Ray, and B. Barman. Exact analysis of laminar dispersion in non-Newtonian flow. *Wärme-und Stoffübertragung*, 23:39–43, 1988.

[35] D. Dutta. *Hydrodynamics dispersion, in "Encyclopedia of Microfluidics and Nanofluidics", edited by D. Li.* 2015.

[36] D. Dutta, A. Ramachandran, and D. T. Leighton. Effect of channel geometry on solute dispersion in pressure-driven microfluidic systems. *Microfluid. Nanofluid.*, 2:275–290, 2006.

[37] M. S. El-Genk and H. H. Saber. Minimum thickness of a flowing down liquid film on a vertical surface. *Int. J. Heat Mass Trans.*, 44:2809–2825, 2001.

[38] M. H. Eres, L. W. Schwartz, and R. V. Roy. Fingering phenomena for driven coating films. *Phys. Fluids*, 12:1278–1295, 2000.

[39] L. Espín and S. Kumar. Forced spreading of films and droplets of colloidal suspensions. *J. Fluid Mech.*, 742:495–519, 2014.

[40] P. L. Evans, L. W. Schwartz, and R. V. Roy. Steady and unsteady solutions for coating flow on a rotating horizontal cylinder: Two-dimensional theoretical and numerical modeling. *Phys. Fluids*, 16:2742–2756, 2004.

[41] P. L. Evans, L. W. Schwartz, and R. V. Roy. Three-dimensional solutions for coating flow on a rotating horizontal cylinder: Theory and experiment. *Phys. Fluids*, 17:072102, 2005.

[42] L. T. Fan and W. S. Hwang. Dispersion of Ostwald-de Waele fluid in laminar flow through a cylindrical tube. *Proc. Roy. Soc. London A*, 283:576–582, 1965.

[43] S. Fomin, K. Kilpatrick, and R. Hubbard. Rimming flow of a power-law fluid: Qualitative analysis of the mathematical model and analytical solutions. *Appl. Math. Comput.*, 216:2169–2176, 2010.

[44] S. Fomin, R. Shankar, N. Danes, A. Yasuda, and V. Chugunov. Rimming flow of a weakly elastic fluid. *Theor. Comput. Fluid Dyn.*, 28:485–498, 2014.

[45] Foter. URL: http://foter.com/photo/dessert-sweet-berry/. Accessed: 26th July 2017.

[46] A. C. Fowler. *Groundwater Flow, Chapter 13 in "Mathematical Models in the Applied Sciences"*. 1998.

[47] D. K. Gartling and N. Phan-Thien. A numerical simulation of a plastic fluid in a parallel-plate plastometer. *J. Non-Newt. Fluid Mech.*, 14:347–360, 1984.

[48] W. N. Gill and R. Sankarasubramanian. Dispersion of a non-uniform slug in time-dependent flow. *Proc. Roy. Soc. London A*, 322:101–117, 1971.

[49] I. S. Gradshteyn and I. M. Ryzhik. *Table of Integrals, Series, and Products, edited by D. Zwillinger, 867–1057.* Academic Press, [online], 8th edition, 1980.

[50] N. L. Grand-Piteira, A. Daerr, and L. Limat. Meandering rivulets on a plane: A simple balance between inertia and capillarity. *Phys. Rev. Letters*, 96:254503, 2006.

[51] A. Griffiths. On the movement of a coloured index along a capillary tube, and its application to the measurement of the circulation of water in a closed circuit. *Proc. Roy. Soc. London A*, 23:190–197, 1910.

[52] R. W. Griffiths. The dynamics of lava flows. *Annu. Rev. Fluid Mech.*, 32:477–518, 2000.

[53] D. C. Guell, R. G. Cox, and H. Brenner. Taylor dispersion in conduits of large aspect ratio. *Chem. Eng. Comm.*, 58:231–244, 1987.

[54] J. H. Harker, J. R. Backhurst, and J. F. Richardson. *Chemical Engineering.* Butterworth-Heinemann, 5th edition, 2013.

[55] M. A. Herrada, A. S. Mohamed, J. M. Montanero, and A. M. Gañán-Calvo. Stability of a rivulet flowing in a microchannel. *Int. J. Multiphase Flow*, 69:1–7, 2015.

[56] L. M. Hocking, W. R. Debler, and K. E. Cook. The growth of leading-edge distortions on a viscous sheet. *Phys. Fluids*, 11:307–313, 1999.

[57] D. Holland, B. R. Duffy, and S. K. Wilson. Thermocapillary effects on a thin viscous rivulet draining steadily down a uniformly heated or cooled slowly varying substrate. *J. Fluid Mech.*, 441:195–221, 2001.

[58] P. D. Howell, H. Kim, M. G. Popova, and H. A. Stone. Rivulet flow over a flexible beam. *J. Fluid Mech.*, 796:285–305, 2016.

[59] B. Hu and S. L. Kieweg. The effect of surface tension on the gravity-driven thin film flow of Newtonian and power-law fluids. *Comput. Fluids*, 64:83–90, 2012.

[60] B. Hu and S. L. Kieweg. Contact line instability of gravity-driven flow of power-law fluids. *J. Non-Newt. Fluid Mech.*, 225:62–69, 2015.

[61] H. E. Huppert. The propagation of two-dimensional and axisymmetric viscous gravity currents over a rigid horizontal surface. *J. Fluid Mech.*, 121:43–58, 1982.

[62] B. Inaglory. URL: https://upload.wikimedia.org/wikipedia/commons/b/b1/P Accessed: 12th September 2016.

[63] M. F. G. Johnson, R. A. Schluter, M. J. Miksis, and S. G. Bankoff. Experimental study of rivulet formation on an inclined plate by fluorescent imaging. *J. Fluid Mech.*, 394:339–354, 1999.

[64] L. Jossic, P. Lefevre, C. de Loubens, A. Magnin, and C. Corre. The fluid mechanics of shear-thinning tear substitutes. *J. Non-Newt. Fluid Mech.*, 161:1–9, 2009.

[65] O. A. Kabov. Interfacial thermal fluid phenomena in thin liquid films. *Int. J. Emerg. Multidisciplinary Fluid Sci.*, 2:87–120, 2010.

[66] O. A. Kabov, M. V. Bartashevich, and V. Cheverda. Rivulet flows in microchannels and minichannels. *Int. J. Emerg. Multidisciplinary Fluid Sci.*, 2:161–182, 2010.

[67] V. O. Kheyfets and S. L. Kieweg. Gravity-driven thin film flow of an Ellis fluid. *J. Non-Newt. Fluid Mech.*, 202:88–98, 2013.

[68] P. A. Kuibin. An asymptotic description of the rivulet flow along an inclined cylinder. *Russ. J. Eng. Thermophys*, 6:33–45, 1996.

[69] L. G. Leal. *Unidirectional and One-Dimensional Flow and Heat Transfer Problems, Chapter 3 in "Advanced Transport Phenomena: Fluid Mechanics and Convective Transport Processes"*. Cambridge University Press, 2007.

[70] C.-Y. Lee, C.-L. Chang, Y.-N. Wang, and L.-M. Fu. Microfluidic mixing: A review. *Int. J. Mol. Sci.*, 12:3263–3287, 2011.

[71] G. A. Leslie, S. K. Wilson, and B. R. Duffy. Three-dimensional coating and rimming flow: a ring of fluid on a rotating horizontal cylinder. *J. Fluid Mech.*, 716:51–82, 2013.

[72] A. E. M. Library. URL: https://aeml.tech.purdue.edu/airframeimages/wing Accessed: 25th July 2017.

[73] G. G. Lipscomb and M. M. Denn. Flow of Bingham fluids in complex geometries. *J. Non-Newt. Fluid Mech.*, 14:337–346, 1984.

[74] E. M. Lungu and H. K. Moffatt. The effect of wall conductance on heat diffusion in duct flow. *J. Eng. Math.*, 16:121–136, 1982.

[75] R. Maiti, R. Khanna, and K. Nigam. Hysteresis in trickle-bed reactors: A review. *Indus. Eng. Chem. Res.*, 45:5185–5198, 2006.

[76] S. Matsuhisa and R. B. Bird. Analytical and numerical solutions for laminar flow of the non-Newtonian Ellis fluid. *A. I. Ch. E. J.*, 11:588–595, 1965.

[77] G. McKinley. Rod-climbing experiment and die-swell. Available from: http://web.mit.edu/nnf/, accessed on 28th June 2017.

[78] G. N. Mercer and A. J. Roberts. A centre manifold description of contaminant dispersion in channels with varying flow properties. *SIAM J. Appl. Math.*, 50:1547–1565, 1990.

[79] K. Mertens, V. Putkaradze, and P. Vorobieff. Morphology of a stream flowing down an inclined plane. Part 1. Braiding. *J. Fluid Mech.*, 531:49–58, 2005.

[80] D. M. Meter and R. B. Bird. Tube flow of non-Newtonian polymer solutions: Part 1. Laminar flow and rheological models. *A. I. Ch. E. J.*, 10:878–881, 1964.

[81] J. Mikielewicz and J. R. Moszynski. Minimum thickness of a liquid film flowing vertically down a solid surface. *Int. J. Heat Mass Trans.*, 19:771–776, 1976.

[82] J. Mikielewicz and J. R. Moszynski. Improved analysis of breakdown of thin liquid-films. *Archi. Mech.*, 30:489–500, 1978.

[83] F. A. Morrison. *Understanding Rheology*. Oxford University Press, 2001.

[84] F. H. H. A. Mukahal, B. R. Duffy, and S. K. Wilson. A rivulet of a power-law fluid with constant contact angle draining down a slowly varying substrate. *Phys. Fluids*, 27:052101, 2015.

[85] F. H. H. A. Mukahal, B. R. Duffy, and S. K. Wilson. Rivulet flow of generalised Newtonian fluids. Submitted for publication, 2016.

[86] F. H. H. A. Mukahal, B. R. Duffy, and S. K. Wilson. Advection and Taylor–Aris dispersion in rivulet flow. To appear in Proc. Roy. Soc. London A, 2017.

[87] F. H. H. A. Mukahal, S. K. Wilson, and B. R. Duffy. A rivulet of a power-law fluid with constant width draining down a slowly varying substrate. *J. Non-Newt. Fluid Mech.*, 224:30–39, 2015.

[88] T. Myers and J. Charpin. A mathematical model for atmospheric ice accretion and water flow on a cold surface. *Int. J. Heat Mass Trans.*, 47:5483–5500, 2004.

[89] T. Myers, H. X. Liang, and B. Wetton. The stability and flow of a rivulet driven by interfacial shear and gravity. *Int. J. Non-Linear Mech.*, 39:1239–1249, 2004.

[90] T. G. Myers. Thin films with high surface tension. *SIAM Rev.*, 40:441–462, 1998.

[91] T. G. Myers. Application of non-Newtonian models to thin film flow. *Phys. Rev. E*, 72:066302, 2005.

[92] T. Nakagawa. Rivulet meanders on a smooth hydrophobic surface. *Int. J. Multiphase Flow*, 18:455–463, 1992.

[93] T. Nakagawa and J. C. Scott. Stream meanders on a smooth hydrophobic surface. *J. Fluid Mech.*, 149:89–99, 1984.

[94] A. Oron, S. H. Davis, and S. G. Bankoff. Long-scale evolution of thin liquid films. *Rev. Mod. Phys.*, 69:931–980, 1997.

[95] M. Pagitsas, A. Nadim, and H. Brenner. Multiple time scale analysis of macrotransport processes. *Physica A*, 135:533–550, 1986.

[96] J. P. Pascal and S. J. D. D'Alessio. Instability of power-law fluid flows down an incline subjected to wind stress. *Appl. Math. Model.*, 31:1229–1248, 2007.

[97] C. Paterson, S. K. Wilson, and B. R. Duffy. Pinning, de-pinning and re-pinning of a slowly varying rivulet. *Europ. J. Mech. B/Fluids*, 41:94–108, 2013.

[98] C. Paterson, S. K. Wilson, and B. R. Duffy. Rivulet flow round a horizontal cylinder subject to a uniform surface shear stress. *Q. J. Mech. Appl. Math.*, 67:567–597, 2014.

[99] C. Paterson, S. K. Wilson, and B. R. Duffy. Strongly coupled interaction between a ridge of fluid and an inviscid airflow. *Phys. Fluids*, 27:072104, 2015.

[100] C. A. Perazzo and J. Gratton. Navier–Stokes solutions for parallel flow in rivulets on an inclined plane. *J. Fluid Mech.*, 507:367–379, 2004.

[101] J. E. Prenosil and P. E. J. Jarvis. Note on Taylor diffusion for a power law fluid. *Chem. Eng. Sci.*, 29:1290–1291, 1974.

[102] D. Pritchard, B. R. Duffy, and S. K. Wilson. Shallow flows of generalised Newtonian fluids on an inclined plane. *J. Eng. Math.*, 94:115–133, 2015.

[103] R. F. Probstein. *Solutions of Uncharged Molecules, Chapter 4 in "Physicochemical Hydrodynamics: an Introduction"*. John Wiley & Sons, 2005.

[104] R. R. Ratnakar and V. Balakotaiah. Exact averaging of laminar dispersion. *Phys. Fluids*, 23:023601, 2011.

[105] O. Reynolds. On the theory of lubrication and its application to Mr. Beauchamp tower's experiments, including an experimental determination of the viscosity of olive oil. *Proc. Roy. Soc. London*, 40:191–203, 1886.

[106] A. C. Robertson, I. J. Taylor, S. K. Wilson, B. R. Duffy, and J. M. Sullivan. Numerical simulation of rivulet evolution on a horizontal cable subject to an external aerodynamic field. *J. Fluids Struc.*, 26:50–73, 2010.

[107] S. Rosenblat. Rivulet flow of a viscoelastic liquid. *J. Non-Newt. Fluid Mech.*, 13:259–277, 1983.

[108] H. H. Saber and M. S. El-Genk. On the breakup of a thin liquid film subject to interfacial shear. *J. Fluid Mech.*, 500:113–133, 2004.

[109] R. Sayag and M. G. Worster. Axisymmetric gravity currents of power-law fluids over a rigid horizontal surface. *J. Fluid Mech.*, 716:R5, 2013.

[110] P. Schmuki and M. Laso. On the stability of rivulet flow. *J. Fluid Mech.*, 215:125–143, 1990.

[111] L. W. Schwartz. Viscous flows down an inclined plane: Instability and finger formation. *Phys. Fluids*, 1:443–445, 1989.

[112] R. Semiat, D. Moalem-Maron, and S. Sideman. Transfer characteristics of convex and concave rivulet flow on inclined surfaces with straight-edged grooves. *Desalination*, 34:267–287, 1980.

[113] D. Slade, S. Veremieiev, Y. C. Lee, and P. H. Gaskell. Gravity-driven thin film flow: The influence of topography and surface tension gradient on rivulet formation. *Chem. Eng. Proc.*, 68:7–12, 2013.

[114] P. C. Smith. A similarity solution for slow viscous flow down an inclined plane. *J. Fluid Mech.*, 58:275–288, 1973.

[115] R. Smith. Longitudinal dispersion of a buoyant contaminant in a shallow channel. *J. Fluid Mech.*, 78:677–688, 1976.

[116] H. A. Stone, A. D. Stroock, and A. Ajdari. Engineering flows in small devices: Microfluidics toward a lab-on-a-chip. *Annu. Rev. Fluid Mech.*, 36:381–411, 2004.

[117] J. M. Sullivan, C. Paterson, S. K. Wilson, and B. R. Duffy. A thin rivulet or ridge subject to a uniform transverse shear stress at its free surface due to an external airflow. *Phys. Fluids*, 24:082109, 2012.

[118] J. M. Sullivan, S. K. Wilson, and B. R. Duffy. A thin rivulet of perfectly wetting fluid subject to a longitudinal surface shear stress. *Q. J. Mech. Appl. Math.*, 61:25–61, 2008.

[119] A. J. Tanasijczuk, C. A. Perazzo, and J. Gratton. Navier–Stokes solutions for steady parallel-sided pendent rivulets. *Europ. J. Mech. B/Fluids*, 29:465–471, 2010.

[120] R. I. Tanner. *Engineering Rheology*. Oxford University Press, 1996.

[121] R. I. Tanner and K. Walters. *Rheology: An Historical Perspective*. Elsevier, 1998.

[122] G. I. Taylor. Dispersion of soluble matter in solvent flowing slowly through a tube. *Proc. Roy. Soc. London A*, 219:186–203, 1953.

[123] G. I. Taylor. Conditions under which dispersion of a solute in a stream of solvent can be used to measure molecular diffusion. *Proc. Roy. Soc. London A*, 225:473–477, 1954.

[124] G. D. Towell and L. B. Rothfeld. Hydrodynamics of rivulet flow. *A. I. Ch. E. J.*, 12:972–980, 1966.

[125] G. A. Truskey, F. Yuan, and D. F. Katz. *Transport phenomena in biological systems*. Pearson/Prentice Hall Upper Saddle River NJ, 2004.

[126] Y. Velísková, M. Sokáč, P. Halaj, M. K. Bara, R. Dulovičová, and R. Schügerl. Pollutant spreading in a small stream: a case study in Mala Nitra Canal in Slovakia. *Env. Proc.*, 1:265–276, 2014.

[127] P. Vlasogiannis, G. Karagiannis, P. Argyropoulos, and V. Bontozoglou. Air–water two-phase flow and heat transfer in a plate heat exchanger. *Int. J. Multiphase Flow*, 28:757–772, 2002.

[128] S. D. R. Wilson and S. L. Burgess. The steady, spreading flow of a rivulet of mud. *J. Non-Newt. Fluid Mech.*, 79:77–85, 1998.

[129] S. K. Wilson and B. R. Duffy. On the gravity-driven draining of a rivulet of viscous fluid down a slowly varying substrate with variation transverse to the direction of flow. *Phys. Fluids*, 10:13–22, 1998.

[130] S. K. Wilson and B. R. Duffy. Strong temperature-dependent-viscosity effects on a rivulet draining down a uniformly heated or cooled slowly varying substrate. *Phys. Fluids*, 15:827–840, 2003.

[131] S. K. Wilson and B. R. Duffy. A rivulet of perfectly wetting fluid draining steadily down a slowly varying substrate. *IMA J. Appl. Math.*, 70:293–322, 2005.

[132] S. K. Wilson and B. R. Duffy. Unidirectional flow of a thin rivulet on a vertical substrate subject to a prescribed uniform shear stress at its free surface. *Phys. Fluids*, 17:108105, 2005.

[133] S. K. Wilson and B. R. Duffy. When is it energetically favorable for a rivulet of perfectly wetting fluid to split? *Phys. Fluids*, 17:078104, 2005.

[134] S. K. Wilson, B. R. Duffy, and R. Hunt. A slender rivulet of a power-law fluid driven by either gravity or a constant shear stress at the free surface. *Q. J. Mech. Appl. Math.*, 55:385–408, 2002.

[135] S. K. Wilson, B. R. Duffy, and A. B. Ross. On the gravity-driven draining of a rivulet of a viscoplastic material down a slowly varying substrate. *Phys. Fluids*, 14:555–571, 2002.

[136] S. K. Wilson, J. M. Sullivan, and B. R. Duffy. The energetics of the breakup of a sheet and of a rivulet on a vertical substrate in the presence of a uniform surface shear stress. *J. Fluid Mech.*, 674:281–306, 2011.

[137] Y. M. Yatim, B. R. Duffy, and S. K. Wilson. Similarity solutions for unsteady shear-stress-driven flow of Newtonian and power-law fluids: slender rivulets and dry patches. *J. Eng. Math.*, 73:53–69, 2012.

[138] Y. M. Yatim, B. R. Duffy, S. K. Wilson, and R. Hunt. Similarity solutions for unsteady gravity-driven slender rivulets. *Q. J. Mech. Appl. Math.*, 64:455–480, 2011.

[139] Y. M. Yatim, S. K. Wilson, and B. R. Duffy. Unsteady gravity-driven slender rivulets of a power-law fluid. *J. Non-Newt. Fluid Mech.*, 165:1423–1430, 2010.

[140] G. W. Young and S. H. Davis. Rivulet instabilities. *J. Fluid Mech.*, 176:1–31, 1987.

[141] W. R. Young and S. Jones. Shear dispersion. *Phys. Fluids*, 3:1087–1101, 1991.

[142] H. Zhang, J. Yue, G. Chen, and Q. Yuan. Flow pattern and break-up of liquid film in single-channel falling film microreactors. *Chem. Eng. J.*, 163:126–132, 2010.

[143] J. Zhang and I. A. Frigaard. Dispersion effects in the miscible displacement of two fluids in a duct of large aspect ratio. *J. Fluid Mech.*, 549:225–251, 2006.